In presenting the dissertation as a partial fulfillment of the requirements for an advanced degree from the Georgia Institute of Technology, I agree that the Library of the Institute shall make it available for inspection and circulation in accordance with its regulations governing materials of this type. I agree that permission to copy from, or to publish from, this dissertation may be granted by the professor under whose direction it was written, or, in his absence, by the Dean of the Graduate Division when such copying or publication is solely for scholarly purposes and does not involve potential financial gain. It is understood that any copying from, or publication of, this dissertation which involves potential financial gain will not be allowed without written permission.

7/25/68

GAS-LIQUID PHASE EQUILIBRIUM IN THE HELIUM-ETHYLENE AND HELIUM-PROPYLENE SYSTEMS BELOW 260 K AND 120 ATMOSPHERES

A THESIS

Presented to

The Faculty of the Graduate Division

by

James Daniel Garber

In Partial Fulfillment

of the Requirements for the Degree

Doctor of Philosophy

in the School of Chemical Engineering

Georgia Institute of Technology

December, 1970

GAS-LIQUID PHASE EQUILIBRIUM IN THE HELIUM-ETHYLENE AND HELIUM-PROPYLENE SYSTEMS BELOW 260 K and 120 ATMOSPHERES

Approved:

Chairman

Date approved by Chairman: 2/5/71

DEDICATION

To the memory of my father

ACKNOWLEDGMENTS

I am very grateful to Dr. W. T. Ziegler, my thesis advisor, for his guidance and encouragement during this research work. He has given me much insight into the general area of thermodynamics, and has helped me to develop the attitudes necessary to carry through a research project. I also wish to thank him for providing employment on other projects that have contributed to my training in thermodynamics. The suggestions and criticisms of Dr. H. A. McGee, Jr. and Dr. R. A. Pierotti while serving on the reading committee are greatly appreciated. Several discussions with Dr. Pierotti concerning some of the theory involved in this work proved to be very helpful. Dr. J. A. Knight, Jr. provided assistance in certain aspects of gas chromatography. His help is very much appreciated.

Other people who have made this work possible are Dr. B. S. Kirk who built the phase equilibrium apparatus used in this work, and Dr. K. F. Liu who provided several computer programs that were useful in making theoretical calculations. I wish to thank the Chemical Engineering Department for providing me with a three year N.D.E.A. fellowship and also the Georgia Tech Foundation which provided other financial support. The use of the facilities at the Rich Electronic Computer Center is also appreciated.

I am very grateful to my wife, Judy, who has provided encouragement,

assistance, and motivation throughout this work. The encouragement of my mother, Mrs. Nola Comeaux, my stepfather, Mr. George J. Comeaux, my brother, Rohn, my two sisters, Marguerite and Mary Ellen, and other relatives is deeply appreciated.

TABLE OF CONTENTS

TABLE OF CONTENTS (Continued)

TABLE OF CONTENTS (Concluded)

LIST OF TABLES

LIST OF TABLES (Continued)

LIST OF TABLES (Concluded)

LIST OF FIGURES

LIST OF FIGURES (Continued)

LIST OF FIGURES (Continued)

LIST OF FIGURES (Concluded)

NOMENCLATURE

$\mathring{A}$ = Angstrom unit, 1×10^{-8} cm.

A_o = empirical parameter in the BWR equation.

a = empirical parameter in the BWR equation.

a_i = hard sphere diameter for molecule.

a_{12} = average hard sphere diameter.

B = second virial coefficient.

B^*_{CL} = reduced classical second virial coefficient from classical Kihara (6-12) core model.

B_K = second virial coefficient calculated from classical Kihara (6-12) core model.

B_o = empirical parameter of BWR equation.

B^*_o = reduced translational quantum second virial coefficient for an ideal gas.

BWR = Benedict-Webb-Rubin equation of state.

B^*_I, B^*_{II} = first and second reduced translational quantum corrections for the second virial coefficient from the Lennard-Jones (6-12) potential function.

b = empirical parameter in BWR equation.

b_o = volumetric parameter in the Lennard-Jones (6-12) intermolecular potential function, Equation (IV-25).

$b_s^{(j)}$ = coefficients for series representation of F_s, Equation (IV-35).

C = third virial coefficient.

$\bar{C}$ = dispersion constant.

C^*_{CL} = reduced classical third virial coefficient from Lennard-Jones (6-12) intermolecular potential function (also written as $C^*_{CL}(T^*)$).

NOMENCLATURE (Continued)

C_o = empirical parameter in BWR equation.

ΔC = non-additivity correction to the third virial coefficient, Equation (IV-51).

C^{add} = classical contribution to the third virial coefficient, Equation (IV-49).

c = empirical parameter in BWR equation; also used in the calculation of the third virial coefficient; see Equation (IV-58).

d = parameter in correlation of Chueh and Prausnitz; see Equation (IV-61).

$\bar{E}_i$ = partial molar internal energy.

e = energy parameter in Lennard-Jones (6-12) intermolecular potential function.

exp = raise 2.30258 to the power of the number in parentheses.

e/k = energy parameter in Lennard-Jones (6-12) intermolecular potential function.

F_1, F_2, F_3 = reduced functions for second virial coefficient from Kihara core model (6-12); Equation (IV-31).

f = fugacity and also used in Equation (IV-50).

$\bar{G}_c$ = partial molar Gibbs free energy for creation of a cavity.

$\bar{G}_i$ = partial molar Gibbs free energy for charging process.

g^o = Gibbs' molar free energy of an ideal gas at 1 atmosphere pressure.

H = Henry's law constant.

H^o = Henry's law constant at zero polarizability.

H_{vap} = heat of vaporization.

h = Plank's constant = 6.6256×10^{-27} erg-sec; also used as peak height on chromatogram.

I = ionization potential.

NOMENCLATURE (Continued)

i = summation index integer.

j = summation index integer.

KIH = Kihara core model (6-12).

KIHCK12 = Kihara core model (6-12) with correction applied to the geometric mixing rule using K_{12} calculated from Equation (V-8).

KIHEK12 = Kihara core model (6-12) with correction applied to the geometric mixing rule using experimental K_{12}.

$\bar{K}$ = Henry's law constant using consistency method.

K_i = Reiss function; see Equation (VIII-6).

K_{LJ} = constant representing the deviation from the Lennard-Jones potential geometric mean of the characteristic energy parameters of components i and j; see Equation (V-9).

K_{12} = constant representing the deviation from the Kihara potential geometric mean of the characteristic energy parameters of components i and j; see Equation (V-7).

k = Boltzmann constant = 1.380308×10^{-16} erg/K molecule.

LJCL = Lennard-Jones classical model.

ℓn = natural (base e) logarithm.

log = common (base 10) logarithm.

M = molecular weight.

M_o = core parameter in Kihara (6-12) core model.

m = mass of molecule, M/N_A.

N = a dummy quantity used to represent various equation of state parameters in writing mixture rules.

N_A = Avogadro's number 6.0238×10^{23} molecules/gm mole.

n = number of gm moles.

n_i = number of moles of component i.

NOMENCLATURE (Continued)

P = *total absolute pressure.*

P_{o1} = vapor pressure of condensible component.

R = gas law constant = 82.0560 atm-cc/gm mole K or 0.0820537 atm-liter/gm mole K.

r = intermolecular distance between centers of molecules.

S_o = core parameter in Kihara (6-12) core model.

s = summation index integer; also an attenuation factor on chromatograph (see Appendix D).

T = temperature, K (formerly $^{\circ}K$).

T^* = kT/e.

T_c^o = classical critical temperature at high temperature for quantum gases, Equation (IV-64).

T_c = critical temperature.

T_{Ri} = reduced temperature, T/T_c, of component i.

t = temperature, $^{\circ}C$.

U = intermolecular potential energy.

U_o = minimum energy of the Kihara potential function.

U_o/k = energy parameter in Kihara (6-12) model.

V = volume of gas.

V_c^o = classical critical volume at high temperature for the quantum gases, Equation (IV-65).

V_c = critical molar volume.

$\overline{V}_c$ = partial molar volume change upon cavity formation.

$\overline{V}_I$ = partial molar volume change upon charging.

V_m = molar volume of gas mixture.

V_o = core parameter in Kihara core model.

NOMENCLATURE (Continued)

V_{o1} = molar volume of component 1 gas at its vapor pressure.

V_1 = molar volume of component 1 gas.

V_2 = molar volume of component 2 gas.

$\overline{V}_i$ = partial molar volume of component i.

v_1 = molar volume of the compressed condensed liquid phase.

v_1^o = saturated molar volume of the condensible component.

x = mole fraction in the condensed phase.

Y = size parameter.

y_i = mole fraction of component i in the gas phase.

y_i^o = mole fraction calculated assuming the gas phase is ideal.

Z = compressibility factor, PV/nRT; also U_o/kT in Kihara core model.

GREEK LETTERS

α = parameter in BWR equation; also the molecular polarizability.

α_P = coefficient of thermal expansion for the pure component.

β_T = isothermal compressibility for the pure component.

$\overline{\beta}_T$ = average isothermal compressibility.

Γ = gamma function.

γ = empirical parameter in BWR equation.

γ_1' = activity coefficient of component 1 in liquid solutions referred to the pure liquid component at the system pressure and temperature.

γ_2' = activity coefficient of component 2 in liquid solutions referred to the infinitely dilute state at the system temperature and pressure.

Λ^* = translational quantum mechanical parameter.

NOMENCLATURE (Concluded)

μ = chemical potential.

μ^{o} = chemical potential of ideal gas at 1 atmosphere.

μ^{*} = chemical potential of pure liquid.

π = pi = 3.14159265.

ρ = distance between molecular cores in the Kihara core model.

$\bar{\rho}$ = number density of fluid molecules, N_A/v_1^o.

ρ_o = shortest distance between molecular cores at minimum potential energy.

σ = length parameter in LJCL (6-12) intermolecular potential.

$\emptyset$ = enhancement factor.

SUBSCRIPTS

1 = condensible component.

01 = gas at its normal vapor pressure (i.e. saturated vapor).

2 = helium.

c = condensible component.

m = gas mixture.

max = maximum value available in the data set.

i,j,k = 1, 2, or m.

v = volatile component.

SUPERSCRIPTS

G = gas.

L = liquid.

' = used to distinguish BWR parameters from virial equation parameters; Equation (IV-72).

∞ = refers to infinite dilution.

SUMMARY

This thesis work has been concerned with the experimental measurement and the theoretical prediction of binary gas-liquid equilibria. The helium-ethylene and helium-propylene systems have been studied below 260 K and 120 atmospheres.

The phase equilibrium apparatus used in this work was a single-pass, continuous flow-type described by Kirk[76] and Kirk and Ziegler.[77] This same apparatus was used by Kirk,[76] Mullins,[107] and Liu[83] for the investigation of phase equilibria of binary systems at cryogenic temperatures and high pressures. The liquid and gas phase equilibrium compositions for these systems were measured using two thermal conductivity chromatographs.

In the helium-ethylene system, seven isotherms in the gas-liquid region were studied. These temperatures were 129.98, 150.01, 162.00, 173.99, 188.02, 202.01, and 216.04 K. Six pressure points, ranging from 20 to 120 atmospheres, were measured along each isotherm. The helium-propylene system was studied in the gas phase along five isotherms. These temperatures were 200.00, 212.49, 224.99, 239.99, and 254.98 K, and the pressure was never greater than 120 atmospheres. The liquid phase of this system was studied at two additional temperatures, 175.00 and 187.49 K.

The uncertainty of the gas and liquid phase measurements in the helium-ethylene system is estimated to be ± 3 percent for the 162.00 K and higher temperatures. The two lower isotherms have an accuracy of ± 4 ½ percent. In the helium-propylene system, the 254.98, 239.99, and

224.99 K isotherms are uncertain to ± 3 percent of the gas phase results and the remaining isotherms, 212.49 and 200.00 K, are uncertain to about ± 4½ percent. The liquid analysis of this system is believed to be accurate to ± 3 percent for these five isotherms, and the lowest two isotherms, 175.00 and 187.49 K, are known to about ± 4½ percent. These uncertainties were determined by the scatter of the chromatograph calibration curve, the pressure gauge uncertainty (one-half percent), and the temperature uncertainty of 0.03 K.

The only experimental data available in the literature for comparison were by Hiza and Duncan[53] for the gas phase of the helium-ethylene system. These data were at the lowest temperatures, 130 and 150 K. Since analysis in this low concentration region was rather difficult in this work, the maximum difference of six percent between the two works is considered to be quite satisfactory.

The theoretical prediction of the gas phase composition for these systems can be adequately described using thermodynamics. An exact equation has been derived for the evaluation of y_1, which requires an assumption for a liquid phase model and an equation of state for the gas mixture. In this work the liquid solution has been assumed to be ideal, $\gamma_1' = 1$. To describe the P-V-T properties of the gas phase the theoretically based virial equation of state and the empirical Benedict-Webb-Rubin equation were used.

The virial equation of state used the Lennard-Jones classical, Kihara core potential, and the Kihara core potential with a modified geometric mixing rule to predict the pure and interaction second virial

coefficients. The third virial coefficients were calculated using the Lennard-Jones classical parameters and the method of Chueh and Prausnitz.[16] The Benedict-Webb-Rubin equation was used in two forms for the calculation of the interaction second virial coefficient. The equation was called BWR(LORENTZ) when the term $(B_o)_{12}$ was calculated using the Lorentz average, and BWR(LINEAR) when the linear average was used for the $(B_o)_{12}$ calculation.

A comparison was made of the available experimental data and the values predicted by theory for the helium-ethylene,[53] helium-ethane,[46,53] helium-propylene, and helium-propane[140] systems. The virial equation using the adjusted geometric mixing rule and the method of Chueh and Prausnitz[16] for the third virial coefficient gave the best agreement with experiment and the BWR(LINEAR) equation also predicted values that were within the experimental uncertainty. The Lennard-Jones classical, Kihara core model, and BWR(LORENTZ) gave less satisfactory results. The inability of these models to predict the correct B_{12} and third virial coefficient values is responsible for the disagreement.

By simply rearranging this theoretical method of predicting y_1, it is possible to use experimental data to extract the second interaction virial coefficient, B_{12}. These data have been extracted and smoothed for the helium-ethylene, helium-ethane, helium-propane, and helium-propylene systems. The uncertainty of these results was estimated by introducing the quoted uncertainty of the experimental data into the calculation. The temperature dependence of these B_{12} curves was found to be much greater than that found by Liu[83] for the helium-argon, helium-oxygen, helium-

nitrogen, helium-methane, and helium-carbon dioxide systems.

As was mentioned earlier, the geometric mixing rule used to predict B_{12} values has been shown to be largely inadequate for systems containing helium. Recent investigators[16,17,33,52,53,83,107] have suggested the introduction of a $(1-K_{12})$ term before the geometric mixing rule of the Kihara energy parameter. Hiza and Duncan[53] have developed an empirical equation which correlates available K_{12} data as a function of ionization potential. In the present work K_{12} values have been extracted for a variety of helium binary systems, and these results were found to compare favorably with the correlation of Hiza and Duncan.

The prediction of the solubility of a high pressure gas in a liquid phase has not received much attention due to the complexity of the problem. An exact expression can be obtained which relates the liquid composition to the fugacity of the gas phase, Henry's law constant, H_2^{∞}, and the partial molar volume at infinite dilution, $\overline{V_2}^{\infty}$. In its most useful form, this equation is known as the Krichevsky-Kasarnovsky equation.[80] Although the fugacity of the gas phase can be described rather easily using an equation of state, values of H_2^{∞} and $\overline{V_2}^{\infty}$ are scarce and very difficult to predict.

Using smoothed gas-liquid equilibrium data, it was possible to extract values of H_2^{∞} and $\overline{V_2}^{\infty}$ from the Krichevsky-Kasarnovsky equation.[80] In this work the fugacity of the gas phase was described using the virial equation. The uncertainty of these values was estimated by introducing the known experimental uncertainty of the data into the calculation.

The method of Pierotti[113,114] has been used to predict values of

H_2^∞ and $\overline{V}_2^\infty$ from first principles. This method is based upon the purely theoretical scaled particle theory. These predicted values of H_2^∞ and $\overline{V}_2^\infty$ are compared to the experimental results. Although in some cases the correct temperature dependency of H_2^∞ and $\overline{V}_2^\infty$ was not predicted, the theoretical values were generally within a factor of two and one-half of the experimental values. Pierotti[113,114,115] has mentioned that two modifications to his method, the dependency of the molecular core parameter with temperature and a correction to the geometric mixing rule used in the interaction energy term, might improve agreement with theory. An attempt was made to check these possible inadequacies, and predictions of H_2^∞ obtained applying these corrections are in excellent agreement with experiment.

CHAPTER I

INTRODUCTION

General Statement of the Problem

There is hardly a chemical process that does not use some aspect of phase equilibrium. Phase equilibrium may take many forms such as distillation, absorption, adsorption, extraction, and crystallization. Thus, it is essential that a chemical engineer have a basic understanding of this subject.

This thesis work is concerned with binary equilibrium between a liquid and a gas phase. The problem is a continuation of work done in this laboratory in which one component, 1, is a liquid or solid and the second component, 2, is a gas which is well above its critical temperature. Therefore, this work consists of experimentally measuring the equilibrium composition of the equilibrium phases at high pressures and the theoretical prediction of these experimental data.

Due to the fact that the gas phase is at high pressure and low temperature, the problem actually becomes the equilibrium of a fluid phase in the presence of a liquid. Under these conditions there may exist strong attractive or repulsive forces between the components of the gas and the liquid phase. If these net forces are attractive, they produce an increase in the partial pressure of the condensible component. This increases the concentration of that component in the gas phase. A very useful measure of the amount of imperfection present in the gas phase is

the enhancement factor, ϕ. The enhancement factor was first defined and used by Dokoupil, et al.[31] This term represents the ratio of the actual mole fraction, y_1, divided by the ideal mole fraction, y_1^o. The ideal mole fraction corresponds to the conditions under which the partial pressure of component 1 equals its vapor pressure

$$Py_1^o = P_{o1} \tag{I-1}$$

The enhancement factor becomes

$$\phi \text{ (enhancement factor)} = \frac{Py_1}{P_{o1}} \tag{I-2}$$

Dr. B. S. Kirk has built a single-pass flow type phase equilibrium apparatus which has been used in this laboratory. The apparatus is briefly described in the following chapter and in more detail by Kirk[76] and Kirk and Ziegler.[77] Binary systems that have been studied in this laboratory have been the hydrogen-methane system by Kirk,[76,77] the hydrogen- and helium-argon systems by Mullins,[107,108] and more recently the helium-carbon dioxide system by Liu.[83] Some of these measurements have been made in the gas-solid and gas-liquid regions which shows the versatility of the phase equilibrium apparatus. A recent survey by Hiza[52] provides an excellent review of the cryogenic binary systems that have been studied.

On the theoretical side of the problem, it is possible to obtain an exact expression for the enhancement factor. The basic thermodynamic criterion of equilibrium between phases is that the chemical potential of

component (i) in each phase must be equal. Using this basis, Kirk,[76] Kirk and Ziegler,[77] Kirk, et al.,[78] Mullins,[107] Liu,[83] Dokoupil,[30] Smith, et al.,[146] MacKendrick, et al.,[88] Prausnitz, et al.,[121] Prausnitz and Chueh,[120] Chiu and Canfield,[15] and Hiza and Duncan[53] have been able to obtain a theoretical expression for the enhancement factor. In many of the studies mentioned above, the agreement between theory and experiment is very good. These calculations require that one has an equation of state that represents the gas mixture. The virial equation of state is perhaps the most interesting equation to use. Since this equation has a theoretical basis, it can provide interesting information about the two and three body interaction forces between dissimilar molecules. Mullins,[107] Hiza,[52] Chueh and Prausnitz,[16] and Hiza and Duncan[53] have demonstrated that the usual geometric combination rule for predicting the interaction virial coefficient using the Kihara potential is largely inadequate for the helium binary systems. Liu[83] has also demonstrated that the same type deviation occurs when the Lennard-Jones classical model is used to represent the second interaction virial coefficient. Some empirical equations as the Benedict-Webb-Rubin (BWR),[46,76,77,88,107,146] Beattie-Bridgeman,[76,77,107] and Redlich-Kwong[119,120] have been shown to predict enhancement factor data better at high pressures than the virial equation, but they suffer from the lack of a theoretical foundation.

With the vast surge in the use of electronic digital computers, many theories of phase equilibrium can now be investigated which once involved calculations that were too laborious. Since most systems encountered in industry are the multicomponent type, the actual merit of this work is to provide the necessary binary data required to eventually

allow prediction of multicomponent phase equilibria. This would indeed alleviate the cumbersome task of making measurements on these systems. A recent paper by Sood and Haselden[148] summarizes the methods presently available for prediction of multicomponent vapor-liquid equilibrium in cryogenic mixtures.

Until a model for the liquid solution is assumed, no enhancement factor calculations can be made. In systems where the gas solubility in the liquid phase is less than 10 percent, it can be assumed that the solution is ideal or the activity coefficient, γ_1', is equal to one. For example, Mullins[107] has shown that the helium-argon system, along the three phase line, has an activity coefficient of unity. This work covers several degrees of temperature and pressures up to 120 atmospheres.

The theoretical prediction of the solubility of a high pressure gas in a cryogenic liquid is a difficult problem. Pierotti[113,114] has presented a method of predicting Henry's law constants from first principles. This method uses the scaled particle theory of Reiss[128] and appears to have the most potential of any theory concerned with the liquid phase.

Selection of a Problem

After a careful examination of existing gas-liquid equilibrium data in the literature, it appeared that binary systems with helium as a component were among the most interesting. Enhancement factors for the various helium binary systems were noted to be always less than three, and the solubility of helium in the liquid phase was usually less than 10 mole percent. The low enhancement factors tend to indicate that the net forces present in the gas phase of these helium binary systems are more

repulsive than the forces in the corresponding hydrogen binaries. The low solubility of helium in the liquid enables one to make assumptions concerning the liquid phase which are probably nearly correct. Helium binary system isobars have been shown by Liu[83] and Hiza and Duncan[53] to exhibit a minimum when plotted versus temperature. This phenomenon appears to be unique to these systems. Due to these several observations and the fact that helium systems have been previously studied in this laboratory, it was decided to choose a binary system involving helium. In selecting a specific system to study, it seemed best to select one that was of practical as well as theoretical interest.

Helium is found chiefly in natural gas wells, and some work has been done to determine the gas-liquid equilibria of these multicomponent mixtures.[6,150] The binary interaction data of these components with helium are of much interest since they could be used to predict the phase equilibrium of these mixtures. Liu[83] has obtained interaction second virial coefficient data for some helium binary systems using experimental phase equilibrium data for helium-nitrogen,[11,28,30,37,69,133] helium-oxygen,[48,144] helium-argon,[94,107,108,144] helium-methane,[40,47,56,70,145] and helium-carbon dioxide.[64,83,88] Since some recent experimental data are now available for the helium-ethane[46,53] and helium-propane[140] systems, it would be interesting to extract these interaction second virial coefficients. Except at low temperatures, the helium-ethylene[53] system has not been studied, and there are no data available for the helium-propylene system. Although the unsaturated hydrocarbons are not expected to be found in helium-gas wells in any sizable concentrations, a study of

these systems would essentially complete the study of the cryogenic helium-hydrocarbon systems. It would be interesting to compare the interaction data of these systems to ethane and propane to examine the effect of the presence of a double bond. There is also the possibility that these systems might show interesting enhancement factor behavior. A large amount of physical property data was also available for these hydrocarbons. This is essential for a complete theoretical investigation to be performed.

CHAPTER II

EXPERIMENTAL APPARATUS

General Description of Apparatus

The phase equilibrium apparatus used in this work has been described in detail by Kirk[76] and also by Kirk and Ziegler.[77] A schematic diagram of the single-pass, continuous flow-type device is shown in Figure 1. This apparatus has been used for phase equilibrium measurements in the gas-solid and gas-liquid regions. The apparatus will be discussed in terms of its use in this work.

This apparatus has been used to determine the equilibrium composition of the gas and liquid phases as a function of temperature and pressure. The maximum pressure used in this work was 120 atm, and the temperature was always below the ice point and above the normal boiling point of liquid nitrogen.

For systems in which the enhancement factor is near one, the operational temperature range depends entirely upon the vapor pressure of the liquid. It is felt that under these circumstances the temperature range used corresponds to the condensible component vapor pressure range of 0.04 to almost 8 atmospheres. At the low vapor pressure end the chromatographic analysis is the limiting factor and at the high vapor pressure end the liquid evaporation rate determines the limiting temperature.

The phase equilibrium cell, in which equilibrium is achieved, is soldered to the inside of a copper block cryostat, which is suspended

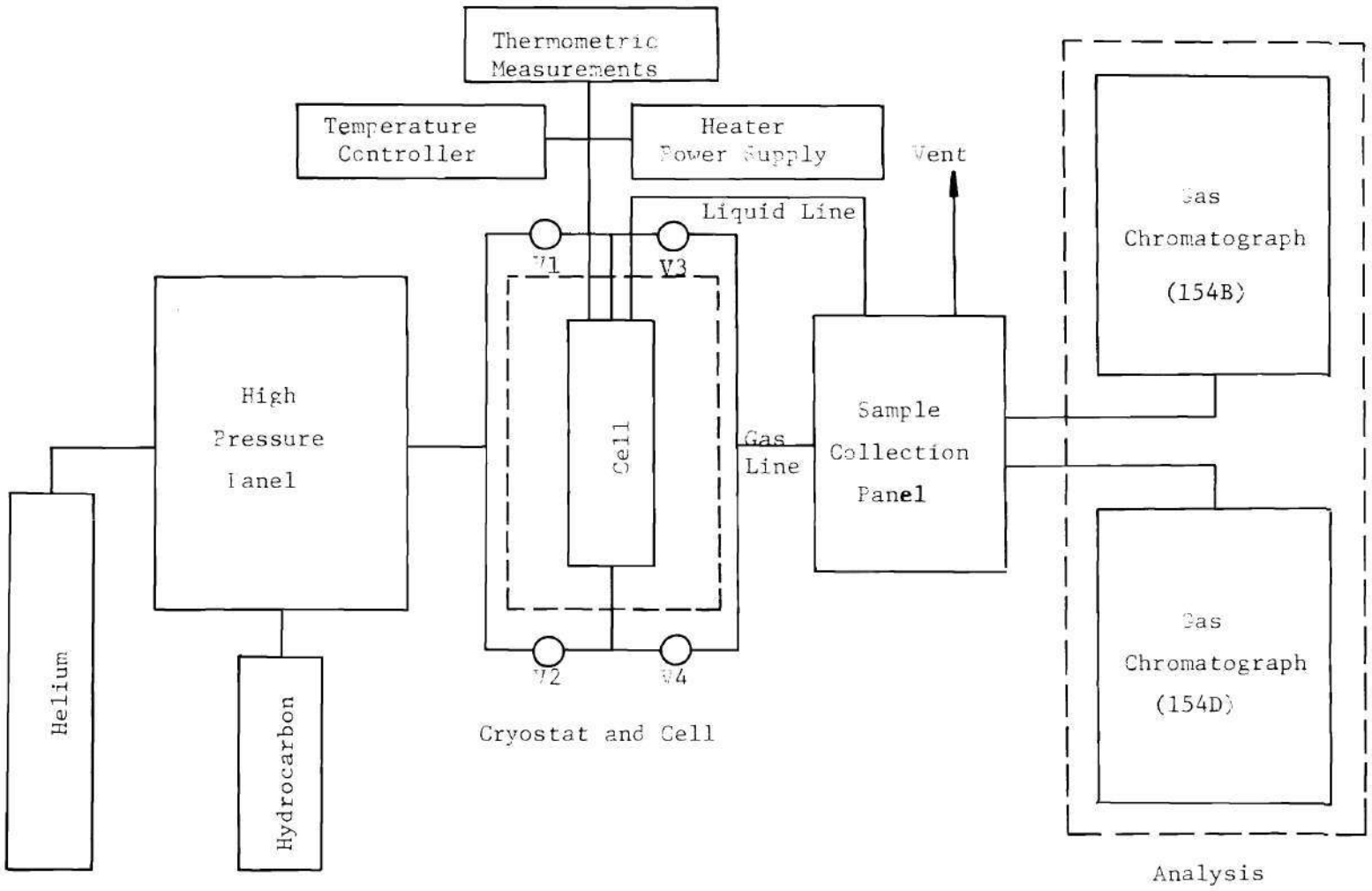

Figure 1. Schematic Diagram of Phase Equilibrium Apparatus.

inside an evacuated container filled with a powder insulation. Between the cell and the copper block cryostat is an annular space partially filled with copper wool. Liquid nitrogen is contained in a reservoir that is suspended beneath the copper block. This cryogen reservoir is connected to the annular space by a small capillary tube extending to the bottom of the reservoir. Refrigeration is provided by vaporization of liquid nitrogen injected into the annular space. A differential pressure regulator maintains a constant pressure above the liquid nitrogen. In this way the amount of refrigeration desired can be controlled by simply opening or closing the throttling valve located on the vent line.

Heat is supplied to the equilibrium cell by a direct current heater wrapped on the copper block. Temperature control is established by balancing a slight excess of refrigeration with heat input which is controlled by an automatic temperature controller. This temperature controller consists of a calibrated twelve junction copper-constantan thermocouple balanced against a reference potentiometer. A galvanometer light, which deflects proportionately to the temperature difference, strikes a photocell which causes a sudden increase in heater input. In this work it was possible to maintain temperatures constant within $\pm$ 0.03 K at any point.

A capsule-type platinum resistance thermometer located in a well at the top shoulder of the cell is used for temperature measurements. This thermometer has been calibrated by the National Bureau of Standards on the International Practical Kelvin Scale (IPTS-48) above 90.18 K and has an assigned ice point of 273.15 K. The NBS-1955 scale is used for any temperature measurement below 90.18 K. All measurements in this work are

reported on the (IPTS-68) as discussed in Appendix C. Difference thermocouples are located along the side and at the ends of the equilibrium cell. These difference couples enable the experimenter to measure the temperature gradients along the cell.

The high pressure panel contains a pressure regulating valve used to establish the pressure of the system. This valve can regulate pressure from 0 to 4500 psi outlet. Two Bourdon pressure gauges were used in this work. One gauge reads from 0 to 3000 psi and the second gauge, which is read from 0 to 600 psi, has a gauge protector set for 450 psi cut-off. These gauges were originally calibrated against a dead weight tester by Kirk.[76] In this work, it was necessary to apply a new correction to the high pressure gauge, see Appendix C. Also located on the high pressure panel are the high pressure gas burette and the condensation burette. These burettes provide one with a reasonable method of introducing a known amount of liquid into the cell.

When temperature and pressure conditions are established in the cell, the analysis of the equilibrium gas and liquid phases terminates the measurements. Gas chromatographs provide a quick and sufficiently accurate method of analysis. The gas phase flows continuously from the cell and a sample can be collected at any time for analysis on a 154D Perkin-Elmer chromatograph. The liquid sample is collected on the sample collecting panel. This panel contains a mercury filled burette which is used to hold the vaporized liquid sample until analysis can be made. The liquid analysis is performed on a 154B Perkin-Elmer chromatograph. Both chromatographs are calibrated to detect the component of lesser concentra-

tion. The columns used in the analysis and the operating conditions of the chromatographs are presented in Appendix D.

Experimental Procedure

The vacuum space around the outside of the copper block must be evacuated with a mechanical pump. A vacuum of about 50 microns assures the operator that temperature control of the copper block can be maintained. The equilibrium cell is flushed with the non-condensible component to assure that no air or condensibles might remain. About two liters of liquid nitrogen are then introduced into the reservoir. This coolant lowers the temperature of the insulation powder in the vacuum space and helps produce a better vacuum, usually about 35 microns. After filling the reservoir, the filling line and the differential pressure regulator are closed. This produces a pressure over the liquid nitrogen and causes liquid to be injected into the annular space between the copper block and the equilibrium cell. To cool down from room temperature to liquid nitrogen temperature takes about six hours and requires about three liters of liquid nitrogen. Once the approximate temperature is established, the reservoir is again filled, and the refrigeration rate is approximately balanced by the heating rate.

The cell pressure and the gas flow rate are established first. A flow rate of 100 cc/hr (at cell T and P) is generally used throughout these runs. With valves V2 and V3 open, and V1 and V4 closed, the liquid component can now be introduced into the cell by using either the high pressure or condensation burette. The total volume of the equilibrium

cell is approximately 40 cc. A liquid capillary line extends through the center of this cell to a point slightly below the middle of the cell. A liquid volume of six cc in the cell causes the liquid level to be flush with the bottom of this capillary line. Therefore, approximately 10 cc of liquid are initially introduced into the cell. This provides the experimenter with enough liquid to allow for the evaporation rate in the single-pass cell and still obtain a liquid sample for analysis. A liquid level indicator is located on the upper portion of the liquid capillary line. This indicator consists of a heater in conjunction with a difference thermocouple. During the withdrawal of a liquid sample through the capillary line, the transition from a liquid phase to a gas phase causes the difference thermocouple to read a higher voltage for the same heater input. This also indicates that the liquid level is flush with the opening in the capillary line and, therefore, six cc of liquid remain in the cell. After the desired temperature has been established, gas samples are continuously analyzed with the 154D chromatograph. When analysis of three consecutive samples differs by less than three percent, it is assumed that equilibrium is reached. During this period the platinum resistance thermometer, pressure gauges, and difference couples are continuously monitored. After equilibrium is established, the liquid sample is collected on the gas collection panel and analyzed on the 154B chromatograph.

During the early part of this work, the liquid level indicator developed a short in its electrical circuit, and it could not be used to check when the liquid level fell below the liquid capillary line. It is

essential that the liquid level is known after each equilibrium point since too much liquid in the cell could cause entrainment. An alternate scheme was developed by which liquid samples were withdrawn from the cell and analyzed until a large helium concentration was detected. This indicated that the liquid level was slightly below the capillary line and about four cc of liquid could now be added to the cell.

One additional modification of the equipment used in this work was concerned with the analysis of helium in the liquid phase. A molecular sieve column is one of the few chromatographic columns which will retain helium long enough for analysis purposes. It also produces good separation of the oxygen and nitrogen peaks from helium. Unfortunately all hydrocarbons except methane are permanently adsorbed in the column packing and saturation of the column develops. In order to use the molecular sieve column for the liquid phase helium analysis, it was necessary to introduce a silica gel column in series with the molecular sieve. The retention time of the hydrocarbon in the silica gel column was longer than the time required for the helium analysis. It was therefore possible to vent the hydrocarbon gas from the silica gel column to the atmosphere. This scheme allowed the molecular sieve to be used. The calibration of the 154B chromatograph, shown in Appendix D, indicates that this method was very satisfactory.

The measurement of a gas-liquid equilibrium point along a given isotherm takes about two and one-half to three hours. Temperature gradients from the top to the bottom of the cell were never greater than 0.03 K.

CHAPTER III

EXPERIMENTAL RESULTS AND DISCUSSION

Experimental Results

Phase equilibrium results for the helium-ethylene and helium-propylene systems are shown in Figures 2 through 9. The actual experimental data are presented in Appendix E. The enhancement factor versus pressure curves represent the same curves from which the smoothed data, Appendix G, have been obtained.

Figures 2 and 3 show a comparison of the available experimental data for the helium-ethylene system by Hiza and Duncan[53] at 130 and 150 K. Figure 4 shows the additional five isotherms for the helium-ethylene system. These isotherms correspond to the following temperatures: 162.00, 173.99, 188.02, 202.01, and 216.04 K. A very interesting plot of enhancement factor versus 100/T for a given pressure is shown in Figure 5. The isobars shown in this Figure were for 120, 60, 20, and 10 atmospheres. The liquid phase compositions are shown in Figure 6 for this system. No liquid phase data are available for comparison.

Since no experimental data were available for the helium-propylene system, no comparison could be made. The five enhancement factor versus pressure isotherms presented in Figure 7 are in the gas-liquid region. These five isotherms were reported at the following temperatures: 200.00, 212.49, 224.99, 239.99, and 254.98 K. A plot of enhancement factor versus

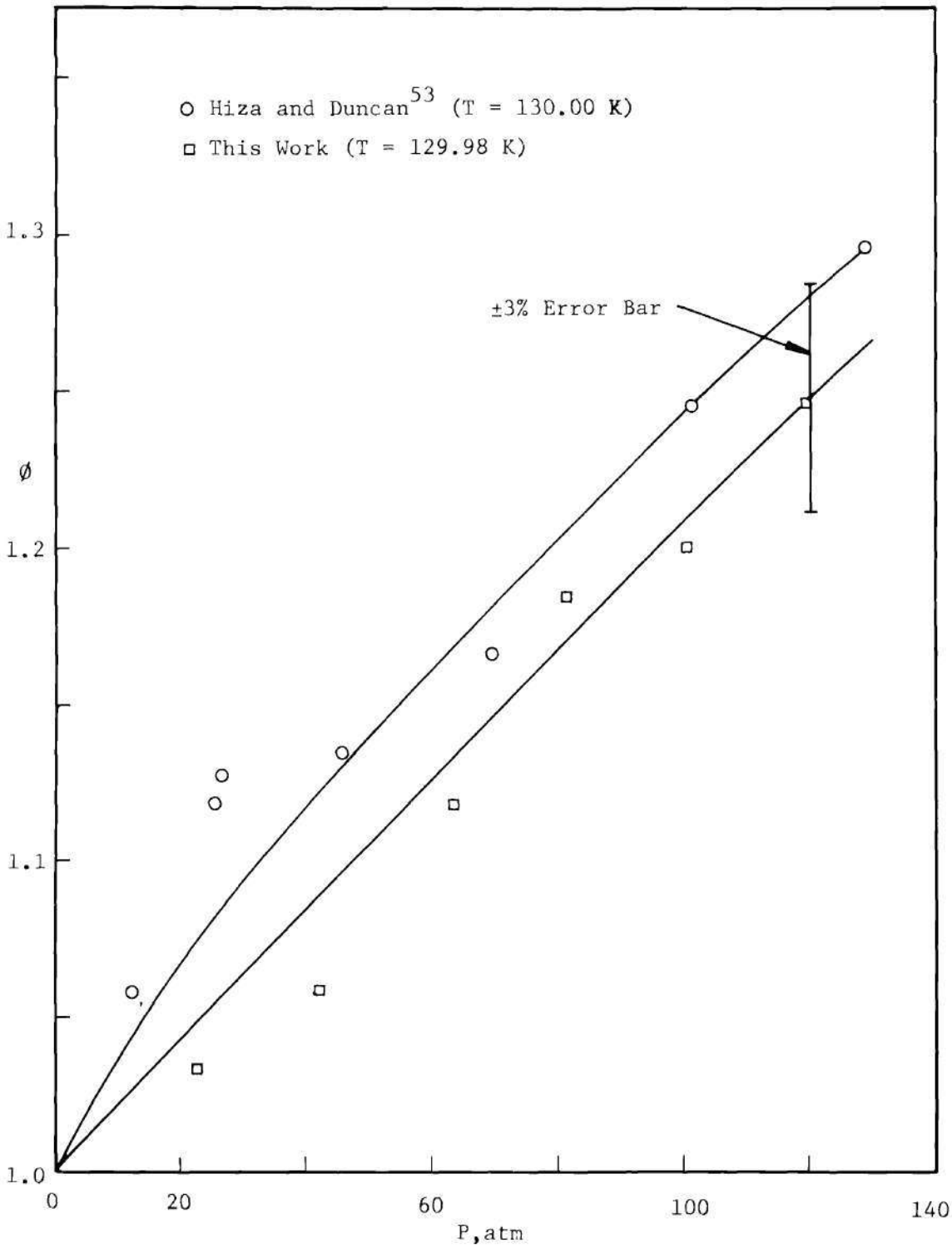

Figure 2. Experimental Enhancement Factors of Ethylene in Helium at 129.98 K.

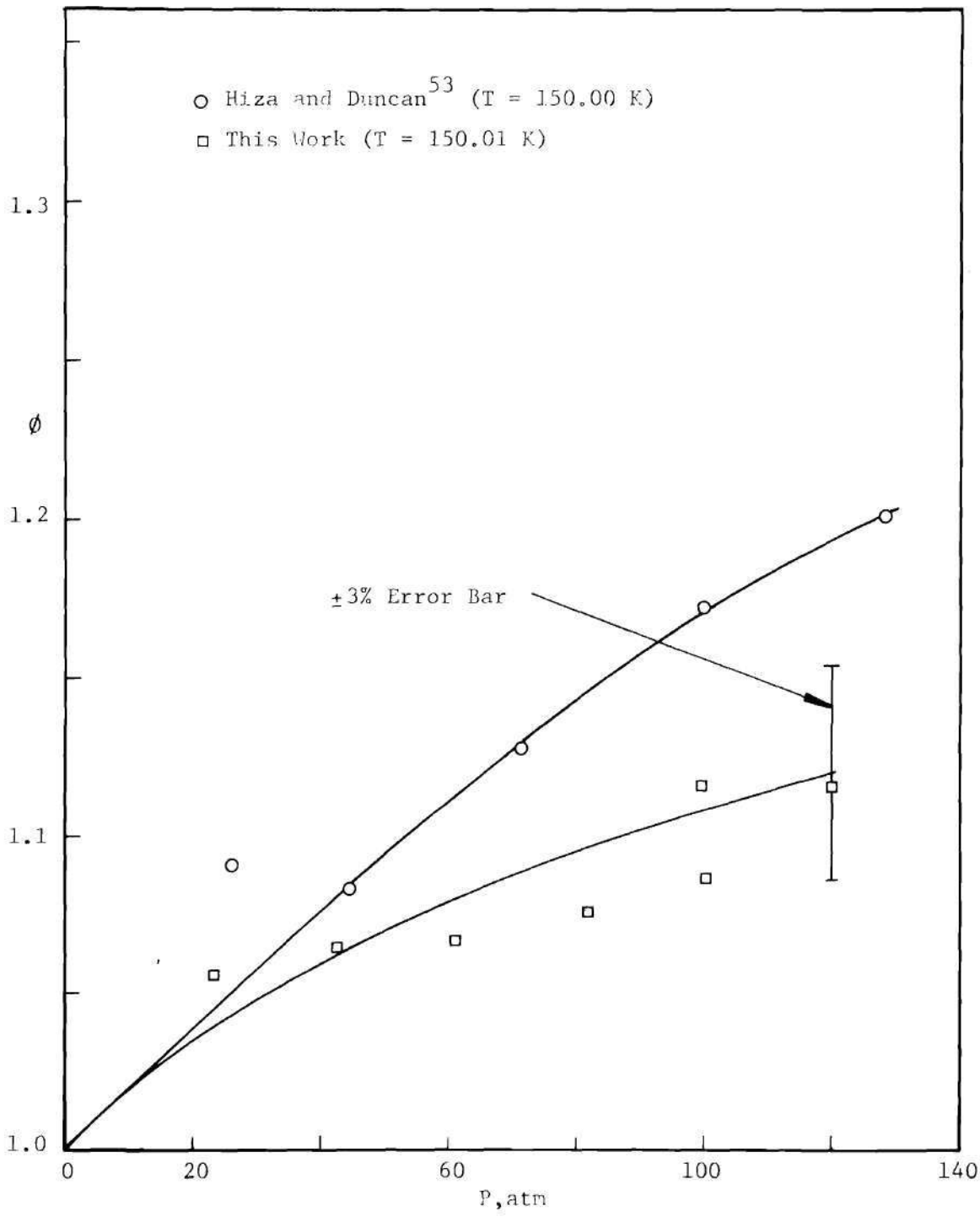

Figure 3. Experimental Enhancement Factors of Ethylene in Helium at 150.01 K.

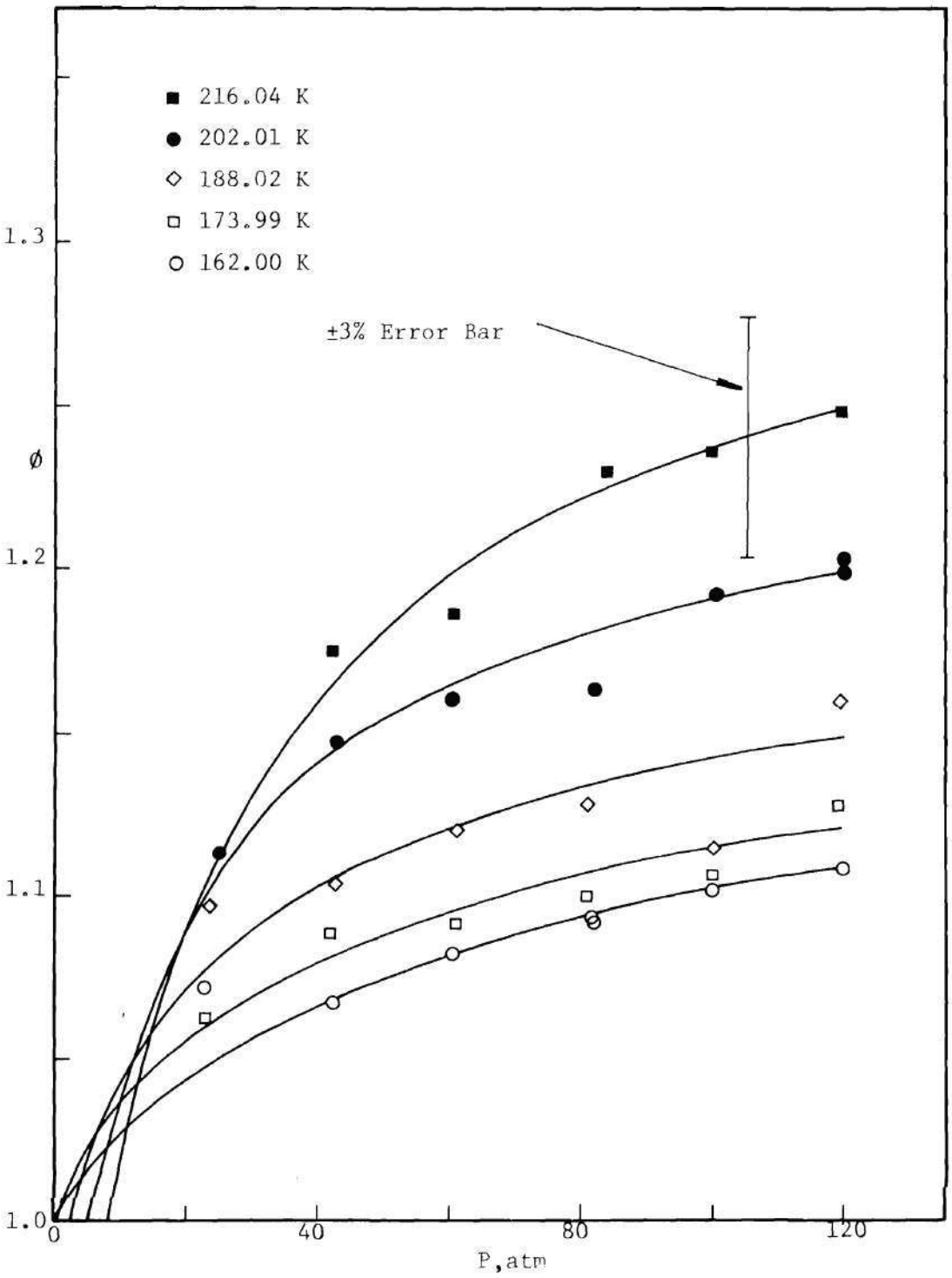

Figure 4. Experimental Enhancement Factors of Ethylene in Helium at 162.00, 173.99, 188.02, 202.01, and 216.04 K.

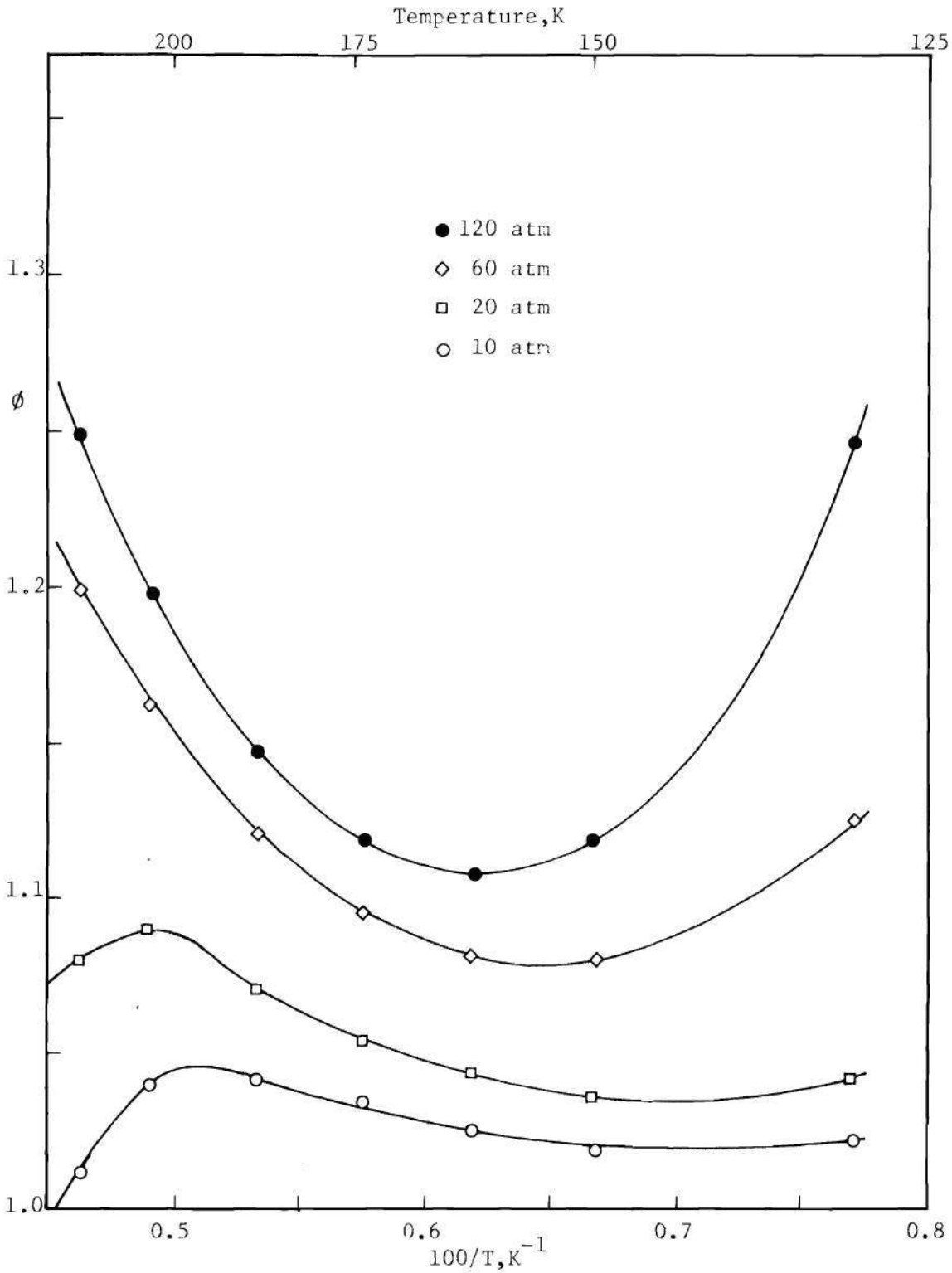

Figure 5. Experimental Enhancement Factors of Ethylene in Helium at 120, 60, 20, and 10 Atmospheres.

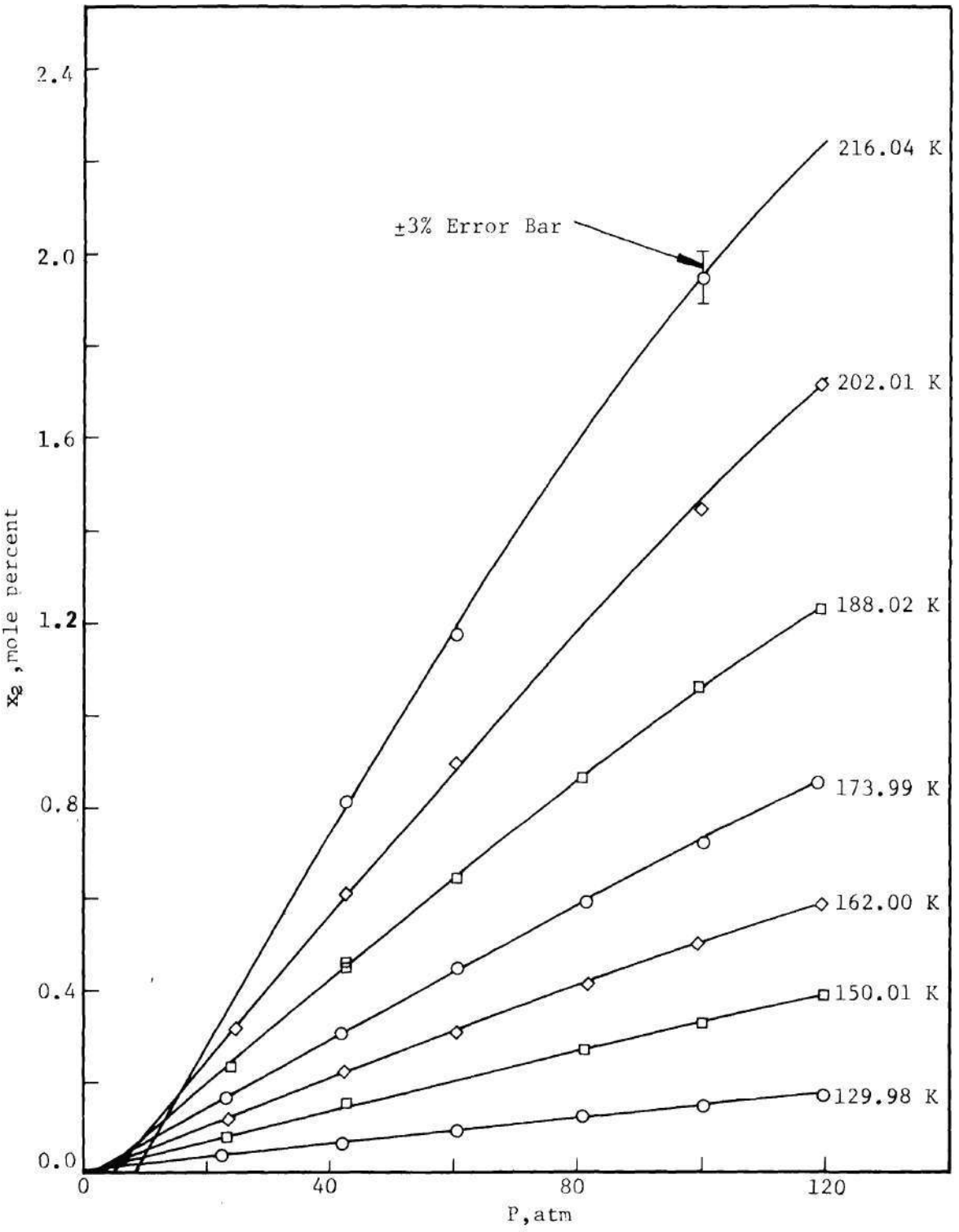

Figure 6. Experimental Solubility of Helium in Liquid Ethylene.

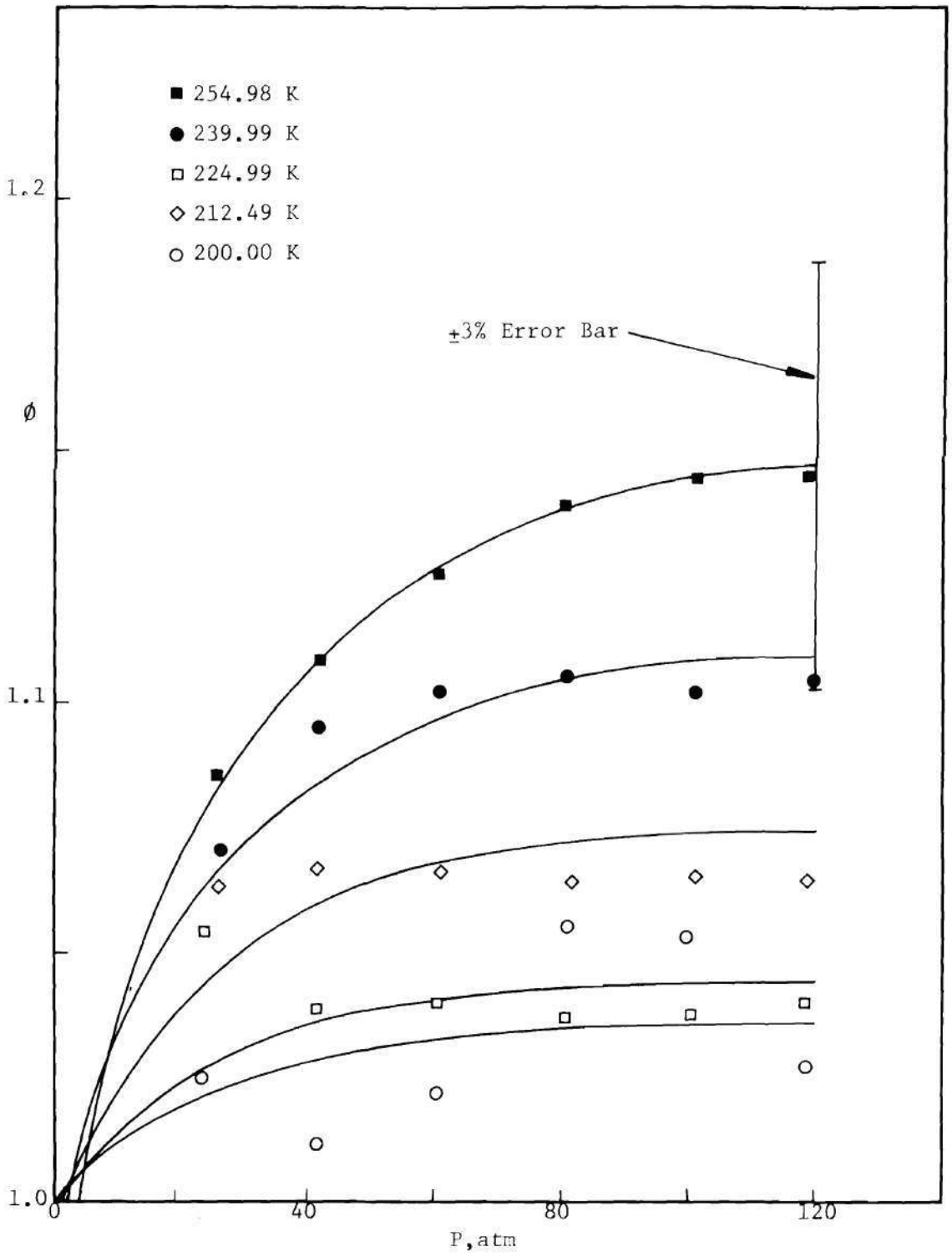

Figure 7. Experimental Enhancement Factors of Propylene in Helium at 200.00, 212.49, 224.99, 239.99, and 254.98 K.

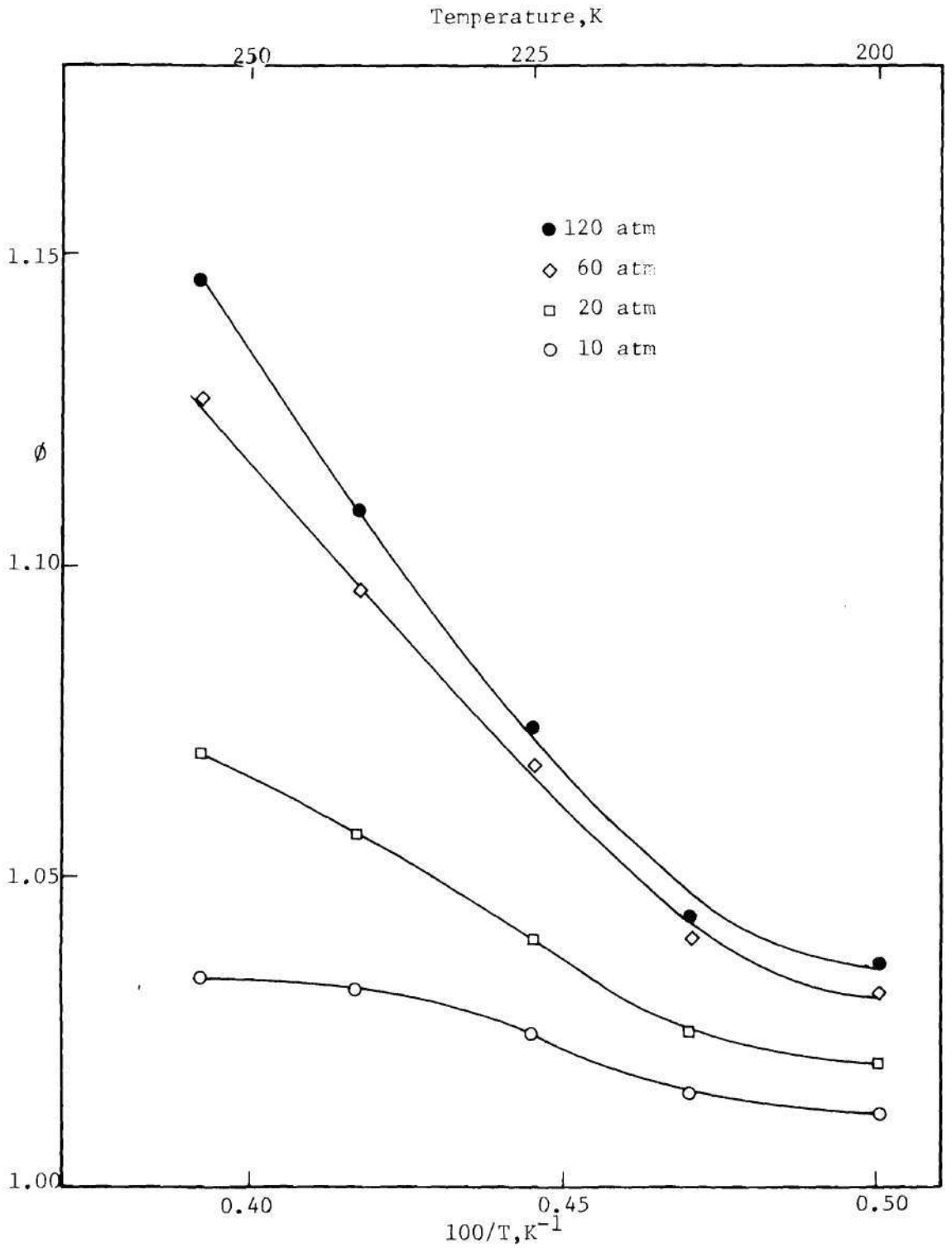

Figure 8. Experimental Enhancement Factors of Propylene in Helium at 120, 60, 20, and 10 Atmospheres.

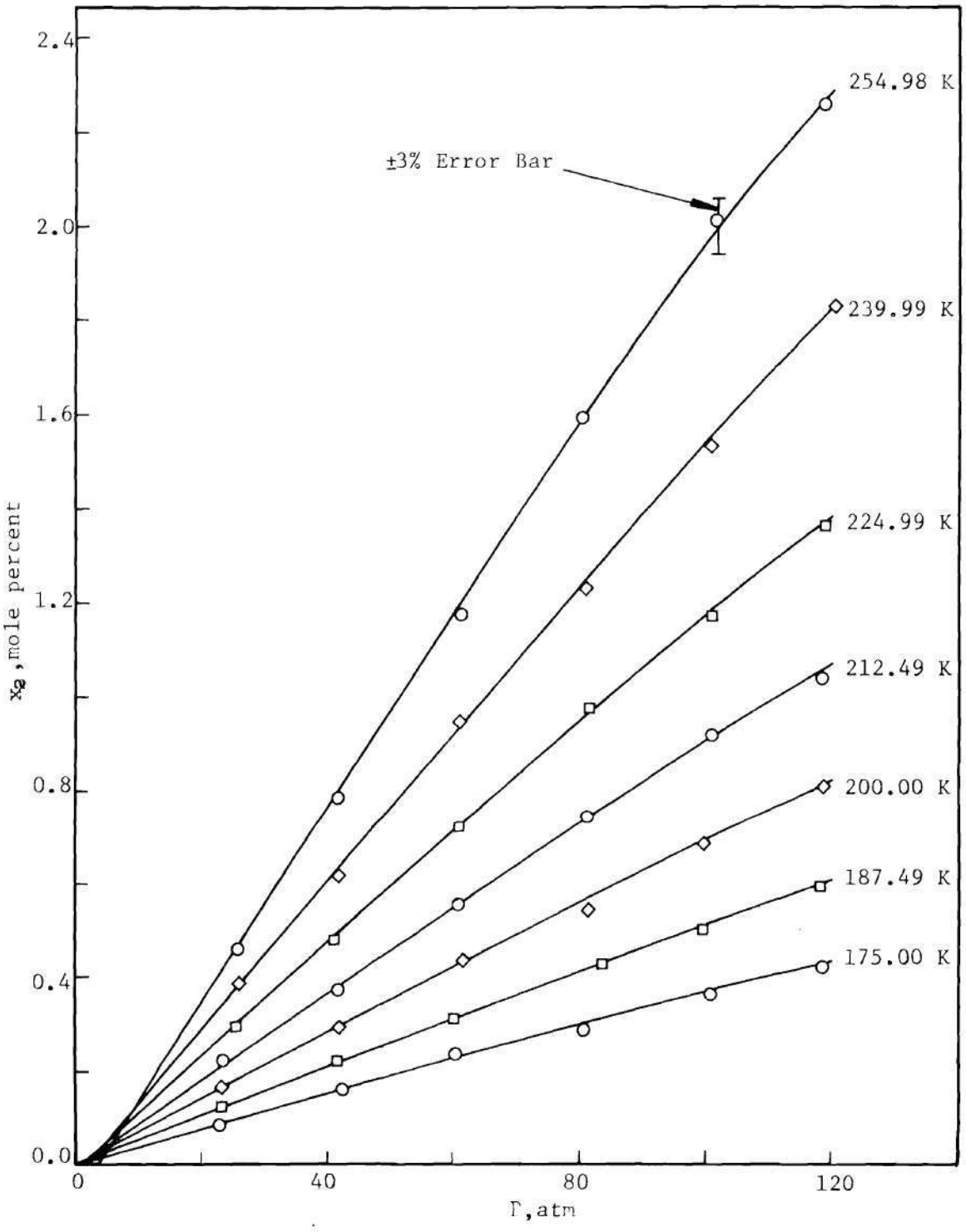

Figure 9. Experimental Solubility of Helium in Liquid Propylene.

100/T for the 120, 60, 20, and 10 atmosphere isobars is presented in Figure 8. The liquid composition as a function of temperature is presented in Figure 9. In addition to the above mentioned isotherms, two additional isotherms were measured in the liquid region. These measurements are reported at 175.00 and 187.49 K.

Discussion of Results

The helium-ethylene system has been shown to exhibit the following trends. For a given pressure, the two lowest enhancement factor isotherms, 129.98 and 150.01, which are shown in Figures 2 and 3, decrease as the temperature increases. The five other enhancement factor isotherms, Figure 4, show the reverse trend by increasing as the temperature increases. This effect is shown very clearly in the isobar curves of Figure 5. This figure plots the enhancement factor versus reciprocal temperature for a given pressure. The minimum in the enhancement factor isobar curves demonstrates this upward trend of the enhancement factor. These results verify the supposition of Hiza and Duncan[53] that this system should show a minimum in the isobar curves. A maximum in the low pressure isobar curves was clearly expected since it is known that, at the temperature corresponding to the vapor pressure of 10 atmospheres, the enhancement factor must go to one. The gas composition ranged from 0.045 to 22.9 mole percent ethylene in the helium.

The liquid solubility shows the reverse solubility effect. This means that the solubility increases with increasing temperature. The solubility curves bend downward at high pressure indicating negative

deviation from Henry's law. The highest isotherm shows only three measured points due to the high liquid evaporation rate. The liquid composition ranged from 0.040 to 1.95 mole percent helium.

The accuracy of the gas and liquid phase results is estimated as ± 3 percent for the 162.00 K and higher isotherms. The two lower isotherms have an estimated accuracy of about ± 4½ percent.

The results of Hiza and Duncan[47] compare favorably with the results of this work. The comparisons made in Figures 2 and 3 show that the results of Hiza and Duncan are consistantly higher than the results of this work. The 130 K results are high by about three percent at all points. The 150 K isotherm, at 120 atmospheres, shows the greatest discrepancy of about six percent. The combined experimental uncertainty of these data in this range is about ± 7 percent. Hiza and Duncan estimate their uncertainty as being about ± 2 percent, but their points show scatter of about ± 3 percent. Considering the total experimental error involved and the difficulty of operating a thermal conductivity chromatograph in the low concentration region, the two sets of data agree fairly well.

The enhancement factors for the helium-propylene system have shown the following trend. Five enhancement factor curves are shown in Figure 7 for this system, and they all apparently increase with increasing temperature. The spacing of the enhancement factor curves shown in Figure 7 indicates that the minimum in the enhancement factor isobar curves is slightly below the lowest measured isotherm, 200.00 K. Figure 8, which shows the experimental isobar curves for this system, tends to confirm this statement. This experiment was initially designed to include two

lower isotherms, 187.50 and 175.00 K, which would have possibly verified the position of this minimum. Although these two isotherms were studied in this work, the results obtained for the gas phase composition, from which the enhancement factor is calculated, are not reported. The values obtained for these isotherms appear to contain a systematic error, which is discussed in detail in Appendix D. The experimental gas phase composition range was from 13.83 to 0.230 mole percent propylene. The three highest isotherms 254.98, 239.99, and 224.99, are uncertain to ± 3 percent, and the remaining two isotherms, 212.49 and 200.00 K, are uncertain to about ± $4\frac{1}{2}$ percent.

The helium solubility in propylene, similar to the helium-propane system, was larger than was shown in the helium-ethylene and helium-ethane systems for the same reduced temperature. The experimental liquid compositions ranged from 0.087 to 2.26 mole percent helium. These curves show the usual reverse solubility and also the usual negative deviation from Henry's law. The liquid analysis in this system is believed to be accurate to ± 3 percent for these five isotherms, but the lowest two isotherms, 175.00 and 187.49 K, are uncertain by about ± $4\frac{1}{2}$ percent.

The uncertainties of these experimental results were estimated from the scatter in the chromatograph calibration curve, the pressure gauge uncertainty of ± $\frac{1}{2}$ percent, and the temperature uncertainty of ± 0.03 K. These uncertainties are reflected in the amount of scatter of points along an experimental isotherm. Appendix D shows the calibration curves for all of the required analyses, and ± 3 percent error bars are shown on all curves.

A single-pass phase apparatus, such as the one used in this work, suffers from the possible inadequacy that one could theoretically reach a steady state situation and not equilibrium. This situation can occur if the flow rate through the equilibrium cell is too fast. Kirk,[76] Mullins,[107] and most recently Liu[83] have all verified that a flow rate of 100 cc/hr at the cell temperature and pressure is sufficient for equilibrium. This flow rate through the cell corresponds to a residence time of 25 minutes. It is not sufficient to assume that this same flow rate would necessarily be sufficient for the systems studied in this work. In the helium-ethylene system, four experimental points were reproduced using a flow rate twice as high as the recommended value of 100 cc/hr. The temperatures of these points ranged from 150 to 202 K and pressures from 42.3 to 119.3 atmospheres. These experimental results agreed well within the quoted experimental accuracy, and they tend to verify that equilibrium results were obtained at flow rates near 100 cc/hr for this system.

In the helium-propylene system, the phase equilibrium measurements along the 175.00 K isotherm at 119 and 23 atmospheres were rerun at twice the normal flow rate. These results agreed with the earlier measurements within the estimated experimental uncertainty. A recent experimental check of the experiment by Mr. Y. K. Yoon[163] verified values of the 200.00 K isotherm. These results were run at flow rates slightly higher than 100 cc/hr, and they are in excellent agreement with those of this work.

CHAPTER IV

THEORETICAL CALCULATION OF THE ENHANCEMENT FACTOR

Introduction

The basic criterion for equilibrium between phases at the same temperature and pressure is that the chemical potential of each component be the same in each phase. For a binary system in gas-liquid equilibrium the following equation is used:

$$\mu_i^L = \mu_i^G \qquad i = 1, 2. \tag{IV-1}$$

Applying this equation to the condensible component 1, Equation (IV-1) becomes

$$\mu_1^L(P,T,x_1) = \mu_1^G(P,T,y_1) \tag{IV-2}$$

The chemical potential of the liquid mixture is given as

$$\mu_1^L(P,T,x_1) = \mu_1^L(P,T) + RT\ \ell n(\gamma_1' x_1) \tag{IV-3}$$

In this equation, the activity coefficient, which is a function of temperature, pressure, and mole fraction of component 1, approaches unity as x_1 approaches unity. It is possible to express the chemical potential in terms of more fundamental measurable quantities. The chemical potential of a pure condensed phase has been given as:

$$\mu_1^L(P,T) = \mu_1^{oL}(P_{o1},T) + \int_{P_{o1}}^{P} v_1\,dP \qquad \text{(IV-4)}$$

where

$$\mu_1^{oL}(P_{o1},T) = \int_{V_{o1}}^{\infty} \left[\left(\frac{\partial P}{\partial n_1}\right)_{V_1,T} - \frac{RT}{V_1}\right] dV_1 - RT\ \ell n\left(\frac{V_{o1}}{RT}\right) + g_1^o \qquad \text{(IV-5)}$$

The chemical potential of component 1 in a binary gas mixture is given as:

$$\mu_1^G(P,T,y_1) = \int_{V_m}^{\infty} \left[\left(\frac{\partial P}{\partial n_1}\right)_{V_m,T,n_2} - \frac{RT}{V_m}\right] dV_m - RT\ \ell n\left(\frac{V_m}{RT}\right) \qquad \text{(IV-6)}$$

$$+ RT\ \ell n\ (y_1) + g_1^o$$

By substitution of Equations (IV-3) and (IV-6) into Equation (IV-2) one obtains:

$$\ell n\left(\frac{Py_1}{P_{o1}}\right) = \ell n\left(\frac{PV_m}{P_{o1}V_{o1}}\right) + \frac{1}{RT}\int_{P_{o1}}^{P} v_1\,dP + \frac{1}{RT}\int_{V_{o1}}^{\infty}\left[\left(\frac{\partial P}{\partial n_1}\right)_{V_1,T}\right. \qquad \text{(IV-7)}$$

$$\left. - \frac{RT}{V_1}\right] dV_1 - \frac{1}{RT}\int_{V_m}^{\infty}\left[\left(\frac{\partial P}{\partial n_1}\right)_{V_m,T,n_2} - \frac{RT}{V_m}\right] dV_m + \ell n\ (\gamma_1' x_1)$$

Equation (IV-7) has been put into an alternate form by Mullins[107]:

$$\ell n\left(\frac{Py_1}{P_{o1}}\right) = + \frac{1}{RT}\int_{P_{o1}}^{P} v_1\,dP + \frac{1}{RT}\int_{V_{o1}}^{\infty}\left[P - \frac{RT}{V_1}\right] dV_1 + Z_{o1} - 1 \qquad \text{(IV-8)}$$

$$- \ell n\ (Z_{o1}) - \frac{1}{RT}\int_{V_m}^{\infty}\left[\left(\frac{\partial P}{\partial n_1}\right)_{V_m,T,n_2} - \frac{RT}{V_m}\right] dV_m \qquad \text{(Continued)}$$

$$+ \ell n\ (Z_m) + \ell n\ (\gamma_1' x_1)$$

From Equations (IV-7) or (IV-8) it is possible to calculate the enhancement factor, Equation (I-2), provided the following information is available: first, the liquid phase data required are saturated molar volume and compressibility data for pure component 1. Second, the composition of the liquid phase must be known. Third, experimental data or an assumption about γ_1' must be made, and fourth, for the gas phase, it is necessary to have an equation of state for pure component 1 and the gas mixture.

The hydrocarbon liquids studied in this work have very few compressibility data. A generalized average isothermal compressibility has been used for these systems. The isothermal compressibility is defined as:

$$\beta_T = - \frac{1}{v_1} \left(\frac{\partial v_1}{\partial P} \right)_T \qquad \text{(IV-9)}$$

and is a function of temperature and pressure. Heck[46] has shown that the average isothermal compressibility can be calculated by:

$$- \bar{\beta}_T = \frac{1}{v_1^o} \left[\frac{v_1 - v_1^o}{P_{max} - P_{o1}} \right]_T \qquad \text{(IV-10)}$$

where the upper pressure P_{max} is the highest value of interest. From Equation (IV-10) an expression for the molar volume of the compressed liquid is obtained:

$$v_1 = v_1^o \left(1 - \bar{\beta}_T (P - P_{o1})\right) \qquad \text{(IV-11)}$$

Using Equation (IV-11) it is now possible to evaluate the first integral in Equation (IV-7) as follows:

$$\frac{1}{RT}\int_{P_{O1}}^{P} v_1\,dP = \frac{v_1^o}{RT}\left[(P - P_{O1})(1 + \bar{\beta}_T P_{O1}) - \frac{\bar{\beta}_T}{2}(P^2 - P_{O1}^2)\right] \qquad \text{(IV-12)}$$

Since values of $\bar{\beta}_T$ are usually much less than one, it is possible to re-write Equation (IV-12) as

$$\frac{1}{RT}\int_{P_{O1}}^{P} v_1\,dP = \frac{v_1^o}{RT}\left[(P - P_{O1}) - \frac{\bar{\beta}_T}{2}(P^2 - P_{O1}^2)\right] \qquad \text{(IV-13)}$$

Equation (IV-13) was used in this work. Heck[46] has shown that in the case of carbon dioxide the above described method compares very well with the more elaborate methods of evaluating this integral. Since the contribution of this term to the enhancement factor is very small, it appears that these assumptions are realistic.

The activity coefficient, γ_1', has been assumed to be unity for the systems studied. This is equivalent to assuming that the solution behaves ideally. Mullins[107] has verified that, for the helium-argon system, the activity coefficient is unity along the three-phase line. This work was performed over a very narrow range of temperature, several degrees, and pressures up to 120 atmospheres. Since the systems studied experimentally in this work show values of x_2 always less than three percent, neglecting the activity coefficient appears to be a good assumption. The helium-ethane and helium-propane systems, which were studied theoretically in this work, each showed maximum values of x_2 of about 10 percent. There

may be some question about the value of γ_1' at this concentration level, but the majority of the x_2 values for these systems were much less than 10 percent.

The remainder of this chapter is concerned with the evaluation of the remaining integrals in Equation (IV-7) or (IV-8) which require a choice of an equation of state for the pure component and the gas mixture. Two equations of state are used in this work: the theoretical virial equation and the empirical Benedict-Webb-Rubin equation. Both of these equations have been extensively used to describe the P-V-T properties of pure components and gas mixtures.

Virial Equation of State

The virial equation of state is an equation of state based on statistical mechanics.[50] This equation has been used to describe the P-V-T properties of pure gases and gas mixtures. Equation (IV-14) shows this equation in its most useful form:

$$\frac{PV}{RT} = 1 + \frac{B}{V} + \frac{C}{V^2} \qquad \text{(IV-14)}$$

The virial coefficients B and C are a function of temperature. For a gas mixture these virials are given by

$$B_m = y_1^2 B_{11} + 2y_1 y_2 B_{12} + y_2^2 B_{22} \qquad \text{(IV-15)}$$

$$C_m = y_1^3 C_{111} + 3y_1^2 y_2 C_{112} + 3y_1 y_2^2 C_{122} + y_2^3 C_{222} \qquad \text{(IV-16)}$$

If Equations (IV-13), (IV-14), (IV-15), and (IV-16) are used together in Equation (IV-8), the following expression is obtained for the enhancement factor:

$$\ell n\ (\phi) = \frac{V_1^o}{RT}\left[(P - P_{o1}) - \frac{\bar{\beta}_T}{2}(P^2 - P_{o1}^2)\right] + \frac{2B_{11}}{V_{o1}} + \frac{3C_{111}}{2V_{o1}^2} \qquad \text{(IV-17)}$$

$$- \ell n\ (Z_{o1}) - \frac{2(y_1 B_{11} + y_2 B_{12})}{V_m} - \frac{3(y_1^2 C_{111} + 2y_1 y_2 C_{112} + y_2^2 C_{122})}{2V_m^2}$$

$$+ \ell n\ (Z_m) + \ell n(x_1)$$

The major difficulty in predicting the enhancement factor is in the calculation of the pure and interaction virial coefficients. Once their values are known, the solution is obtained by a simultaneous solution of Equation (IV-14) and (IV-17) for V_m and y_1.

Although Equation (IV-17) has been derived for gas-liquid equilibrium, its application to the gas-solid region requires only two assumptions. First, the solid is assumed to be pure component 1. Mullins[107] studied the freezing point curve in the helium-argon system to pressures of 120 atmospheres and concluded that the solid was essentially pure. Since the pressure of this present work does not exceed 120 atmospheres, this appears to be a reasonable assumption. Therefore, the term, $\ell n\ (x_1)$, is equal to zero. The second assumption is that the solid phase is essentially incompressible at the pressures used in this work. The value of $\bar{\beta}_T$ is therefore taken to be zero. The value of the molar volume becomes that of the saturated solid component 1 at that temperature.

Calculation of Virial Coefficients

Second Virial Coefficient

A potential energy function represents the potential energy experienced by two molecules as a function of the distance between the molecules. If the potential function is given for pure or mixed interactions, it is possible to calculate the corresponding second virial coefficient using the following relation from Hirschfelder, et al.[50]:

$$B(T) = \int_{r=0}^{r=\infty} \left(1 - \exp\left(-\frac{U(r)}{kT}\right)\right) db_o(r) \qquad \text{(IV-18)}$$

where

$$b_o(r) = \frac{2\pi N_A}{3} r^3 \qquad \text{(IV-19)}$$

Two potential functions, the Lennard-Jones (6-12) and the Kihara (6-12), have been used in this work to describe the interaction between molecules.

The Lennard-Jones (6-12) potential function[50] represents the sum of two potential functions. One function is an attractive energy inversely proportional to the sixth power of the distance of separation, and the other function is a repulsion energy inversely proportional to the twelfth power of the distance between molecules:

$$U(r) = 4e\left[\left(\frac{\sigma}{r}\right)^{12} - \left(\frac{\sigma}{r}\right)^{6}\right] \qquad \text{(IV-20)}$$

The value of r represents the distance between the two point masses. The value of σ corresponds to the distance between molecules, r, when $U(r) = 0$ and e corresponds to the minimum in the potential function.

This minimum occurs at

$$r = 2^{\frac{1}{6}}\sigma. \tag{IV-21}$$

The other potential energy function used in this work is the Kihara core model.[73,74] The Kihara and Lennard-Jones models differ in their description of the molecule. The potential function used in this model is very similar to Equation (IV-20):

$$U(\rho) = U_o \left[\left(\frac{\rho_o}{\rho}\right)^{12} - 2\left(\frac{\rho_o}{\rho}\right)^{6}\right] \tag{IV-22}$$

The value of ρ represents the shortest distance between the molecular cores. The two adjustable parameters, U_o and ρ_o, are interrelated since ρ_o corresponds to the distance ρ when the potential function is a minimum $U = U_o$.

Lennard-Jones Classical Model (LJCL). Using Equations (IV-20) and (IV-18), Hirschfelder, et al.[50] have obtained a reduced second virial coefficient, B^*_{CL}, which is a function of reduced temperatures:

$$B_{ij} = (b_o)_{ij}\, B^*_{CL}\, (T^*_{ij}) \tag{IV-23}$$

where

$$T^*_{ij} = \frac{T}{\left(\frac{e}{k}\right)_{ij}} \tag{IV-24}$$

and $(b_o)_{ij}$ is related to σ by

$$(b_o)_{ij} = \frac{2\pi N_A\, \sigma^3_{ij}}{3} \tag{IV-25}$$

For pure components, i is equal to j; i is not equal to j for mixtures. Mixing rules are required for the interaction parameters. The most commonly used ones are

$$\left(\frac{e}{k}\right)_{ij} = \left(\frac{e}{k}\right)_i^{\frac{1}{2}} \left(\frac{e}{k}\right)_j^{\frac{1}{2}} \tag{IV-26}$$

$$(b_o)_{ij} = \tfrac{1}{8} \left(b_{oi}^{\frac{1}{3}} + b_{oj}^{\frac{1}{3}}\right)^3 \tag{IV-27}$$

Equation (IV-27) is equivalent to using

$$\sigma_{12} = \frac{\sigma_1 + \sigma_2}{2} \tag{IV-28}$$

in Equation (IV-25). Hence, from the pure potential parameters, it is possible to obtain estimates for the mixture parameters.

The reduced second virial coefficient, B^*_{CL}, is evaluated from the expression:

$$B^*_{CL}(T^*) = \sum_{j=o}^{\infty} b^{(j)} \left(T^*_{ij}\right)^{-(1+2j)/4} \tag{IV-29}$$

where

$$b^{(j)} = -\left(\frac{2^{(j+\frac{1}{2})}}{4\ j!}\right) \left(\frac{2j - 1}{4}\right) \tag{IV-30}$$

The values of $b^{(j)}$ have been recomputed by Kirk[76] and agree well with those of Hirschfelder, et al.[50] except at $b^{(16)}$ which was $-0.3386316 \times 10^{-5}$ as compared to $-0.3387440 \times 10^{-5}$ computed by Hirschfelder, et al. The

values of Kirk have been used in this work.

Kihara Core Model (KIH). The Kihara model[73] assumes an impenetrable core rather than a point mass as does the Lennard-Jones model. In the Kihara core model, molecular cores are described in terms of three parameters, M_o, S_o, and V_o. The following equation from Prausnitz and Myers[122] is used in these calculations for pure and mixed virial coefficients:

$$\frac{(B_K)_{ij}}{N_A} = \frac{2\pi}{3}(\rho_o)^3_{ij}F_3 + \frac{M_{oi} + M_{oj}}{2}(\rho_o)^2_{ij}F_2 + \left(\frac{S_{oi} + S_{oj}}{2} + \frac{M_{oi}M_{oj}}{4\pi}\right)(\rho_o)_{ij}F_1 + \frac{V_{oi} + V_{oj}}{2} + \frac{M_{oi}S_{oj} + M_{oj}S_{oi}}{8\pi} \qquad \text{(IV-31)}$$

Mixture rules required for the interaction parameters are

$$(U_o)_{ij} = (U_{oi})^{\frac{1}{2}}(U_{oj})^{\frac{1}{2}} \qquad \text{(IV-32)}$$

$$(\rho_o)_{ij} = \frac{\rho_{oi} + \rho_{oj}}{2} \qquad \text{(IV-33)}$$

The functions F_1, F_2, and F_3 are all functions of Z, where $Z = (U_o)_{12}/kT$. These functions can be calculated from the relation given by Kihara.[73]

$$F_s = -\frac{s}{12}\sum_{j=0}^{\infty}\left[\frac{2^j}{j!}\Gamma\left(\frac{6j - s}{12}\right)\right]Z^{(6j+s)/12} \qquad \text{(IV-34)}$$

or can be rewritten:

$$F_s = \sum_{j=o}^{\infty} b_s^{(j)} \, Z^{(6j+s)/12} \qquad \text{(IV-35)}$$

where s = 1, 2, and 3. Mullins[107] has calculated the values of the first 40 terms of $b_s^{(j)}$. These results have been presented by Kirk,[76] and they are used in this work.

DeBoer and Michels[27] have presented an expression to calculate the contribution of the quantum corrections to the calculation of the second virial coefficient. For pure quantum gases like helium, hydrogen, and neon, these quantum corrections are essential. Prausnitz and Myers[122] have indicated that, for interactions between one quantum and a non-quantum gas, these corrections may still be necessary. For this reason quantum corrections are included for these helium system. The second virial coefficient becomes:

$$B_{ij} = (B_K)_{ij} + (b_o)_{ij} \left[(\Lambda^*_{ij})^2 B^*_I + (\Lambda^*_{ij})^4 B^*_{II} - (\Lambda^*_{ij})^3 B^*_o \right] \qquad \text{(IV-36)}$$

The reduced quantum mechanical parameter Λ^* can be calculated by:

$$\Lambda^{*2}_{ij} = \frac{h^2}{k \, \sigma^2_{ij} \, m_{ij} \, (U_o/k)_{ij}} \qquad \text{(IV-37)}$$

Using the Kihara core model parameter, it is possible to obtain a value for[122]:

$$\sigma_{ij} = 2^{-\frac{1}{6}} \rho_{oij} + \frac{M_{oi} + M_{oj}}{4\pi} \qquad \text{(IV-38)}$$

$$m_{ij} = \frac{M_{ij}}{N_A} \tag{IV-39}$$

where

$$\frac{1}{M_{ij}} = \frac{1}{M_i} + \frac{1}{M_j} \tag{IV-40}$$

The two correction terms, B_I^* and B_{II}^*, are given by the equations[50]:

$$B_I^* = \sum_{j=0}^{\infty} b_I^{(j)} \, (T^*)^{-(6j+13)/12} \tag{IV-41}$$

$$B_{II}^* = \sum_{j=0}^{\infty} b_{II}^{(j)} \, (T^*)^{-(6j+23)/12} \tag{IV-42}$$

where

$$b_I^{(j)} = - \left(\frac{11 - 36j}{768 \, \pi^2}\right)\left(\frac{2^{(6j+13)/6}}{j!}\right) \Gamma\left(\frac{6j - 1}{12}\right) \tag{IV-43}$$

$$b_{II}^{(j)} = - \left(\frac{3024j^2 + 4728j + 767}{491520 \, \pi^4}\right)\left(\frac{2^{(6j+23)/6}}{j!}\right) \Gamma\left(\frac{6j + 1}{12}\right) \tag{IV-44}$$

The first 42 values of $b_I^{(j)}$ and $b_{II}^{(j)}$ have been computed by Kirk[76] and are used in this work. The last term in Equation (IV-36) is the ideal gas quantum correction, B_o^*, given by the equation:

$$B_o^* = \frac{3}{32 \, \pi^{\frac{3}{2}} \, (T^*)^{\frac{3}{2}}} \tag{IV-45}$$

All Kihara second virial coefficient calculations for helium and the mixed virials include quantum corrections.

Kihara Core Model with K_{12} (KIHK12). The idea of a correction to the geometric mixing rule for the energy parameter in the Kihara potential function has been a topic of considerable interest. It was shown by Prausnitz[16,17,33] that the introduction of a correction to the geometric mixing rule enabled the Kihara potential to represent the interaction second virial coefficient data more exactly. The correction factor $(1 - K_{12})$, where K_{12} is an empirical constant for each binary system, has also been used by other investigators.[52,53,107] In all cases investigated, the linear average for $(\rho_o)_{12}$ was assumed to be valid. Liu[83] has recently attempted to extend this idea to the Lennard-Jones potential function. Some experimental values of K_{12} are presented in Chapter V.

Mathematically this method requires changing the depth of the Kihara mixture potential well by a factor $(1 - K_{12})$:

$$(U_o)_{12} = (1 - K_{12}) (U_o)_{12(\text{Geometric})} \qquad \text{(IV-46)}$$

where

$$(U_o)_{12(\text{Geometric})} = (U_{o1} U_{o2})^{\frac{1}{2}} \qquad \text{(IV-47)}$$

Therefore, the only change made in the Kihara core model program was to introduce the $(1 - K_{12})$ factor. In cases where the K_{12} value was experimentally determined the predicted enhancement factors were called KIHEK12.

As is discussed further in the following chapter, Hiza and Duncan[53] have presented an excellent correlation of K_{12} as a function of ionization potential. Values of K_{12} calculated from their equation were used to calculate the enhancement factor equation, and they were called KIHCK12.

Third Virial Coefficient

The third virial coefficient like the second virial coefficient is a correction to the ideal gas law. Being a higher order term in the virial expansion, the third virial coefficient is concerned with the three-molecule interactions. To describe the interaction of three molecules, a three-body potential energy function is required. Since little is known about three-body forces, a common assumption made in molecular physics is to use pairwise additivity of the intermolecular potentials. This corresponds to the assumption

$$U_{ijk} = U_{ij} + U_{ik} + U_{jk} \qquad \text{(IV-48)}$$

Using this potential function, the classical third virial coefficient of a gas can be written as,[141]

$$C^{add} = -\frac{8\pi^2 N_A^2}{3} \iiint f_{12} f_{13} f_{23} r_{12} r_{13} r_{23} \, dr_{12} dr_{13} dr_{23} \qquad \text{(IV-49)}$$

where

$$f_{ij} = \exp(-U_{ij}/kT) - 1 \qquad \text{(IV-50)}$$

Numerical calculations of Equation (IV-49) have been performed for the Lennard-Jones potential by Bird, et al.,[5] Kihara,[71,72] Rowlinson, et al.,[137] and Sherwood and Prausnitz.[141] For the Kihara potential function, calculations have been made by Sherwood and Prausnitz[141] assuming a spherical core.

It has been shown by Kihara[73,74] that, at low temperatures, there

are large discrepancies that arise between the measured third virial coefficients of the inert gases and the theoretically calculated values assuming pairwise additivity. Although the third virial coefficients at low temperatures have a large uncertainty, Graben and Present[41] have pointed out that the non-additivity contributions to the third virial coefficient calculation can be significant, especially at low temperatures. The non-additivity correction as described by Sherwood and Prausnitz[141] is given as,

$$\Delta C = -\frac{8\pi^2 N_A^2}{3}\iiint \exp\left(-\frac{\Sigma U_{ij}}{kT}\left(\exp\left(-\frac{\Delta U}{kT}\right)-1\right)\right) \qquad \text{(IV-51)}$$

$$\times\, r_{12}\, r_{13}\, r_{23}\, dr_{12}\, dr_{13}\, dr_{23}$$

where

$$\Sigma U_{ij} = U_{12} + U_{13} + U_{23} \qquad \text{(IV-52)}$$

and $\Delta U\,(r_{12}, r_{13}, r_{23})$ is the three-body interaction energy. If ΔU is taken as zero, then

$$C = C^{add} \qquad \text{(IV-53)}$$

otherwise

$$C = C^{add} + \Delta C \qquad \text{(IV-54)}$$

To add to the complexity of this problem, the non-additivity term ΔC is split up into a dispersion (attractive) and overlap (repulsion) portion. So Equation (IV-54) becomes

$$C = C^{add} + \Delta C(\text{overlap}) + \Delta C(\text{dispersion}) \qquad \text{(IV-55)}$$

ΔC(dispersion) has been calculated for the Lennard-Jones (6-12) potential by Fowler and Graben,[38] Graben and Present,[41] and Sherwood and Prausnitz.[141] Similar calculations were performed by Sherwood and Prausnitz on the Kihara (6-12) potential. Sherwood and Prausnitz[142] have demonstrated that ΔC(dispersion) is always positive and that its contribution becomes more significant at low temperatures.

Calculations of ΔC(overlap) have been made, but they involve additional difficulties. Graben, et al.[42] and Sherwood, et al.[143] have made calculations for the Lennard-Jones (6-12) potential. Both papers confirmed that the ΔC(overlap) term is definitely not negligible. The sign of this term is negative and its magnitude is almost exactly the same as the ΔC(dispersion) values. Although the uncertainty of these numbers is very large, the effect is essentially that of cancellation of the non-additivity effects. No values of ΔC(overlap) appear to have been calculated for the Kihara core potential.

The paper of Sherwood and Prausnitz,[141] which presents

$$C = C^{add} + \Delta C(\text{dispersion}) \qquad \text{(IV-56)}$$

for the Lennard-Jones and Kihara (6-12) models, bears out the above discussion concerning the Lennard-Jones ΔC(overlap) contribution. Their comparison of the calculated Lennard-Jones model values are all considerably higher than experiment and undoubtedly the inclusion of ΔC(overlap) would improve the predicted results. That paper also shows that the Kihara model calculations which include the ΔC(dispersion) values represent the experimental data for argon, krypton, and nitrogen very well, but they

appear to be excessively high for xenon, carbon dioxide, carbon tetrafluoride, and heavy hydrocarbons.

Because of the evident uncertainty in the third virial calculations, it was decided to use two different models for these calculations. The first model is the Lennard-Jones classical (6-12), and the other model is the recent corresponding-states correlation of Chueh and Prausnitz.[16] Since some third virial coefficient data are available for the pure hydrocarbons and helium (see Appendix F), it is felt that a comparison of methods is in order. Unfortunately, due to the steepness in the experimental third virial coefficient curve at $T_{R_1} \leq 0.80$, and since few data are available in the negative region, little comparison could be made below that reduced temperature.

Lennard-Jones Classical Model (LJCL). In past theoretical work done in this laboratory to predict the enhancement factor, the Lennard-Jones model has been used to describe the third virial coefficient. The expression used to calculate the third virial coefficient is given by Hirschfelder, et al.[50]

$$C_{ijk} = C_{ijk}^{add} = (b_o)_{ijk}^2 \, C_{CL}^* \, (T_{ijk}^*) \qquad \text{(IV-57)}$$

where the reduced third virial coefficient is given by

$$C_{CL}^* \, (T_{ijk}^*) = \sum_{j=o}^{\infty} c^{(j)} \, (T_{ijk}^*)^{-(j+1)/2} \qquad \text{(IV-58)}$$

The $c^{(j)}$ values used in this work were the first 21 values given by Rowlinson, et al.[137] For mixtures the following combination rules were used:

$$\left(\frac{e}{k}\right)_{ijk} = \left(\frac{e}{k}\right)_i^{\frac{1}{3}} \left(\frac{e}{k}\right)_j^{\frac{1}{3}} \left(\frac{e}{k}\right)_k^{\frac{1}{3}} \qquad \text{(IV-59)}$$

and

$$(b_o)_{ijk} = \frac{1}{27}\left[(b_o)_i^{\frac{1}{3}} + (b_o)_j^{\frac{1}{3}} + (b_o)_k^{\frac{1}{3}}\right]^3 \qquad \text{(IV-60)}$$

The pure and mixture third virial coefficients calculated do not include any non-additivity corrections. This method of predicting the third virial coefficients has been used only in the Lennard-Jones program to predict the enhancement factor.

Method of Chueh and Prausnitz. In an attempt to alleviate some of the difficulties encountered in the third virial coefficient calculations, Chueh and Prausnitz[16] have presented an approximate corresponding-states correlation for the third virial coefficient of non-polar gases. This correlation uses reliable experimental data in a reduced form. The generalization is expressed as a function

$$\frac{C}{V_c^2} = f_c\left(\frac{T}{T_c}, d\right) \qquad \text{(IV-61)}$$

and

$$\frac{C}{V_c^2} = (0.232\ T_R^{-0.25} + 0.468\ T_R^{-5})(1 - \exp\ (1 - 1.89\ T_R^{\ 2})) \qquad \text{(IV-62)}$$

$$+ d \exp\ (- 2.49 + 2.30\ T_R - 2.70\ T_R^{\ 2})$$

where

$$T_R = \frac{T}{T_c} \qquad \text{(IV-63)}$$

The term containing the parameter d becomes important at $T_R < 2.0$. Although no correlation has been presented by them for d, its value appears to be directly related to the molecular size and polarizability of the molecule. Chueh and Prausnitz[16] give some values of d for pure gases, and they show how to estimate d using reduced third virial coefficient data. In this work, the parameter d was estimated for a variety of compounds using third virial coefficient data. These data for ethane, ethylene, propane, and propylene are presented in Appendix F, and the data for the other compounds come from the book of Dymond and Smith.[32] These values of d are presented in Table 28 of Appendix F. Other physical property data required for these calculations are also presented in this table.

For the quantum gases, a modification of the corresponding states behavior is required since these gases must be described by quantum rather than classical, statistical mechanics. Chueh and Prausnitz[16] have presented a method of obtaining effective critical constants, that is, the effective critical constants in the limit of high temperatures. For helium, these constants are $T_c^o = 10.47$ K and $V_c^o = 37.5$ cc/gm mole. The equations given by Chueh and Prausnitz[16] are

$$T_c = \frac{T_c^o}{1 + \frac{21.8}{M\,T}} \qquad \text{(IV-64)}$$

and

$$V_c = \frac{V_c^o}{1 - \frac{9.91}{M\,T}} \qquad \text{(IV-65)}$$

These critical constants are now used to calculate the third virial coefficient using Equation (IV-62).

To calculate the third virial coefficients of mixtures, Chueh and Prausnitz[16] have recommended the approximation suggested by Orentlicher and Prausnitz[111] as the best now available. Applying this approximation for mixture virial coefficients to the correlation of Chueh and Prausnitz, one obtains

$$C_{ijk} = (C_{ij}C_{ik}C_{jk})^{\frac{1}{3}} \tag{IV-66}$$

where

$$C_{ij} = V_{cij}^2 \, f_c \left(\frac{T}{T_{cij}}, \, d_{ij}\right) \tag{IV-67}$$

For mixtures containing one or more quantum gases, the binary critical constants are

$$T_{cij} = \frac{(1 - K_{12})(T_{ci}^{o} T_{cj}^{o})^{\frac{1}{2}}}{\left(1 + \frac{21.8}{M_{12}T}\right)} \tag{IV-68}$$

and

$$V_{cij} = \frac{\left(V_{ci}^{o\frac{1}{3}} + V_{cj}^{o\frac{1}{3}}\right)^3}{8\left(1 - \frac{9.91}{M_{12}T}\right)} \tag{IV-69}$$

where

$$d_{ij} = \frac{d_i + d_j}{2} \tag{IV-70}$$

and

$$M_{ij} = \frac{2M_i M_j}{M_i + M_j} \tag{IV-71}$$

The K_{12} used in Equation (IV-68) is obtained from interaction second virial coefficient data. This K_{12} is the previously mentioned correction to the geometric mixing rule for the Kihara potential function, Equation (IV-46). Due to this correspondence to the Kihara model, this method of Chueh and Prausnitz[16] is used to calculate all third virial coefficients in the Kihara enhancement factor programs. All of the third virial coefficients, C_{111}, C_{112}, C_{122}, and C_{222}, are calculated from this method when $T_R \geq 0.80$. Due to the steepness of the third virial coefficient curve at $T_R < 0.80$, Chueh and Prausnitz recommend setting the coefficients C_{111} and C_{112} equal to zero, but the other coefficients, C_{222} and C_{122}, are still calculated. This recommendation was followed in this work.

Benedict-Webb-Rubin Equation of State (BWR)

The Benedict-Webb-Rubin equation of state is an empirical equation which contains eight adjustable parameters. This equation of state has been used to predict enhancement factors in gas-liquid and gas-solid binary systems.[46,76,77,88,107,146] BWR parameters for helium have only recently become available[46] and thus, very few calculations have been made for these binary systems.[46,88] Since originally the BWR equation was written for use on hydrocarbons and hydrocarbon mixtures, it would be interesting to see how this equation predicts phase equilibrium for the helium-hydrocarbon systems and to determine if the empirical BWR equation is able to predict the unusual shapes shown by the isobar curves for the helium systems.

The method of prediction of enhancement factors using the BWR

equation has been described in great detail by Heck.[46] In this work the same approach has been followed, and only the equations used and the method of solution of these equations will be presented here. The BWR equation for mixtures can be written as

$$P = \frac{RT}{V_m} + \frac{RTB'_m}{V_m^2} + \frac{RTC'_m}{V_m^3} + \frac{a_m \alpha_m}{V_m^6} + \frac{c_m \left(1 + \frac{\gamma_m}{V_m^2}\right) \exp\left(-\frac{\gamma_m}{V_m^2}\right)}{V_m^3 T^2} \qquad \text{(IV-72)}$$

where

$$B'_m = (B_o)_m - \frac{(A_o)_m}{RT} - \frac{(C_o)_m}{RT^3} \qquad \text{(IV-73)}$$

$$C'_m = b_m - \frac{a_m}{RT} \qquad \text{(IV-74)}$$

The mixture rules used are

$$N_m = y_1^2 N_{11} + 2y_1 y_2 N_{12} + y_2^2 N_{22} \qquad \text{(IV-75)}$$

for $N = A_o$, B_o, C_o, and γ. Values of N_{12} are given by

$$N_{12} = (N_1 N_2)^{\frac{1}{2}} \qquad \text{(IV-76)}$$

for A_o, C_o, and γ. The calculation of $(B_o)_{12}$ has been a subject of much interest. Heck[46] uses the more common Lorentz average for his calculations. Mullins[107] has pointed out that, according to Benedict, et al.,[3] the linear average should be used in the prediction of phase equilibrium, and he demonstrated that the linear average gives the best results for the hydrogen-argon system. In this work both the

$$(B_o)_{12}(\text{LINEAR}) = \frac{(B_{o11} + B_{o22})}{2} \qquad \text{(IV-77)}$$

and

$$(B_o)_{12}(\text{LORENTZ}) = \tfrac{1}{8}\left[(B_{o11})^{\frac{1}{3}} + (B_{o22})^{\frac{1}{3}}\right]^3 \qquad \text{(IV-78)}$$

averages have been investigated. The enhancement factors predicted are called BWR(LINEAR) and BWR(LORENTZ), respectively. The other parameters, a, b, c, and α, are combined using the following rule

$$N_m = y_1^3 N_{111} + 3y_1^2 y_2 N_{112} + 3y_1 y_2^2 N_{122} + y_2^3 N_{222} \qquad \text{(IV-79)}$$

where

$$N_{ijk} = (N_i N_j N_k)^{\frac{1}{3}} \qquad \text{(IV-80)}$$

Equation (IV-72) applies to pure components by letting $y_2 = 0$ and so obtaining

$$N_m = N_{111} \qquad \text{(IV-81)}$$

Equation (IV-7) and the BWR equation for mixtures and pure components are combined to give the enhancement factor equation[46]

$$\ell n\phi = \ell n\left(\frac{PV_m}{P_{o1}V_{o1}}\right) + \frac{v_1^o}{RT}\left[(P - P_{o1}) - \frac{\bar{\beta}_T}{2}(P^2 - P_{o1}^2)\right] + \frac{2B'_{11}}{V_{o1}} \qquad \text{(IV-82)}$$

$$+ \frac{3C'_{111}}{2V_{o1}^2} + \frac{6\,a_1\alpha_1}{5RTV_{o1}^5} + \frac{c_1}{RT^3\gamma_1} + \frac{c_1}{RT^3}\exp\left(-\frac{\gamma_1}{V_{o1}^2}\right)\left[\frac{\gamma_1}{V_{o1}^4} + \frac{1}{2V_{o1}^2} - \frac{1}{\gamma_1}\right]$$

(Continued)

$$- \frac{2[y_1 (B'_{11} - B'_{12}) + B'_{12}]}{V_m} - \frac{3[y_1^2 (C'_{111} - 2C'_{112} + C'_{122})}{2V_m^2}$$

$$+ \frac{2y_1 (C'_{112} - C'_{122}) + C'_{122}]}{2V_m^2} - \frac{3(a_m \alpha_{1mm} + \alpha_m a_{1mm})}{5RTV_m^5} - \frac{3c_{1mm}}{RT^3 \gamma_m}$$

$$+ \frac{2c_m \gamma_{1m}}{RT^3 \gamma_m^2} + \frac{\exp\left(-\frac{\gamma_m}{V_m^2}\right)}{RT^3} \left[\frac{3c_{1mm}}{\gamma_m} - \frac{2c_m \gamma_{1m}}{\gamma_m^2} + \frac{3c_{1mm}}{2V_m^2} - \frac{2c_m \gamma_{1m}}{\gamma_m V_m^2} - \frac{c_m \gamma_{1m}}{V_m^4}\right]$$

$$+ \ell n \, (\gamma_1' x_1)$$

In this equation the combination rule

$$N_{1mm} = (N_1 N_m N_m)^{\frac{1}{3}} \qquad \text{(IV-83)}$$

is used for α, a, and c, where N_m is given by Equation (IV-79). For γ, the combination rule

$$N_{1m} = (N_1 N_m)^{\frac{1}{2}} \qquad \text{(IV-84)}$$

is used, where N_m is given by Equation (IV-75).

Provided the BWR constants are available for the two pure components, the prediction of the enhancement factor amounts to a solution of Equations (IV-72) and (IV-82) for V_m and y_1. The method of solution is basically the Newton-Raphson method as described by Heck.[46] In this work, the activity coefficient has been taken as unity and the value of x_1 used in this calculation was the experimental value.

Kirk[76] has shown that Equation (IV-72) can be put in a form similar to the virial equation, Equation (IV-14), with some of the higher order

volume terms missing. This was done by expanding the exponential term and collecting similar terms. The following equations are reported by Kirk for the virial coefficients

$$B_{ij} = (B_o)_{ij} - \frac{(A_o)_{ij}}{RT} - \frac{(C_o)_{ij}}{RT^3} \qquad \text{(IV-85)}$$

$$C_{ijk} = b_{ijk} - \frac{a_{ijk}}{RT} + \frac{c_{ijk}}{RT^3} \qquad \text{(IV-86)}$$

In this way it was possible to get values for the pure and interaction virial coefficients from the BWR equation. Values calculated using these equations are presented in Chapter V and Appendix F.

CHAPTER V

DETERMINATION OF THE INTERACTION SECOND VIRIAL COEFFICIENT FROM PHASE EQUILIBRIUM DATA

General Discussion

Although pure virial coefficients have been measured for a variety of gases, data concerning the interaction virial coefficients are very scarce. Most of the data found are at room temperature. The interaction second virial coefficient, B_{12}, physically represents the two-body interaction between two dissimilar molecules. If one had a potential function for the interaction pair, it would be easy to calculate B_{12} using Equation (IV-18). If the interacting molecules are very dissimilar, the interaction potential function is hard to predict and actual experimental data are necessary.

There are a variety of methods by which B_{12} may be extracted from measurements on binary gas mixtures. These methods are:

(1) P-V-T measurements on the gas mixture at low pressures.[161]

(2) The Burnett method.[9]

(3) Measurement of the pressure change on mixing two gases at constant volume and temperature.[23]

(4) The Joule-Thomson expansion.

(5) Velocity of sound techniques.[159]

(6) Beam scattering experiments.[21]

(7) Phase equilibrium measurements.[107]

All of these methods of obtaining B_{12} require an accurate knowledge of the pure virial coefficients. In the first six methods, when one component is below its critical, the composition of the condensible component must always be kept less than the equilibrium gas phase composition or else a condensed phase will form. Hence, these methods become awkward to use at low temperatures. In addition to this, accurate volume measurements at low temperature are extremely difficult. There are some data available at low temperatures using the Burnett method,[12,20,58,60,105,106] and more recently Brewer and Vaughn[8] and Brewer[7] have measured the pressure change upon mixing for a variety of gas mixtures down to -150°C.

Due to the problems associated with making direct measurements on gas mixtures at cryogenic temperatures, most of the low temperature B_{12} data found in the literature have been extracted from phase equilibrium measurements. The method referred to has been used by Reuss and Beenakker,[131] Dokoupil,[30] Mullins,[107] Liu,[83] and Chiu and Canfield.[15] This method is described in the following section.

Extraction of B_{12} from Phase Equilibrium Data

Since the measurements of phase equilibrium data provide the enhancement factor and the liquid phase composition, it is possible to rearrange the virial form of the enhancement factor, Equation (IV-17), to give

$$B_{12} = \frac{V_m}{2y_2}\left\{\frac{2B_{11}}{V_{01}} + \frac{3C_{111}}{2V_{01}^2} - \ell n\,(Z_{01}) - \frac{3}{2V_m^2}\,(y_1^2 C_{111} + 2y_1 y_2 C_{112} \qquad \text{(V-1)}\right.$$

$$\left. + y_2^2 C_{122}) + \frac{v_1^o}{RT}\left[(P - P_{01}) - \frac{\bar{\beta}_T}{2}\,(P^2 - P_{01}^2)\right] - \frac{2y_1 B_{11}}{V_m}\right\} \qquad \text{(Continued)}$$

$$+ \ln (Z_m) + \ln (x_1) - \ln \left(\frac{Py_1}{P_{o1}}\right)\Big\} \qquad (V\text{-}1)$$

Along a given isotherm, Equation (V-1) is solved for B_{12} at each pressure. The calculated values of B_{12} are plotted versus $(P - P_{o1})$ and by extrapolation to $(P - P_{o1}) = 0$, the true value of B_{12} is obtained. This method was described and used by Mullins[107] and more recently by Liu.[83] The manner in which this equation was used in this work is now discussed.

Since the solution to this equation requires a value for the gas phase molar volume, V_m, it is necessary to calculate the virial coefficients B_{22}, B_{12}, and C_{222} in addition to the coefficients shown in Equation (V-1). Mullins[107] and Liu[83] used the Lennard-Jones (6-12) model to predict the third virial coefficients (C_{111}, C_{112}, C_{122}, and C_{222}). This method appears to work well for systems involving simple molecules and where $T_{R1} < 0.80$. For larger molecules, the third virial coefficient is not adequately described by the Lennard-Jones parameters as is shown in Appendix F. This is especially critical where $T_{R1} \geq 0.80$, and the value of all the third virial coefficients become important. In this work the third virial coefficients, C_{111}, C_{112}, and C_{122}, have been calculated using the method of Chueh and Prausnitz[16] as described in Chapter IV. The parameters required for this calculation are shown in Table 28 of Appendix F. The values of C_{222} were taken directly using the selected curve shown in Figure 49. The second virial coefficient of helium, B_{22}, was calculated from Lennard-Jones parameters, and the second virial coefficient of the condensed component, B_{11}, was calculated using both the Lennard-Jones and Kihara parameters. A trial value of B_{12} was needed for

the calculation of V_m. This value was calculated initially using the Lennard-Jones parameters. After an initial run of the program, a new and improved value of B_{12} could be calculated. Similarly, the parameter K_{12}, which is used in the third virial coefficient calculation, was initially estimated using the empirical equation of Hiza and Duncan,[53] Equation (V-8). The third virial coefficient calculations do not appear too sensitive to this parameter. After one iteration of the B_{12} program, very good final estimates of B_{12} and K_{12} could be made.

One other modification was made of the existing B_{12} program. Since compressibility data for the condensed liquid phase were generally not available, it was necessary to use the average isothermal compressibility, $\bar{\beta}_T$. The modification that was made in this program is the same as described in Chapter IV.

In the systems studied in this work, the values calculated using this method generally compared well with the values from the original program of Liu[83] at low temperatures, $T_{R1} < 0.80$. The agreement was always within one cc/gm mole. At higher temperatures, $T_{R1} > 0.80$, the present method of extracting B_{12} and the original program of Liu begin to differ. The program of Liu appears to diverge from reality. It is above this temperature that the third virial coefficients, C_{111} and C_{112}, become very important.

At each temperature, two experimental values of B_{12} were obtained. This was accomplished by keeping all coefficients constant in this calculation except B_{11}. The B_{11} values used were calculated using the Kihara potential parameters and the Lennard-Jones parameters. This indicates the

effect of the virial coefficient B_{11} on the calculation of B_{12}. The squares represent the calculations using Kihara potential parameters, and the circles represent the calculation using the Lennard-Jones parameters. In each of the following figures, the curves labeled LJCL, KIH, KIHCK12, KIHEK12, BWR(LINEAR), and BWR(LORENTZ) represent the theoretical values of B_{12} calculated by these models. These various models were described in detail in Chapter IV.

B_{12} for the Helium-Ethane System

Phase equilibrium data from Heck[46] and Hiza and Duncan[53] have been used to extract the B_{12} values for this system. The experimental data were first smoothed and presented in Table 33 of Appendix G. Since Hiza and Duncan did not measure the liquid phase composition, it was necessary to estimate values of x_2 at 150 and 130 K. This was done using values from the helium-ethylene system at the same reduced temperature, and the values so obtained are presented in Table 33. At 150 K the effect of neglecting x_2 completely produced an uncertainty of only $\pm$ 0.1 cc/gm mole. The calculated values of B_{12} are presented in Figure 10. The agreement between the B_{12} values extracted from the two works is good except at 150 K. The value of B_{12} at that temperature is definitely high, which indicates that the enhancement factor values are too low. Smoothed values of B_{12} were read from Figure 10 at even temperature intervals and are given in Table 1. The uncertainty of these results was estimated to be $\pm$ 3 cc/gm mole. This was done by introducing the uncertainty of the enhancement factor and x_2 into the B_{12} program and recalculating B_{12}.

The various theoretical curves are shown in Figure 10.

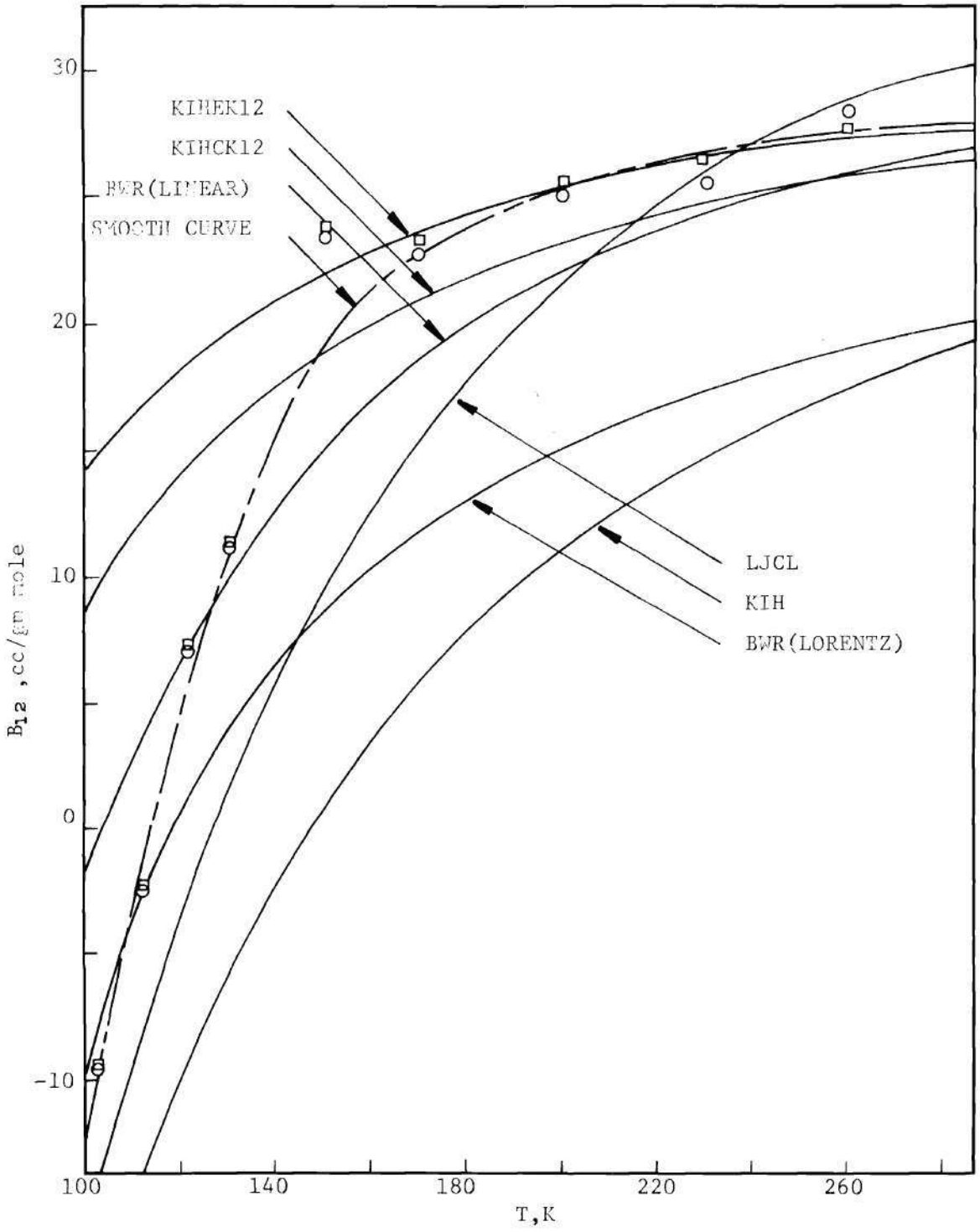

Figure 10. Comparison of Predicted and Experimental B_{12} for the Helium-Ethane System.

Table 1. B_{12} for the Helium-Ethane System

T,K	B_{12}, cc/gm mole
100	-11.4 ± 3
120	4.7 ± 3
140	15.8 ± 3
160	21.5 ± 3
180	24.1 ± 3
200	25.5 ± 3
220	26.5 ± 3
240	27.1 ± 3
260	27.5 ± 3
280	27.9 ± 3

The KIH and BWR(LORENTZ) models predict values that are too low, but the LJCL, KIHEK12, KIHCK12, and BWR(LINEAR) models appear to fit the data quite well.

B_{12} for the Helium-Ethylene System

B_{12} values for the helium-ethylene system have not been determined previously. The phase equilibrium data for this system consist of this work and the work of Hiza and Duncan.[53] The data for both of these works were smoothed and are presented in Table 34 of Appendix G. Since at 130 K the effect of letting $x_2 = 0.0$ instead of the experimental value produced a change in B_{12} of 0.08 cc/gm mole, no attempt was made to estimate x_2 values at lower temperatures. Figure 11 shows there is generally good agreement between the B_{12}'s from this work and those from the work of Hiza and Duncan. However, the two isotherms that overlap, 150 and 130 K, disagree by approximately 2.8 cc/gm mole. The B_{12}'s of Hiza and Duncan appear to be a little on the low side. Smoothed values of B_{12} are presented

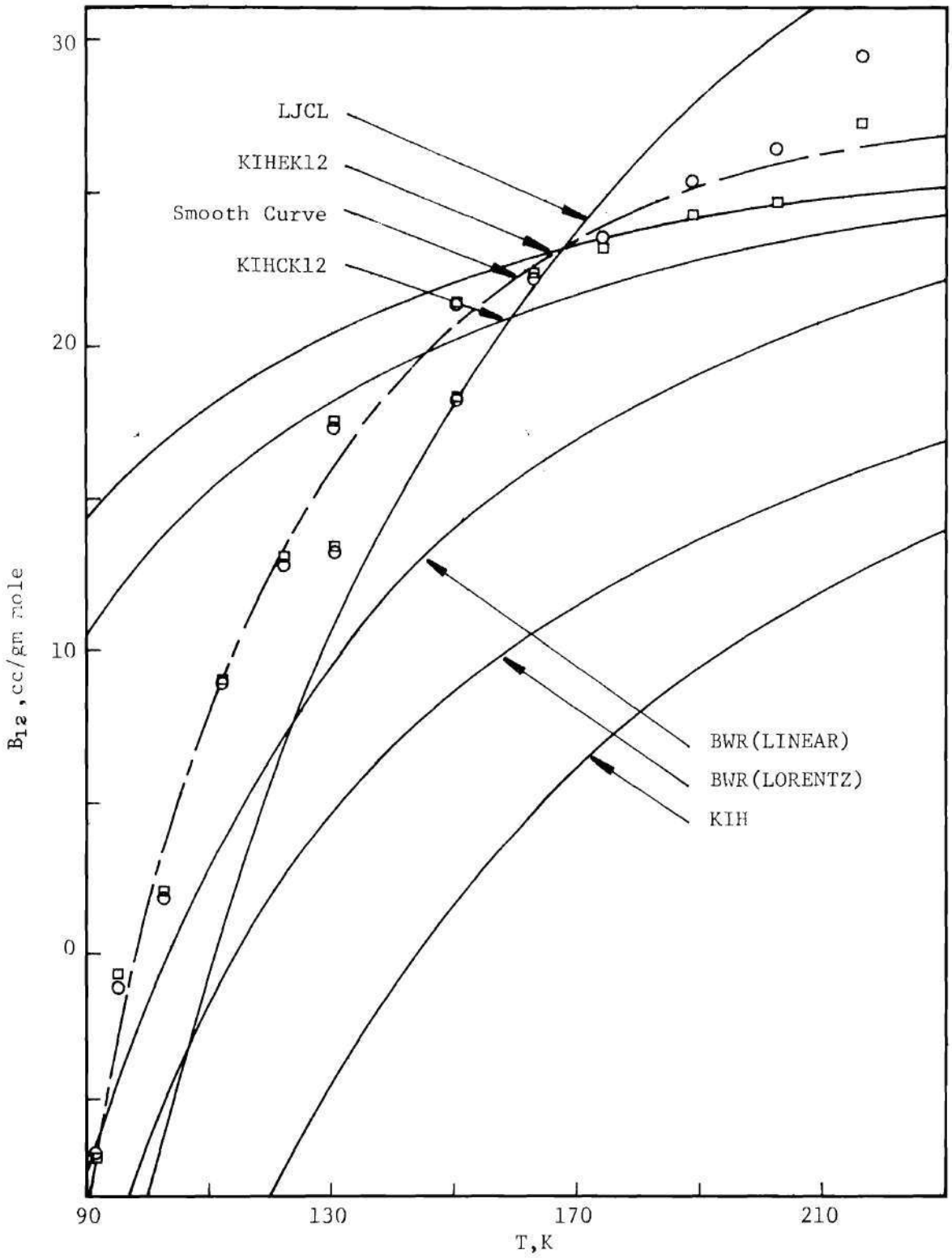

Figure 11. Comparison of Predicted and Experimental B_{12} for the Helium-Ethylene System.

at even temperature intervals in Table 2. The error bar on the data was determined by varying the input enhancement factor and x_2 values by the estimated experimental error. The uncertainty was shown to be about ± 3.5 cc/gm mole throughout the temperature range discussed.

Table 2. B_{12} for the Helium-Ethylene System

T,K	B_{12}, cc/gm mole
90	- 7.2 ± 3.5
100	1.8 ± 3.5
110	8.1 ± 3.5
120	12.7 ± 3.5
130	16.1 ± 3.5
140	18.8 ± 3.5
150	21.0 ± 3.5
160	22.3 ± 3.5
170	23.7 ± 3.5
180	24.6 ± 3.5
190	25.3 ± 3.5
200	25.9 ± 3.5
210	26.3 ± 3.5
220	26.6 ± 3.5

Figure 11 shows the agreement between experimental B_{12}'s and the theoretically calculated values. The LJCL, KIHEK12, and KIHCK12 models represent the data best. The BWR(LINEAR), BWR(LORENTZ), and KIH models predict values of B_{12} that are too low.

B_{12} for the Helium-Propane System

Several experimental B_{12} values have been determined by Brewer[7] for the helium-propane system. In addition to this, phase equilibrium measurements have been made by Schlinder, et al.[140] for this system.

These data of Schlinder, et al. have been smoothed in this work and are presented in Table 35 of Appendix G. The B_{12} values extracted in this work using the data of Schindler, et al. are presented together with the B_{12} values obtained by Brewer in Figure 12. The data of Brewer were corrected by using the pure virial values for propane, B_{11}, selected in this work, Figure 56. These adjusted values show good agreement with the values obtained from Schlinder's data except at 248.15 K, where their values differ by about 20 cc/gm mole.

The experimental curve is very steep at low temperatures, and it shows a strong downward bend at about 285 K. If more weight were given to the experimental point of Brewer at 248.15 K, then the bend in the curve would be shifted to still lower temperatures. The accuracy of the B_{12}'s presented in Figure 12 is about 4.0 cc/gm mole. Smoothed values of B_{12} at even temperature intervals are presented in Table 3.

The theoretical values of B_{12} are shown in Figure 12. Values predicted by the BWR(LINEAR), KIHCK12, and KIHEK12 models are in very good agreement with experiment at temperatures above 270 K. The LJCL model predicts values that are much higher than experiment. The BWR(LORENTZ) and KIH models again predict values that are too low.

B_{12} for the Helium-Propylene System

The phase equilibrium measurements presented in this work represent the only source available for extraction of B_{12} data. The smoothed enhancement factor and liquid composition data are presented in Table 36 of Appendix G. Figure 13 shows the extracted B_{12} data, and Table 4 gives smoothed values of B_{12} at even temperature intervals. Because the enhance-

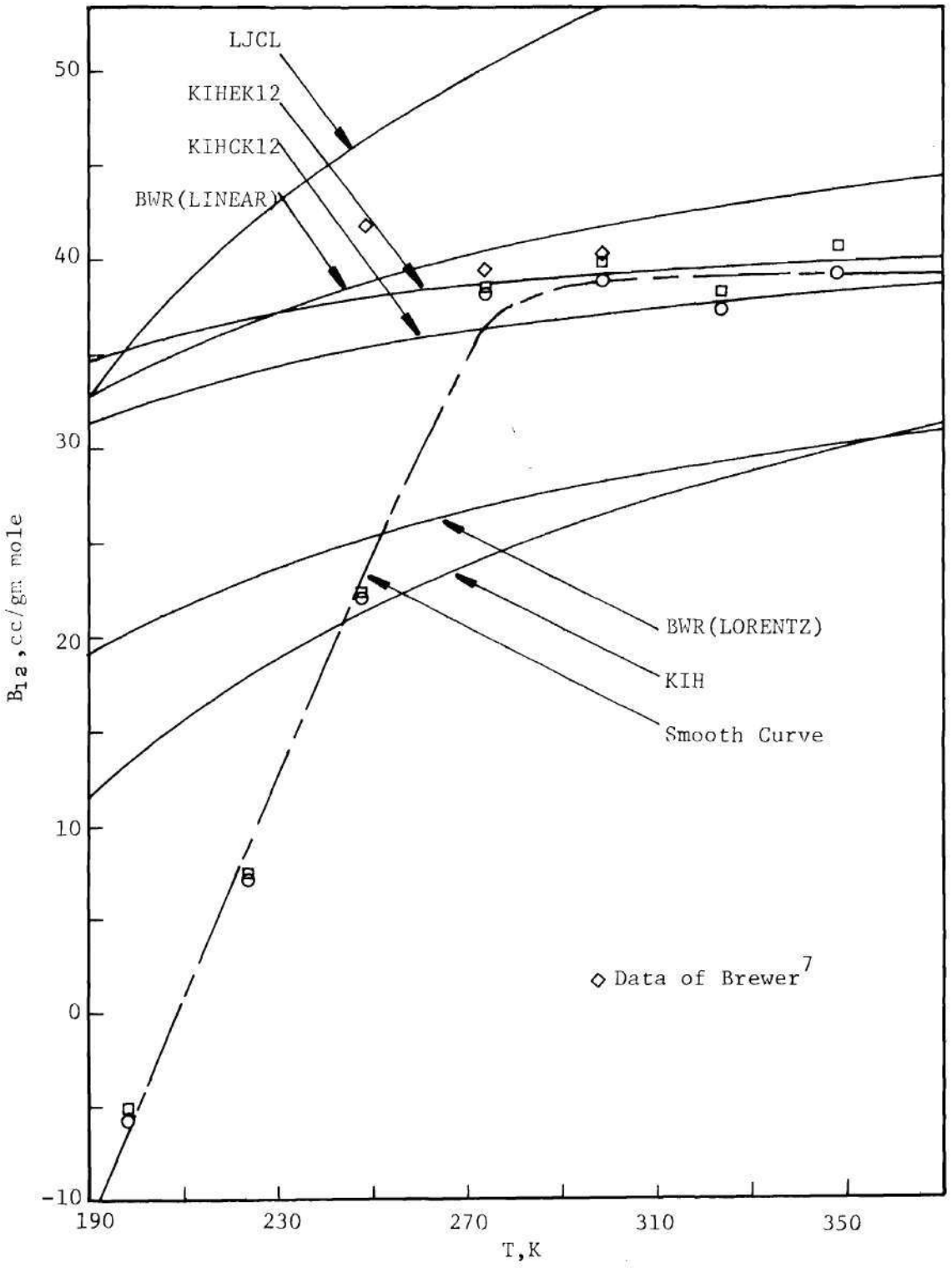

Figure 12. Comparison of Predicted and Experimental B_{12} for the Helium-Propane System.

Table 3. B_{12} for the Helium-Propane System

T,K	B_{12}, cc/gm mole
200	- 5.30 ± 4
210	0.62 ± 4
220	6.70 ± 4
230	12.4 ± 4
240	19.5 ± 4
250	25.5 ± 4
260	30.6 ± 4
270	35.1 ± 4
280	37.7 ± 4
290	38.6 ± 4
300	39.0 ± 4
310	39.1 ± 4
320	39.2 ± 4
330	39.2 ± 4
340	39.3 ± 4
350	39.3 ± 4
360	39.3 ± 4

Table 4. B_{12} for the Helium-Propylene System

T,K	B_{12}, cc/gm mole
200	32.0 ± 6
210	33.4 ± 6
220	34.0 ± 6
230	34.5 ± 6
240	34.8 ± 6
250	35.0 ± 6
260	35.2 ± 6

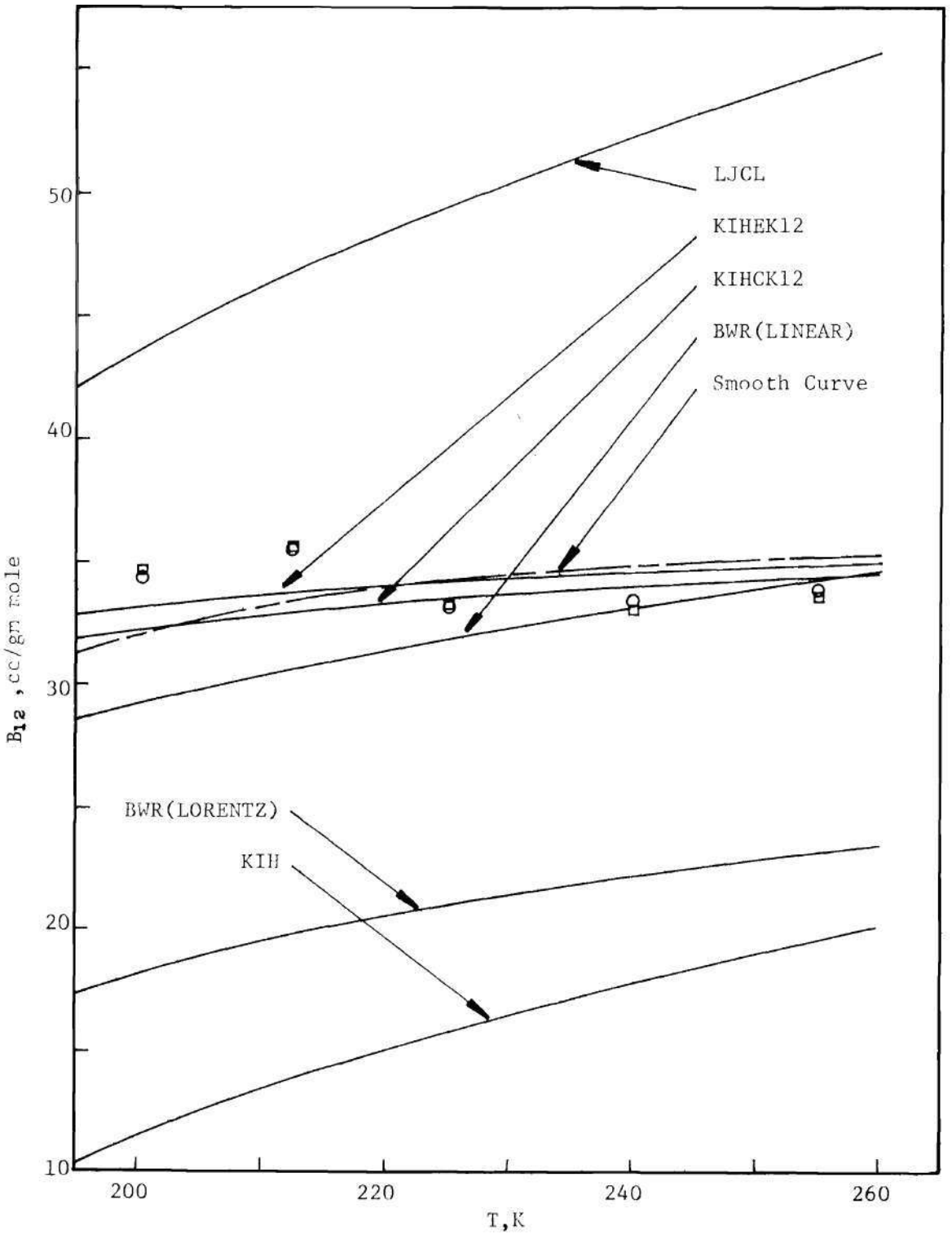

Figure 13. Comparison of Predicted and Experimental B_{12} for the Helium-Propylene System.

ment factors are very close to one, a ± 3 percent variation of the experimental data produces a large average uncertainty in B_{12} of ± 6 cc/gm mole. Although the large uncertainty of these values makes the precise shape of this curve hard to determine, it appears that the curve is starting to bend downward as it is expected to do at lower temperatures. The large uncertainty means that all the data could be fitted with a straight line at 34 cc/gm mole.

The various theoretical models are shown in Figure 13. The BWR(LINEAR), KIHEK12, and KIHCK12 models again predicted the best B_{12} values. The LJCL values are excessively high, and the KIH and BWR(LORENTZ) values are too low.

Summary of Helium Binary B_{12} Data

A survey of B_{12} data for helium binary systems is presented in this section and summarized in Table 5. This collection of data might prove useful in prediction of multicomponent gas-liquid equilibrium. It might also prove helpful in spotting some generalizations about the two-body interaction forces. Some systems presented here are not considered cryogenic gases, but they are included to make the survey more general.

A very good analysis of B_{12} data, for helium cryogenic gas systems, has been performed by Liu.[83] He has extracted B_{12} values from phase equilibrium data and combined these results with the available higher temperature data. He has studied the helium-carbon dioxide, helium-argon, helium-methane, helium-nitrogen, and helium-oxygen systems. Other papers showing B_{12} data for helium binary systems have been presented by Brewer,[7] Brewer and Vaughn,[8] King and Robertson,[75] Jones and

Table 5. List of B_{12} Data for Helium Binary Systems

System	Reference	T,K	B_{12}, cc/gm mole
He-Ne	8	123.15	8.68
		173.15	10.91
		223.15	11.74
		273.15	12.11
		323.15	12.71
	57	273.15	13.5
		373.15	13.9
		473.15	13.2
		573.15	12.8
		673.15	11.7
He-Ar	83	70	- 7.8 ± 2.5
		80	- 2.9 ± 2.5
		90	0.8 ± 2.5
		100	3.7 ± 2.5
		110	6.1 ± 2.5
		150	12.1 ± 2.5
		200	15.6 ± 2.5
		250	17.4 ± 2.5
		300	18.6 ± 0.3
	67	303.15	18.77 ± 0.10
		373.15	19.73 ± 0.08
		473.15	20.26 ± 0.2
		573.15	20.45 ± 0.2
		673.15	20.35 ± 0.3
		773.15	19.75 ± 0.3
He-Kr	7	148.15	15.53
		173.15	16.07
		198.15	17.66
		223.15	18.70
		273.15	18.32
		323.15	20.99
He-Xe	7	173.15	23.24
		198.15	25.72
		223.15	25.43
		273.15	26.86
		323.15	28.78

Table 5. (Continued)

System	Reference	T,K	B_{12}, cc/gm mole
$He-H_2$	8	123.15	15.14
		148.15	15.92
		173.15	16.20
		198.15	16.43
		223.15	16.20
		248.15	16.43
		273.15	16.37
	39	298.15	16.01
		323.15	15.82
		298.15	16.4
		323.15	15.6
		348.15	15.4
		373.15	15.3
		398.15	15.1
		423.15	15.0
		448.15	14.9
$He-N_2$	83	80	3.0 ± 2.5
		90	6.1 ± 2.5
		100	8.5 ± 2.5
		110	10.6 ± 2.5
		120	12.3 ± 2.5
	12	133.15	13.80 ± 2.5
		143.14	15.31 ± 2.5
		158.15	16.50 ± 2.5
		183.15	17.85 ± 2.5
		223.15	20.16 ± 2.5
	162	273.15	21.66 ± 2.5
		448.15	22.92 ± 0.4
		523.15	22.41 ± 0.4
		598.15	21.73 ± 0.4
		673.15	21.20 ± 0.4
		748.15	20.33 ± 0.4
$He-O_2$	83	70	-12.1 ± 2.5
		90	- 2.0 ± 2.5
		110	4.1 ± 2.5
		130	8.0 ± 2.5
		150	10.7 ± 2.5
$He-CO_2$	83	180	10.9 ± 5
		200	13.5 ± 5
		220	15.7 ± 5
		240	17.6 ± 5
		260	19.1 ± 5
		280	20.4 ± 5

Table 5. (Concluded)

System	Reference	T,K	B_{12}, cc/gm mole
He-CO	7	123.15	14.31
		148.15	16.64
		173.15	18.41
		223.15	20.62
		273.15	21.53
He-CH_4	83	60	-11.0 ± 3
		80	4.6 ± 3
		100	10.9 ± 3
		120	14.6 ± 3
		140	17.2 ± 3
		160	19.1 ± 3
		180	20.6 ± 3
He-CF_4	67	303.15	26.51 ± 0.8
		373.15	30.19 ± 0.9
		473.15	33.20 ± 0.5
		573.15	37.42 ± 0.8
		673.15	40.47 ± 0.4
		773.15	43.13 ± 0.4
He-C_4H_{10}	65	373.25	47.9 ± 5
		398.15	50.5 ± 5
		423.15	52.7 ± 5
		448.15	52.4 ± 5
		473.25	46.7 ± 5
		498.25	53.6 ± 5
He-$C_{10}H_8$	75	305.15	67.5 ± 2.8
		347.15	74.7 ± 2.8

Kay,[65] Kalfoglou and Miller,[67] and Witonsky and Miller.[162] These results have been presented in Table 5. The systems are presented in order of the most simple to the most complex molecular interactions. The helium-hydrocarbon results presented in the previous section are considered a part of this summary. The uncertainty of the values presented in Table 5 has been estimated where possible. The values presented by Brewer[7] have an uncertainty that is hard to estimate since they are completely dependent upon the values for the pure virial coefficients.

Several observations can be made from the results in Table 5. First, within a given series, as the helium-inert gases or helium-hydrocarbon series, it appears that, for a given reduced temperature, T_{R_1}, the values of B_{12} increase as the molecules become larger. Second, almost all of the B_{12} values are positive except at the lowest temperatures. This accounts for the fact that enhancement factors of these systems are very close to unity. Third, Table 5 reveals that several of the B_{12} curves show a maximum. These are the helium-neon, helium-argon, helium-hydrogen, and helium-nitrogen systems. The appearance of this maximum is somewhat unexpected, and this trend is discussed somewhat further at this point.

The general shape of the second virial coefficient curve for pure components has been discussed in detail by Hirschfelder, et al.[50] They have pointed out that all pure second virial coefficient curves, at high enough temperatures, should pass through a point of $B(T) = 0.0$ at the Boyle temperature and that, at still higher temperatures, this curve should pass through a maximum. Using the Lennard-Jones (6-12) parameters, Hirsch-

felder, et al.[50] have produced a reduced second virial coefficient curve that reveals the following results:

$$B(T) = 0.0 \qquad \text{at} \qquad T^* = 3.43 \tag{V-2}$$

and

$$\frac{dB(T)}{dT} = 0.0 \qquad \text{at} \qquad T^* = 25 \tag{V-3}$$

where

$$T^* = T/(e/k). \tag{V-4}$$

Thus, depending upon the magnitude of (e/k), the Lennard-Jones energy parameter, one might expect to see different portions of the second virial coefficient curve. The only pure gas which has been shown to reproduce the expected curve is helium. Using the value of (e/k) given in Table 27, a Boyle temperature of 24 K and a maximum in the B(T) curve at 174 K can be calculated using Equations (V-2) and (V-3). Figure 48 shows that these temperatures are in good agreement with experiment. Hydrogen, neon, argon, and nitrogen all exhibit a Boyle temperature, but their experimental data fall short of the maximum in the curve.

The discussion above tends to shed some light on the unusual behavior of the $B_{12}(T)$ curves for the helium binary systems. The presence of helium in these mixtures has the effect of lowering the Boyle point and the maximum in the second virial interaction coefficient curve. Figure 14 reveals the maximum in the $B_{12}(T)$ curve for the helium-hydrogen system. A summary of this type information has been presented in Table 6. It is interesting to note that, although the maximum in the helium-nitrogen

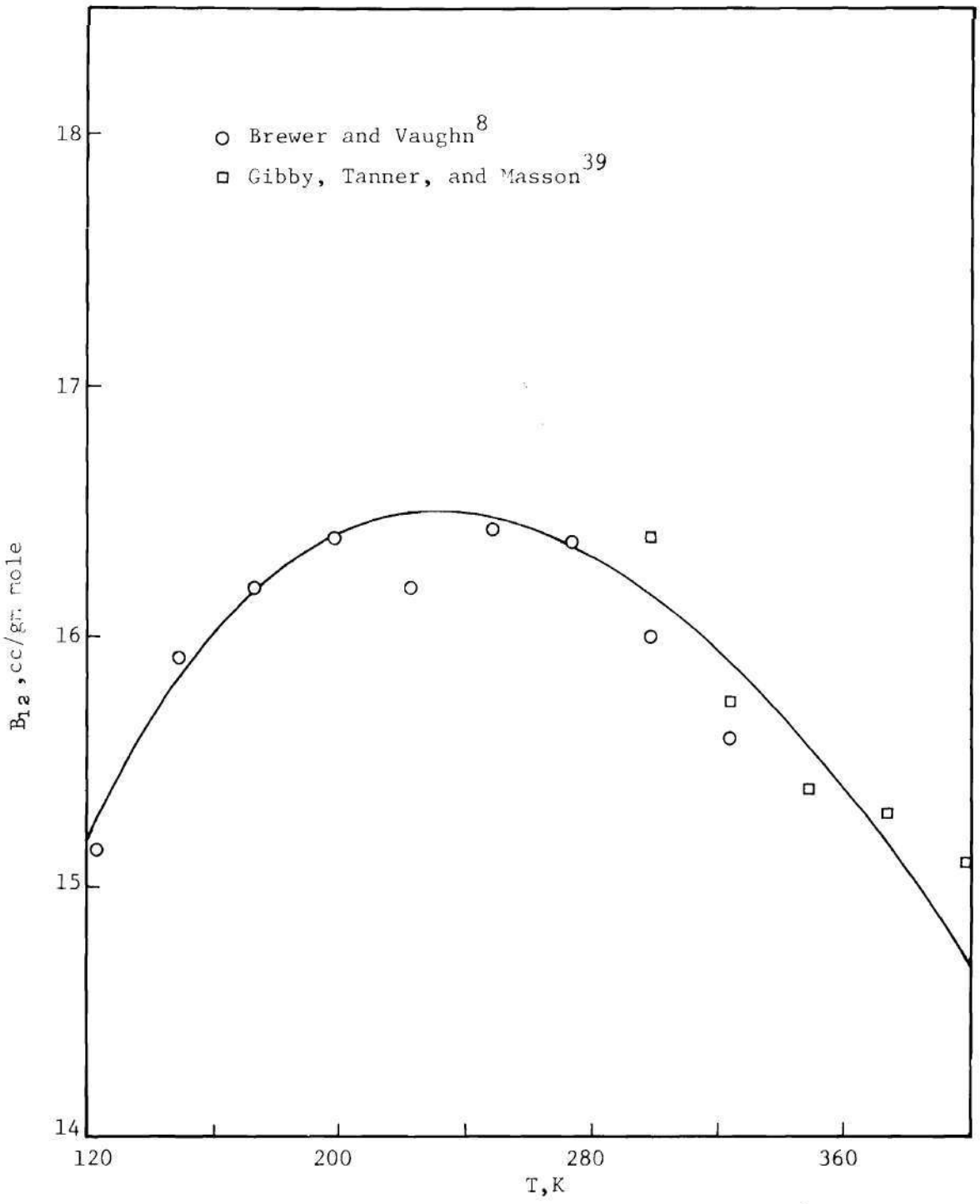

Figure 14. B_{12} for the Helium-Hydrogen System.

and helium-argon system curves differs by about 220 K, the critical temperatures of nitrogen and argon differ by only 25 K. This tremendous shift in the maximum of the B_{12} curve may be due to some forces present in the nitrogen versus the argon interaction with helium. No attempt is made here to speculate on the type of forces responsible for this shift. The same type of shift seems to occur when comparing the helium-hydrogen and the helium-neon curves.

Table 6. Temperature at Which the B_{12} versus Temperature Curve Reaches a Maximum

Binary Mixture	Approximate Temperature of Maximum, K
He-He	174
He-H_2	225
He-Ne	400
He-Ar	600
He-N_2	380

It is possible to make estimates of the interaction energy parameter, $(e/k)_{12}$, for mixtures. This can be done by using Equation (V-2) or (V-3) provided one has either the Boyle temperature or the temperature where the slope of the $B_{12}(T)$ curve is zero. This method has been used by Mullins[107] to obtain (e/k) for pure helium. Liu[83] has obtained $(e/k)_{12}$ values for some helium binary systems by least square fitting the Lennard-Jones parameters to the experimental B_{12} data. Using the Boyle temperature data for the helium-nitrogen, helium-argon, and helium-oxygen systems,

the value of $(e/k)_{12}$ calculated from Equation (V-2) agreed to within several percent of the values obtained by Liu.

Deviations from the Geometric Mixing Rule

The calculation of the second interaction virial coefficient, B_{12}, would be a very easy chore if one had the correct intermolecular potential function. Since both the Lennard-Jones and Kihara (6-12) potentials have been used to describe interactions between like molecules, it is assumed that these potential functions will describe interactions between unlike molecules. For the calculation of an interaction virial coefficient, the Lennard-Jones potential function is dependent upon σ_{12}, the collision diameter, and $(e/k)_{12}$, the depth of the potential well. The usual way of getting these parameters is by using Equations (IV-26) and (IV-28).

Hudson and McCoubrey[62] have shown that, for the Lennard-Jones (6-12) potential, an approximate solution of the London theory of dispersion forces[50] yields:

$$e_{12} = \left[\frac{2(I_1 I_2)^{\frac{1}{2}}}{I_1+I_2}\right]\left[2^6 \frac{\sigma_1^3 \sigma_2^3}{(\sigma_1+\sigma_2)^6}\right](e_1 e_2)^{\frac{1}{2}} \qquad \text{(V-5)}$$

and

$$\sigma_{12} = \frac{\sigma_1 + \sigma_2}{2} \qquad \text{(V-6)}$$

Equation (V-6) is in the familiar linear form, but Equation (V-5) appears grossly different from the general geometric mixing rule. If the two interacting molecules have the same ionization potential, $I_1 = I_2$,

and the collision diameters are the same, $\sigma_1 = \sigma_2$, then equation (V-5) reduces to the more familiar geometric mixing rule, Equation (IV-26). Hence, it is shown theoretically that, for molecules that are very dissimilar in their values of I and σ, one can expect deviations from the geometric mixing rule. Work by Hudson and McCoubrey[62] and Huff and Reed,[63] using Equation (V-5), indicated an improvement of predicted B_{12} values when molecules are relatively similar, but the results are more random than consistent. Eckert, et al.[33] have given consideration to changing the linear mixing rule for σ_{12}, but the results appear unsatisfactory. Since the Lennard-Jones (6-12) potential function differs from the Kihara core potential only in its description of the molecular core, it is likely that Equation (V-5) or perhaps a similar equation applies to the geometric mixing rule for the energy parameter of the Kihara potential.

Binary systems containing helium or neon have been shown by Chueh and Prausnitz,[16] Hiza and Duncan,[53] Mullins,[107] Hiza,[52] and Liu[83] to give large deviations from the geometric mean. For example, the helium-neon and helium-methane binary systems show 40 and 28 percent deviations from the Kihara potential geometric mixing rule for the energy parameter, respectively.

In an attempt to improve the Kihara potential, Mullins,[97] Chueh and Prausnitz,[16,17] Eckert, et al.,[33] Hiza and Duncan,[53] and Hiza[52] have introduced a correction to the geometric mixing rule:

$$U_{o12} = (1-K_{12}) \; (U_{o_1} U_{o_2})^{\frac{1}{2}} \qquad \text{(V-7)}$$

The K_{12} factor must be obtained from experimental interaction gas phase data. If a good estimation of K_{12} could be made, it would be possible to predict a very good value of B_{12}, which is the most important term in the theoretical prediction of the enhancement factors except at the highest pressures where the third and higher virial coefficients become important. All values of K_{12} discussed in this section are in reference to Equation (V-7).

Since Equation (V-5) indicates that K_{12} should be a function of ionization potential and collision diameter, Hiza and Duncan[53] investigated both of these parameters, and they developed an empirical correlation which relates the K_{12} of Equation (V-7) to the ionization potential.

$$K_{12} = 0.17 \ (I_v - I_c)^{\frac{1}{2}} \ \ell n \left(\frac{I_v}{I_c}\right) \qquad \text{(V-8)}$$

where v and c refer to the volatile and condensible components, respectively. The correlation was developed for gas mixtures that have large K_{12} values. Hiza[52] has shown that this correlation, which is based upon experimental data, provides a good correction to the geometric mixing rule. Since interaction virial coefficients, B_{12}, have been determined in the present work for the helium-hydrocarbon systems, it seemed quite interesting to determine their respective K_{12} values and thereby check the usefulness of Equation (V-8).

Liu[83] has used the same type of correction for the Lennard-Jones (6-12) potential,

$$\left(\frac{e}{k}\right)_{12} = (1 - K_{LJ}) \left(\frac{e}{k_1} \ \frac{e}{k_2}\right)^{\frac{1}{2}} \qquad \text{(V-9)}$$

Unfortunately, the two Lennard-Jones parameters, (e/k) and σ, are very sensitive to the temperature range of the second virial coefficient fit. Recent papers by Lin and Robinson[82] and Hanley and Klein[45] have revealed difficulties in obtaining these parameters from second virial coefficient data. Because of the strong temperature dependency of these parameters, the possibility of a useful correlation coming from these results is highly unlikely. The Kihara core model involves an additional core parameter, and its parameters are not as sensitive to temperature. For this reason, corrections to the geometric mixing rule of the energy parameter obtained using these energy parameters should be of more interest.

Hiza and Duncan[53] extracted B_{12} from the enhancement factor data by assuming $y_1 = 0.0$ and that the condensed phase was pure and incompressible. At these temperatures, the vapor pressure is much less than one and so V_{01} is much greater than one. This is equivalent to reducing equation (IV-17) to

$$\ell n\phi = \frac{v_1^o (P - P_{01})}{RT} + \ell n (Z_2) - \frac{2B_{12}}{V_2} - \frac{3C_{122}}{2V_2^2} \qquad \text{(V-10)}$$

By selecting the proper value of K_{12} for the calculation of B_{12}, it was possible to reproduce the experimental data. Therefore, in this way a value of K_{12} could be obtained at each temperature, and it would hopefully be a constant. Unfortunately, this method does not allow one to extract K_{12} values in cases where y_1 or x_2 cannot be neglected (usually above $T_{R1} = 0.5$).

Chueh and Prausnitz[16] and Solen, et al.[147] have presented values

of K_{12} in the literature, and these values have compared well with the results of Hiza[52] and with the results of this work. Prausnitz states that K_{12} is evaluated from information on the i-j interaction data given by the second interaction virial coefficients. This seems to verify that their approach to obtaining K_{12} is similar to that of Hiza and Duncan.[53] Their work appears to be extended to higher reduced temperatures.

The method used in this work to extract K_{12} from B_{12} data is similar to that used by Hiza and Duncan. The values of B_{12} were extracted from the phase equilibrium data using Equation (V-1). The Kihara virial coefficient with quantum corrections, Equation (IV-36), was then fitted graphically to these data by adjusting the value of K_{12} in Equation (IV-46). In this fit the linear average for $(\rho_o)_{12}$, Equation (IV-33), was used. Therefore the only unknown in Equation (IV-36) was the value of K_{12}. In all systems studied, the Kihara parameters were taken from the paper of Prausnitz and Myers.[122] Some of these parameters are presented in Table 27, Appendix F. The fit was over a specified temperature range since in some systems the K_{12} values are a function of temperature.

This apparent temperature dependence of K_{12} has been noticed by Hiza and Duncan,[53] and they reference a similar problem experienced by Prausnitz. The problem becomes more pronounced as the molecules become more complex. The results of Liu[83] show that this temperature dependency is present in the helium-methane system. The results of this work have revealed that the effect is very strong in the remaining helium-hydrocarbon systems. The effect of changing the value of K_{12} is to simply move the B_{12} curve up or down, and so this lack of temperature dependency of the

theoretical model is more basic than simply changing the geometric mixing rule. Undoubtedly, part of the reason for this poor representation of the data is a lack of the (6-12) potential function to describe these interactions adequately. Perhaps the repulsion portion of the potential should be changed to a lower number, due to the softer core of these larger molecules. A recent book by Margenau and Kestner[91] may help produce some insight into the selection of a realistic potential function for interacting molecules.

In Table 7, the values of K_{12} extracted in this work are given. The temperature range over which the fit was made is also shown. This table includes a fit of some data presented in Table 5. K_{12} values available for these systems from Hiza[52] and Solen, et al.[147] are shown for comparison. Since the real objective of this section was to check the correlation of Hiza and Duncan,[53] Equation (V-8), values of K_{12} calculated from this equation are also presented. Values of the ionization potential used in this equation are taken from Reed[127] and the 49th edition of the Handbook of Chemistry and Physics. The agreement of these calculated values with experiment is very satisfactory.

Although no reference is made to the temperature range of their fit, the K_{12} values of Solen, et al.[147] are in excellent agreement with the values of this work. This seems to verify that their method of obtaining K_{12} was the same as the method used in this work. Since Hiza used a simplified enhancement factor equation to calculate B_{12}, it is certain that most of his values are over a lower temperature range than those in this work. Hence, some disagreement between these two investigators may be due to the temperature dependency of K_{12}.

Table 7. Values of K_{12} for Helium Binary Systems

Gas	I*	K_{12} Calculated	K_{12} Experimental		
		Equation (V-8)	This Work**	Hiza[52]	Solen, et al.[147]
He	24.46[127]				
Ne	21.5 [127]	0.037			0.04
Ar	15.76[127]	0.221	0.22 (65-150 K)	0.22	0.22
Kr	14.00[127]	0.308	0.53 (150-330 K)	0.312	
Xe	12.13	0.418		0.40	
H_2	15.6	0.228		0.30	0.24
N_2	15.51	0.232	0.26 (65-120 K)		0.23
O_2	12.16[127]	0.420	0.12 (70-150 K)		0.10
CO_2	14.4	0.293	0.20 (220-280 K)		0.20
CO	14.1	0.302	0.39 (123-283 K)		
CH_4	13.12[127]	0.356	0.49 (95-190 K)		0.46
C_2H_6	11.65[127]	0.451	0.55 (170-290 K)		0.55
C_2H_4	10.56[127]	0.532	0.60 (130-220 K)	0.40	
C_3H_8	11.21[127]	0.483	0.60 (260-350 K)		0.60
C_3H_6	9.80[127]	0.595	0.63 (200-255 K)		

*Values of I not referenced, were taken directly from the 49th edition of the Handbook of Chemistry and Physics.

**These values represent an average value over the specified temperature range.

These results show that helium interactions with large molecules tend to give large deviations from the Kihara geometric mixing rule. An attempt was made to obtain K_{12} for the helium-n-butane system. No value of K_{12} would give values of B_{12} as large as the experimental results. It is suspected that the Kihara parameters used may be the reason for this result. Since no parameters for n-butane were available from Prausnitz and Myers,[122] Kihara spherical core parameters from Tee, et al.[155] were used. It is likely that the value of K_{12} is sensitive to the core parameters of the Kihara potential. Although this area has not been pursued, it certainly bears further consideration.

CHAPTER VI

COMPARISON OF EXPERIMENTAL AND PREDICTED ENHANCEMENT FACTORS

The various theoretical models discussed in Chapter IV have been used to calculate enhancement factors for the helium-ethane, -ethylene, -propane, and -propylene systems. The virial equation of state used the LJCL, KIH, KIHCK12, and KIHEK12 models to calculate the virial coefficients. The BWR(LINEAR) equation was also used. These predicted values are presented in Tables 33 through 36 of Appendix G. Figures 15 through 18 show a graphical comparison of these five different sets of predicted enhancement factors with a representative isotherm of each system. An additional theoretically predicted enhancement factor curve showing the BWR(LORENTZ) values is shown in the figures for comparison. The isotherm selected for each system was within the temperature range of the experimental K_{12} value. Figure 19 shows an isobar curve for the helium-ethane system. This 20 atmosphere isobar demonstrates the minimum and maximum which can occur in the various helium binary enhancement factor curves. The three basic theoretical models LJCL, KIH, and BWR(LINEAR) show that these models are able to qualitatively represent the enhancement factor isobar curves reasonably well for these systems.

Several comments should be made about the basic differences the various models possess. The three models, KIH, KIHEK12, and KIHCK12, differ only in their calculation of the interaction terms, B_{12}, C_{112}, and C_{122}. The pure second and third virial coefficients are identical in

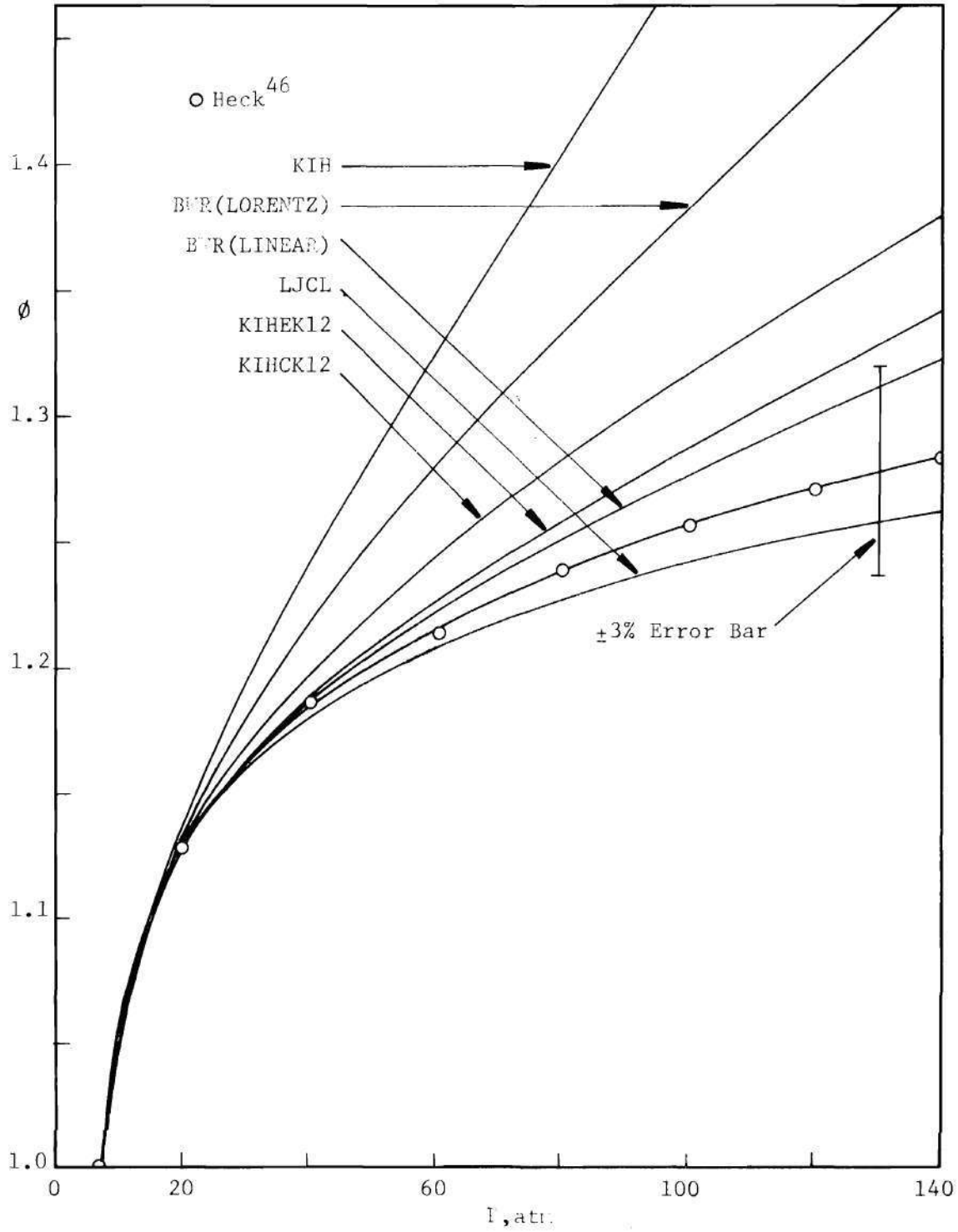

Figure 15. Theoretical and Experimental Enhancement Factors in the Helium-Ethane System at 230.00 K.

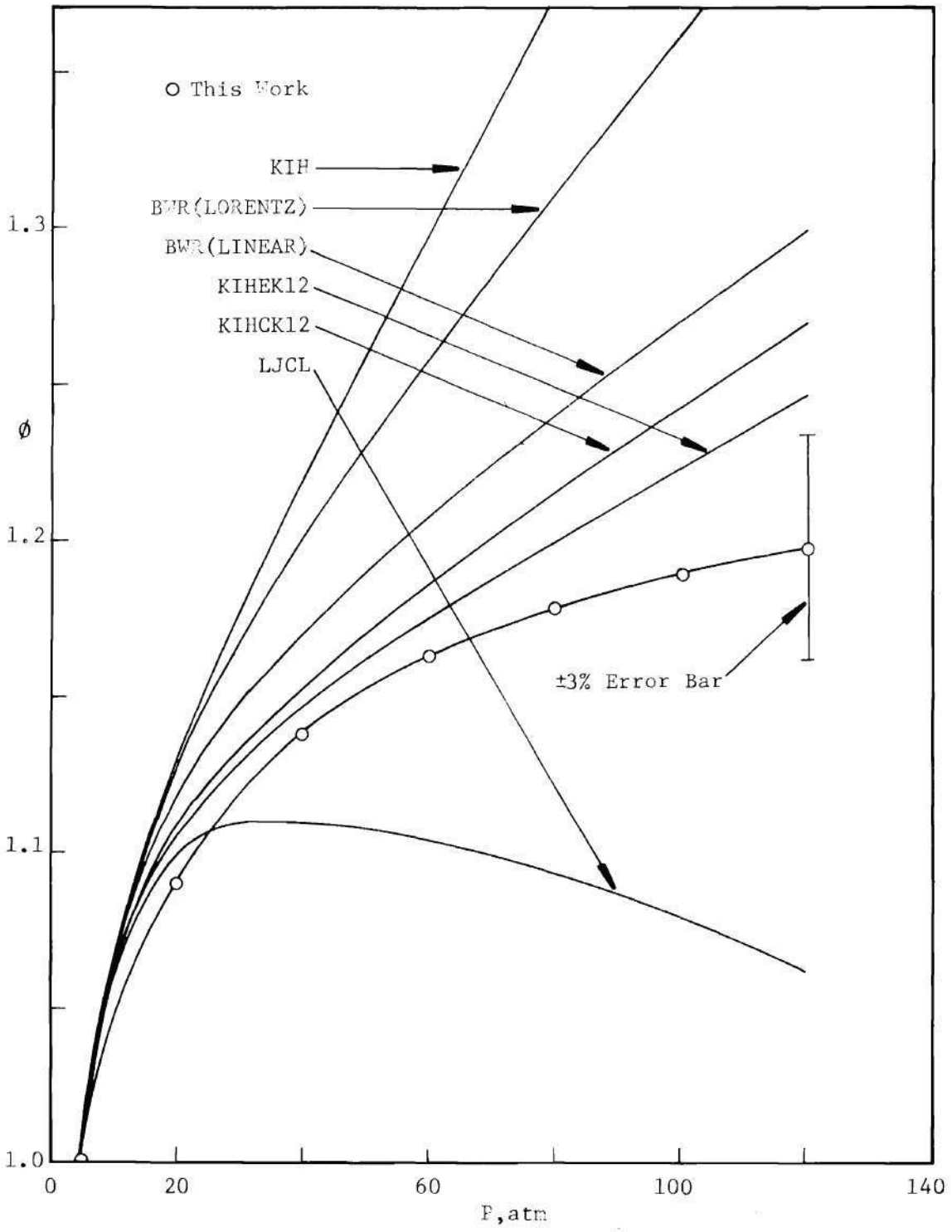

Figure 16. Theoretical and Experimental Enhancement Factors in the Helium-Ethylene System at 202.01 K.

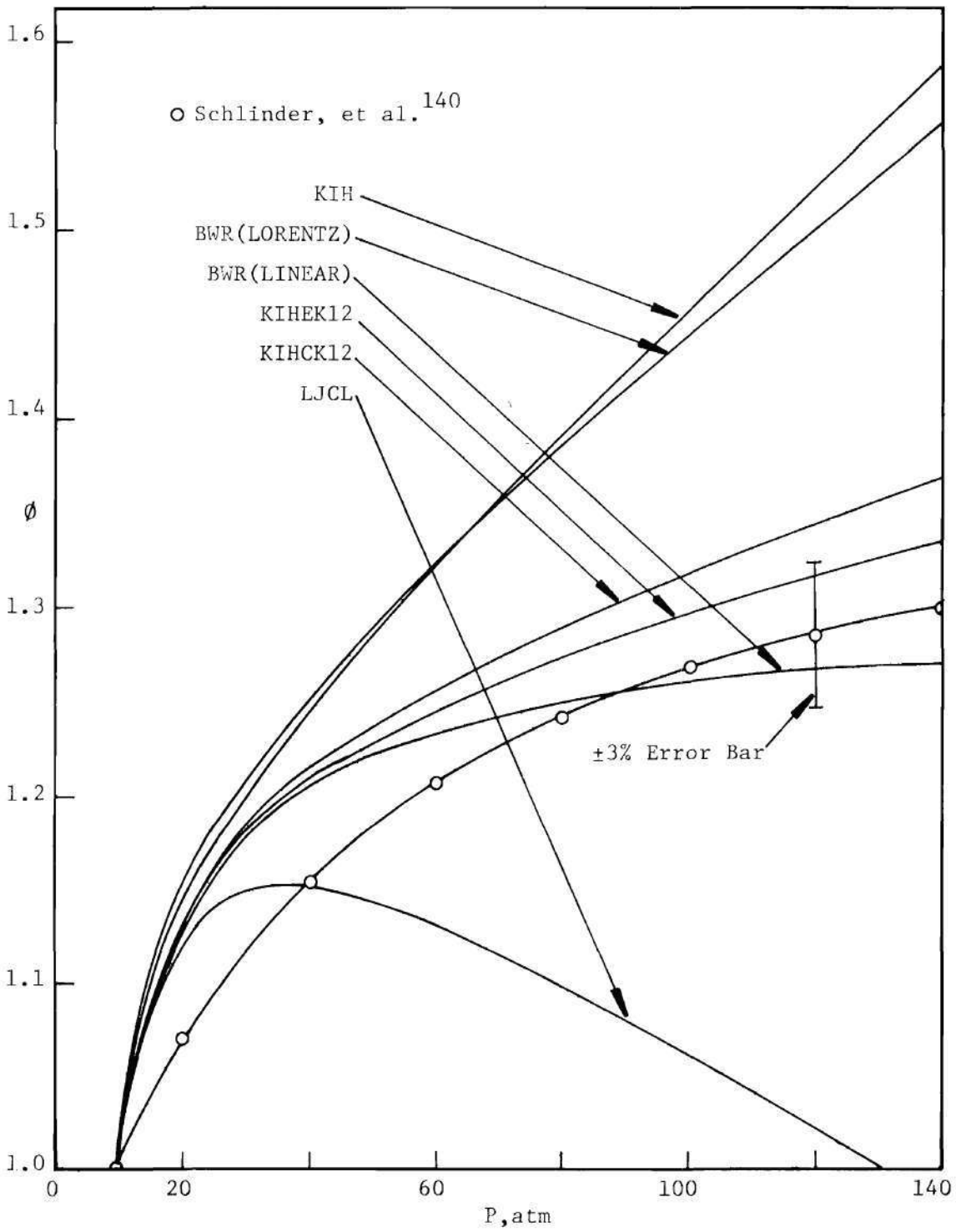

Figure 17. Theoretical and Experimental Enhancement Factors in the Helium-Propane System at 298.15 K.

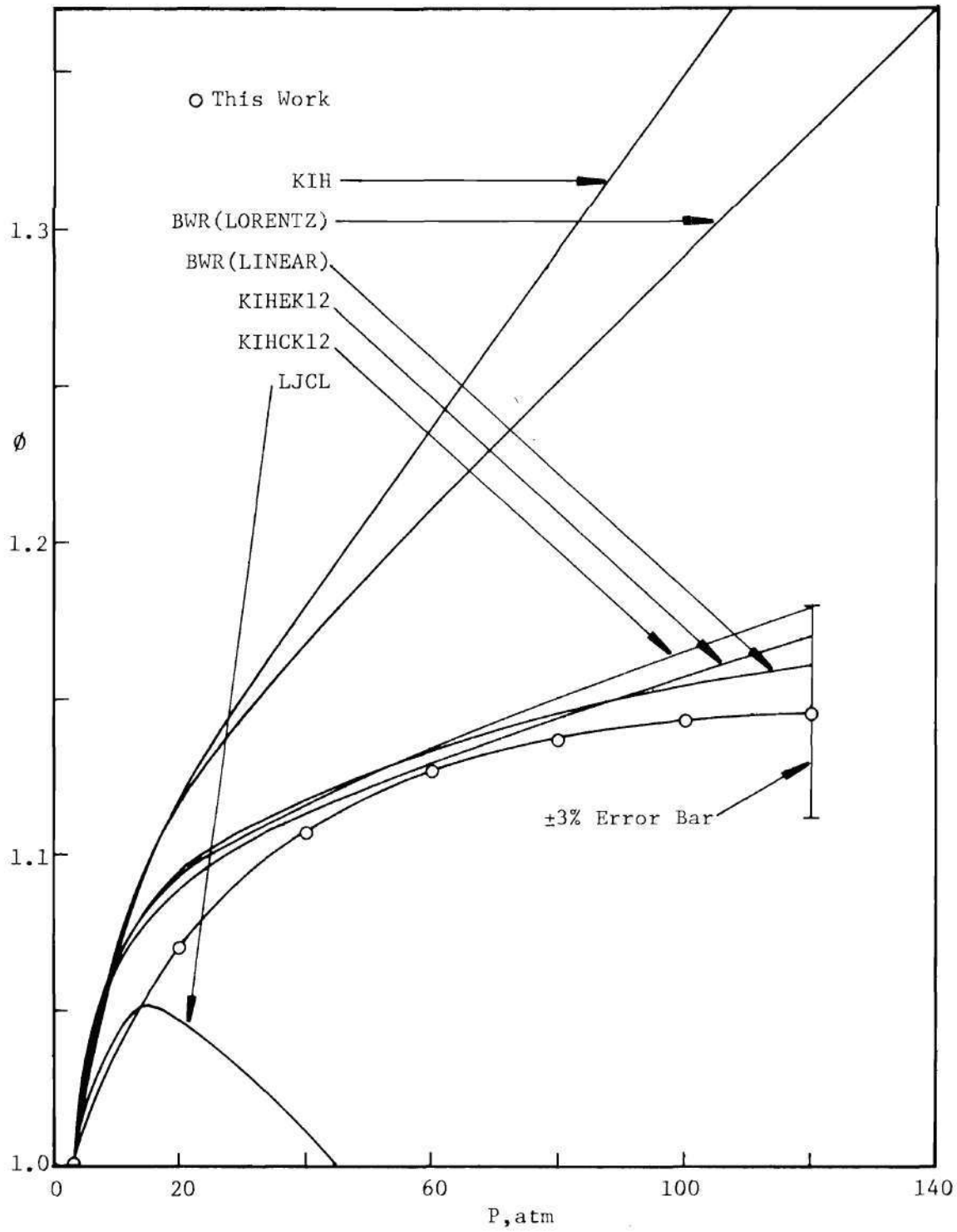

Figure 18. Theoretical and Experimental Enhancement Factors in the Helium-Propylene System at 254.98 K.

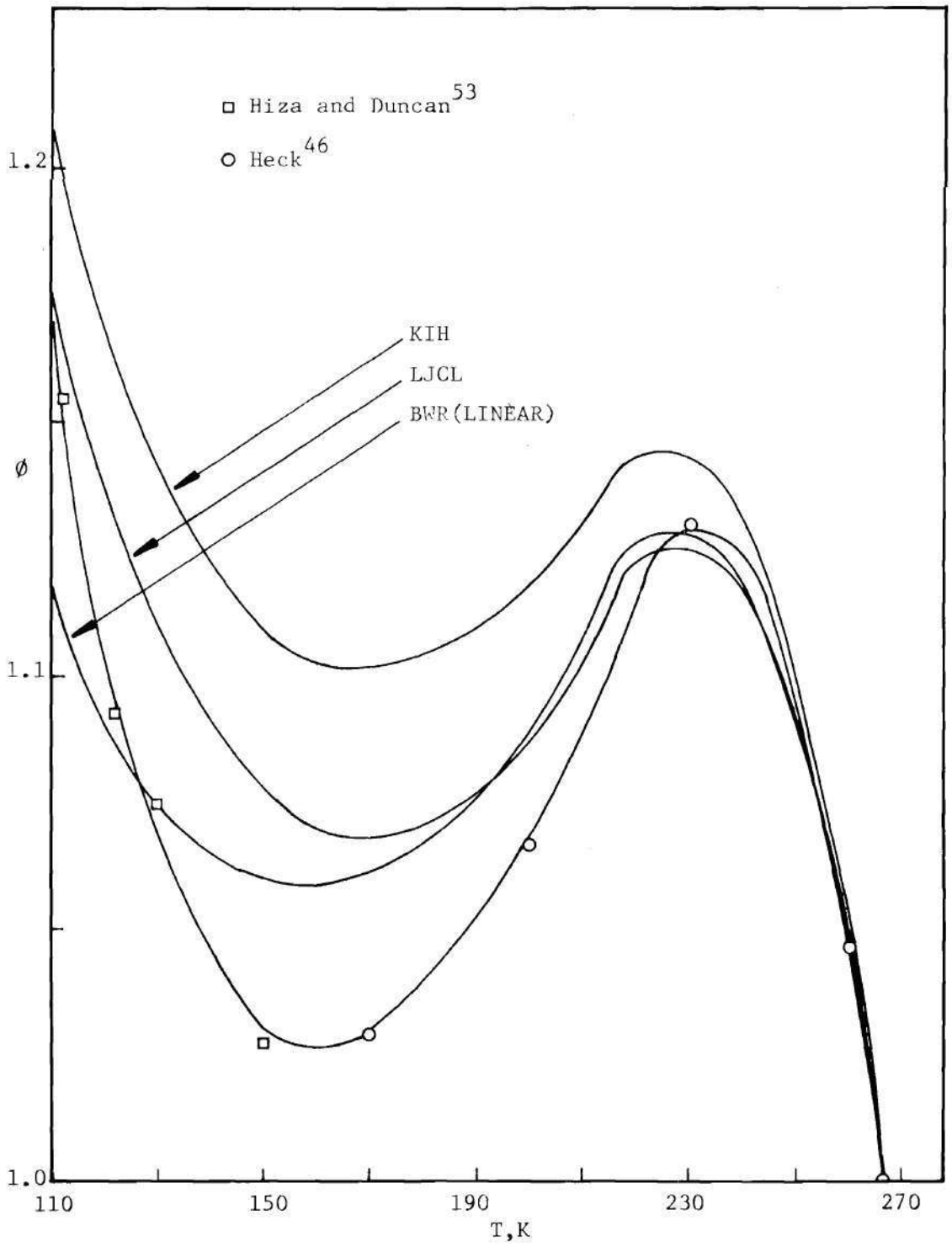

Figure 19. Theoretical and Experimental Enhancement Factors at 20 Atmospheres for the Helium-Ethane System.

these models. Hence, at low pressures by looking at the experimental and calculated B_{12} curves, it is possible to see the effect B_{12} has on the enhancement factor calculations. The LJCL model predicts virial coefficients that are all different from the KIH models. The BWR equation is represented by the BWR(LINEAR) and the BWR(LORENTZ) models. These two models differ only in their predicted value of B_{12} which is shown in Chapter V. Thus, the basic differences between all of these models are shown on the B_{12} curves in Chapter V, and the second and third virial coefficient curves presented in Appendix F.

For the helium-ethane system, Figure 15 shows that the LJCL, KIHEK12, and BWR(LINEAR) models predict enhancement factors that agree well with experiment. The KIHCK12 predicted values differ by a maximum of six percent. The BWR(LORENTZ) and KIH models show values too high by about 11 and 20 percent, respectively.

The helium-ethylene system isotherm presented in Figure 16 shows that the KIHCK12 and KIHEK12 models represent the data within five percent. The LJCL model predicts values that are too low by as much as 11 percent. The BWR(LINEAR) values are high by a maximum of about nine percent, and the BWR(LORENTZ) and KIH values are considerably higher than experiment.

Figure 17 presents an isotherm of the helium-propane system. The BWR(LINEAR), KIHEK12, and KIHCK12 values agree with experiment within five and one-half percent at all points. The LJCL model predicts values too low by about 25 percent, and the BWR(LORENTZ) and KIH values are too high by about 19 percent.

The helium-propylene isotherm is given in Figure 18. The BWR-(LINEAR), KIHEK12, and KIHCK12 models predict values that are all within the experimental accuracy. The KIH and BWR(LORENTZ) models are high by about 25 and 10 percent, respectively. The LJCL model is again predicting values considerably lower than the experimental results.

The enhancement factors predicted by the KIH model were always larger than the enhancement factors predicted by the other models. As the Kihara K_{12} factor is increased from zero, the B_{12} values increase and the enhancement factors decrease. Since the B_{12} term contributes negatively to the enhancement factor when B_{12} is positive, this is the expected trend. These figures generally show that the Kihara K_{12} factor can produce a sizable difference in predicted enhancement factors. The K_{12} values calculated from the correlation of Hiza and Duncan,[53] Equation (V-8), predicted enhancement factors that were slightly higher than the experimental K_{12} values, but they were still in good agreement with experimental enhancement factors. These results tend to give support to this correlation. The pure third virial coefficients used with this model were calculated using the method of Chueh and Prausnitz[16] and are given in Appendix F.

The B_{12} values predicted by the LJCL model were quite satisfactory for the helium-ethane and helium-ethylene systems. Unfortunately, the values for the helium-propane and helium-propylene systems were excessively high. This accounts for the agreement and disagreement of this model at the low pressures for these systems. The strong bending effect shown at high pressures by this model for the helium-ethylene, -propane, and

-propylene systems is indicative of an incorrectly predicted third virial coefficient. Values of the pure third virial coefficients for the Lennard-Jones model are compared to experimental data in Appendix F. In the case of ethane, the agreement is fairly good, but the predicted values for ethylene, propane, and propylene are much larger than experiment. Since the third virial coefficient contributes negatively to the enhancement factor calculation, the bending of the curve is the expected result for these systems.

The BWR(LORENTZ) model predicted theoretical enhancement factors that were always higher than experiment. By simply changing the mixing rule for $(B_o)_{12}$, as Mullins[107] has suggested, the new BWR(LINEAR) model gives results that agree very well with experiment. The values of B_{12} predicted by these models are shown in the experimental B_{12} curves of Chapter V. The linear rule gives B_{12} values that are in much better agreement with experiment as are the enhancement factors predicted by this model. The BWR third virial coefficients predicted using Equation (IV-86) are compared to experimental values in Appendix F. Equation (IV-86) definitely has an incorrect functional form, since at low temperature the theoretical values of C_{111} increase exponentially instead of decreasing with decreasing temperature as do the experimental results. Although this error in the third virial coefficient calculation exists, the predicted enhancement factors agree very well with experiment even at high pressures. There are several possible reasons why the theoretical enhancement factor curves agree with experiment. First, the value of C_{111} starts becoming large at $T_{R_1} < 0.80$, which is the point where this term begins to

contribute very little to the enhancement factor calculation. Second, at this temperature the value of C_{222} is still being calculated correctly. Third, some of the higher order volume terms in the BWR equation, Equation (IV-72), may be compensating for this incorrectly predicted virial coefficient.

Appendix G presents the smoothed experimental and theoretical enhancement factors in Tables 33 to 36 for these four helium binary systems. The theoretical calculations are made over the entire experimental temperature range for the KIH, KIHCK12, KIHEK12, LJCL, and BWR(LINEAR) models. These tables indicate that, as the theoretical B_{12} curves begin to deviate from the experimental B_{12} curves, the various theoretical models incorrectly predict values of the enhancement factor. Therefore, the KIHCK12, KIHEK12, and BWR(LINEAR), while predicting very good enhancement factors at the higher temperatures, do in fact give poor agreement at low temperatures, where the theoretical B_{12} curves do not show the correct temperature dependency. The theoretical and experimental B_{12} curves are presented in Chapter V.

Figure 19 shows the experimental 20 atmosphere enhancement factor isobar for the helium-ethane system together with theoretically predicted enhancement factors. The ability of the theoretical models to predict the minimum and maximum of these isobar curves is a subject of considerable interest. Liu[83] first became aware of this ability of the LJCL and KIH theoretical models in his work on the helium-carbon dioxide system. His theoretical calculations reveal that the same is true for the helium-oxygen, -nitrogen, and -methane systems. More recently, the minimum in

the enhancement factor isobars has been shown to occur experimentally in the helium-ethane,[46,53] -ethylene, and -propane[140] systems. Figure 5 shows the experimental isobars for the helium-ethylene system. Over the range of experiment, the helium-argon system has not shown a minimum either experimentally or theoretically. In observing this phenomenon, Liu[83] states that it is the combination of the relative sizes of the various terms that is important and that no single term by itself could have produced the unusual behavior. Since that time, additional helium systems have shown this type phenomenon, and also the theoretical enhancement factors predicted by the empirical BWR equation have been shown to reproduce this trend. It may now be possible to make a more positive statement as to which terms might be responsible for this unexpected agreement between theory and experiment. This minimum in the enhancement factor isobar curves has not been shown in the various hydrogen binary systems.[54,55,77,107] Therefore, it is speculated that this observation is unique to the helium systems.

The 20 atmosphere enhancement factor isobar curve has been selected for several reasons. First, the maximum in the curve is more pronounced at low pressures. Second, an additional experimental point is obtained. This point corresponds to the temperature where the vapor pressure of ethane is 20 atmospheres since at this point the enhancement factor must be equal to unity. Third, at this low pressure it is possible to neglect the third virial coefficients and Equation (IV-17) becomes:

$$\ell n\ (\phi) = \frac{v_i^o}{RT}\left[(P - P_{o1}) - \frac{\bar{\beta}_T}{2}(P^2 - P_{o1}^2)\right] + \frac{2B_{11}}{V_{o1}} \quad \text{(Continued)} \qquad \text{(VI-1)}$$

$$- \ell n\ (Z_{01}) - \frac{2(y_1 B_{11} + y_2 B_{12})}{V_m} + \ell n\ (Z_m) + \ell n\ (x_1)$$

The magnitude of these various terms in the helium-argon system, which does not show this minimum, and those of the helium-ethane system have been examined. The major difference between these two systems is the magnitude of B_{11} and the sign of B_{12}. For argon the B_{11} value is less negative than for ethane, and B_{12} is very close to zero while the corresponding value for ethane is large and positive. It now appears that the magnitude of the term $- \frac{2}{V_m} (y_1 B_{11} + y_2 B_{12})$ in Equation (IV-17) is responsible for the predicted minimum in these various helium binary systems. As the temperature increases the only variable that changes appreciably is y_1. Since the value of B_{11} is negative, the term begins to add excessively to the value of $\ell n(\phi)$. The positive value of B_{12} subtracts from $\ell n(\phi)$ appreciably at low temperatures. This has the effect of lowering $\ell n(\phi)$ and thereby making the minimum more pronounced. In the helium-argon system, the B_{11} value of argon is not large enough to cause a minimum in the curve.

Although this investigation has not been comprehensive, it does provide a little insight into the unusual results obtained for these systems. The position of the minimum in these curves is a function of the mole fraction, the magnitude of the second virial coefficient, B_{11}, and the second interaction virial coefficient B_{12}.

CHAPTER VII

EXPERIMENTAL HENRY'S LAW CONSTANTS AND PARTIAL MOLAR VOLUMES AT INFINITE DILUTION

Introduction

In 1803 William Henry observed that the solubility of a gas in a liquid is directly proportional to its partial pressure in the vapor phase. The relation used to express this observation is

$$Py_2 = Hx_2 \tag{VII-1}$$

Equation (VII-1) is used even today, but its applications are limited to systems where the partial pressure and solubility of the solute are small and the temperature is well below the critical of the solvent. Hence, just as the ideal gas law is a simplified form of the more complex virial equation, Equation (VII-1) represents a simplification of a more exact thermodynamic relation.

The type of systems considered in this chapter are binary systems, which have one of their components well above its critical temperature, a gas, and one below its critical, a liquid. Therefore conditions are such that

$$T > T_{c_2} \tag{VII-2}$$

$$T < T_{c_1} \tag{VII-3}$$

The criterion for phase equilibrium as stated in Chapter IV can be

used to describe this phenomenon. For the equilibrium of component 2, in the gas and liquid phases, one obtains the expression

$$\mu_2^G(P,T,y_2) = \mu_2^L(P,T,x_2) \qquad \text{(VII-4)}$$

It is now possible to substitute known thermodynamic relations for the above quantities. For the chemical potential of the liquid phase, we use the relation

$$\mu_2^L(P,T,x_2) = \mu_2^*(P,T) + RT\ \ell n(\gamma_2' x_2) \qquad \text{(VII-5)}$$

Since component 2 is above its critical temperature, the definition of γ_2' must be specified as

$$\gamma_2'(P,T,x_2) \rightarrow 1 \qquad \text{as } x_2 \rightarrow 0 \qquad \text{and } P \rightarrow P_{o1} \qquad \text{(VII-6)}$$

The chemical potential of the gas phase may be related to the fugacity of the mixture by

$$\mu_2^G(P,T,y_2) - \mu_2^o(P=1,T) = RT\ \ell n \left(\frac{f_2^G}{f_2^o}\right) \qquad \text{(VII-7)}$$

The chemical potential $\mu_2^o(P=1,T)$ of the reference state is for an ideal gas at one atmosphere, hence the reference fugacity, f_2^o, is taken equal to one atmosphere. Substitution of Equations (VII-5) and (VII-7) into Equation (VII-4) yields

$$\ell n \left(\frac{f_2^G(P,T,y_2)}{x_2} \right) = \ell n \; H_2(P,T) + \ell n \; (\gamma_2') \qquad \text{(VII-8)}$$

where

$$\ell n \; H_2(P,T) = \frac{\mu_2^*(P,T) - \mu_2^o(P=1,T)}{RT} \qquad \text{(VII-9)}$$

Equation (VII-9) is the definition of the thermodynamic Henry's law constant, $H_2(P,T)$. It is dimensionless and is a function of temperature and pressure. The Henry's law constant at infinite dilution, H_2^∞, is equal to Equation (VII-9) in the limit as $x_2 \rightarrow 0$ and $P \rightarrow P_{o1}$ at the given temperature.

Differentiating Equation (VII-5) with respect to pressure at constant composition yields

$$\left(\frac{\partial \mu_2^L}{\partial P} \right)_{T,x} = \left(\frac{\partial \mu_2^*(P,T)}{\partial P} \right)_T + RT \left(\frac{\partial \ell n(\gamma_2')}{\partial P} \right)_{T,x} \qquad \text{(VII-10)}$$

If the region of interest is near $x_2 = 0$, we have the condition that $\gamma_2' = 1$ and we obtain

$$\left(\frac{\partial \mu_2^*(P,T)}{\partial P} \right)_T = \overline{V}_2^\infty \qquad \text{(VII-11)}$$

Likewise differentiating Equation (VII-9) gives

$$\left(\frac{\partial \ell n \; H_2(P,T)}{\partial P} \right)_T = \frac{1}{RT} \left(\frac{\partial \mu_2^*}{\partial P} \right)_T = \frac{\overline{V}_2^\infty}{RT} \qquad \text{(VII-12)}$$

and after integration of this equation

$$\ell n\ H_2(P,T) = \ell n\ H_2^{\infty}(P_{O1},T) + \frac{1}{RT}\int_{P_{O1},T}^{P,T} \overline{V}_2^{\infty}\, dP \qquad \text{(VII-13)}$$

Substitution of Equation (VII-13) into Equation (VII-8) gives[107,110,147]

$$\ell n\left(\frac{f_2^G}{x_2}\right) = \ell n\ H_2^{\infty}(P_{O1},T) + \frac{1}{RT}\int_{P_{O1},T}^{P,T} \overline{V}_2^{\infty}\, dP + \ell n\ (\gamma_2') \qquad \text{(VII-14)}$$

Equation (VII-14) is an exact solution to the problem of gas solubility in a liquid phase. If one assumes that $\overline{V}_2^{\infty}$ is independent of pressure, then

$$\ell n\left(\frac{f_2^G}{x_2}\right) = \ell n\ H_2^{\infty}(P_{O1},T) + \frac{\overline{V}_2^{\infty}(P - P_{O1})}{RT} + \ell n\ (\gamma_2') \qquad \text{(VII-15)}$$

To predict values of the gas solubility, x_2, from Equation (VII-15), the following properties of the system are needed:

(1) The fugacity of the gas phase, f_2^G.

(2) Henry's law constant at infinite dilution, $H_2^{\infty}(P_{O1},T)$.

(3) The partial molar volume at infinite dilution, $\overline{V}_2^{\infty}$.

(4) The activity coefficient of the solution, γ_2'.

Equation (VII-15) is often used to extract H_2^{∞} and $\overline{V}_2^{\infty}$ values from phase equilibrium data. Since these two quantities have well-defined physical meanings, their values may give some insight into the types of interactions occurring in the liquid phase. Values of H_2^{∞} and $\overline{V}_2^{\infty}$ from binary systems might prove useful in the prediction of multicomponent gas phase liquid solubilities. An equation of state for the gas phase allows one to compute f_2^G. Equation (VII-15) suggests that a plot of $\ell n\left(\frac{f_2^G}{x_2}\right)$ versus

$(P - P_{01})$ should give a straight line in the neighborhood of $(P - P_{01}) = 0$, whose intercept at $(P - P_{01}) = 0$ is equal to $\ell n\ H_2^{\infty}$ and whose slope is equal to $\overline{V_2^{\infty}}/(RT)$. If the γ_2' term becomes large at high pressures, the line would curve up or down depending on whether the system exhibits positive or negative deviation from Henry's law. The liquid composition for all the systems considered in this work were very often less than 10 mole percent, which suggests that γ_2' may not deviate appreciably from unity. A value of γ_2' close to unity is important since a larger value could definitely affect the slope of the line and thereby cause errors in the $\overline{V_2^{\infty}}$ calculation. If the solution is assumed to be ideal, Equation (VII-15) reduces to the Krichevsky-Kasarnovsky[80] equation.

$$\ell n \left(\frac{f_2^G}{x_2}\right) = \ell n\ H_2^{\infty}\ (P_{01}, T) + \frac{\overline{V_2^{\infty}}\ (P - P_{01})}{RT} \qquad \text{(VII-16)}$$

This is the equation that has been used in this work.

Since values of y_1 and x_2 have already been smoothed for the helium binary systems, the only problem involved in this calculation is the evaluation of the gas phase fugacity, f_2^G. It is possible to evaluate the fugacity from the following equation, where the reference state is the same as in Equation (VII-7).

$$\ell n\ f_2^G = + \frac{1}{RT} \int_V^{\infty} \left[\left(\frac{\partial P}{\partial n_2}\right)_{V,T,n-1} - \frac{RT}{V}\right] dV - \ell n \left(\frac{V}{n_2 RT}\right) \qquad \text{(VII-17)}$$

There are many possible equations of state for the gas mixture, but since data for the virial equation have been extracted in Chapter V, it will

be used in this calculation. The virial equation for a mixture has already been presented as Equation (IV-14). Substituting the differentiated form of this equation into Equation (VII-17) and integrating, one obtains the following expression for the left side of Equation (VII-16)

$$\ln\left(\frac{f_2^G}{x_2}\right) = \frac{2(y_1 B_{12} + y_2 B_{22})}{V_m} + \frac{3(y_1^2 C_{112} + 2y_1 y_2 C_{122} + y_2^2 C_{222})}{2V_m^2} \qquad \text{(VII-18)}$$

$$+ \ln\left(\frac{y_2 RT}{x_2 V_m}\right)$$

The evaluation of V_m was made using the virial equation through the third virial coefficient. Values of x_2, y_1, B_{12}, and C_{222} were read into the calculations. The C_{222} values are given in Figure 49 of Appendix F, and the values of B_{12} were obtained from Liu[83] and from this work. B_{22} and B_{11} were calculated from Lennard-Jones and Kihara parameters, respectively. These parameters are those presented in Appendix F. The method of Chueh and Prausnitz[16] was used to calculate the third virial coefficients, C_{111}, C_{112}, and C_{122}. The parameters needed for this calculation are presented in Table 28 of Appendix F. The K_{12} values used in this calculation are those determined in this work, and they are given in Table 7.

A paper was recently published by Solen, et al.[147] which presents H_2^∞ for different helium binary systems. This work of Solen, et al. used a form of the Redlich-Kwong equation to calculate the gas phase fugacity. Their values of H_2^∞ are based on a vapor pressure of zero for all experimental points, which is the approach shown in an earlier paper of Prausnitz.[118] To compare the values of Solen, et al. to those of this work,

it was necessary to use their value of $\bar{V}_2^{\infty}$ and the following equation

$$H_2^{\infty}\ (P = P_{O1}, T) = H_2^{\infty}\ (P = 0, T)\ \exp\left(\frac{\bar{V}_2^{\infty} P_{O1}}{RT}\right) \qquad \text{(VII-19)}$$

Their values of $\bar{V}_2^{\infty}$ are not compared in this chapter since they were calculated using the theoretical method of Chueh and Prausnitz[18] and are not extracted from the experimental data.

Other investigators have attempted to extract H_2^{∞} and $\bar{V}_2^{\infty}$ using the Lewis-Randall rule to calculate the fugacity.[145] This rule defines the fugacity of component i in the mixture as

$$f_i^G = y_i f_{(pure)}^G \qquad \text{(VII-20)}$$

where $f_{(pure)}^G$ is the fugacity of pure component i. This is equivalent to letting $y_1 = 0$ in Equation (VII-18). Hence, this rule becomes invalid as the value of y_1 differs from zero.

Another means of correlating liquid phase solubility data is to plot

$$\bar{K} \equiv \frac{P - P_{O1}}{x_2} \quad \text{versus} \quad (P - P_{O1}) \qquad \text{(VII-21)}$$

Then

$$\bar{K}^{\infty} \equiv \lim_{x_2 \to 0} \frac{P - P_{O1}}{x_2} \qquad \text{(VII-22)}$$

This method is used in checking thermodynamic consistency of data and is hereafter called the consistency method. Mullins,[107] Hiza, et al.,[47,54,55] and Heck[46] have used this method, and they describe this $\bar{K}^{\infty}$ as a pseudo

Henry's law constant. This method is not easily related to the limiting form of Equation (VII-15) and therefore has no apparent thermodynamic significance. However, values of H_2^{∞} ($P = P_{o1}, T$) predicted using this method appear to agree well with the values calculated from the more elaborate methods. Because of the simplicity of this calculation, values using this method have been calculated for comparison.

The following sections present the Henry's law constants extracted in this work together with those extracted by other people for the various cryogenic liquids that have helium dissolved in them. This is a comparative presentation of the methods available for the extraction of Henry's law constants from solubility data. The smoothed values of H_2^{∞} that are presented in the following Tables represent an average of the values from the available methods. The experimental values of $\overline{V_2}^{\infty}$ that have been extracted in this work have been smoothed and are presented in the following tables. No independent experimental values of $\overline{V_2}^{\infty}$ were available for comparison.

Extraction of H_2^{∞} and $\overline{V_2}^{\infty}$ from Phase Equilibrium Data

H_2^{∞} ($P = P_{o1}, T$) and $\overline{V_2}^{\infty}$ for the Helium-Argon System

Phase equilibrium data of Mullins[107] are used over a temperature range of 86.02 to 108.02 K and pressures up to 120 atmospheres. The smoothed y_1 and x_2 phase equilibrium values are taken from Liu.[83]

Figure 20 shows the values of H_2^{∞} as a function of temperature for the helium-argon system. The values obtained in this work for the helium-argon system are in good agreement with those of Solen, et al.,[147] after

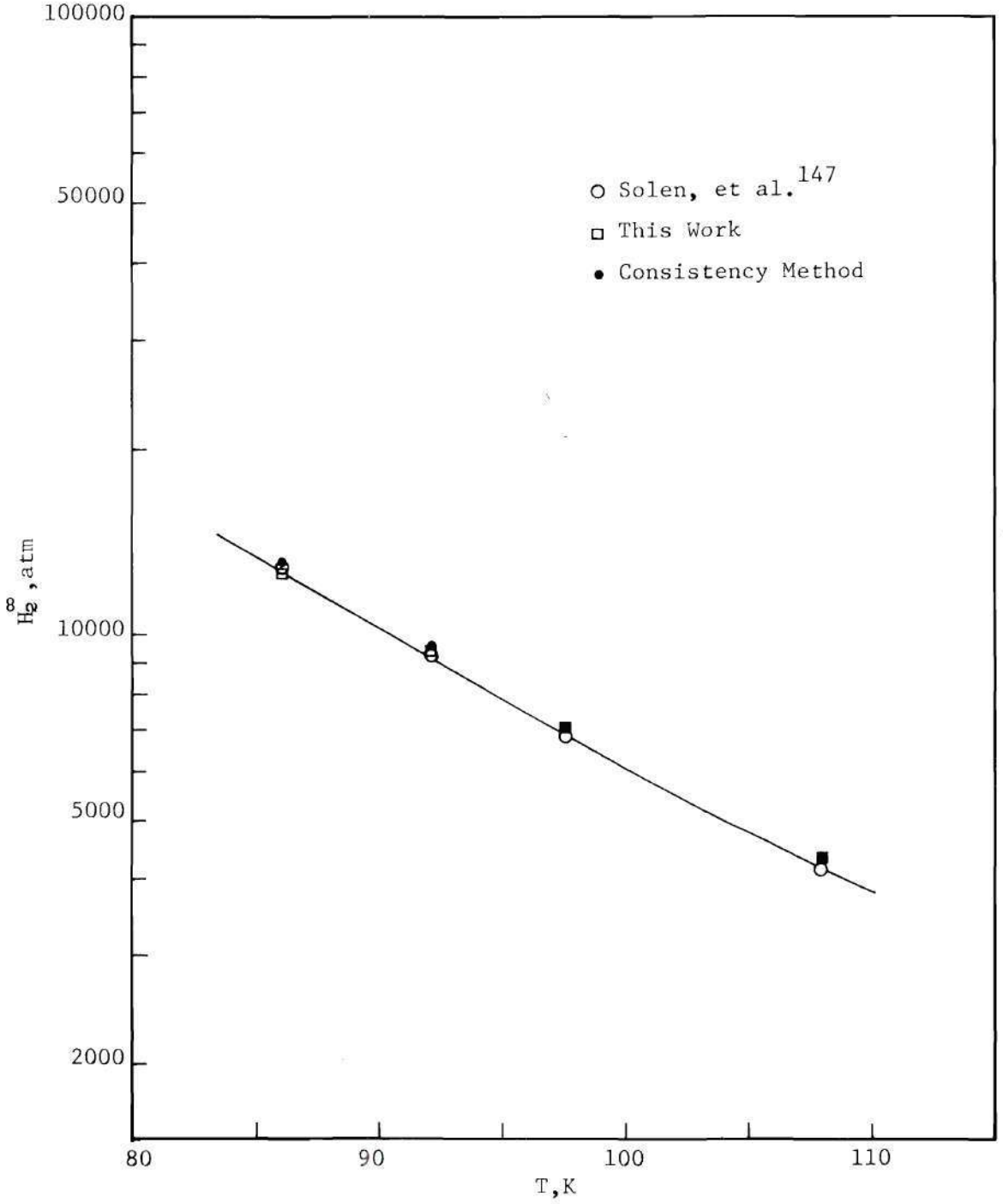

Figure 20. Experimentally Determined Henry's Law Constants for the Helium-Argon System.

correction using Equation (VII-19). Values obtained using the consistency method give surprisingly good agreement, considering the simplicity of the method.

Smoothed values of H_2^∞ and $\overline{V}_2^\infty$ are presented in Table 8. The uncertainty of these numbers, due to the estimated uncertainty of x_2 and y_1, was 2.6 percent of H_2^∞ and five percent of the $\overline{V}_2^\infty$ values.

Table 8. H_2^∞ and $\overline{V}_2^\infty$ for the Helium-Argon System

T,K*	H_2^∞, atm		$\overline{V}_2^\infty$, cc/gm mole	
	Calculated	Smoothed	Calculated	Smoothed
86.02	12,660 ± 266	12,660	22.7 ± 0.2	22.7
91.98	9,285 ± 208	9,375	23.1 ± 0.5	22.9
97.51	7,037 ± 167	7,055	23.1 ± 0.78	23.1
108.02	4,374 ± 114	4,225	23.9 ± 1.3	23.9

*Corresponding vapor pressure values are given by Liu.[83]

H_2^∞ ($P = P_{o1}, T$) and $\overline{V}_2^\infty$ for the Helium-Oxygen System

The phase equilibrium data for this system have been determined by Herring and Barrick.[48] Their work covers a temperature range of 69.9 to 149.91 K and pressures up to 200 atmospheres. The data have been smoothed by Liu[83] and are used in this work.

Figure 21 shows the values of H_2^∞ calculated from these data together with the results from Solen, et al.[147] and the consistency method. Agreement is very good at low temperatures, but at high temperatures the differences become systematically larger. The maximum difference between

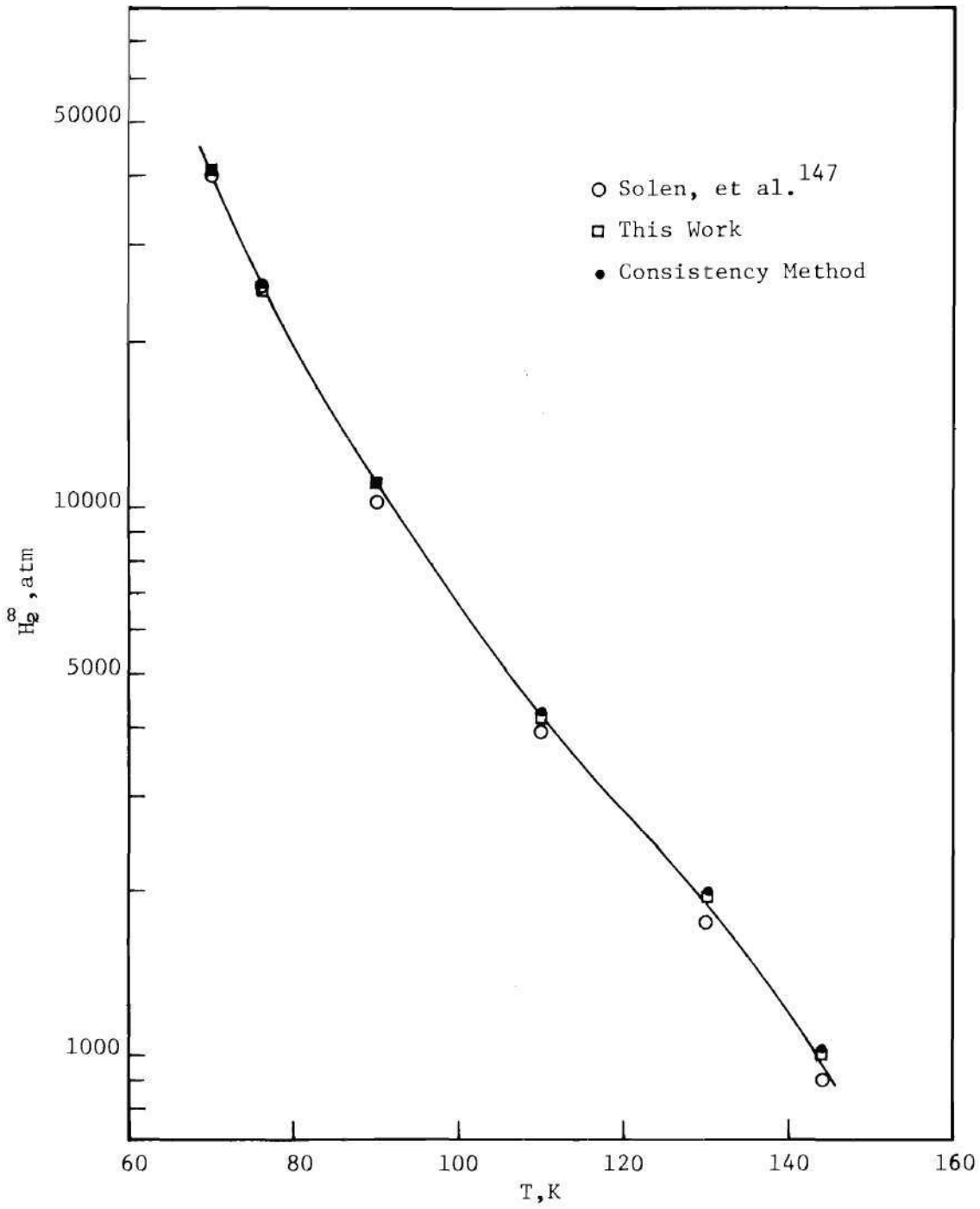

Figure 21. Experimentally Determined Henry's Law Constants for the Helium-Oxygen System.

this work and that of Solen is about ± 10 percent.

The smoothed values of H_2^∞ and $\overline{V}_2^\infty$ are presented in Table 9 together with their uncertainty due to a ± 3 percent error in y_1 and x_2. This produced a maximum error of 5.5 percent in H_2^∞ and of 7.5 percent in $\overline{V}_2^\infty$ at 143.93 K.

Table 9. H_2^∞ and $\overline{V}_2^\infty$ for the Helium-Oxygen System

T,K*	H_2^∞, atm		$\overline{V}_2^\infty$, cc/gm mole	
	Calculated	Smoothed	Calculated	Smoothed
69.90	41,110 ± 1,280	39.750	15.1 ± 0	16.7
75.90	24,390 ± 803	25,100	19.0 ± 0.12	17.1
89.98	11,260 ± 396	11,250	18.0 ± 0.29	18.0
109.96	4,184 ± 182	4,180	21.4 ± 0.98	19.4
129.95	1,956 ± 97	1,880	17.9 ± 1.4	21.0
143.93	1,004 ± 54	965	22.6 ± 1.8	22.6

*Corresponding vapor pressure values are given by Liu.[83]

H_2^∞ ($P = P_{O1}, T$) and $\overline{V}_2^\infty$ for the Helium-Nitrogen System

Gas-liquid phase equilibrium of this system has been measured by Rodewald, et al.[133] and DeVaney, et al.[28] These data cover a temperature range of 64.9 to 120.0 K and pressures up to 140 atmospheres. These data have been separately smoothed by Liu.[83] Several isotherms from the data of Rodewald, et al.[133] at low temperatures (64.9 to 77.2 K) and all of the data of DeVaney, et al.[28] were used in this work to calculate H_2^∞. The paper by Solen, et al.[147] calculated H_2^∞ using the data of Rodewald.

Figure 22 indicates the disagreement between the two sets of

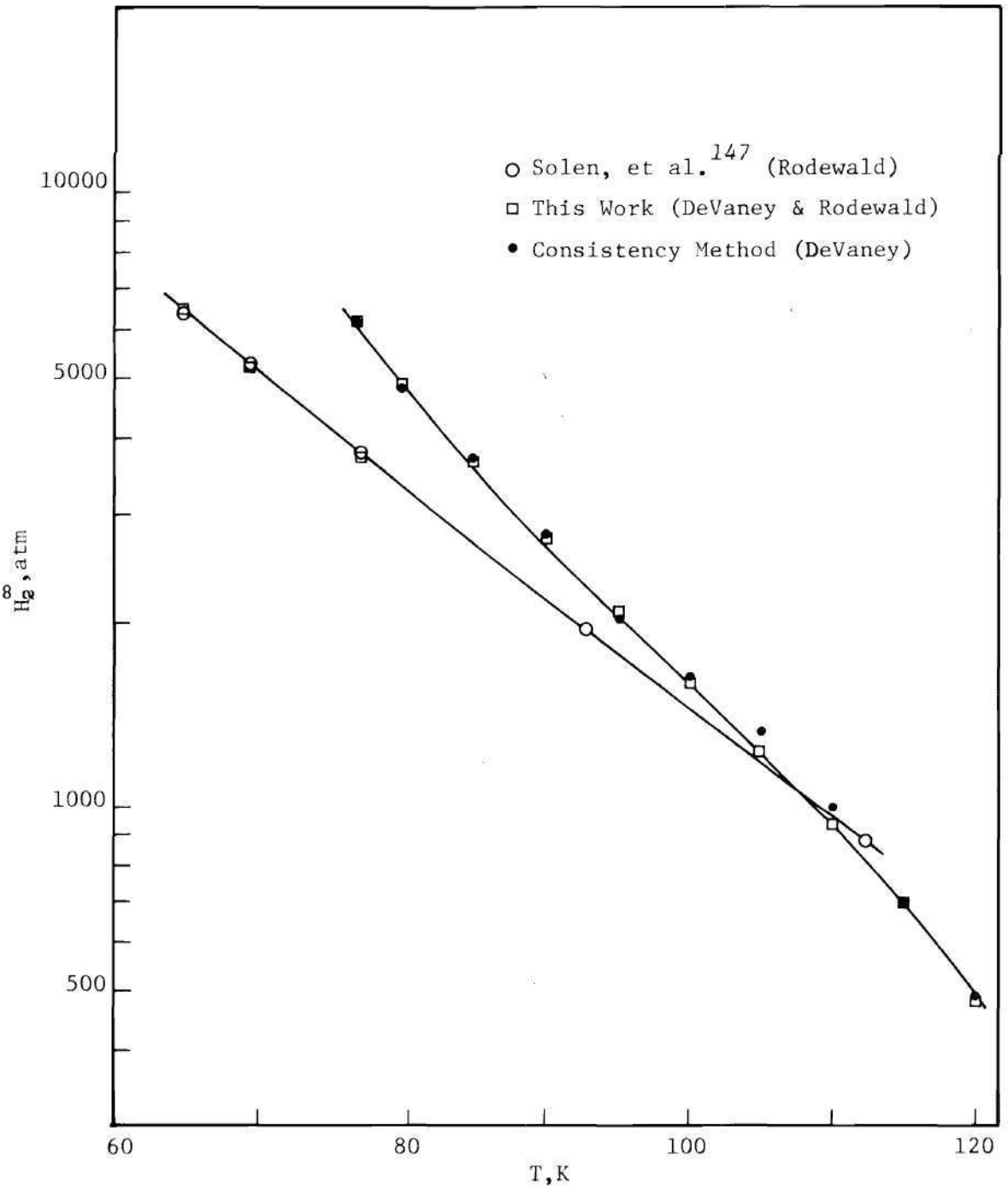

Figure 22. Experimentally Determined Henry's Law Constants for the Helium-Nitrogen System.

experimental data by the large difference between the extracted Henry's law constants. Within each set of data the agreement between methods is quite good. The smoothed molar volume data were obtained using the data of DeVaney.

A ± 3 percent uncertainty in y_1 and x_2 produces a maximum error of seven percent in H_2^{∞} and eight percent in $\overline{V}_2^{\infty}$ at the highest temperature. Both the rough and smoothed H_2^{∞} and $\overline{V}_2^{\infty}$ values are given in Table 10.

Table 10. H_2^{∞} and $\overline{V}_2^{\infty}$ for the Helium-Nitrogen System

T,K*	H_2^{∞}, atm		$\overline{V}_2^{\infty}$, cc/gm mole	
	Calculated	Smoothed	Calculated	Smoothed
77.0	6,119 ± 190	6,100	13.1 ± 0.1	12.9
80.0	4,803 ± 161	4,940	13.9 ± 0.36	13.1
85.0	3,618 ± 135	3,620	12.7 ± 0.80	13.9
90.0	2,740 ± 114	2,720	13.8 ± 1.2	15.2
95.0	2,069 ± 93.7	2,065	17.2 ± 1.7	17.3
100.0	1,595 ± 78.5	1,585	20.9 ± 2.1	20.3
105.0	1,242 ± 64.0	1,240	23.7 ± 2.6	24.5
110.0	926.3 ± 52.8	933	31.1 ± 3.0	30.1
115.0	696.5 ± 42.5	683	38.8 ± 3.5	38.8
120.0	479.7 ± 31.2	481	51.8 ± 3.9	51.4

*Corresponding vapor pressure values are given by Liu.[83]

H_2^{∞} ($P = P_{O1}$,T) and $\overline{V}_2^{\infty}$ for the Helium-Carbon Dioxide System

Phase equilibrium measurements in the gas-liquid region have been made by Barrick, et al.[2] These data cover the temperature range of 219.9 to 274.9 K and pressures up to 200 atmospheres. These data have been smoothed by Liu[83] and were all used except for the lowest temperature,

219.9 K. The calculations of $\ell n \left(\frac{f_2}{x_2}\right)$ at this temperature showed great scatter.

Figure 23 shows that the results of this work and those of Solen, et al.[147] for H_2^∞ differ by a maximum of seven percent. Calculated and smoothed values for H_2^∞ and $\overline{V}_2^\infty$ are presented in Table 11. A ± 3 percent uncertainty in y_1 and x_2 produces a maximum error of six percent in H_2^∞ and a four percent change in $\overline{V}_2^\infty$ at the highest temperature, 274.9 K.

Table 11. H_2^∞ and $\overline{V}_2^\infty$ for the Helium-Carbon Dioxide System

T,K*	H_2^∞, atm		$\overline{V}_2^\infty$, cc/gm mole	
	Calculated	Smoothed	Calculated	Smoothed
229.9	8,356 ± 243	8,480	20.2 ± 0.0	20.4
244.9	5,445 ± 214	5,450	28.9 ± 0.44	28.8
259.9	3,740 ± 186	3,640	42.9 ± 0.87	37.3
274.9	2,490 ± 150	2,500	39.9 ± 1.3	46.1

*Corresponding vapor pressure values are given by Liu.[83]

H_2^∞ ($P = P_{01}$,T) and $\overline{V}_2^\infty$ for the Helium-Methane System

Two sets of phase equilibrium data have been smoothed by Liu.[83] The data of Heck and Hiza[47] cover a temperature range of 94.97 to 184.83 K and pressures up to 200 atmospheres. The second set of data are from Sinor, et al.[145] and cover a temperature range of 113.15 to 188.15 K and pressures up to 130 atmospheres. Since both sets of data appear equally smooth, it was decided to calculate H_2^∞ from both. The liquid phase data of Sinor, et al.[154] smoothed by Liu were found to contain an error at

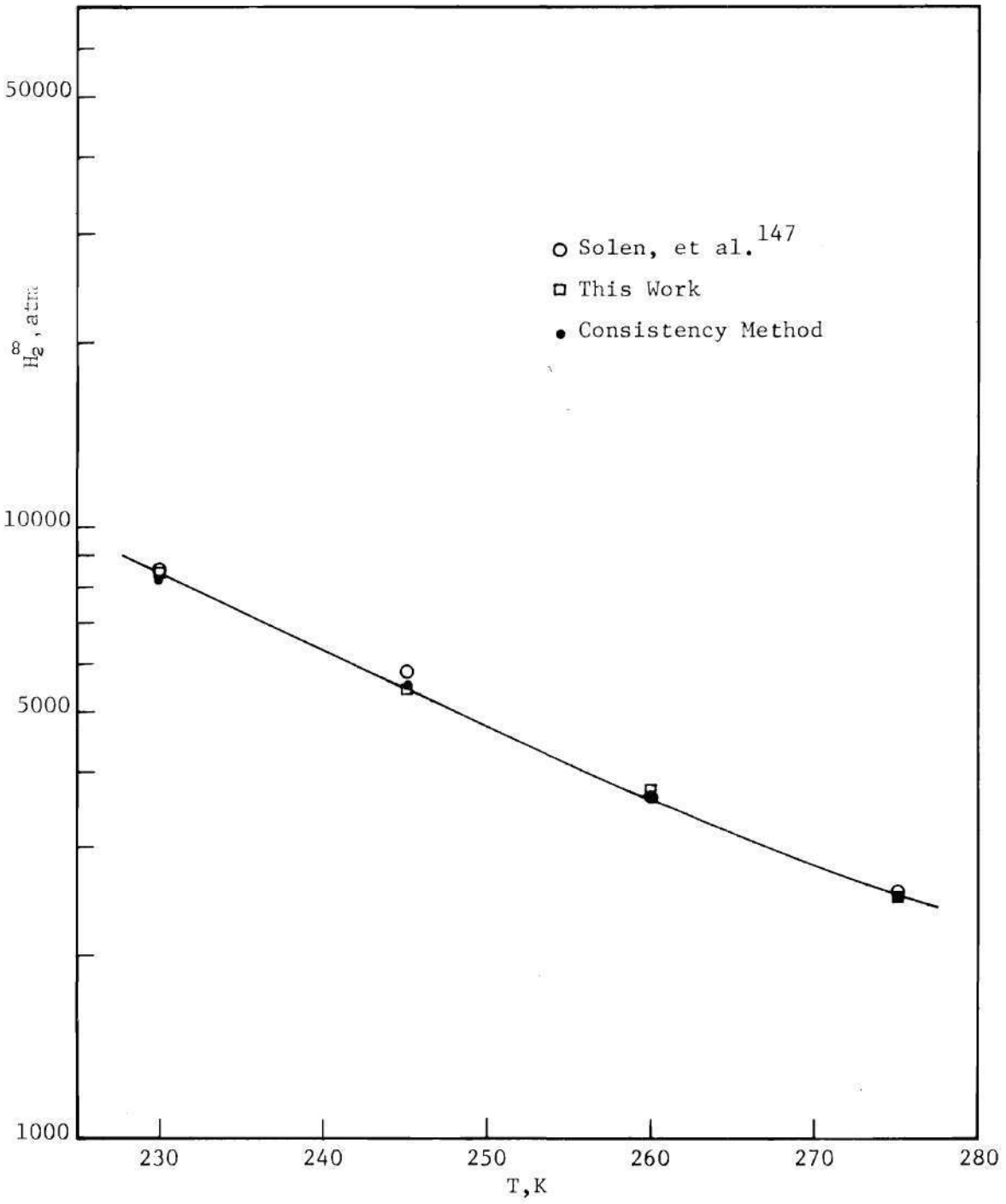

Figure 23. Experimentally Determined Henry's Law Constants for the Helium-Carbon Dioxide System.

113.15 K. These values were corrected for use in this work.

Figure 24 shows that the H_2^∞ values calculated from the two sets of data agreed very well. Solen, et al.[147] used the data of Heck and Hiza[47] in their work. The maximum difference between this work and that of Solen, et al.[147] was 10 percent.

The experimental uncertainty of ± 3 percent in y_1 and x_2 produced a maximum uncertainty of six percent in H_2^∞ and three percent in $\overline{V_2}^\infty$ at the highest temperatures. The smoothed and calculated values of H_2^∞ and $\overline{V_2}^\infty$ are presented in Table 12.

H_2^∞ ($P = P_{01}, T$) and $\overline{V_2}^\infty$ for the Helium-Ethane System

The gas-liquid equilibrium for this system has been studied by Heck.[46] These data have been smoothed and are presented in Appendix G. The temperature range is 170 to 290 K and pressures are up to 200 atmospheres. These same data were used by Solen, et al.[147] to obtain H_2^∞. Their results compare well with the results of this work as is shown in Figure 25. The two methods differ by a maximum of about four percent. The calculated and smoothed H_2^∞ and $\overline{V_2}^\infty$ values are presented in Table 13.

The introduction of an uncertainty of ± 3 percent in y_1 and x_2 produced a maximum uncertainty of four percent in H_2^∞ and of six percent in $\overline{V_2}^\infty$.

H_2^∞ ($P = P_{01}, T$) and $\overline{V_2}^\infty$ for the Helium-Ethylene System

The only complete set of gas-liquid equilibrium data for this system was done in this work. The smoothed data for this system are presented in Appendix G. These data cover the temperature range of 129.98 to 216.04 K and pressures up to 120 atmospheres. Since these data were

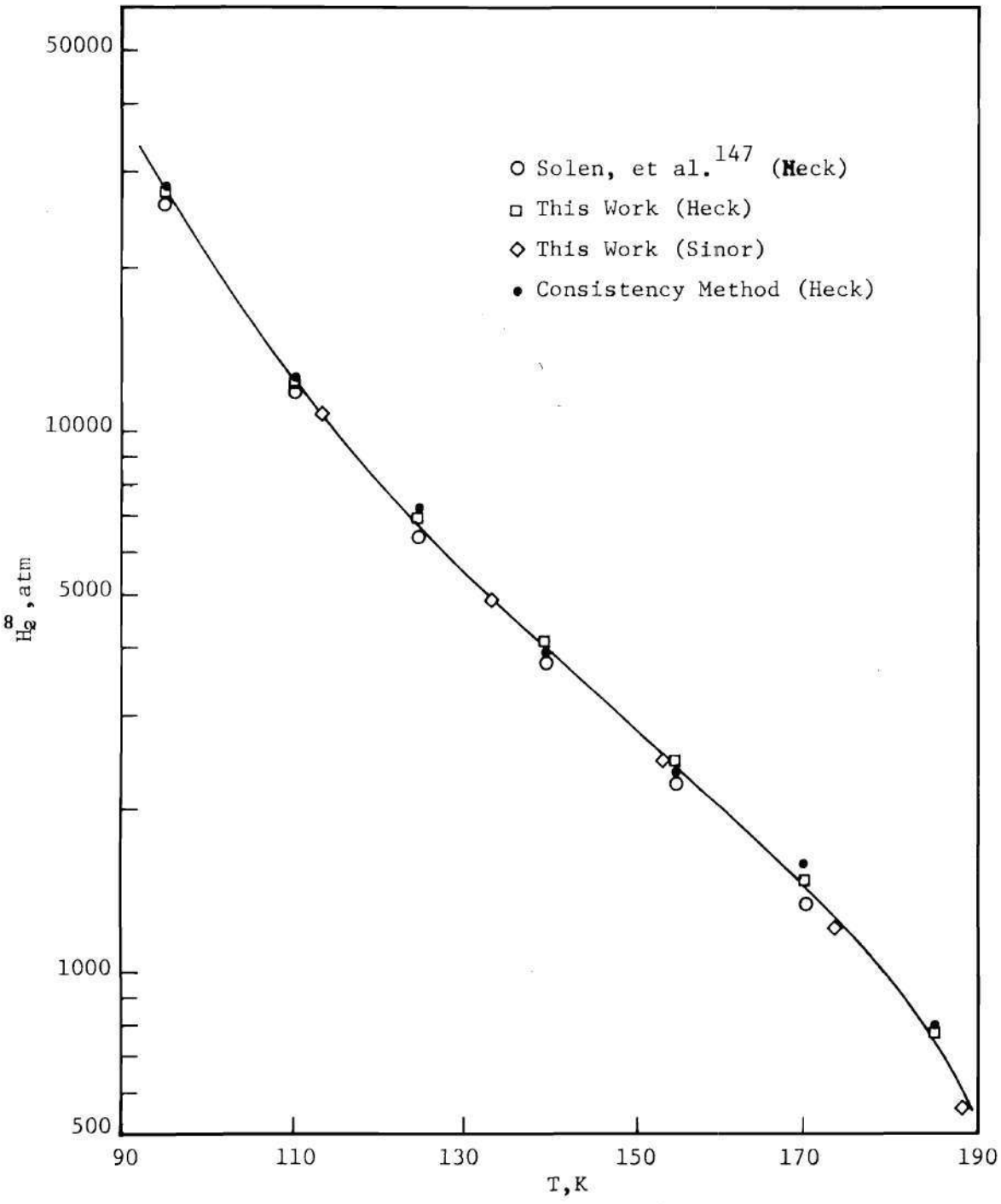

Figure 24. Experimentally Determined Henry's Law Constants for the Helium-Methane System.

Table 12. H_2^{∞} and $\overline{V_2}^{\infty}$ for the Helium-Methane System

T,K*	H_2^{∞}, atm		$\overline{V_2}^{\infty}$, cc/gm mole	
	Calculated	Smoothed	Calculated	Smoothed
94.97	27,640 ± 692	27,100	23.1 ± 0.3	24.8
109.90	12,335 ± 363	12,350	28.4 ± 0.5	25.7
113.15	11,085 ± 336	10,800	25.1 ± 0.6	26.0
124.85	6,974 ± 236	6,775	28.2 ± 0.7	27.2
133.15	4,886 ± 177	4,890	31.0 ± 0.8	28.2
139.83	4,138 ± 158	3,950	30.9 ± 0.9	29.5
153.15	2,503 ± 106	2,510	31.2 ± 1.1	33.1
154.80	2,518 ± 106	2,390	33.8 ± 1.1	33.4
169.81	1,491 ± 70	1,440	42.0 ± 1.3	41.6
173.15	1,222 ± 63.5	1,260	44.1 ± 1.3	43.9
184.83	775.9 ± 43	758	63.4 ± 1.5	56.8
188.15	570.8 ± 33	600	54.2 ± 1.5	60.0

*Corresponding vapor pressure values are given by Liu.[83]

Table 13. H_2^{∞} and $\overline{V_2}^{\infty}$ for the Helium-Ethane System

T,K*	H_2^{∞}, atm		$\overline{V_2}^{\infty}$, cc/gm mole	
	Calculated	Smoothed	Calculated	Smoothed
170	14,370 ± 374	14,550	23.4 ± 1.4	23.4
200	7,058 ± 206	6,920	26.4 ± 1.2	26.4
230	3,810 ± 124	3,720	30.9 ± 1.1	31.9
260	1,937 ± 69	1,930	48.9 ± 0.95	48.0
290	953.5 ± 37	970	75.6 ± 0.80	76.3

*Corresponding vapor pressure values are given in Table 30.

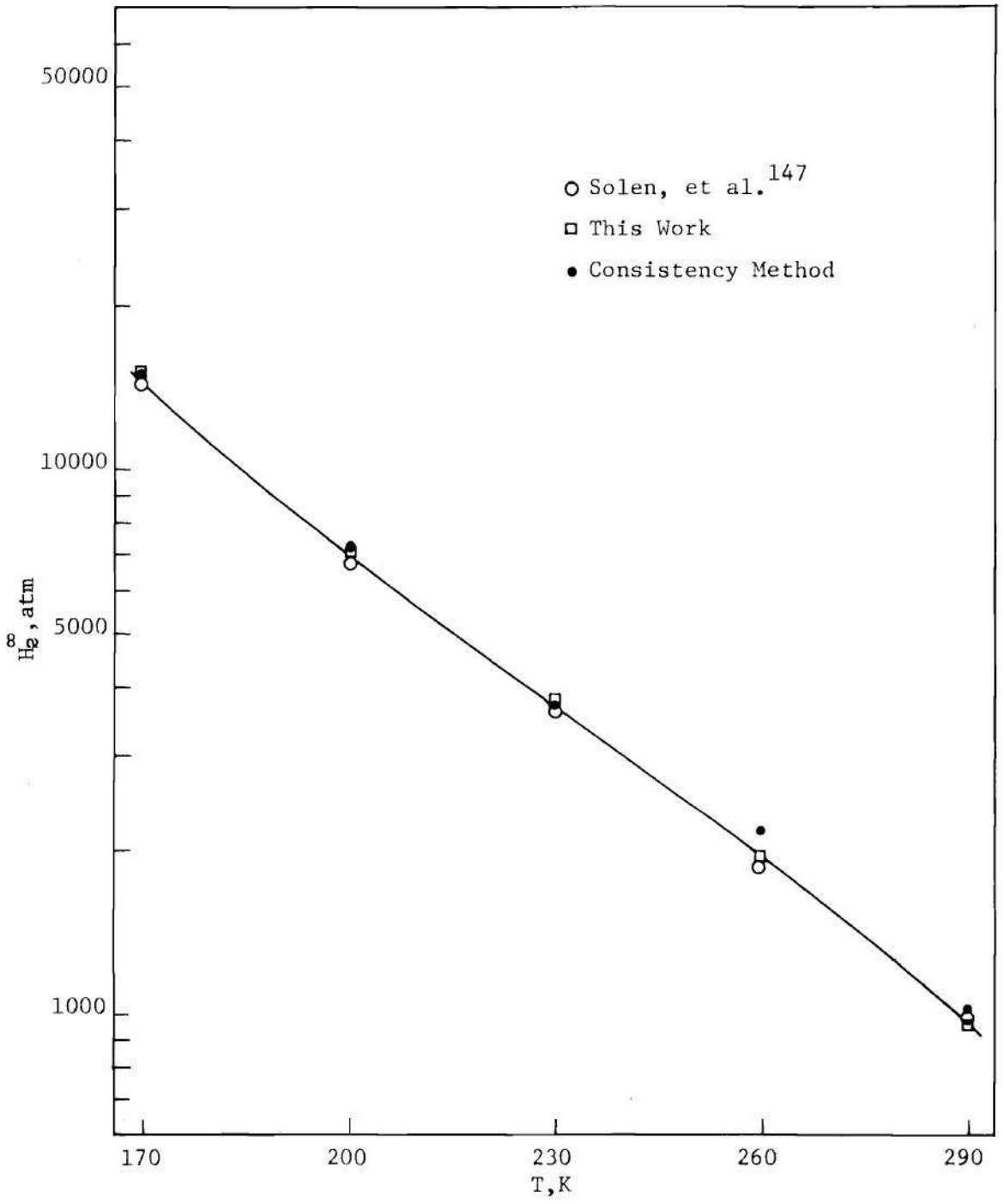

Figure 25. Experimentally Determined Henry's Law Constants for the Helium-Ethane System.

not available to Solen, et al.,[147] the only comparison is with the consistency method. Figure 26 shows that the results are quite smooth and agreement is very good.

Table 14 presents the calculated and smoothed values of H_2^∞ and $\overline{V}_2^\infty$. The experimental uncertainty of y_1 and x_2 produced a maximum uncertainty of four percent in H_2^∞ and about two percent in $\overline{V}_2^\infty$.

Table 14. H_2^∞ and $\overline{V}_2^\infty$ for the Helium-Ethylene System

T, K*	H_2^∞, atm		$\overline{V}_2^\infty$, cc/gm mole	
	Calculated	Smoothed	Calculated	Smoothed
129.98	62,640 ± 1,880	62,800	18.3 ± 0.4	20.5
150.01	27,640 ± 895	27,700	22.9 ± 0.3	21.3
162.00	18,215 ± 615	18,350	23.9 ± 0.3	21.9
173.99	12,559 ± 441	12,650	23.4 ± 0.7	22.8
188.02	8,543 ± 314	8,520	23.7 ± 0.2	24.5
202.01	5,978 ± 230	5,900	26.4 ± 0.1	27.4
216.04	4,143 ± 166	4,190	36.7 ± 0.1	35.3

*Corresponding vapor pressure values are given in Table 29.

H_2^∞ ($P = P_{O1}$, T) and $\overline{V}_2^\infty$ for the Helium-Propane System

Schindler, et al.[140] have obtained gas-liquid equilibrium data for this system over the temperature range of 198.15 to 348.15 K and pressures up to 200 atmospheres. These data have been smoothed and they are presented in Appendix G. Figure 27 shows a comparison of the calculated Henry's law constants. Agreement is fairly good between this work and that of Solen, et al.[147] The two methods differ by a maximum of about 13 percent at the highest temperature.

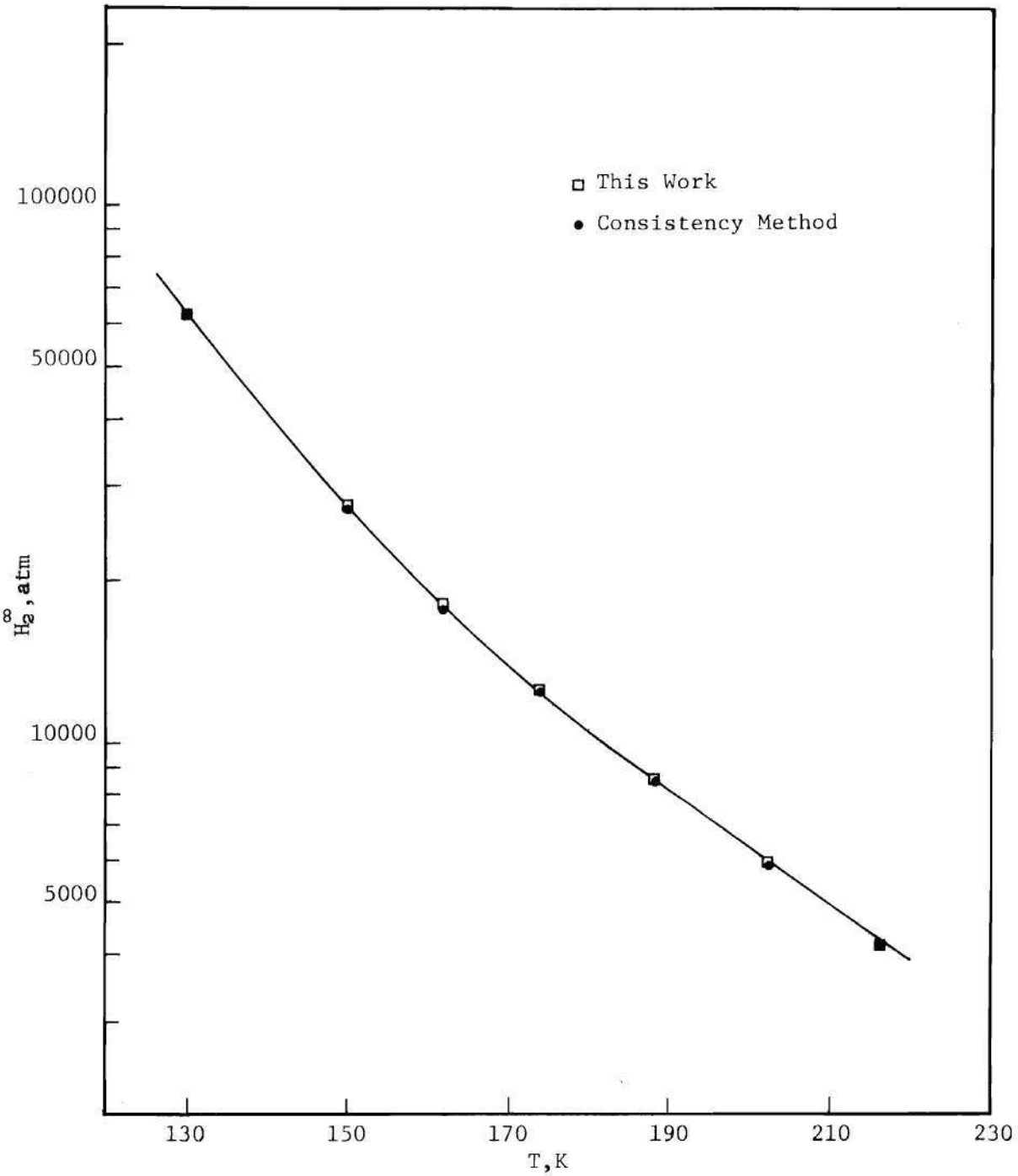

Figure 26. Experimentally Determined Henry's Law Constants for the Helium-Ethylene System.

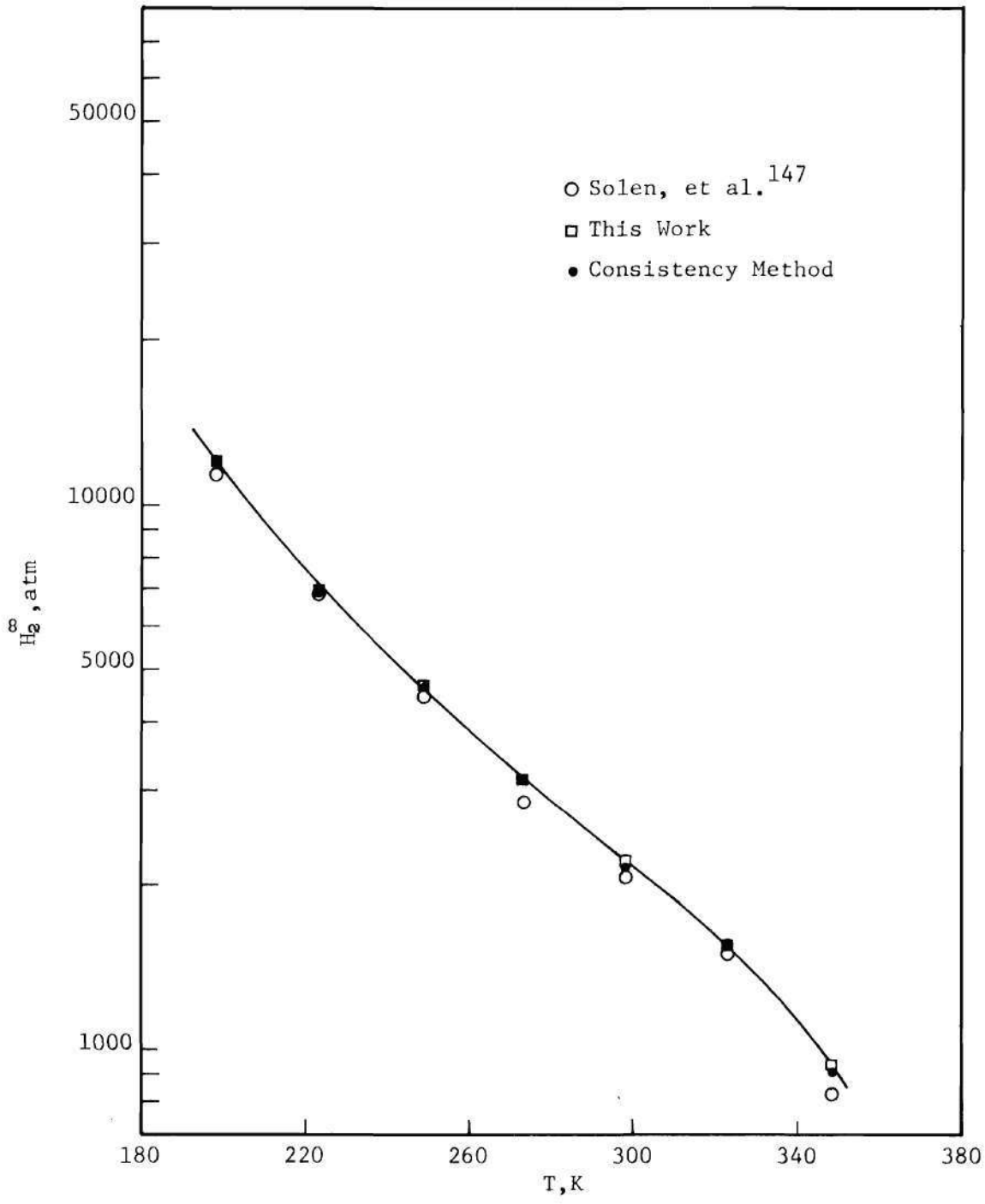

Figure 27. Experimentally Determined Henry's Law Constants for the Helium-Propane System.

Smoothed values of H_2^∞ and $\overline{V}_2^\infty$ are presented in Table 15. The maximum uncertainty in these calculations due to the uncertainty in y_1 and x_2 was about four percent of H_2^∞ and five percent of $\overline{V}_2^\infty$.

Table 15. H_2^∞ and $\overline{V}_2^\infty$ for the Helium-Propane System

T,K*	H_2^∞, atm		$\overline{V}_2^\infty$, cc/gm mole	
	Calculated	Smoothed	Calculated	Smoothed
198.15	12,035 ± 392	11,850	25.7 ± 0.5	27.7
223.15	6,998 ± 234	7,000	31.8 ± 0.8	29.6
248.15	4,640 ± 162	4,620	31.1 ± 1.2	32.0
273.15	3,174 ± 114	3,190	34.9 ± 1.5	35.0
298.15	2,237 ± 84	2,235	42.1 ± 1.9	39.6
323.15	1,553 ± 60	1,545	43.8 ± 2.2	47.8
348.15	946 ± 38	940	68.9 ± 2.5	69.0

*Corresponding vapor pressure values are given in Table 32.

H_2^∞ ($P = P_{O1}, T$) and $\overline{V}_2^\infty$ for the Helium-Propylene System

The phase equilibrium study done in this work represents the only data available for this system. These data have been smoothed and are presented in Appendix G. Calculations have been made over the temperature range of 200.00 to 254.98 K. The consistency method has been used over the entire range of 175.00 to 254.98 K, and the results, which are presented in Figure 28, agree very favorably.

Calculated and smoothed values of H_2^∞ and $\overline{V}_2^\infty$ are presented in Table 16. The uncertainty in y_1 and x_2 produces a maximum uncertainty of four percent in H_2^∞ and eight percent in $\overline{V}_2^\infty$.

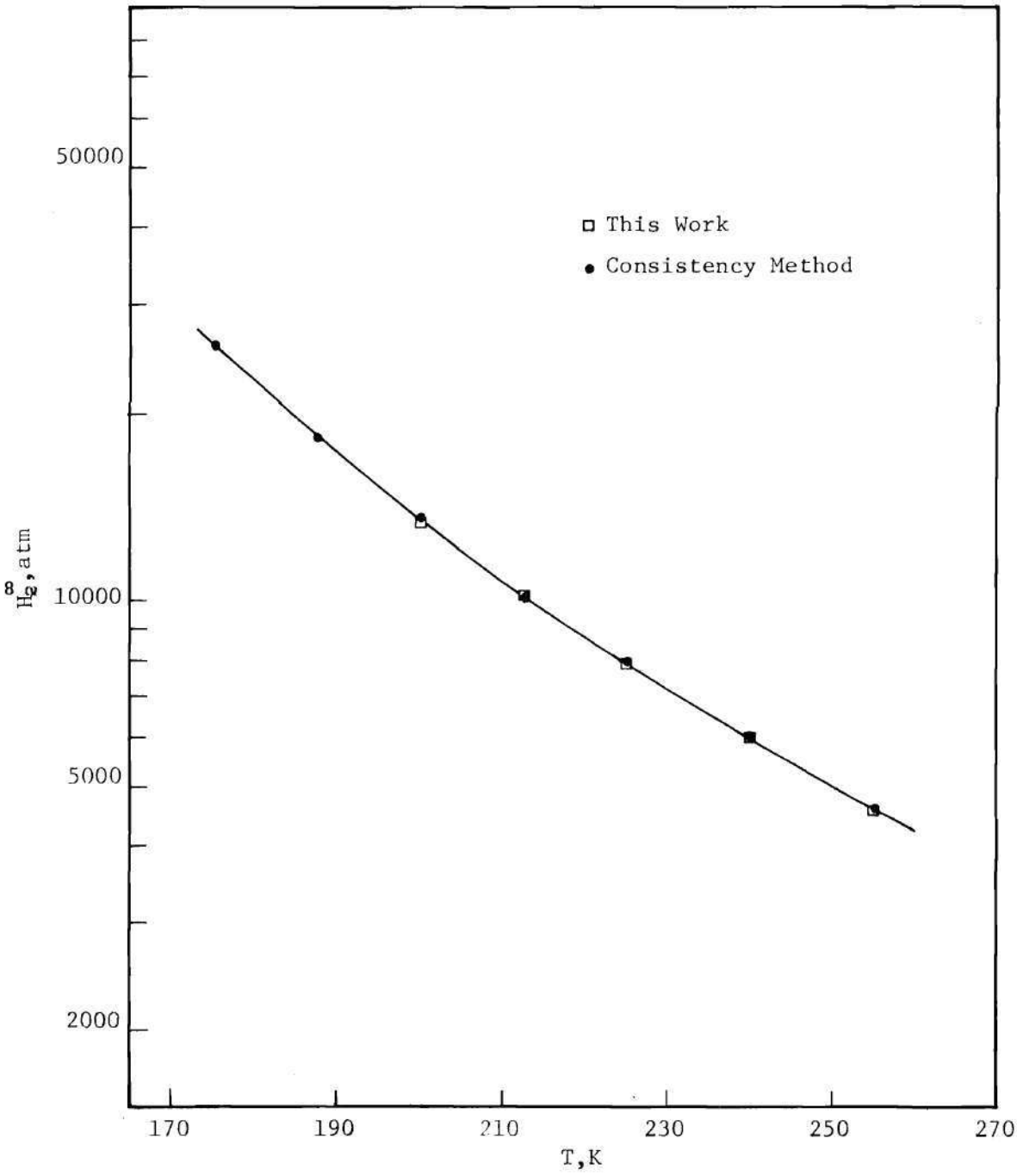

Figure 28. Experimentally Determined Henry's Law Constants for the Helium-Propylene System.

Table 16. H_2^{∞} and $\overline{V_2}^{\infty}$ for the Helium-Propylene System

T,K*	H_2^{∞}, atm		$\overline{V_2}^{\infty}$, cc/gm mole	
	Calculated	Smoothed	Calculated	Smoothed
175.00		26,000**		
187.49		18,350**		
200.00	13,557 ± 389	13,650	21.5 ± 1.2	21.0
212.49	10,225 ± 310	10,300	23.8 ± 2.0	21.9
224.99	7,996 ± 249	7,990	23.2 ± 2.7	23.2
239.99	6,063 ± 208	6,000	23.3 ± 3.6	25.5
254.98	4,598 ± 165	4,620	28.9 ± 4.5	29.0

*Corresponding vapor pressure values are given in Table 31.

**Extrapolated using the consistency method.

Discussion of Results

The results of these calculations confirm that the H_2^∞ values extracted, using the virial equation to calculate the gas phase fugacity, are in excellent agreement with the results calculated by Solen, et al.[147] using the modified Redlich-Kwong equation to describe the fugacity. In most cases the same experimental data were used to calculate H_2^∞; therefore, any difference between these two calculated values is a direct reflection of the inability of the two methods to predict the same fugacity. The maximum difference between the two methods was found to be 13 percent, and the two methods had a tendency to differ for $T_{R1} \geqq 0.8$. In most cases the agreement was within the experimental uncertainty. The smoothed values of H_2^∞ were determined by weighting both sets of results.

The consistency method has been shown to give surprisingly good agreement with the results derived from the more elaborate procedures. In almost every case, the results of the consistency method agreed better with the results of this work than those of Solen, et al. These results indicate that at least for the helium systems this method is very satisfactory. These results never deviate from the smooth curve by more than 10 percent.

Since the values of $\overline{V}_2^\infty$ used by Solen, at al.[147] were calculated from an empirical method of Chueh and Prausnitz[18] instead of experimental data, no comparison is made here. However, in the following chapter a comparison is made. Since the slope of the $\ell n \left(\frac{f_2^G}{x_2}\right)$ versus $(P - P_{01})$ curve determines the value of $\overline{V}_2^\infty$, it is expected that some scatter of these values is reflected by the difficulty of drawing a line through the

calculated values. Most of the differences between the actual and smoothed values of $\overline{V_2}^{\infty}$ can be accounted for because of the experimental uncertainty.

Table 17 presents the values of H_2^{∞} and $\overline{V_2}^{\infty}$ for the various helium binary systems at a reduced temperature of 0.75. By using a reduced temperature basis, it is possible to make a comparison of H_2^{∞} and $\overline{V_2}^{\infty}$ values for the various systems. The results obtained are very interesting. The helium-nitrogen system shows the lowest H_2^{∞} value. This means that helium is most soluble in this system. The helium-carbon dioxide system shows an extremely high value of H_2^{∞} which indicates that the solubility of helium is very low. Within the helium-hydrocarbon series there appears to be no systematic trend. The helium-propane system shows the lowest value of H_2^{∞} in this series. Apparently helium is more soluble in the heavier hydrocarbons than the lighter ones. The $\overline{V_2}^{\infty}$ values for these hydrocarbons are all above 30 cc/gm mole and they appear to increase with the molecular weight. The helium-nitrogen system shows the smallest value of $\overline{V_2}^{\infty}$.

Table 17. Values of H_2^{∞} and $\overline{V}_2^{\infty}$ Compared at a Given Reduced Temperature ($T_{R1} = 0.75$)

System	T,K	H_2^{∞}, atm	$\overline{V}_2^{\infty}$, cc/gm mole
He-Ar	113	3,420	24.3
He-O_2	116	3,280	20.6
He-N_2	94.5	2,120	17.2
He-CO_2	228	9,100	19.1
He-CH_4	143	3,470	30.7
He-C_2H_6	229	3,800	31.8
He-C_2H_4	212	4,610	33.1
He-C_3H_8	277	3,050	35.9
He-C_3H_6	274	3,500*	33.5*

*Values of H_2^{∞} and $\overline{V}_2^{\infty}$ are extrapolated.

CHAPTER VIII

THEORETICAL PREDICTION OF HENRY'S LAW CONSTANT AND PARTIAL MOLAR VOLUME AT INFINITE DILUTION

General Discussion

In previous chapters, the gas phase has been generally described using the virial equation of state instead of semi-empirical or empirical equations of state. The reason for this preference is that the virial equation is derivable from statistical mechanics and the other models are not. Hence, any improvement on the theoretical model is somewhat of an extension of the existing theory of gases.

In an attempt to describe the properties of a liquid phase, different theories of statistical mechanics of fluids have been developed. As in the case of the gas phase, there are some theories that are fundamental in nature, based on first principles, and some which are semi-empirical or empirical. Some of the fundamental theories that have been used are the Mayer cluster theory,[93] the radial distribution function theory,[49] the Percus-Yevick theory,[112] and the most recent scaled particle theory of fluids.[128] Theories which are considered semi-empirical or heuristic are the free volume theories,[123] quasi-lattice theories,[49] and the significant structure volume theory.[14]

As is expected, the heuristic models in general give best agreement with experimental results since their form has been chosen to fit the data. The fundamental theories are appealing due to their theoretical

basis.

The problem of predicting the solubility of a high-pressure gas in a liquid phase has not yet been solved. If good estimates of H_2^∞ and $\overline{V}_2^\infty$ could be obtained, one could use Equation (VII-16) to determine the liquid composition. Hence the problem becomes one of finding a theory which will predict these two quantities. Recent work by Miller and Prausnitz[104] has shown that the free volume theory[124,138] gives an expression for the Henry's law constant. The systems they considered are at high pressures and one component is above its critical temperature. Their paper indicates that only one adjustable parameter, K_{12}, which has been discussed in Chapter V, is required for these calculations. Although the method appears to predict satisfactory values for H_2^∞, there is evidence that a change in K_{12} amounting to $\pm$ 0.05 produces a 30 percent change in H_2^∞. As has been indicated in Chapter V, the value of K_{12} can be a strong function of temperature. This implies that their method may have large possible errors.

Using another semi-empirical method, Chueh and Prausnitz[18] have developed a method of calculating $\overline{V}_2^\infty$ in nonpolar liquid mixtures. Their method consists of extending to mixtures the corresponding states correlation of Lyckman, et al.[85] for calculation of molar volumes of saturated liquid mixtures. These mixture volumes are used to calculate partial molar volumes from a modification of the Redlich-Kwong equation. This method was used to calculate $\overline{V}_2^\infty$ in the paper by Solen, et al.[147]

The above methods represent the best ways of estimating H_2^∞ and $\overline{V}_2^\infty$ from semi-empirical methods. The results are admittedly good, but these

models tend to divorce themselves from what is actually occurring physically in the system. It would indeed be refreshing to find a model, based upon first principles, which could predict H_2^{∞} and $\overline{V_2}^{\infty}$. Of the fundamental theories mentioned, the scaled particle theory appears to produce the most consistent results. Therefore, this chapter will be devoted to the application of this theory to high pressure gas solubility.

Method of Pierotti

The scaled particle theory was first presented in 1957 by Reiss, et al.[128,129,130] The theory calculated the reversible work required to introduce a hard sphere (component 2) into a fluid (component 1) by producing a spherical cavity of radius, a_2. This theory does not contain any adjustable parameters, and the physical properties calculated by this method are obtained from formulas containing quantities which are obtained from independent measurements.

Pierotti[113,114] has presented equations for the work required to introduce a real gas in a solvent. This method has been used by him to calculate Henry's law constants, heat of solution, partial molar volumes, and heat of vaporization in aqueous[114,115] and non-aqueous[113] solutions. Pierotti indicates that there are two steps in the introduction of a gas molecule in a solvent. First, a hole, the size of the solute molecule, is created in the solvent. Second, the solute molecule interacts with the solvent when placed in the cavity. The Lennard-Jones (6-12) pairwise potential is used to describe this interaction.

The equations used in this method are as follows[113,128]:

$$\ell n\ H_2^{\infty} = \frac{\overline{G}_i}{RT} + \frac{\overline{G}_c}{RT} + \ell n \left(\frac{RT}{v_1^o}\right) \qquad \text{(VIII-1)}$$

$$\overline{V}_2^{\infty} = \overline{V}_I + \overline{V}_c + \beta_T RT \qquad \text{(VIII-2)}$$

$$H_{vap} = RT + \alpha_P RT^2 \left(\frac{(1 + 2Y)^2}{(1 - Y)^3}\right) \qquad \text{(VIII-3)}$$

$$\beta_T = \frac{a_1^3 N_A (1 - Y)^4}{6RT\ Y(1 + 2Y)^2} \qquad \text{(VIII-4)}$$

$$\alpha_P = \frac{1 - Y^3}{T(1 + 2Y)^2} \qquad \text{(VIII-5)}$$

$\overline{G}_c$ represents the partial molar Gibbs free energy of creating a cavity in a fluid and is given by Reiss[128] as:

$$\overline{G}_c = K_0 + K_1 a_{12} + K_2 a_{12}^2 + K_3 a_{12}^3 \qquad \text{(VIII-6)}$$

where

$$K_0 = RT \left[- \ell n\ (1 - Y) + \left(\frac{9}{2}\right) \left(\frac{Y}{(1 - Y)}\right)^2\right] - \frac{\pi P a_1^3}{6} \qquad \text{(VIII-7)}$$

$$K_1 = - \left(\frac{RT}{a_1}\right) \left[\frac{6Y}{(1 - Y)} + 18 \left(\frac{Y}{(1 - Y)}\right)^2\right] + \pi P a_1^2 \qquad \text{(VIII-8)}$$

$$K_2 = \left(\frac{RT}{a_1^2}\right) \left[\left(\frac{12Y}{(1 - Y)}\right) + 18 \left(\frac{Y}{(1 - Y)}\right)^2\right] - 2\pi P a_1 \qquad \text{(VIII-9)}$$

$$K_3 = (4/3)\ \pi P \qquad \text{(VIII-10)}$$

where

$$Y = \frac{\pi a^3 \bar{\rho}}{6} \qquad \text{(VIII-11)}$$

$$a_{12} = \frac{a_1 + a_2}{2} \qquad \text{(VIII-12)}$$

$\bar{G}_i$ is the partial molar Gibbs free energy for the interaction term. If the entropy term is neglected, $\bar{G}_i$ is approximated by the partial molar internal energy, $\bar{E}_i$, where

$$\bar{E}_i = - \frac{5.33\ \pi \bar{\rho} \bar{C}}{6 a_{12}^3} \qquad \text{(VIII-13)}$$

The dispersion constant $\bar{C}$ can be expressed in terms of the Lennard-Jones (6-12) parameters:

$$\bar{C} = 4(e_1 e_2)^{\frac{1}{2}} \left(\frac{a_1 + a_2}{2}\right)^6 \qquad \text{(VIII-14)}$$

The heat of vaporization, H_{vap}, can be calculated using Equation (VIII-3) provided a value of α_P, coefficient of thermal expansion, can be obtained. The values of β_T and α_P can be calculated from Equations (VIII-4) and (VIII-5) provided one knows the value of a_1, the effective hard core diameter.

In the calculation of the partial molar volume, $\bar{V}_2^{\infty}$, $\bar{V}_I$ represents the volume change upon charging, and $\bar{V}_c$ is the volume change upon cavity formation. If $\bar{V}_I$ in Equation (VIII-2) is set equal to zero, we obtain

$$\bar{V}_2^{\infty} = \bar{V}_c + \beta_T RT \qquad \text{(VIII-15)}$$

where $\bar{V}_c$ can be calculated from the relation

$$\bar{V}_c = 82.0560\ \beta_T\ TY \left\{ \left[\frac{6}{(1 - Y)} + \frac{6Y}{(1 - Y)^2} \right] \left[2\left(\frac{a_{12}}{a_1}\right)^2 - \left(\frac{a_{12}}{a_1}\right) \right] + \left[\frac{36Y}{(1 - Y)^2} + \frac{36Y^2}{(1 - Y)^3} \right] \left[\left(\frac{a_{12}}{a_1}\right)^2 - \left(\frac{a_{12}}{a_1}\right) + \frac{1}{4} \right] + \frac{1}{(1 - Y)} \right\} + \frac{\pi a_2^3 N_A}{6} \qquad \text{(VIII-16)}$$

The Dependence of a_1 Upon Temperature

The preceding equations indicate that the value of a_1 is a very important input number in these calculations. The number a_1 represents the effective hard core diameter of the solvent molecule. To determine a value of a_1, one generally assumes that the intermolecular potential function has the Lennard-Jones form, and a_1 can be extracted from second virial coefficient data. The value of a_1 corresponds to the intermolecular distance at which the potential function passes through zero. This corresponds to the parameter σ in the Lennard-Jones potential. Since molecules do not actually possess hard cores, a_1 is defined as an average diameter. In non-spherical molecules it may be possible to choose a value of a_1 which hopefully would include the rotational averaging and core softness. Values of the Lennard-Jones parameters used in this work are presented in Table 18.

Pierotti[115] and Reiss[128] have clearly demonstrated the variation of a_1 for various molecules with temperature. For a given solvent the

Table 18. Lennard-Jones (6-12) Parameters

Gas	Parameter Number	Parameters		Reference
		e/k,K	σ, Å*	
He		6.96	2.63	107
Ar	1	122	3.40	50
	2	118.13	3.499	155
	3	119.3	3.4302	167
N_2	1	95.2	3.745	109
	2	90.467	3.935	165
	3	96.26	3.694	155
	4	95.9	3.71	50
CH_4	1	148.9	3.783	109
	2	148.2	3.817	50
	3	142.87	4.010	155
C_2H_6	1	200.5	4.939	109
	2	243	3.954	50
C_2H_4	1	199.2	4.523	50
	2	202.52	4.433	155
	3	194.4	4.595	109
C_3H_8	1	242	5.637	50
	2	233.28	5.711	155
	3	195.0	6.700	109
C_3H_6	1	215.67	5.75	160
	2	209.1	5.897	109
	3	167.66	6.959	(This Work)

*In this section, σ is equal to a.

value of a_1 seems to decrease as the temperature increases. Pierotti[113] has shown that, since the dispersion constant, $\overline{C}$, is related to the polarizability of the solute, α_2, a plot of $\ell n\ H_2^{\infty}$ versus α_2 should produce a smooth curve for various solutes in a given solvent. The extrapolation of this curve to zero polarizability gives a finite value of $\ell n\ H_2^{o\infty}$. This indicates that, although the interaction term in Equation (VIII-1) is zero, the solubility is nonzero. Equation (VIII-1) now becomes

$$\ell n\ H_2^{o\infty} = \frac{\overline{G}_c}{RT} + \ell n\left(\frac{RT}{v_1^o}\right) \qquad \text{(VIII-17)}$$

Pierotti[113] has also shown that it is possible to correlate the collision diameter, a_2, of the rare gases with their polarizabilities. Extrapolation of this curve to zero polarizability gives a value for a_2 equal to 2.58 Å. Therefore, the extrapolation of the $\ell n\ H_2^{\infty}$ versus α_2 curve to zero polarizability is equivalent to determining the solubility of a hard sphere of diameter 2.58 Å in the particular solvent. Since the value of a_2 at $\alpha_2 = 0$ is now known, Equation (VIII-17) can be solved for a_1 provided values of $\ell n\ H_2^{o\infty}$ are known. This procedure is followed at various temperatures so that the temperature dependency of a_1 can be established. Pierotti[113,114] has used this method to calculate a_1 versus temperature for benzene and water, and his results indicate that these molecules show very little temperature dependency. More recently, Heck[46] has successfully used this correlation for solutes in carbon dioxide.

Heck has presented a critical comparison of experimental Henry's law constants and those calculated from the scaled particle theory.

His theoretical work consists of using different Lennard-Jones parameters for the solute and solvent molecules. Since different people have fitted different temperature ranges of second virial coefficient data, it is possible to have a wide selection of Lennard-Jones parameters. For example, Heck gives values of a_1 that vary from 3.34 to 4.55 Å for carbon dioxide and from 3.954 to 5.22 Å for ethane. The spherical inert gases appear to have a narrower range of a_1 values. For example, neon shows a range of 2.749 to 2.82 Å. In his comparative study, Heck observed that the Lennard-Jones parameters that fitted the second virial coefficients best did not necessarily predict the best Henry's law constants. In most cases the predicted curves did not have the correct temperature dependency. The solvents that he considered were neon, oxygen, ethane, and carbon dioxide with the solutes being either helium, hydrogen, or neon. His final conclusion was that the liquid phase composition cannot be calculated by the method of Pierotti.

In this chapter, an attempt is made to explain these results observed by Heck. Pierotti[113,114] has stated that the temperature dependency of a_1 and the geometric mixing rule in the interaction term are probably the largest sources of error present in his method. Both of these potential sources of error are investigated in this work. Values of a_1 as a function of temperature are obtained for different solvents. The method used is that described previously in this section. The values of $\ell n\ H_2^{\infty}$ used in this work were values extracted from the solubility data of helium and hydrogen gases dissolved individually in the solvent. Experimental values of the Henry's law constants for the helium systems are

taken from Chapter VII, and the H_2^{∞} values for the hydrogen systems are taken from Orentlicher and Prausnitz.[110] Values of α_2 used in this work were taken from the paper of Pierotti.[113] The values of a_1 extracted from Equation (VIII-17) are considered experimental data and these results are compared to a_1 values obtained from Equations (VIII-3), (VIII-4), and (VIII-5) which relate a_1 to the heat of vaporization, isothermal compressibility, and thermal expansion for the pure solvent. The various values of σ in the Lennard-Jones parameters given in Table 18 are also used for comparison. A comparison was made in all cases where these physical properties of the liquid phase were available. Hopefully these results might indicate which physical properties would provide good estimates of a_1 versus temperature.

a_1 versus Temperature for Argon. Since the scaled particle theory has been derived for hard spheres dissolved into a fluid of spherical particles, this solvent should provide an excellent test of the theory. Values of a_1 extracted from $\ell n\ H_2^{O\infty}$ data using Equation (VIII-17) are shown in Figure 29 together with a_1 values calculated from Equations (VIII-3), (VIII-4), and (VIII-5) involving H_{vap}, β_T, and α_p, respectively. The experimental values of isothermal compressibility and coefficient of thermal expansion were taken from Rowlinson[136] and heat of vaporization values from Ziegler, et al.[167] and Din.[29] The comparison of a_1 values computed by the last three methods with values of a_1 computed from $H_2^{O\infty}$ data shows that the values of a_1 computed using H_{vap} give the best agreement while values of a_1 computed using β_T and α_p are smaller. The value of a_1 computed using α_p gave the poorest agreement showing a rapid decrease

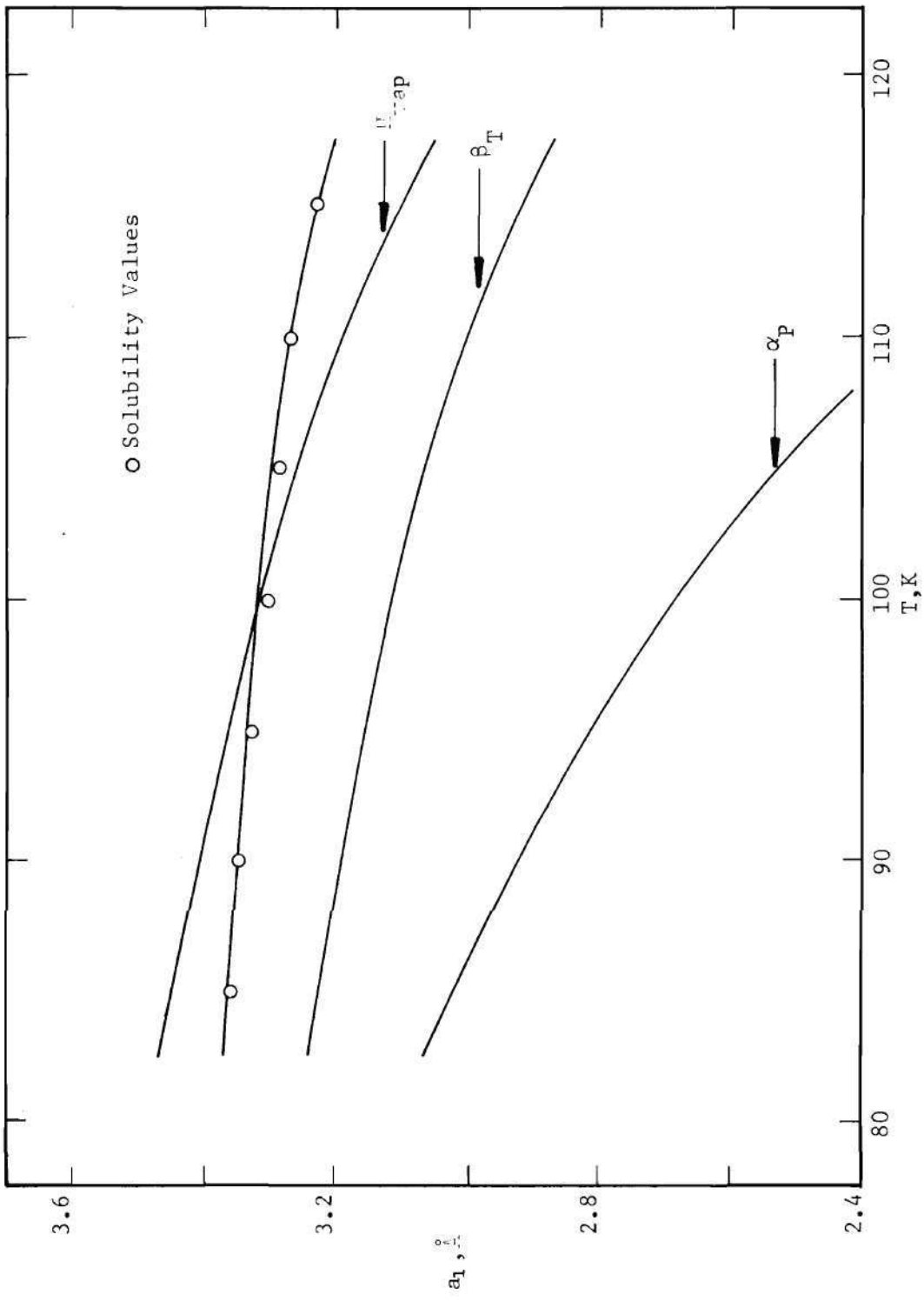

Figure 29. Variation of a_1 with Temperature for Argon.

at higher temperatures. Values of σ from the Lennard-Jones parameters given in Table 18 are somewhat higher than the experimental values of a_1. The values of σ, in Table 18, are not a function of temperature and would be represented as a straight line in Figure 29.

a_1 versus Temperature for Nitrogen. Since there are two sets of Henry's law constants available for the solubility of helium in nitrogen, Figure 22, it was felt that a_1 values should be extracted using both sets of H_2^{∞} values. The first data set was that of DeVaney[28] and represents the H_2^{∞} values extracted in this work, and the second set were those H_2^{∞} values extracted from the data of Rodewald[133] by Solen, et al.[147] The two sets of a_1 values extracted from these data using Equation (VIII-17) are shown in Figure 30. They have somewhat different slopes, but agree to within about 0.15 Å. Also shown in Figure 30 are values of a_1 extracted from Equations (VIII-3), (VIII-4), and (VIII-5) which involve H_{vap}, β_T, and α_P for pure liquid nitrogen. The experimental values of β_T and α_P were taken from Rowlinson[136] and values of H_{vap} were taken from Ziegler, et al.[165] and Din.[29] The values of a_1 calculated using these last three methods show that the a_1 values computed using H_{vap} give the best agreement while values calculated from β_T and α_P are smaller. Again the values computed from α_P gave the poorest agreement. The parameters σ from the Lennard-Jones potential function are given in Table 18 for nitrogen. These values of σ are all larger than the experimental results.

a_1 versus Temperature for Methane. The values of a_1 extracted from $H_2^{o\infty}$ data using Equation (VIII-17) are shown in Figure 31. At higher temperatures this curve shows a leveling off effect not shown in the

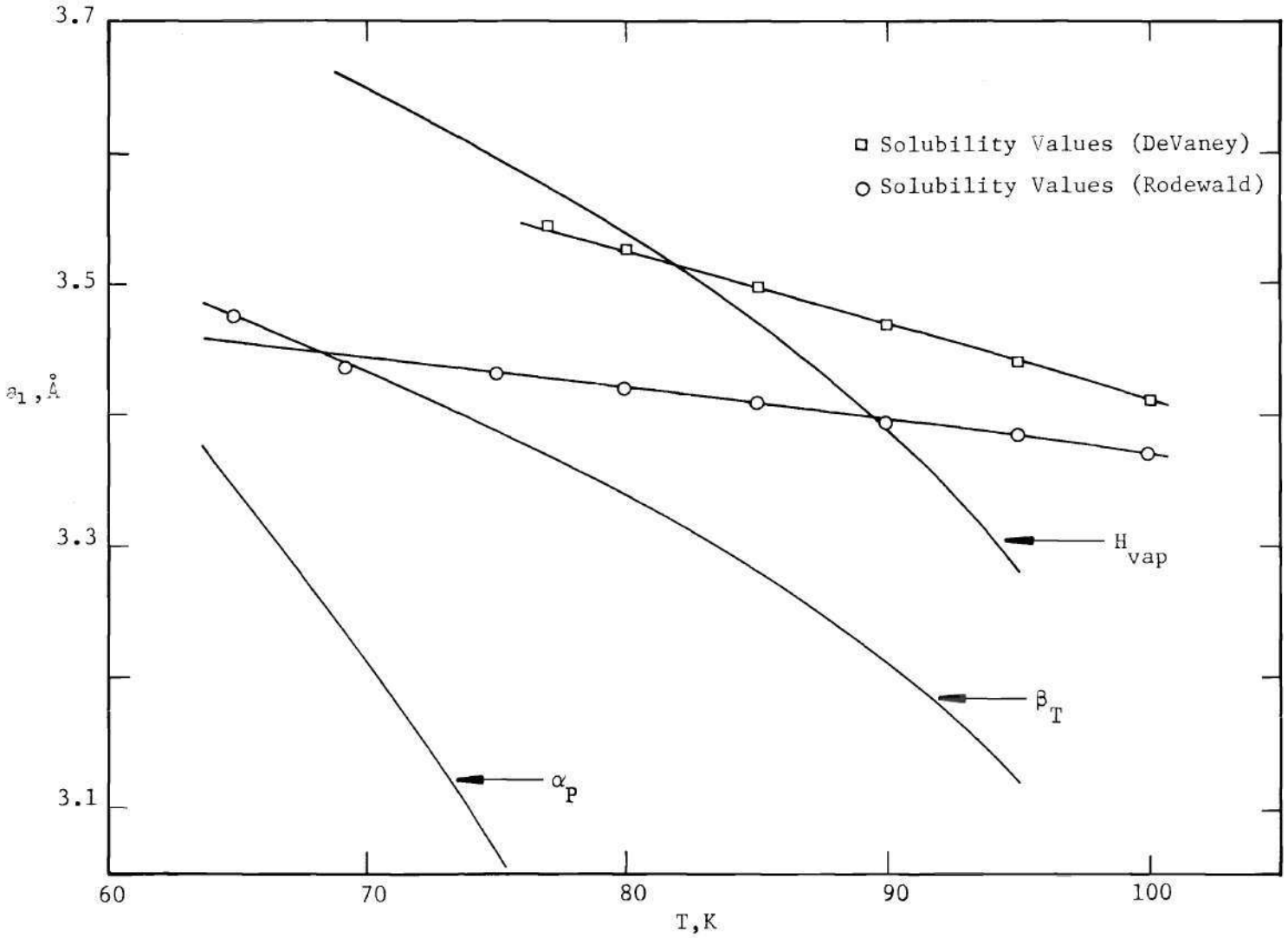

Figure 30. Variation of a_1 with Temperature for Nitrogen.

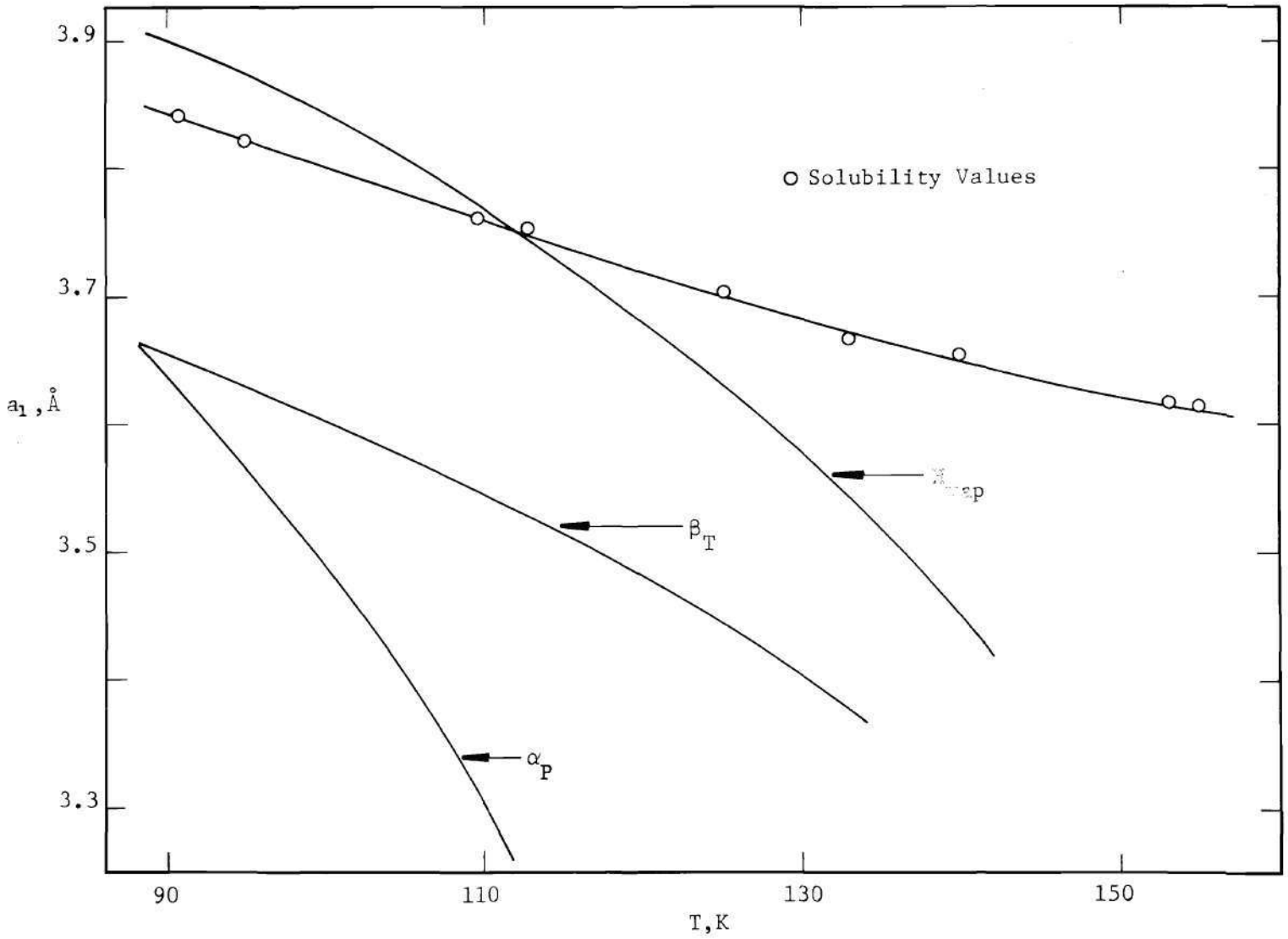

Figure 31. Variation of a_1 with Temperature for Methane.

previous curves. Values of a_1 calculated from the physical properties, H_{vap}, β_T, and α_P, are shown in Figure 31 for comparison. The experimental values of β_T and α_P for pure liquid methane were taken from Rowlinson,[136] and the values of H_{vap} were those of Ziegler, et al.[168] and Din.[29] The values of a_1 from H_{vap} are in reasonably good agreement with the experimental a_1 values. The a_1 values extracted from β_T and α_P are smaller than experiment. Again the values computed from α_P gave the poorest agreement. The values of σ from the Lennard-Jones potential, presented in Table 18, show good to poor agreement.

a_1 versus Temperature for Other Solvents. Values of a_1 have been extracted from $H_2^{o\infty}$ data for ethylene, ethane, propylene, and propane using Equation (VIII-17). These results are presented in Figure 32. The calculations were made possible because of the H_2^{∞} data available for helium and hydrogen dissolved in these solvents. Due to a lack of sufficient physical property data, it was not possible to compare these a_1 values with values of a_1 calculated from other physical properties. The a_1 values calculated for these systems are generally lower than the Lennard-Jones parameter σ presented in Table 18.

Theoretical Values of H_2^{∞} and $\overline{V}_2^{\infty}$ Calculated from Pierotti's Method

The previous section has revealed that, over a wide temperature range, most cryogenic liquids exhibit a sizable change in their molecular core diameter, a_1. The larger molecules tend to show the largest variation of a_1. For example, Figure 32 indicates that ethane changes from

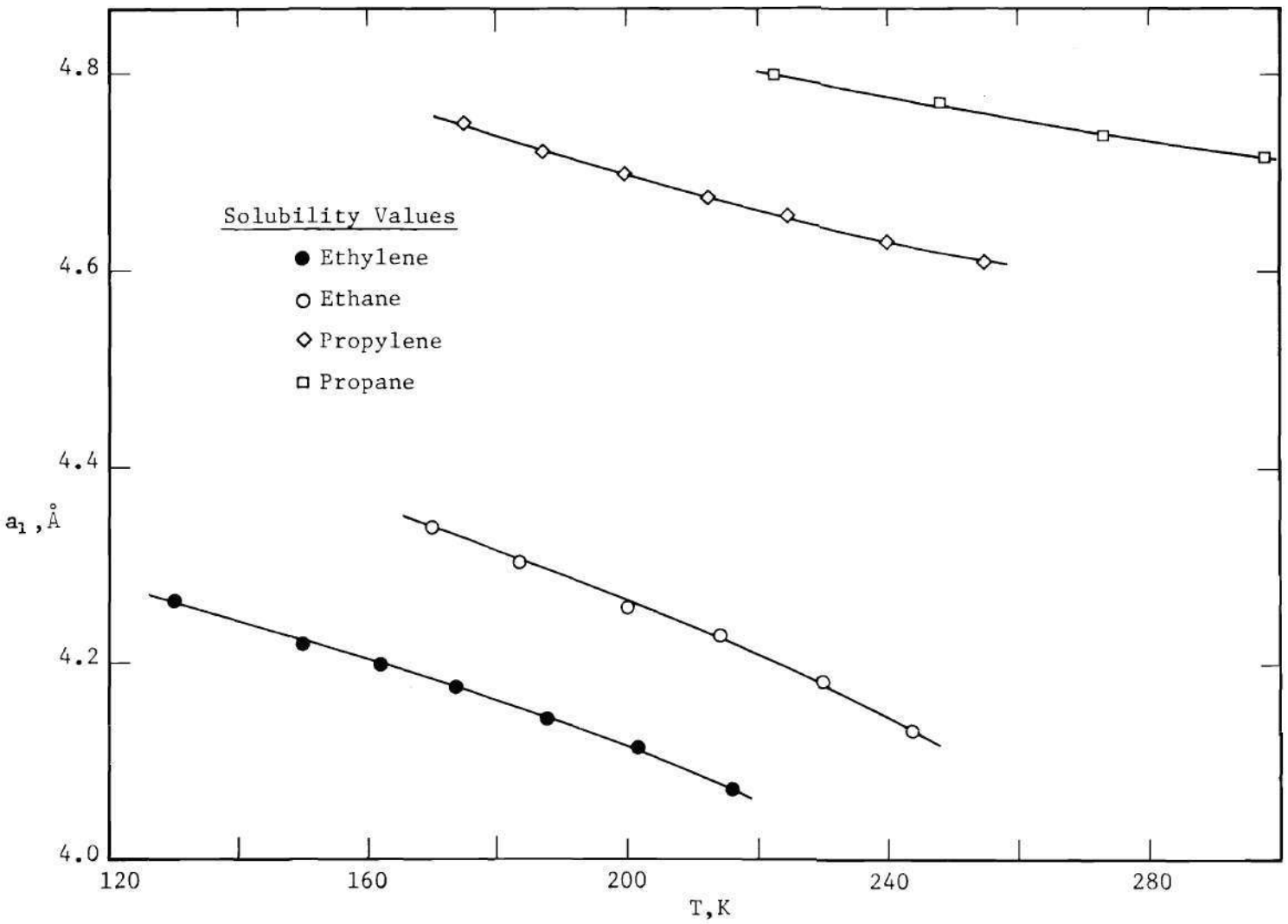

Figure 32. Variation of a_1 with Temperature for Ethane, Ethylene, Propane, and Propylene.

a_1 = 4.33 to 4.13 Å over a temperature range of 75 K. The values of a_1 from the Lennard-Jones parameters are not in agreement with solubility a_1 values for large molecules. The purpose of this section is to examine the effect of a_1 on the calculation of H_2^∞ and $\overline{V_2^\infty}$, and thus to investigate the usefulness of this method in predicting the solubility of gases in liquids.

Since the molecular core diameter, a_1, has been determined versus temperature, it is now possible to check the contribution of the interaction term, $\overline{G}_i$, in Equation (VIII-1) in the calculation of H_2^∞. The evaluation of the interaction energy term, Equation (VIII-13), requires the calculation of the geometric average of the Lennard-Jones energy parameter. Deviations from the geometric mixing rule for both the Lennard-Jones and Kihara potential models have been discussed previously in Chapter V. Therefore, it seems likely to assume that this interaction energy term might be corrected by including the $(1 - K_{LJ})$ factor before the geometric mixing rule in Equation (VIII-14). This gives

$$\overline{C} = 4(1 - K_{LJ})(e_1 e_2)^{\frac{1}{2}} \left(\frac{a_1 + a_2}{2}\right)^6 \qquad \text{(VIII-18)}$$

Liu[83] has obtained a correction to the Lennard-Jones geometric mixing rule for the helium-argon, -nitrogen, and -methane systems. His correction is based upon a least square fit of this potential function to the interaction second virial coefficient. This assumes that the linear average is valid for the calculation of σ_{12}, Equation (IV-28). By calculating the values of H_2^∞ from Equation (VIII-1) using the experimental a_1 data, it is possible

to check the importance of the interaction energy, $\bar{G}_i$, in these calculations. It is hoped that, if a correction to the interaction term is necessary in this method of Pierotti, it would correspond to the $(1 - K_{LJ})$ factor found by Liu.

The calculation of $\bar{V}_2^{\infty}$, using Equation (VIII-2), requires an accurate knowledge of the coefficient of isothermal compressibility, β_T. Of the systems studied in this work, data of this type are available for argon, nitrogen, and methane. Calculations made using the method of Pierotti and those calculated using the method of Chueh and Prausnitz[18] are compared to the experimental results of this work for these three systems. In all these calculations, the Lennard-Jones parameters used for helium are those presented by Mullins[107] (see Table 18). The number of the theoretical curves in the following figures corresponds to the number assigned to the respective Lennard-Jones parameters in Table 18.

H_2^{∞} and $\bar{V}_2^{\infty}$ for the Helium-Argon System

Figure 33 shows the calculated values of H_2^{∞} together with the experimental results from Table 8. Most of the theoretical curves are within a factor of two of the experimental values. These curves do not take variations of a_1 with temperature into account, but the variations are not considerable. The theoretical values of H_2^{∞} predicted using the a_1 values extracted from solubility data, Figure 29, show the correct temperature dependency. These values are a factor of two and one-half times too low, and a value of $K_{LJ} = 0.485$ in Equation (VIII-18) is required to bring the theoretical curve into agreement with experiment. This correction to the geometric mixing rule is quite a bit larger than

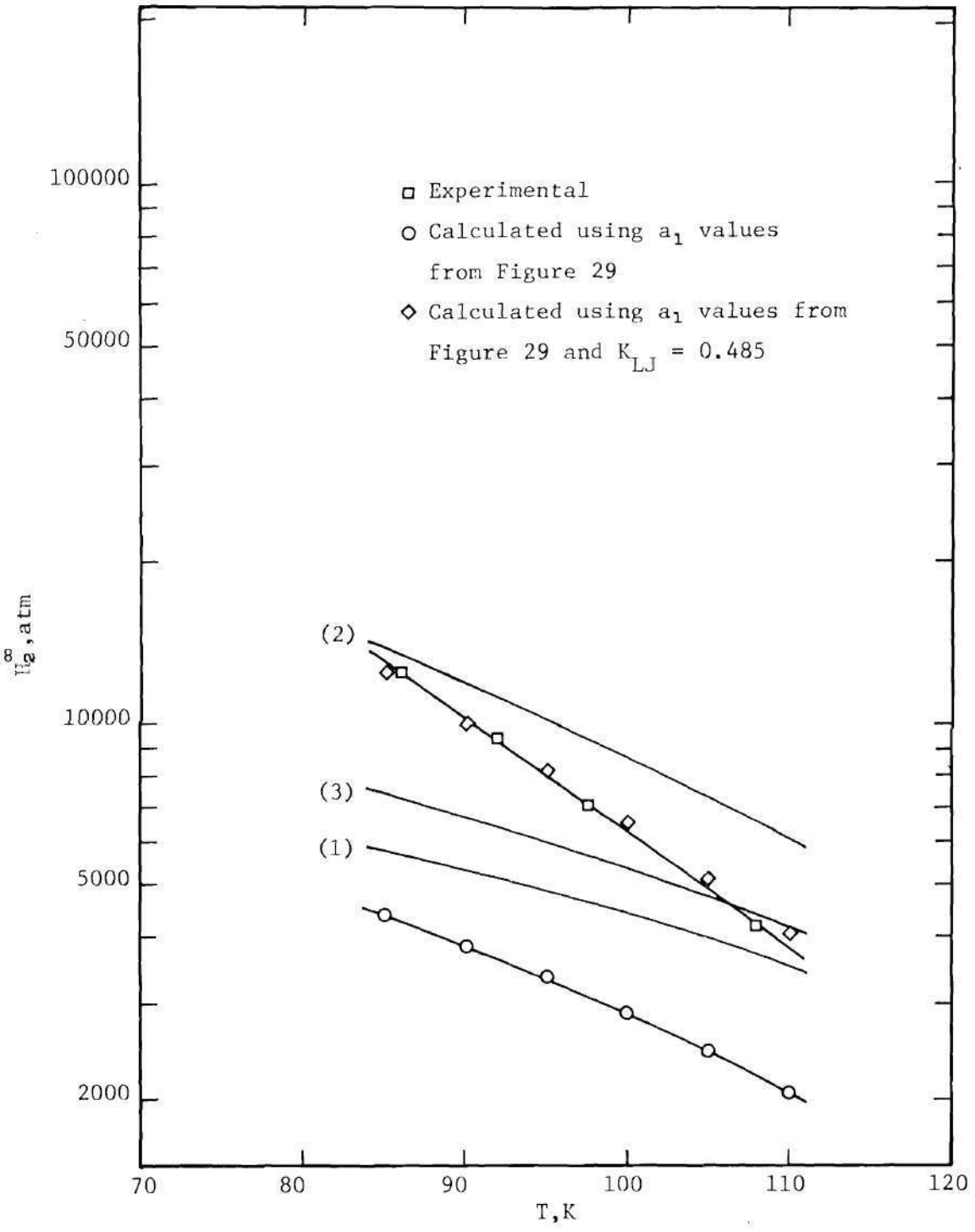

Figure 33. Comparison of Theoretical and Experimental H_2^∞ for the Helium-Argon System.

the value of $K_{LJ} = 0.122$ found by Liu[83] using interaction second virial cofficient data.

A comparison of the calculated and the smoothed experimental values of $\overline{V_2}^{\infty}$ is shown in Figure 34. The calculation of $\overline{V_2}^{\infty}$ is completely dependent upon the values of a_1 and β_T. The larger values of a_1 have the effect of raising the theoretically predicted curves, but the slope appears to remain unchanged. The values of $\overline{V_2}^{\infty}$ predicted using the a_1 values extracted from solubility data compare very well with the values predicted by the empirical method of Chueh and Prausnitz.[18] Unfortunately, all of the theoretically calculated values of $\overline{V_2}^{\infty}$ are too high when compared to the experimental values. The theoretical curves all show signs of bending upward at lower temperatures than the experimental curve.

H_2^{∞} and $\overline{V_2}^{\infty}$ for the Helium-Nitrogen System

The experimental H_2^{∞} values of both DeVaney and Rodewald from Table 10 are presented together with theoretical values in Figure 35. The various Lennard-Jones parameters from Table 18 predict values that are closer to the data of DeVaney than that of Rodewald, but they are generally high. The variation of these curves with temperature is generally in agreement with experiment. The H_2^{∞} values predicted using the experimental a_1 solubility values from Figure 30 are shown in Figure 35. These values are calculated for both the experimental data of DeVaney and Rodewald. The variation of H_2^{∞} with temperature is in excellent agreement with experiment, but again the predicted values are too low. The K_{LJ} values required to bring the theoretical curve into agreement with experiment were $K_{LJ} = 0.466$, for the data of DeVaney, and $K_{LJ} = 0.500$, for the data of Rodewald. These

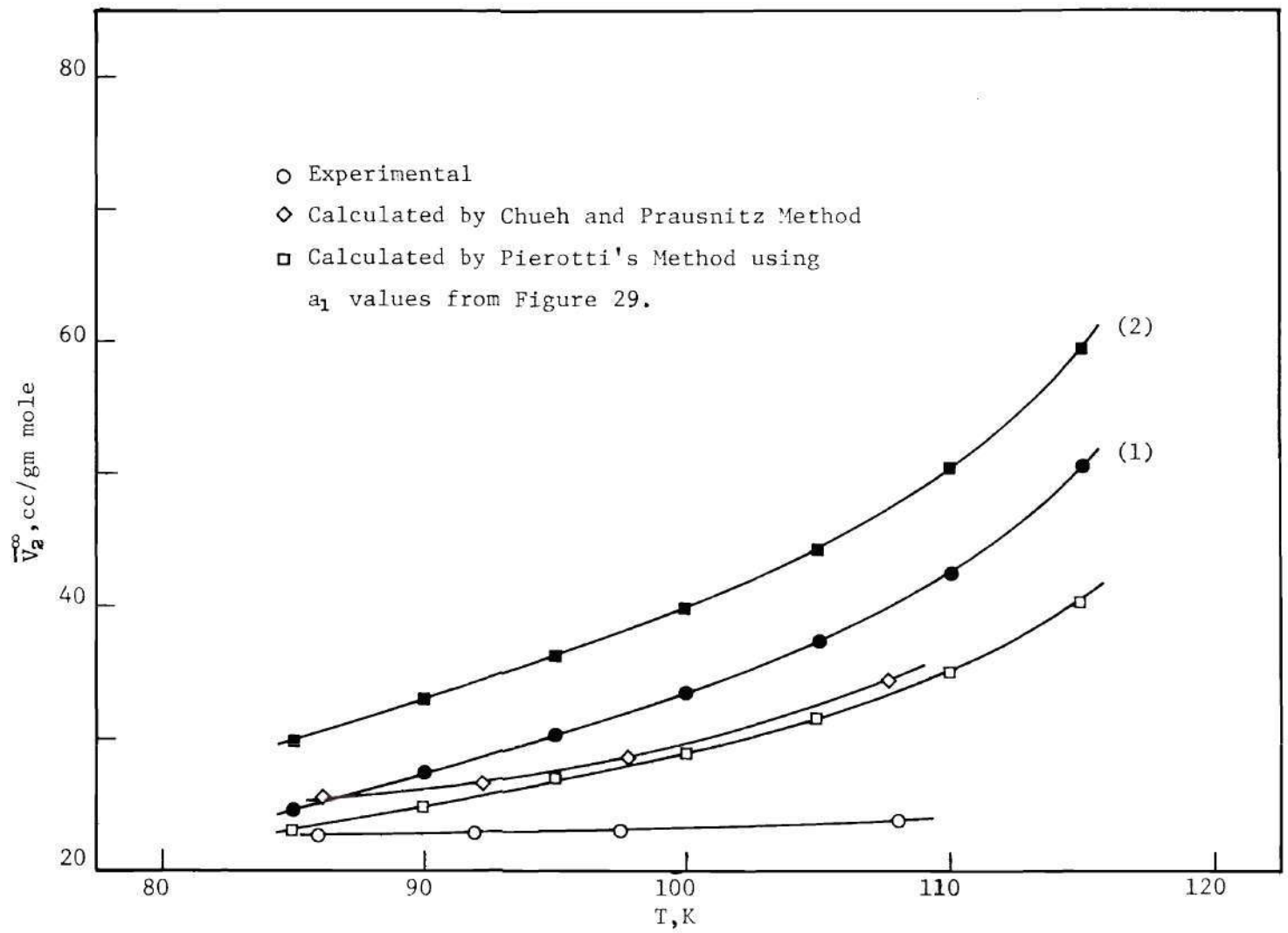

Figure 34. Comparison of Theoretical and Experimental $\bar{V}_2^\infty$ for the Helium-Argon System.

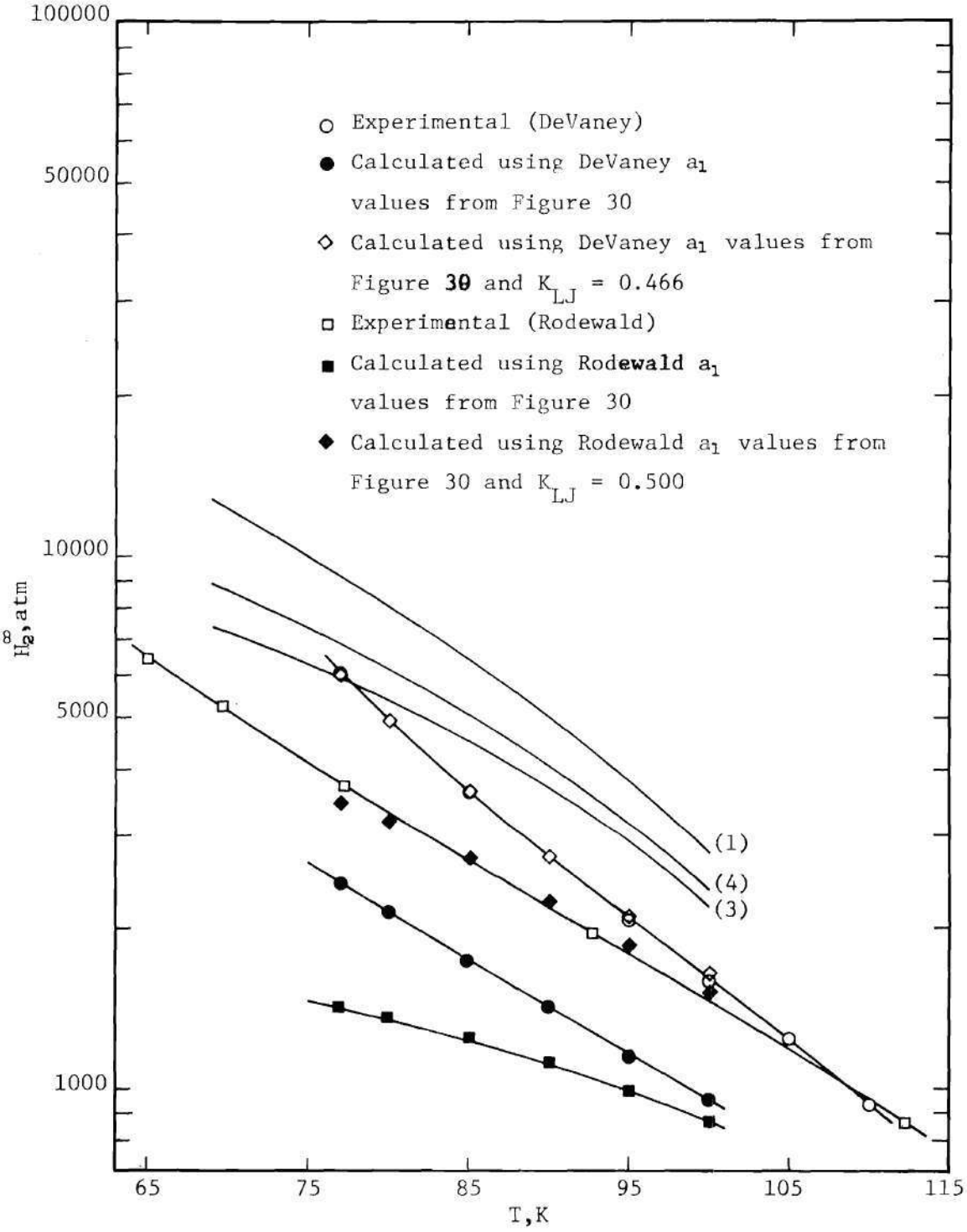

Figure 35. Comparison of Theoretical and Experimental H_2^{∞} for the Helium-Nitrogen System.

values of K_{LJ} do not compare too well with the value of $K_{LJ} = 0.127$, determined by Liu[83] using the interaction second virial coefficient data.

In Figure 36, the values of $\overline{V_2}^{\infty}$ calculated from the various theoretical models are compared to smoothed values taken from Table 10. All of the models predict values of $\overline{V_2}^{\infty}$ that are too high. The a_1 solubility values of DeVaney predict $\overline{V_2}^{\infty}$ values that are in excellent agreement with values calculated using the method of Chueh and Prausnitz. The values calculated using the Lennard-Jones parameters are excessively high.

H_2^{∞} and $\overline{V_2}^{\infty}$ for the Helium-Methane System

Figure 37 shows the theoretical Henry's law constants, H_2^{∞}, together with the smooth experimental values from Table 12. The predicted values of H_2^{∞} using the Lennard-Jones parameters shown in Table 18 do not show the correct temperature dependency. This indicates that this system has an a_1 value that is a strong function of temperature as has been shown in Figure 31. These curves are generally still within a factor of two of the experimental values. If the experimental values of a_1 from Figure 31 are used, the temperature dependency of H_2^{∞} is reproduced very well. The calculated curve falls below the experimental curve. To bring the two curves into agreement, it is necessary to use a value of $K_{LJ} = 0.364$. This value agrees fairly well with the value of $K_{LJ} = 0.224$ calculated by Liu[83] using interaction second virial coefficient data.

The theoretically calculated values of $\overline{V_2}^{\infty}$ and experimental values from Table 12 are shown in Figure 38. The theoretical values of $\overline{V_2}^{\infty}$ are all higher than the experimental results. The values predicted using the a_1 solubility values are in excellent agreement with those predicted by

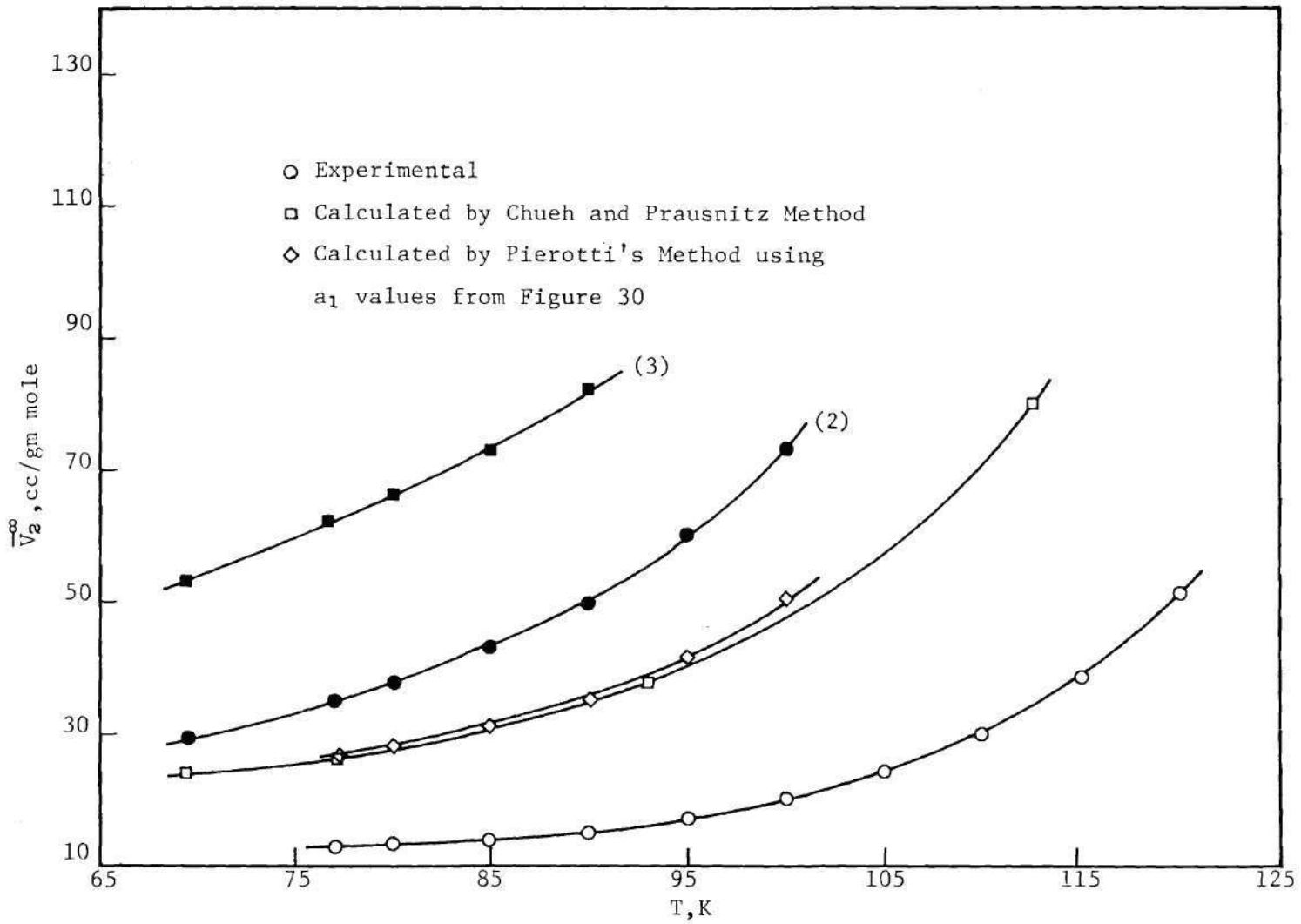

Figure 36. Comparison of Theoretical and Experimental $\overline{V}_2^\infty$ for the Helium-Nitrogen System.

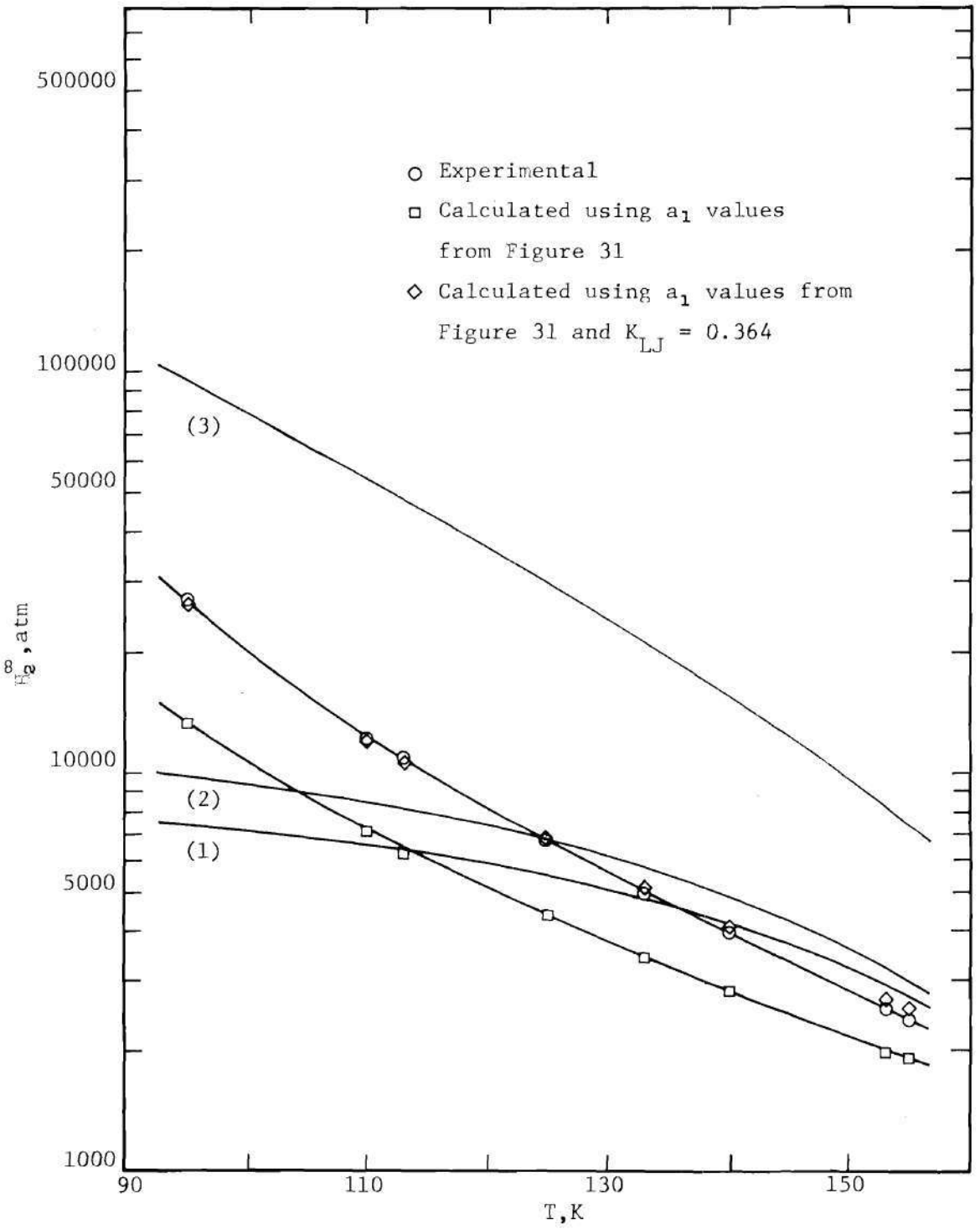

Figure 37. Comparison of Theoretical and Experimental H_2^∞ for the Helium-Methane System.

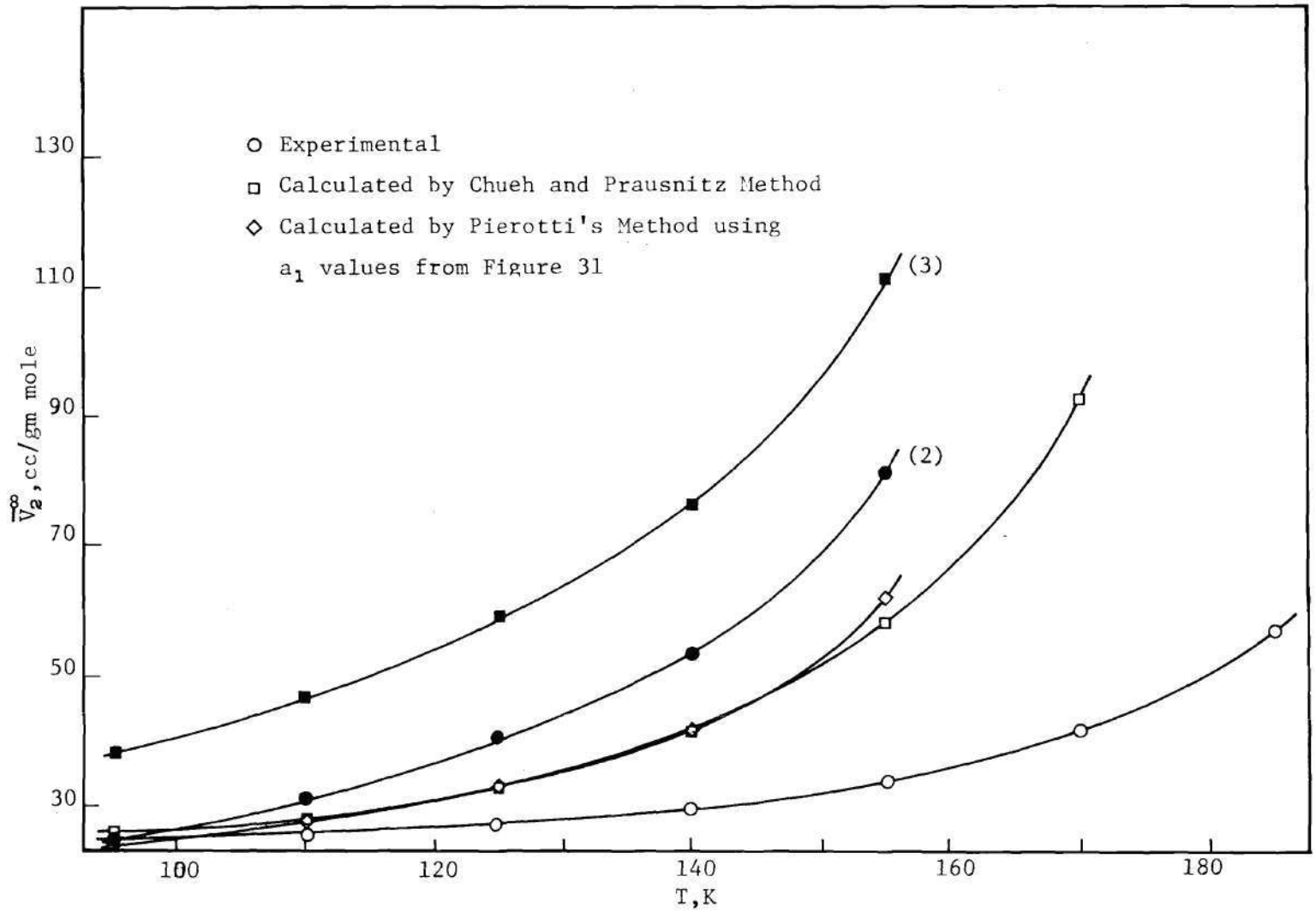

Figure 38. Comparison of Theoretical and Experimental $\bar{V}_2^\infty$ for the Helium-Methane System.

the method of Chueh and Prausnitz. The values predicted by the Lennard-Jones parameters are higher than the other theoretical values.

H_2^∞ for the Helium-Ethane System

In Figure 39, a comparison is made between the theoretical values of H_2^∞ computed using various values of a_1 and the experimental values of H_2^∞ from Table 13. This system has Lennard-Jones parameters that have σ values ranging from 3.954 to 4.939 Å. The effect of this wide variation of a_1 upon H_2^∞ is shown in Figure 39. These calculations reveal that the predicted values show a lack of temperature dependency and large differences when compared to experiment. The values of H_2^∞ predicted from the solubility a_1 values from Figure 32 show the correct temperature dependency. The values of H_2^∞ predicted by this method are again too low and a value of $K_{LJ} = 0.345$ was required to bring the two curves into agreement.

H_2^∞ for the Helium-Ethylene System

In Figure 40, a comparison is made between the theoretical values of H_2^∞ and experimental values of H_2^∞ taken from Table 14. The values predicted using the available Lennard-Jones parameters are shown to give values of H_2^∞ that are excessively high. The temperature dependency of these values is fairly good. The temperature dependency of the values of H_2^∞ predicted using the extracted a_1 solubility values show excellent agreement with experiment. A value of $K_{LJ} = 0.245$ is required to produce excellent agreement between theory and experiment.

H_2^∞ for the Helium-Propane and Helium-Propylene Systems

A close inspection of Equation (VIII-1) reveals that, if the value of Y, Equation (VIII-11), becomes greater than unity, then the method of

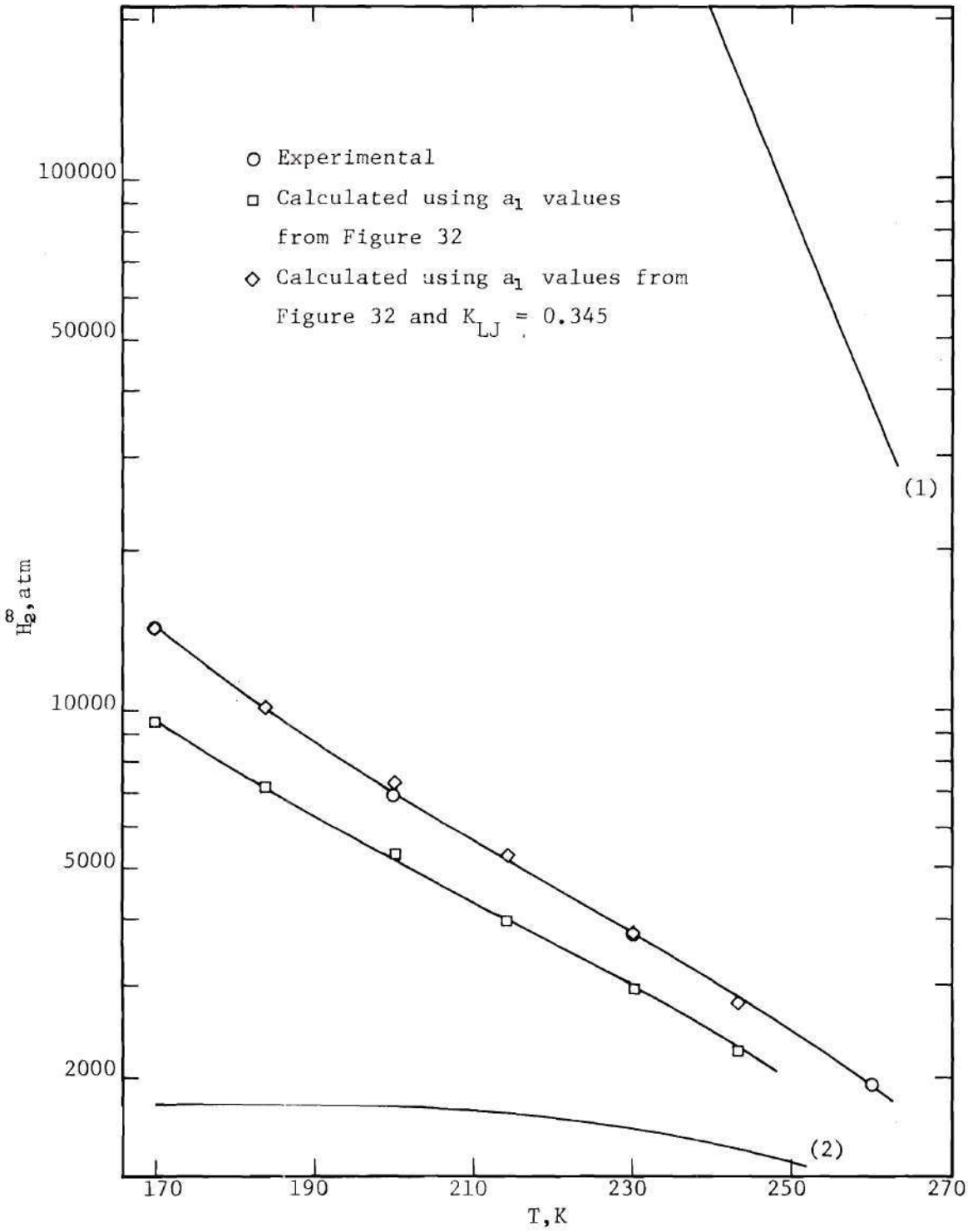

Figure 39. Comparison of Theoretical and Experimental H_2^∞ for the Helium-Ethane System.

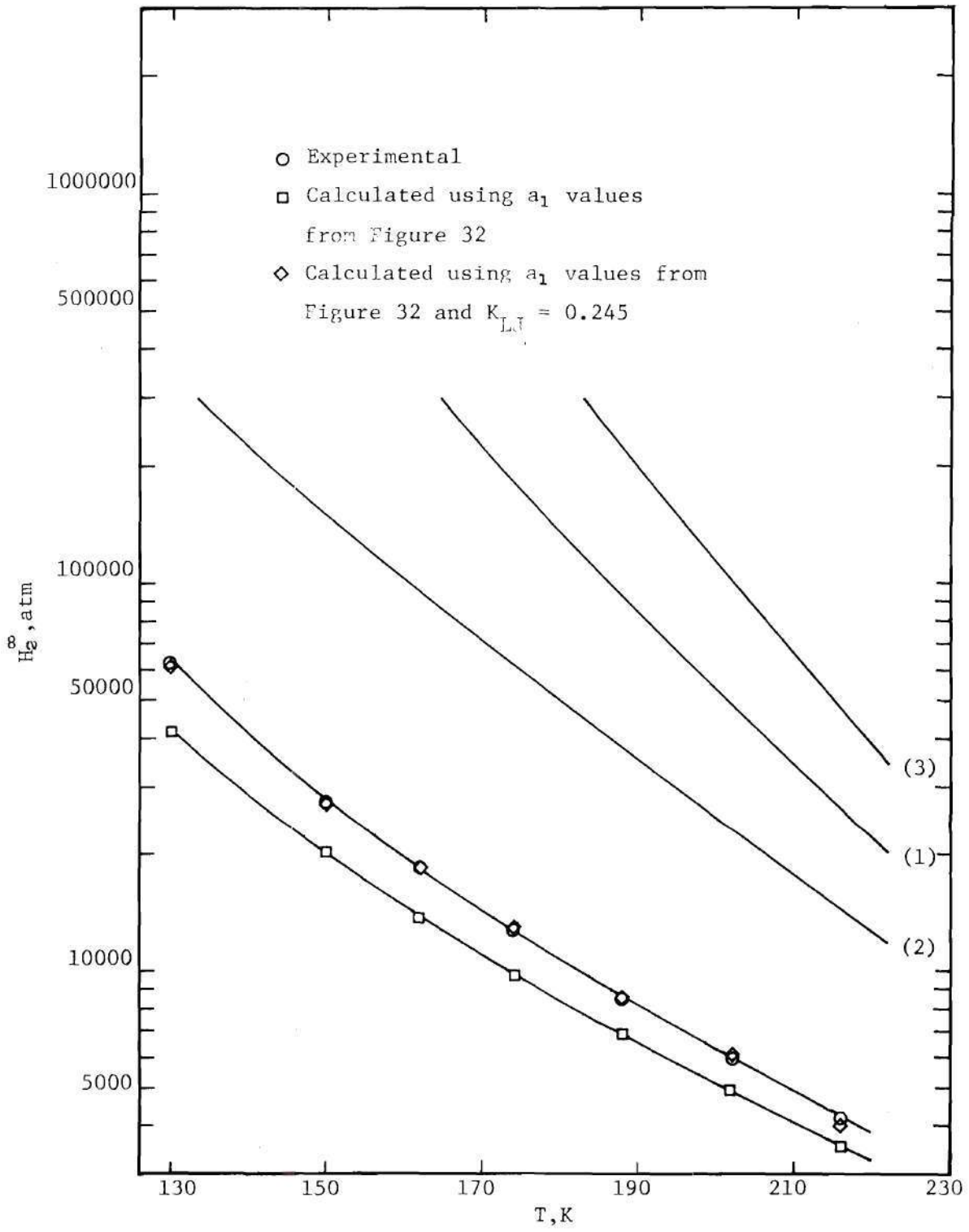

Figure 40. Comparison of Theoretical and Experimental H_2^{∞} for the Helium-Ethylene System.

Pierotti will not work. The value of Y is a function of a_1 and the molar volume. In both of these systems, the values of σ, from Table 18, were so large that all values of Y calculated were greater than unity; therefore, no theoretical calculations could be made using Lennard-Jones parameters. Figure 41 shows the comparison between the theoretical values of H_2^∞ calculated using solubility a_1 values from Figure 32 and the experimental values of H_2^∞ given in Table 15 for the helium-propane system. The agreement is very good and a value of $K_{LJ} = 0.228$ was required for the adjustment of the interaction curve. Figure 42 shows the same type of comparison for the helium-propylene system. The temperature dependency is very good between the theoretical and experimental curve. The values of a_1 used to calculate the theoretical curve come from Figure 32 and the experimental values of H_2^∞ come from Table 16. A value of $K_{LJ} = 0.20$ was required to produce agreement between these two curves.

Discussion of Results

The previous sections of this chapter have revealed some interesting information about the use of the scaled particle theory in describing the solubility of gases in liquids. Provided the Lennard-Jones parameters for the cryogenic liquid do not show considerable scatter, as was found to be the case for argon, notrogen, and methane, the predicted H_2^∞ and $\overline{V_2}^\infty$ values are generally within a factor of two of the experimental values. Unfortunately, the temperature dependency of the predicted H_2^∞ values is not consistent with experiment.

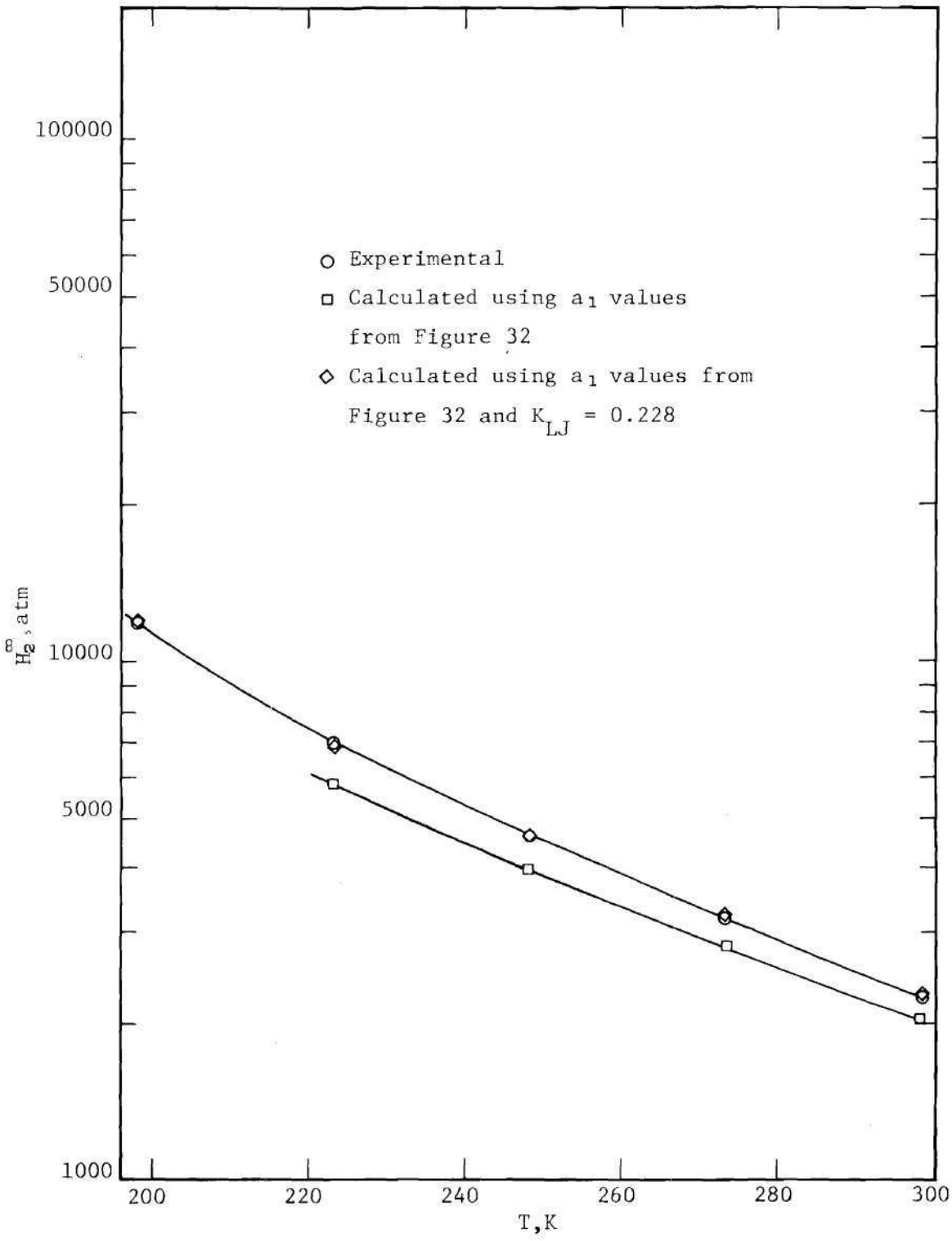

Figure 41. Comparison of Theoretical and Experimental H_2^∞ for the Helium-Propane System.

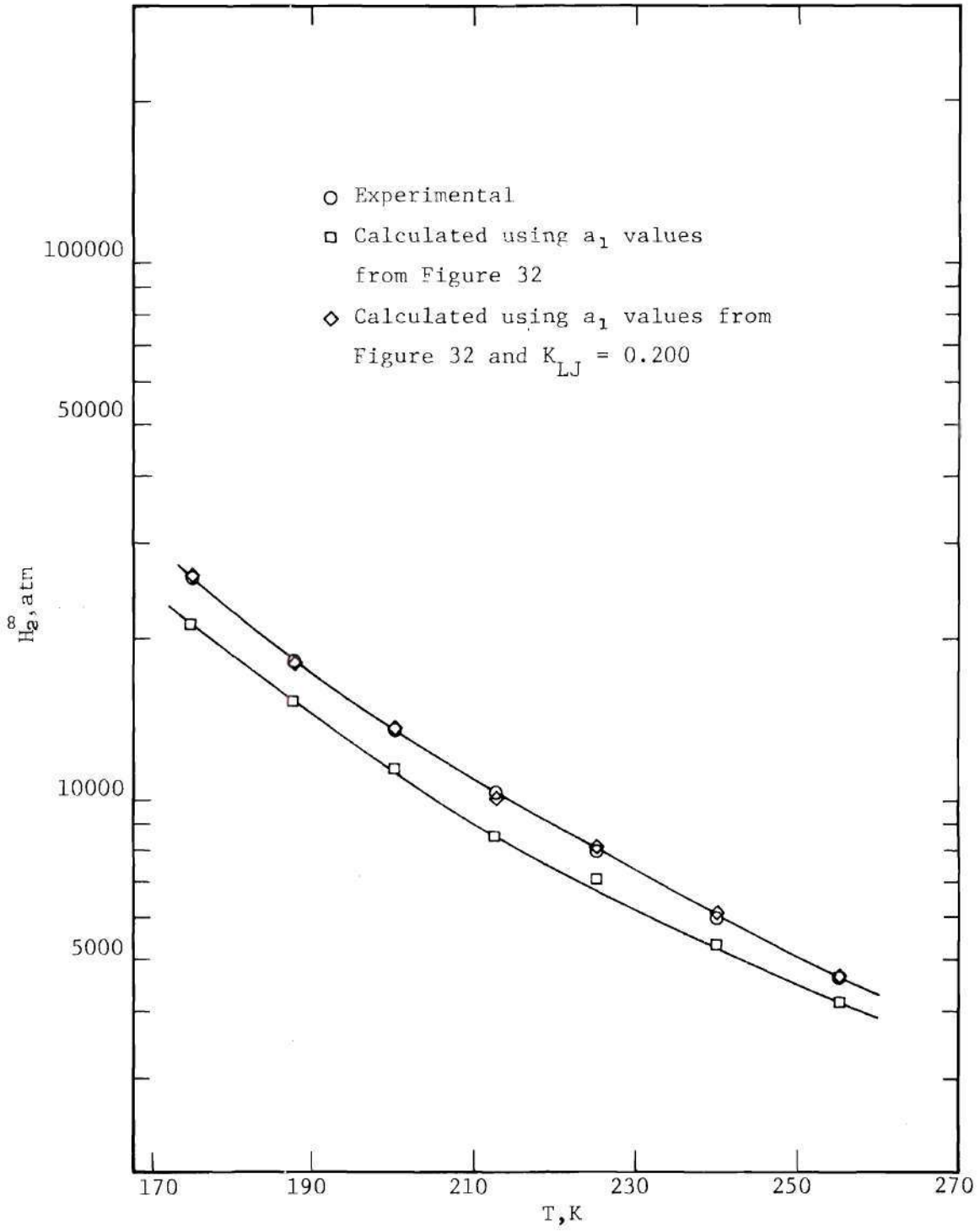

Figure 42. Comparison of Theoretical and Experimental H_2^{∞} for the Helium-Propylene System.

To predict values of H_2^{∞} that are in excellent agreement with experiment, it is necessary to make two modifications of this method of Pierotti. The first modification is that the value of a_1 must be treated as a function of temperature instead of being assumed to have a constant value. The amount of variation in a_1 is apparently a function of the temperature range and the size of the molecule. Values of a_1 versus temperature have been extracted from $H_2^{o\infty}$ data, and these results are compared to a_1 values extracted from physical property data (heat of vaporization, coefficient of isothermal compressibility, and coefficient of thermal expansion). This comparison was made for argon, nitrogen, and methane. Although the agreement between these curves is not very good, it appears that the heat of vaporization can give a_1 values that are in reasonable agreement with experiment. The β_T and α_P values of a_1 are consistently lower than experiment, and they tend to diverge considerably at higher temperatures.

The second modification of Pierotti's method is involved with the interaction term. It now appears that the error in the theoretically predicted H_2^{∞} values due to the interaction term cannot be entirely explained by a faulty geometric mixing rule for the energy parameters in the Lennard-Jones model, Equation (VIII-18). The values of K_{LJ} that correct the geometric average in this work do not have the same values as the K_{LJ} values that Liu[83] obtained from the second interaction virial coefficient. The values obtained in this work imply that a reduction of the interaction term by as much as 48.5 percent is necessary in the helium-argon system. Without the interaction term correction being applied, the predicted values

of H_2^{∞} using the a_1 solubility values would still agree within a factor of two with experiment. The K_{LJ} values extracted in this work become smaller as the molecule becomes larger. For example, the helium-argon value of K_{LJ} was found to be 0.485, and the corresponding value for the helium-propylene was 0.200. This is opposite to the trend found by Liu,[83] using interaction second virial coefficient data. No attempt was made to try to correlate these K_{LJ} values, but it may be possible to make estimates of K_{LJ} parameters for other systems by using the values presented in this work as a guide.

The values of $\overline{V_2^{\infty}}$ that were predicted using the method of Pierotti with the a_1 solubility values agreed very well with the values predicted by Chueh and Prausnitz.[18] However, both of these calculated results are consistently high by a factor of two when compared to the experimental results. Values of $\overline{V_2^{\infty}}$ obtained using the Lennard-Jones parameter, σ, as a constant, showed approximately the correct temperature dependency. Due to the questionable uncertainty in extracting $\overline{V_2^{\infty}}$ from the slope of the $\ell n \frac{f_2^G}{x_2}$ versus $(P - P_{01})$ curve, these results are not very conclusive.

It is not possible to explain some of the results Heck[46] observed using the method of Pierotti. The inability of the theoretical model to predict the correct temperature dependency as stated by Heck is due to the variation of a_1 with temperature. Heck made theoretical calculations, using the method of Pierotti, for molecules whose various sets of Lennard-Jones parameters show large variations in the parameter σ. For example, in the case of ethane the three available sets of parameters gave values of σ ranging from 3.954 to 5.22 Å. These values of σ for carbon dioxide

ranged from 3.34 to 4.07 Å for two sets of parameters. This wide range of a_1 values, used to calculate H_2^{∞}, gave results that varied from too low to excessively high when compared to experimental values. These same observations were noticed in this work in some cases, but for molecules where the various σ values are fairly constant from one set of parameters to the next, as in the case of argon, the predicted values of H_2^{∞} are in very good agreement with experiment (see Figure 33).

In cases where the values of σ from the Lennard-Jones potential show large variations, it is recommended that a value of a_1 be extracted from the H_{vap}, using Equation (VIII-3). Heck's attempt to use the heat of vaporization as a means of obtaining a_1 proved unfruitful, not because of a lack of the theory, but because he used an incorrect equation. The equation used was taken from Pierotti's first paper,[113] which contained a typographical error. It is hoped that this chapter has cleared up some of the statements made by Heck, and that it has reinstated the method of Pierotti as a suitable method of estimating the solubility of a high pressure gas in a liquid.

CHAPTER IX

CONCLUSIONS AND RECOMMENDATIONS

Conclusions

The gas-liquid equilibrium for the helium-ethylene and helium-propylene systems has been studied at temperatures below 255 K and pressures up to 120 atmospheres. The gas and liquid compositions have been determined along seven different isotherms for the helium-ethylene system. The seven isotherms correspond to temperatures of 129.98, 150.01, 162.00, 173.99, 188.02, 202.01, and 216.04 K. These results are believed to be accurate to ± 3 percent for the 162.00 K isotherm and higher temperature isotherms. The two lowest isotherms are believed to be accurate to ± $4\frac{1}{2}$ percent. The helium-propylene system was studied in the gas phase along five isotherms. These temperatures were 200.00, 212.49, 224.99, 239.99, and 254.98 K. The liquid phase of this system was studied at two additional temperatures, 175.00 and 187.49 K. The gas phase analyses at these two lowest temperatures were suspected to contain a possible 10 to 15 percent systematic error, and they are not reported. In this system the gas phase results along the 224.99, 239.99, and 254.98 K isotherms are uncertain to ± 3 percent, and the remaining isotherms, 200.00 and 212.49 K, are uncertain to about ± $4\frac{1}{2}$ percent. The liquid analysis of this system is believed to be accurate to ± 3 percent for these five isotherms, and the lowest two isotherms, 175.00 and 187.49 K, are known to about ± $4\frac{1}{2}$ percent.

The only experimental data available for comparison were done by Hiza and Duncan[53] on the helium-ethylene system. They made measurements on the gas phase composition at 130 and 150 K. Their results are in good agreement with the results of this work. The agreement is always well within the combined experimental uncertainty of ± 7 percent.

The temperatures reported in this work are based upon the International Practical Temperature Scale of 1968 and pressure gauge corrections are taken from Appendix C. The gas imperfection correction was applied to the mixtures used to construct the chromatographic calibration curve. This correction amounted to + 0.5 percent for the helium-ethylene mixtures and 1.4 percent for the helium-propylene mixtures. Hence, it is evident that neglecting this correction could produce a sizable error in these data.

The interaction second virial coefficient, B_{12}, has been extracted from available phase equilibria data for the helium-ethylene, helium-ethane, helium-propylene, and helium-propane systems. The enhancement factor equation, using the virial equation of state, has been rearranged and solved for B_{12}. This program, which calculates the third virial coefficients using the method of Chueh and Prausnitz,[16] can be used in the region of $T_{R1} \geq 0.80$. The original program of Liu appears to give erroneous results when used above this reduced temperature. The results of this work tend to reveal that, as the disparity between interacting molecules becomes greater, the B_{12} values become large and positive. The curve of B_{12} versus temperature for these systems shows strong temperature dependency. Comparison of the extracted B_{12} values with the theoretically

calculated results showed that the models lacked the proper temperature dependency.

Recent investigators[16,17,33,52,53,83,107] have attempted to correct the faulty geometric mixing rule for the Lennard-Jones (6-12) and Kihara (6-12) core models. A correction is applied by introducing a constant factor before the geometric average. In the case of the Kihara core model, this factor is given as $(1 - K_{12})$. Hiza and Duncan[53] have developed a correlation which related this K_{12} to a function of the ionization potential. Since this K_{12} factor has become increasingly important in describing phase equilibria, values of this factor were extracted from available B_{12} data. A variety of helium binary systems was investigated, and the K_{12} factors extracted from experiment are in good agreement with the correlation of Hiza and Duncan.[53] Because of the strong temperature dependency shown by some of the B_{12} results, the values of K_{12} calculated in this work were determined over a specified temperature range.

Theoretical enhancement factors were predicted for the helium-ethylene, helium-ethane, helium-propylene, and helium-propane systems using the virial and BWR equations of state to describe the gas phase. In this work the liquid solution was assumed to be ideal, and the experimental mole fraction, x_1, was used in the calculation. The virial equation using the Kihara core potential with the correction to the geometric mixing rule for the calculation of B_{12} and the third virial coefficients calculated using the method of Chueh and Prausnitz[16] gave the best agreement with experiment. The Lennard-Jones (6-12) and Kihara model without the geometric correction were generally in poor agreement with experiment.

The BWR(LINEAR) equation predicted values that agreed very well with experiment, but the BWR(LORENTZ) values are considerably poorer. Both the virial and BWR equations were able to predict the minimum and maximum present in the enhancement factor isobar curves.

The Krichevsky-Kasarnovsky equation can be used to correlate the liquid phase data of helium binary systems. The virial equation apparently does an adequate job of calculating the fugacity since the H_2^∞ results compared favorably with those of Solen, et al.,[147] who used the Redlich-Kwong equation to calculate the fugacity. For these helium systems, the results of the consistency method of calculating H_2^∞ have been shown to be in excellent agreement with the results calculated by the more elaborate methods. Values of H_2^∞ and $\overline{V}_2^\infty$ have been extracted for the systems studied in this work and those studied by Liu.[83]

The method of Pierotti[113,114] can be used to provide good estimates of H_2^∞ and $\overline{V}_2^\infty$ for these helium systems. These values predicted from first principles are generally within a factor of two and one-half of the experimental results. By taking into account the temperature dependency of the core diameter, a_1, it is possible to represent the temperature dependency of the experimental curve. An additional correction applied to the Lennard-Jones geometric mixing rule, involved in the interaction energy term, produces results which agree very well with experiment. The predicted value of $\overline{V}_2^\infty$ using the temperature dependency of the core diameter, a_1, agrees with experiment by a factor of two. These results agree almost exactly with the theoretical values reported by Solen, et al.[147] using the relation of Chueh and Prausnitz.[18]

Recommendations

The following is a list of recommendations for future work in phase equilibria.

1. The work done on the helium-propylene system should be extended to lower temperatures. Additional gas phase data at lower temperatures would perhaps confirm that the enhancement factors begin to increase with decreasing temperature. These data would also provide values of B_{12} and thereby demonstrate the temperature dependency of B_{12} for this system.

2. The method of Huff and Reed[63] should be used to predict values of B_{12} for various helium binary systems. Jones and Kay[65] have demonstrated that this method works well for the helium-n-butane system.

3. The Kihara spherical core parameters[109,156] have been shown to fit the second virial coefficient data for various molecules very well. It would be interesting to use these parameters to extract K_{12} values and to see how these values compare to the values of K_{12} obtained using the parameters of Prausnitz and Myers.[122] This would give some indication as to the dependency of K_{12} upon the Kihara parameters used.

4. In selecting a set of Lennard-Jones parameters to fit the second virial coefficient data, consideration of the predicted values of the third virial coefficient should be taken into account. The least squares fit of the Lennard-Jones (6-12) potential function to virial coefficient values has the following characteristic. As the fit is applied to the low temperature end of the data, the value of b_o increases rapidly and e/k decreases. Since the third virial coefficient calculations require the use of b_o^2, it is easy to see why these parameters tend to predict high values

for the third virial coefficient. Since some pure third virial coefficients are now available, a least squares fit of the Lennard-Jones (6-12) parameters should take into account this additional information.

5. A recent paper by Sze and Hsu[153] gives the second virial coefficient for the Lennard-Jones (6-m) potential in reduced form. The value of m was varied from 8 to 150. This parameter represents the hardness or softness of the molecular core. Since there is no reason why every molecular core described by the Lennard-Jones potential should obey the (6-12) potential, it would be interesting to try different values of m in the potential. The larger molecules should have lower values of m since their molecular cores are softer. This type of Lennard-Jones potential might give a better temperature dependency for the predicted B_{12} curves.

6. Multicomponent vapor-liquid equilibrium data are available for helium-natural gas mixtures.[6,150] Most of the necessary helium binary interaction data required for a theoretical calculation of multicomponent vapor-liquid equilibria of these systems have been presented in this work and that of Liu.[83] It would be very interesting to try to predict the equilibrium compositions of the multicomponent mixture and make comparisons with experiment. Comparisons of this type are very rare since few experimental data on multicomponent systems are available.

7. The value of the molecular core, a_1, used in the method of Pierotti, has been determined as a function of temperature for various cryogenic solvents. These values of a_1 could be used to predict the solubility of hydrogen, neon, argon, and other gases in these cryogenic liquids.

The only additional data required would be an adjustment of the geometric mixing rule.

8. Perhaps some attempt should be made to determine the usefulness of the following empirical relations: (1) the Redlich-Kwong equation[119,120] to predict enhancement factor data; (2) the method of Miller and Prausnitz[104] to predict the values of H_2^{∞}; and (3) the method of Chueh and Prausnitz[18] to predict values of $\overline{V}_2^{\infty}$.

APPENDICES

APPENDIX A

EXPERIMENTAL VAPOR PRESSURE OF ARGON AND CARBON DIOXIDE

Since the argon and carbon dioxide gases used by Mullins[107] and Liu[83] were still available for use, the measurement of the vapor pressure of these gases provided a check as to whether the pressure gauges and platinum resistance thermometer were still operating properly.

Table 19 shows the experimental vapor pressure of argon measured in this work and a comparison of these data with those calculated from the experimental curves of McCain and Ziegler,[95] Van Itterbeek, et al.,[158] and Michels, et al.[103] Measurements were made over the temperature range of 119.98 to 147.48 K, which corresponds to a pressure range of 12.28 to 42.88 atmospheres. These data agree very well with the work of Mullins[107] as indicated by Table 21.

Experimental vapor pressure results for carbon dioxide are presented in Table 20, and a comparison is made with the results calculated from the experimental curve of Meyers and Van Dusen.[98] The temperature range covered in this work was 208.13 to 238.15 K, which corresponds to a pressure range of 2.85 to 11.93 atmospheres. The results of this work agree very well with the data obtained by Liu[83] shown in Table 21.

The pressure gauges, one a low pressure gauge (0 to 600 psi, five inch diameter) and the other a high pressure gauge (0 to 3000 psi, five inch diameter), have been originally calibrated by Kirk[76] and were found by him to require the addition of 1 and 15 psi, respectively, to the gauge

Table 19. Experimental Vapor Pressure of Argon

T,K	Vapor Pressure, atm				
	This Work		McCain & Ziegler[95]	Van Itterbeek, et al.[158]	Michels et al.[103]
	Low Pressure Gauge	High Pressure Gauge			
119.98	12.03	12.28	12.020	12.019	11.976
124.99	15.65	15.96	15.674	15.673	15.624
129.98	20.03	20.51	20.031	20.030	19.990
134.99	25.24	25.68	25.214	25.212	25.195
139.98	31.34	31.66	31.290	31.288	31.295
144.98		38.66	38.417	38.414	38.427
147.48		42.88	42.409	42.405	42.412
Average difference between high pressure gauge and investigators			0.37	0.37	0.38
Average difference between low pressure gauge and investigators			0.014	0.014	0.04

Table 20. Experimental Vapor Pressure of Carbon Dioxide

T,K	Vapor Pressure, atm		
	This Work		Myers and Van Dusen[98]
	Low Pressure Gauge	High Pressure Gauge	
208.13	2.854	3.284	2.8285
213.14	4.045	4.507	4.0407
218.13	5.529	5.943	5.4733
223.16	6.766	7.031	6.7498
228.14	8.258	8.727	8.2203
233.14	9.986	10.29	9.9239
238.15	11.93	12.20	11.880
Average difference between high pressure gauge and investigator			0.41
Average difference between low pressure gauge and investigator			0.04

Table 21. Summary of Vapor Pressure Measurements on Phase Equilibrium Equipment

Investigator	Gas	Average Deviation from Michels, et al.[103] atm		Average Deviation from Myers and Van Dusen,[98] atm	
		High Pressure Gauge	Low Pressure Gauge	High Pressure Gauge	Low Pressure Gauge
Mullins[107]	Argon	0.34	0.07		
This Work	Argon	0.38	0.04		
Liu[83]	Carbon Dioxide			0.34	0.04
This Work	Carbon Dioxide			0.41	0.04

reading. These corrections were used in the measurements reported in Tables 19, 20, and 21. All temperature measurements were made on a platinum resistance thermometer calibrated by the National Bureau of Standards on the International Practical Temperature Scale of 1948 (IPTS-48).

These results tend to confirm that the apparatus is operating, at pressures less than 50 atmospheres, in a manner similar to that found by Mullins and Liu. Phase equilibrium measurements made on the helium-carbon dioxide system, presented in Appendix B, confirm that, at high pressures, the gauges are also operating in a manner similar to that found by Liu.[83]

The results of Table 21 imply that applying the plus one psi correction as stated by Kirk[76] for the low pressure gauge caused the gauge to give results that agreed well with data from other experimenters. However, applying the + 15 psi correction to the high pressure gauge causes this gauge to give pressure measurements that are about plus five psi too high. A change of this high pressure gauge correction from + 15 to 10 psi enables the gauge to represent the experimental data much better. This matter has been discussed in detail in Appendix C.

APPENDIX B

HELIUM-CARBON DIOXIDE SYSTEM MEASUREMENTS

To develop experimental technique in the operation of the phase equilibrium apparatus and to check the pressure gauges at high pressure, several experimental enhancement factors of the helium-carbon dioxide system were determined. The gas phase composition was measured for three different pressure points along an isotherm previously studied by Barrick, et al.[2] and Liu.[83] Figure 43 shows these results together with the data of Barrick, et al.[2] and Liu.[83] The accuracy of the measurements of this work was within the experimental uncertainty of ± 3 percent as stated by Liu.

The gas mixing burette built by Kirk[76] was used to prepare several helium-carbon dioxide gas mixtures. These mixtures were run on the 154B gas chromatograph to check Liu's calibration curve. These results were also within the experimental error of the chromatographic analysis.

Both of these experiments gave the experimenter confidence that the phase equilibrium apparatus and the gas mixing burette were being operated in a correct manner.

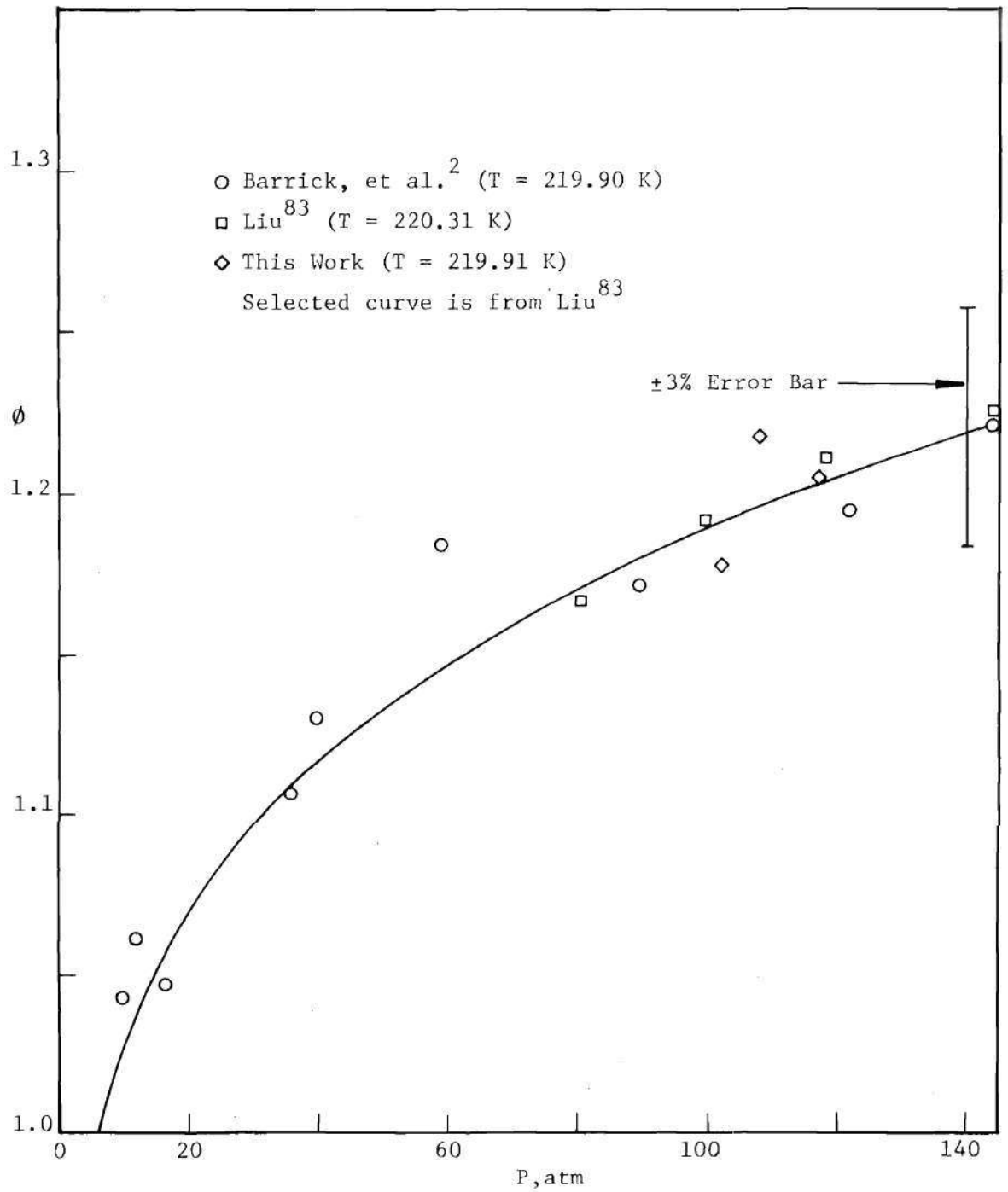

Figure 43. Experimental Enhancement Factors in the Helium-Carbon Dioxide System at 219.91 K.

APPENDIX C

CORRECTION OF THE HIGH PRESSURE GAUGE AND TEMPERATURE MEASUREMENTS ON THE IPTS-68

At the beginning of this work, it appeared that applying the plus 15 psi correction to the high pressure gauge and the plue one psi correction to the low pressure gauge found by Kirk caused there to be a sizable difference in readings on the two gauges. Two different sets of measurements were responsible for this observation.

As the initial check on the pressure gauges, Table 21 in Appendix A summarizes the three different sets of vapor pressure measurements of Mullins,[107] Liu,[83] and this work. This table gives the average difference between the experimental vapor pressures measured in this laboratory, and the values measured experimentally by other investigators. Assuming that the temperature measurements are valid, which is the most likely assumption, it appears that the average difference between the three investigators confirms that the plus one psi correction for the small gauge reading causes it to read approximately 0.04 atmospheres or 0.60 psi too high, and the plus 15 psi correction to the high pressure gauge reading appears to be on the average 0.37 atmospheres or 5.5 psi too high. The uncertainty in reading these pressure gauges is about 0.75 psi for the low gauge and 2.5 psi for the high pressure gauge. This confirms that the low pressure gauge is operating within its experimental uncertainty, but the correction applied to the high pressure gauge causes it

to produce values that are high.

As a second check on the pressure gauges, the equilibrium cell was pressurized over the range of 10 to 480 psi and both gauges were read. With no gauge corrections being applied, the average difference between readings was found to be 8.6 psi. The procedure was repeated by depressurizing from 480 to 10 psi, and this time the average difference was 10.8 psi. Taking an average of these two numbers and adding plus one psi to account for the correction to the small gauge, a final difference of 10.7 psi would have to be added to the high pressure gauge, instead of plus 15 psi as Kirk's calibration showed, to have it agree with the low pressure gauge readings.

Since the vapor pressure measurements have indicated that the large gauge should be corrected by + 9.5 psi, and the comparison between gauges indicated a + 10.7 psi correction, it was decided to adopt a new correction value of + 10 psi. Hence, all of the pressure measurements shown in this thesis, except those in Appendices A and B, have been corrected by plus one psi for the small gauge and + 10 psi for the large gauge.

Temperature measurements made in this work were obtained by using a platinum resistance thermometer. The thermometer has been calibrated by the U. S. National Bureau of Standards on the International Practical Temperature Scale of 1948. To convert these temperatures to the Kelvin scale, the following relation was used

$$T(K) = t(^{\circ}C) + 273.15$$

A recent paper by Barber[1] provides the correction from the IPTS of 1948 to the IPTS of 1968. This correction is given over the temperature range of -180 to 100°C. All temperatures measured in this work, except those in Appendices A and B, are reported on the IPTS-68.

APPENDIX D

CALIBRATION OF GAS CHROMATOGRAPHS

The calibration of a thermal conductivity gas chromatograph to detect a given component over a wide range of composition is a formidable task. Initially in the calibration, a column must be found which not only separates any known impurities from the main peak, but it must also allow the main component to pass through the column in a reasonable time and with a quick response to the recorder. This assures the experimenter of a very sharp and symmetrical peak. After consideration is given to other variables as: gas sample valve size, recorder chart speed, carrier gas, recorder voltage, and detector voltage setting, the next important step is to make up standard lecture bottles of approximate composition over the entire composition region. A bottle is made for each chromatograph attenuation switch used. This enables the experimenter to correct for day-to-day changes in the response from the thermistor sensing device located in the thermal conductivity cell. The assigned peak heights of these standard bottles are established at the time of the chromatographic calibration. During phase equilibrium measurements, the unknown sample is analyzed and immediately afterwards the standard bottle for that attenuation switch is also analyzed. If the standard bottle peak height shows a drift from its value at the time of the original calibration, the unknown sample peak height is changed by a proportional

amount. This corrected peak height for the unknown sample now allows one to calculate the corresponding value of the mole fraction using the original calibration curve. Standard bottles for these different switches are usually of such a composition that their peak heights are approximately 75 units (three fourths of the width of the recorder chart paper). This minimizes the amount of correction that has to be made for the chromatographic drift.

The actual chromatograph calibration curve is constructed by making up samples of known composition that contain the component to be analyzed together with the second component. To make these gas mixtures, a gas mixing burette designed and built by Kirk[76] was used. This apparatus can be used to prepare binary mixtures in which either component could range from a few hundred parts per million to 100 mole percent. In systems where molecules with large negative second virial coefficients are present, as in ethylene or propylene, it is necessary to make gas imperfection corrections to the compositions of the mixtures made up in the gas mixing burette.

Helium-Ethylene System

This binary system was studied over the temperature range 129.98 to 216.04 K, which corresponds to the composition range of 0.0405 to about 25 mole percent ethylene in helium. Figure 44 shows the calibration curve obtained for ethylene in helium using a 154D Perkin-Elmer chromatograph. This calibration range required the use of nine standard bottles. Corrections of about + 0.5 percent were made to correct this

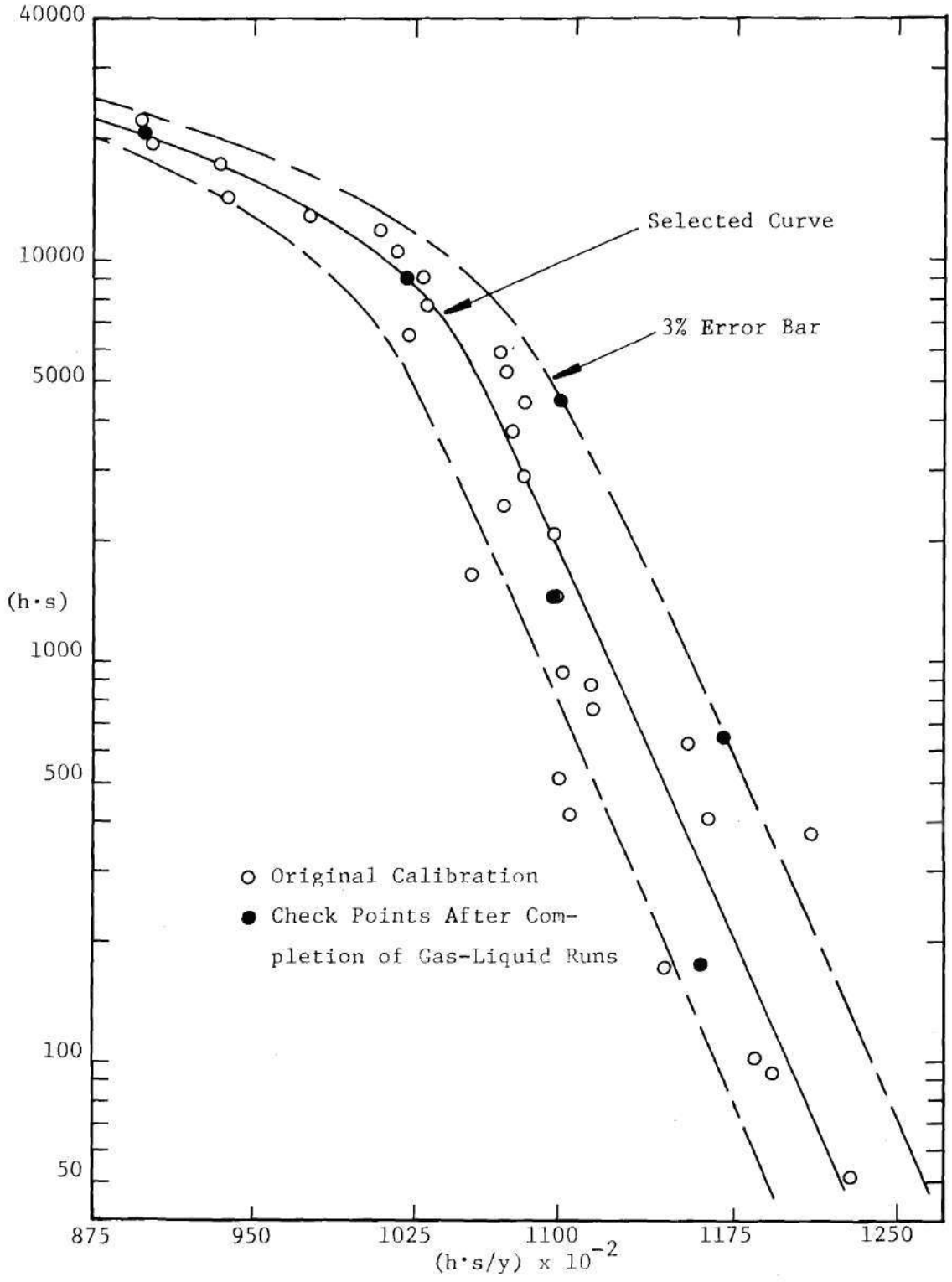

Figure 44. Calibration Curve of Ethylene in Helium.

system for gas imperfection in the gas mixtures.

The solubility of helium in ethylene over this temperature range covers a much smaller composition range. The calibration curve showed a range of composition from 0.0295 to 4.77 mole percent using a 154B Perkin-Elmer chromatograph. Seven standard bottles were made for this calibration and Figure 45 shows the final selected calibration curve.

Helium-Propylene System

This system was studied along five different isotherms all in the gas-liquid region. Therefore, it was again necessary to establish calibration curves for the determination of gas and liquid compositions. The chromatograph calibration curves for the determination of propylene in the gas phase is shown in Figure 46. The curve covers a composition range from 0.0363 to 30.9 mole percent, and required the use of nine standard bottles on the 154D chromatograph. In this calibration the gas mixtures made up in the gas burette were corrected for gas imperfection by about 1.4 percent.

The calibration curve used for the analysis of helium in liquid propylene was the same curve established for the analysis of helium in liquid ethylene on the 154B chromatograph, Figure 45. It was quite apparent that, due to the modification applied to the 154B chromatograph, the component present with the helium should not affect the analysis of the helium. A check of the calibration curve using a few helium-propylene mixtures verified this hypothesis as is shown in Figure 45.

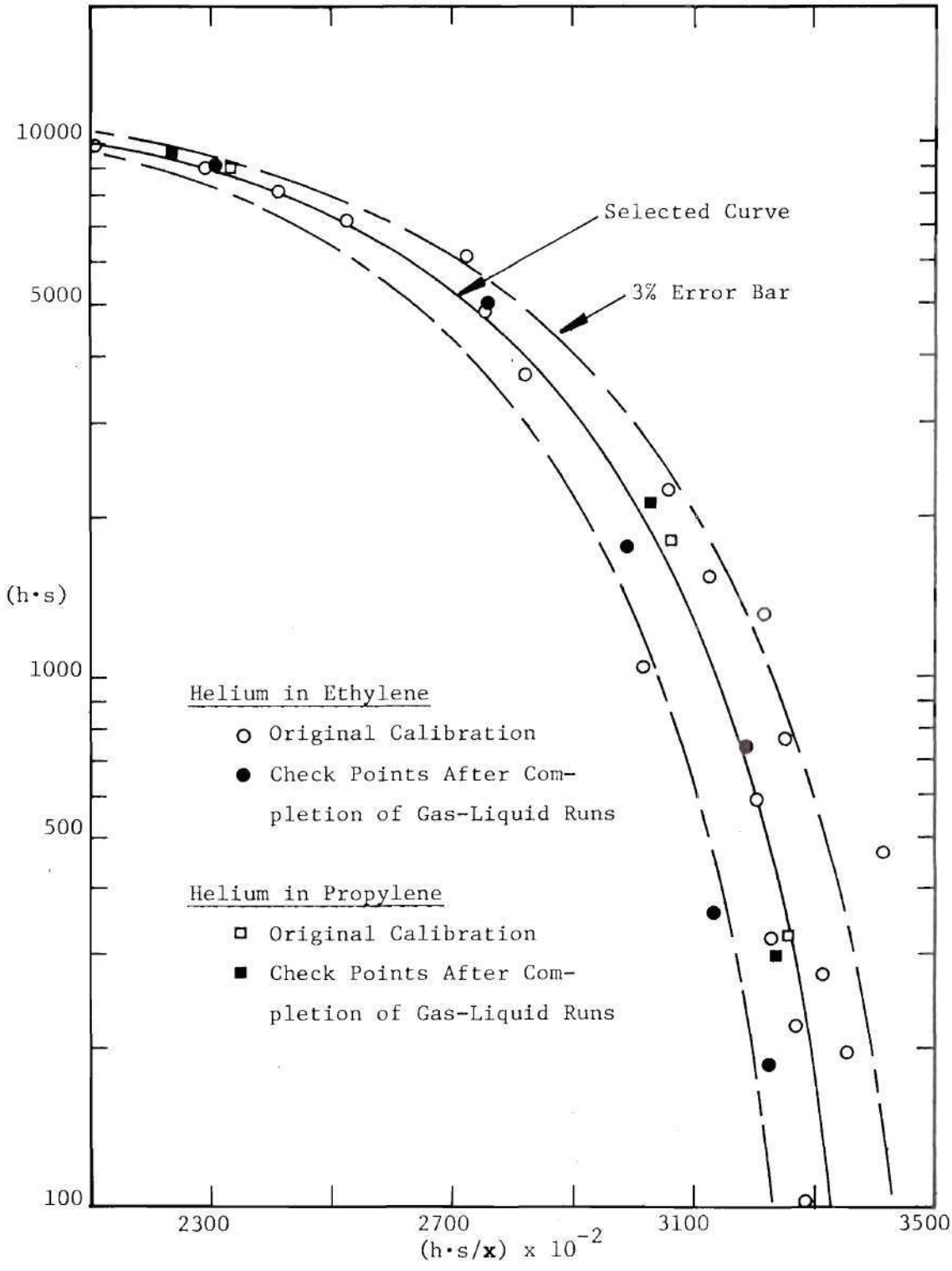

Figure 45. Calibration Curve of Helium in Ethylene and Propylene.

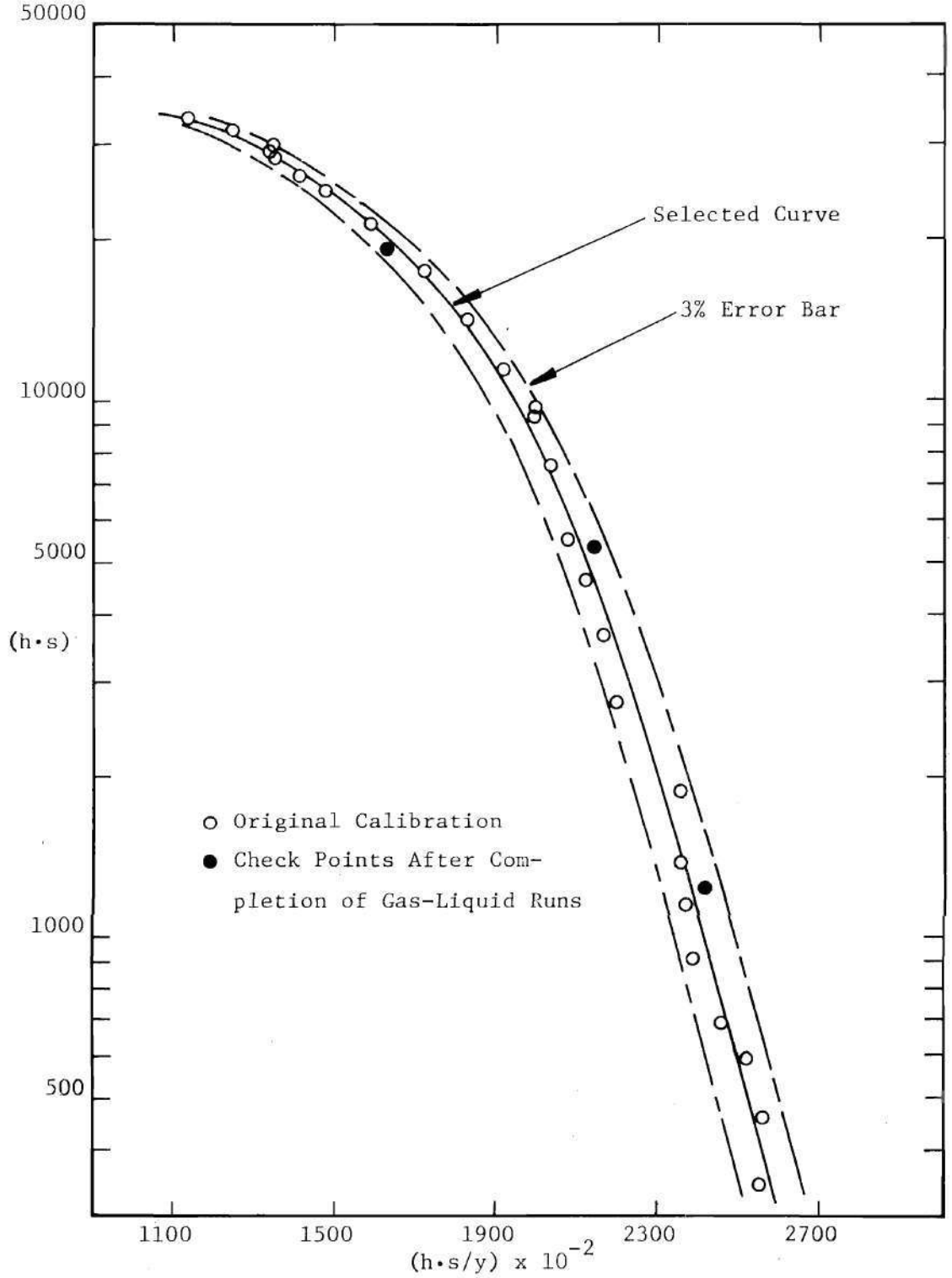

Figure 46. Calibration Curve of Propylene in Helium.

Comments on Calibration Curves

In all calibration curves shown in this work, the ± 3 mole percent error lines are used to indicate the degree of scatter present during the calibration. At the low composition end of the curve, the scatter is usually larger than three percent. This scatter indicates the approximate uncertainty in the phase equilibrium measurements due to analysis. Table 22 gives specific operational information about the chromatographic columns and conditions used in each analysis.

Since it took several days for the chromatograph calibration to be completed, it was necessary to choose a mean room temperature and pressure. All peak heights measured during this calibration were corrected to this standard set of ambient conditions by assuming that the change in the number of moles contained in the sample was proportional to the change in temperature and pressure. During an experimental run, this correction was not done since the standard bottle height automatically corrects for temperature and pressure variations by changing its height from its calibration value.

The rerun points shown on all three calibration curves were all performed after the phase equilibrium runs were completed. These points gave confidence that the calibration curve stayed constant during the entire experiment.

It was mentioned in Chapter III that, due to some experimental enhancement factors obtained in the helium-propylene system at the two lowest isotherms, 187.5 and 175.0 K, the calibration curve for propylene, Figure 46, was suspected of containing a systematic error in the

Table 22. Operating Conditions of Chromatographs

	Systems of Analysis			
	He in C_2H_4	He in C_3H_6	C_2H_4 in He	C_3H_6 in He
Chromatograph	154B	154B	154D	154D
Perkin-Elmer Column Type	Molecular Sieve	Molecular Sieve	Silica Gel	Dimethyl-sulfolane
Length, meter	2	2	1	2
Oven Temperature, °C	32	32	41	29
Carrier Gas	Argon	Argon	Helium	Helium
Flow Rate, cc/min	58	58	337	99
Sample Size, cc	10	10	15.6	15.6
Detector Voltage mv at Shunt	60	60	4.6	4.6
Recorder Voltage mv at Shunt	7	7	0.75*	3.0*
Chart Speed, inches/min	1.5	1.5	1.5	1.5

*These voltages caused a deflection of 90 and 95, respectively, on the recorder.

lowest concentration region. The reason for this hypothesis is that the lowest isotherm, 175.0 K, gave values of the enhancement factor that were less than unity. Although enhancement factors less than one have been observed in the helium-mercury[152] and helium-napthalene[75] systems, and a good summary of this phenomenon is presented by Haar and Sengers,[43] there are several reasons why it is not expected to occur in the helium-propylene system. First, from a corresponding states basis, this system would not agree with the other helium-hydrocarbon systems. Second, the reliable theoretical enhancement factor models do not predict that this should occur. Third, use of these enhancement factor data to extract interaction virial coefficient data would lead to a B_{12} curve that has a negative slope. A negative slope in this type of curve has never been shown except in mixtures where both components are well above their critical temperatures (see Chapter V). All of these results pointed to a possible error in these enhancement factor measurements at low temperature. A preliminary investigation did not reveal any possible source of direct error. The fact that the liquid compositions compared very well with the helium-propane solubility values seemed to indicate that perhaps a systematic error was present in the propylene calibration curve. Unfortunately, by the time all observations were made, the standard bottles used in the propylene analysis were destroyed and no check of the calibration curve could be made. Mr. Y. K. Yoon,[163] who is presently working on the helium-tetrafluoromethane system, did discover that a systematic error was present in the gas mixing burette. Apparently a capillary stopcock used on this apparatus had developed a slight blockage. Since each dilu-

tion of the original sample would include this error, in the lowest concentration region, 0.04 mole percent, this blockage could account for an enhancement factor error of 10 to 15 percent too low. Since phase equilibrium measurements on the helium-ethylene system appear to agree well with data from an independent investigator, it appears that the blockage occurred some time after the helium-ethylene system was run. It now appears probable that the gas phase composition measurements at the lowest temperatures for the helium-propylene system may have been in error by as much as 15 percent. For these reasons, the enhancement factors at 175.00 and 187.49 K have not been reported.

APPENDIX E

SUMMARY OF PHASE EQUILIBRIUM DATA FOR THE HELIUM-ETHYLENE AND HELIUM-PROPYLENE SYSTEMS

Phase equilibrium data for the helium-ethylene and the helium-propylene systems are presented in Tables 23 through 26. These tables present the gas-liquid equilibrium compositions for these two systems as a function of pressure and temperature. Six pressure points, ranging from approximately 120 to 20 atmospheres, were measured along each isotherm.

The first column in these tables gives the code number of the sample. The first number represents the pressure setting, the first letter represents the isotherm being measured and the second number represents the sample number.

Pressure gauge corrections were made using the results given in Appendix C and adding the barometric pressure to the gauge reading. Temperature of the equilibrium cell and the cell difference thermocouple were continuously monitored during each run. At a given pressure point, the equilibrium temperature could easily be controlled to ± 0.03 K. The cell difference thermocouple values ranged from 0.00 to a maximum of 0.03 K in the helium-ethylene system and from 0.00 to 0.022 K in the helium-propylene system. The temperature assigned to the gas equilibrium sample was the temperature indicated by the platinum resistance thermometer at the time of the analysis. All temperatures were measured on the (IPTS-48),

but using the procedure described in Appendix C, they have been corrected to the (IPTS-68). The temperature of the liquid sample was the temperature indicated by the platinum resistance thermometer at the moment of withdrawal. No correction was made for the small thermal gradient along the bomb, since one half of the bomb temperature difference was always less than 0.015 K.

The flow rate used in almost all of these experimental points was 100 cc/hr at the cell temperature and pressure. This corresponds to a residence time of 25 minutes in the cell. As was mentioned in Chapter III, this flow rate was found to be sufficient for equilibrium to be reached.

Table 23. Experimental Gas Phase Equilibrium Composition in the Helium-Ethylene System

Sample No.	T K	P atm	P_{01} atm	100 y_1 mole percent	ϕ
1A3	129.976	119.65	0.04346	0.0458	1.261
1A4	129.973	119.65	0.04345	0.0454	1.249
1A5	129.972	119.65	0.04344	0.0447	1.231
SELECTED	129.97	119.65			1.247
2A3	129.992	100.05	0.04354	0.0519	1.193
2A4	129.991	100.05	0.04353	0.0519	1.193
2A5	129.970	100.05	0.04343	0.0525	1.210
SELECTED	129.98	100.05			1.199
3A4	129.987	80.45	0.04351	0.0635	1.174
3A5	129.988	80.45	0.04352	0.0645	1.192
3A6	129.985	80.45	0.04350	0.0639	1.182
SELECTED	129.99	80.45			1.183
4A3	129.978	63.16	0.04347	0.0766	1.112
4A4	129.978	63.16	0.04347	0.0769	1.117
4A5	129.977	63.16	0.04347	0.0774	1.124
SELECTED	129.98	63.16			1.118
5A2	129.973	41.93	0.04345	0.1105	1.066
5A3	129.974	41.93	0.04345	0.1096	1.058
5A4	129.975	41.93	0.04346	0.1091	1.053
SELECTED	129.97	41.93			1.059
6A2	129.979	22.35	0.04348	0.2023	1.040
6A3	129.982	22.35	0.04349	0.1989	1.022
6A4	129.990	22.35	0.04353	0.2019	1.037
SELECTED	129.98	22.35			1.033
1B3	150.019	119.24	0.26989	0.2544	1.124
1B4	150.022	119.24	0.26995	0.2507	1.107
1B5	150.023	119.24	0.26997	0.2538	1.121
SELECTED	150.02	119.24			1.117
2B3	150.018	99.91	0.26987	0.2914	1.079
2B4	150.014	99.91	0.26979	0.2950	1.092
2B5	150.015	99.91	0.26981	0.2936	1.087
SELECTED	150.02	99.91			1.086

Table 23. (Continued)

Sample No.	T K	P atm	P_{01} atm	100 y_1 mole percent	ϕ
3B2	150.020	99.78	0.26991	0.3021	1.117
3B3	150.018	99.78	0.26987	0.3016	1.115
3B4	150.009	99.78	0.26968	0.3025	1.119
SELECTED	150.02	99.78			1.117
4B2	150.020	80.59	0.26991	0.3624	1.082
4B3	150.019	80.59	0.26989	0.3640	1.087
4B4	150.025	80.59	0.27002	0.3562	1.063
SELECTED	150.02	80.59			1.077
5B3	149.986	60.24	0.26920	0.4770	1.067
5B4	149.985	60.24	0.26918	0.4764	1.066
5B5	149.981	60.24	0.26889	0.4760	1.066
SELECTED	149.99	60.24			1.066
6B3	150.003	42.07	0.26956	0.6788	1.059
6B4	150.011	42.07	0.26972	0.6865	1.071
6B5	150.000	42.07	0.26949	0.6813	1.064
SELECTED	150.01	42.07			1.065
7B3	150.010	22.95	0.26970	1.235	1.051
7B4	150.002	22.95	0.26954	1.242	1.058
7B5	150.009	22.95	0.26968	1.246	1.060
SELECTED	150.01	22.95			1.056
1C5	162.002	119.10	0.63208	0.5896	1.111
1C6	162.013	119.10	0.63253	0.5868	1.105
1C7	162.007	119.10	0.63228	0.5878	1.107
SELECTED	162.01	119.10			1.108
2C3	162.017	99.61	0.63270	0.7044	1.109
2C4	162.021	99.61	0.63286	0.6987	1.100
2C5	162.022	99.61	0.63290	0.6963	1.096
SELECTED	162.02	99.61			1.102
3C4	162.001	81.27	0.63204	0.8482	1.091
3C5	162.008	81.27	0.63233	0.8463	1.088
3C6	162.013	81.27	0.63253	0.8505	1.093
3C7	162.008	81.27	0.63233	0.8549	1.099
SELECTED	162.01	81.27			1.093

Table 23. (Continued)

Sample No.	T K	P atm	P_{01} atm	100 y_1 mole percent	ϕ
4C3	161.996	81.06	0.63183	0.8528	1.094
4C4	161.997	81.06	0.63182	0.8503	1.091
4C5	162.000	81.06	0.63200	0.8503	1.091
SELECTED	162.00	81.06			1.092
5C3	161.987	60.38	0.63146	1.134	1.084
5C4	161.983	60.38	0.63130	1.135	1.086
5C5	161.983	60.38	0.63130	1.124	1.075
SELECTED	161.98	60.38			1.082
6C5	161.991	42.01	0.63163	1.617	1.075
6C6	161.984	42.01	0.63134	1.588	1.057
6C7	161.989	42.01	0.63154	1.606	1.068
SELECTED	161.99	42.01			1.067
7C8	161.996	22.91	0.63183	2.961	1.074
7C9	161.983	22.91	0.63130	2.936	1.065
7C10	161.991	22.91	0.63163	2.966	1.076
SELECTED	161.99	22.91			1.072
1D9	174.001	118.77	1.3043	1.236	1.126
1D10	173.990	118.77	1.3035	1.239	1.129
1D11	173.993	118.77	1.3037	1.241	1.131
SELECTED	174.00	118.77			1.129
2D4	174.029	99.71	1.3064	1.448	1.105
2D5	174.010	99.71	1.3050	1.454	1.111
2D6	174.032	99.71	1.3066	1.445	1.103
SELECTED	174.02	99.71			1.106
3D4	173.990	80.66	1.3035	1.781	1.102
3D5	173.990	80.66	1.3035	1.776	1.099
3D6	173.991	80.66	1.3036	1.774	1.098
SELECTED	173.99	80.66			1.100
4D6	173.981	60.24	1.3029	2.363	1.093
4D7	173.972	60.24	1.3022	2.357	1.090
4D8	173.974	60.24	1.3024	2.360	1.092
SELECTED	173.98	60.24			1.092
5D7	173.985	41.87	1.3032	3.391	1.089
5D8	173.977	41.87	1.3026	3.389	1.089
5D9	173.973	41.87	1.3023	3.384	1.088
SELECTED	173.98	41.87			1.089

Table 23. (Continued)

Sample No.	T K	P atm	P_{01} atm	100 y_1 mole percent	ϕ
6D4	173.987	22.92	1.3033	6.056	1.065
6D5	173.988	22.92	1.3034	6.028	1.060
6D6	173.984	22.92	1.3031	6.035	1.061
SELECTED	173.99	22.92			1.062
1E3	188.015	119.17	2.6632	2.592	1.160
1E4	188.019	119.17	2.6637	2.589	1.158
1E5	188.023	119.17	2.6642	2.600	1.163
SELECTED	188.02	119.17			1.160
2E4	188.031	99.51	2.6652	2.979	1.112
2E5	188.046	99.51	2.6671	2.993	1.117
2E6	188.034	99.51	2.6656	3.002	1.121
2E7	188.030	99.51	2.6651	2.982	1.113
SELECTED	188.02	99.51			1.116
3E5	188.046	80.72	2.6671	3.725	1.127
3E6	188.044	80.72	2.6686	3.709	1.122
3E7	188.057	80.72	2.6685	3.757	1.136
3E8	188.048	80.72	2.6674	3.742	1.132
SELECTED	188.05	80.72			1.129
4E3	188.034	60.24	2.6656	4.952	1.119
4E4	188.035	60.24	2.6657	4.960	1.121
4E5	188.043	60.24	2.6667	4.957	1.120
SELECTED	188.04	60.24			1.120
5E2	187.961	42.35	2.6565	6.910	1.102
5E3	187.974	42.35	2.6581	6.791	1.082
5E4	187.963	42.35	2.6568	6.834	1.089
SELECTED	187.97	42.35			1.091
6E5	188.003	42.20	2.6618	6.962	1.104
6E6	187.976	42.20	2.6584	6.960	1.105
6E7	188.003	42.20	2.6618	6.979	1.106
SELECTED	187.99	42.20			1.105
7E4	187.991	23.80	2.6603	12.22	1.093
7E5	187.993	23.80	2.6605	12.29	1.099
7E6	187.993	23.80	2.6605	12.31	1.101
7E7	187.996	23.80	2.6609	12.25	1.096
SELECTED	187.99	23.80			1.097

Table 23. (Continued)

Sample No.	T K	P atm	P_{01} atm	100 y_1 mole percent	ϕ
1F4	201.995	119.51	4.8760	4.919	1.206
1F5	202.001	119.51	4.8772	4.888	1.198
1F6	201.997	119.51	4.8764	4.911	1.204
SELECTED	202.00	119.51			1.203
2F3	202.002	119.30	4.8774	4.914	1.202
2F4	201.999	119.30	4.8768	4.893	1.197
2F5	202.000	119.30	4.8770	4.901	1.199
SELECTED	202.00	119.30			1.199
3F3	201.987	99.64	4.8744	5.852	1.196
3F4	201.986	99.64	4.8742	5.819	1.190
3F5	201.984	99.64	4.8738	5.838	1.194
SELECTED	201.99	99.64			1.193
4F5	202.014	81.13	4.8797	7.030	1.169
4F6	202.015	81.13	4.8799	7.013	1.166
4F7	202.023	81.13	4.8815	6.966	1.158
SELECTED	202.02	81.13			1.164
5F4	202.047	60.17	4.8862	9.418	1.160
5F5	202.044	60.17	4.8856	9.442	1.163
5F6	202.035	60.17	4.8838	9.409	1.159
SELECTED	202.04	60.17			1.161
6F6	202.016	42.54	4.8801	13.13	1.145
6F7	202.016	42.54	4.8801	13.17	1.148
6F8	202.016	42.54	4.8801	13.19	1.150
SELECTED	202.02	42.54			1.148
7F3	202.021	24.61	4.8811	21.93	1.106
7F4	202.022	24.61	4.8813	22.07	1.113
7F5	202.029	24.61	4.8826	22.20	1.119
SELECTED	202.02	24.61			1.113
1G2	216.021	119.09	8.2324	8.626	1.248
1G3	216.009	119.09	8.2289	8.606	1.246
1G4	215.999	119.09	8.2260	8.627	1.249
SELECTED	216.01	119.09			1.248
2G3	216.050	99.77	8.2407	10.27	1.244
2G4	216.049	99.77	8.2404	10.18	1.233
2G5	216.040	99.77	8.2378	10.17	1.232
SELECTED	216.04	99.77			1.236

Table 23. (Concluded)

Sample No.	T K	P atm	P_{01} atm	100 y_1 mole percent	ϕ
3G2	216.026	83.11	8.2338	12.16	1.227
3G3	216.050	83.11	8.2407	12.29	1.239
3G4	216.017	83.11	8.2312	12.07	1.219
3G5	216.037	83.11	8.2369	12.22	1.233
SELECTED	216.03	83.11			1.230
4G3	216.032	60.25	8.2355	16.24	1.188
4G4	216.037	60.25	8.2369	16.26	1.189
4G5	216.042	60.25	8.2384	16.17	1.183
SELECTED	216.04	60.25			1.187
5G3	216.046	42.29	8.2395	23.03	1.182
5G4	216.047	42.29	8.2398	22.78	1.169
5G5	216.048	42.29	8.2401	22.88	1.174
SELECTED	216.05	42.29			1.175

Table 24. Experimental Values of Equilibrium Liquid Phase Compositions in the Helium-Ethylene System

Sample No.	T K	P atm	100 x_2 mole percent
1A1	129.971	119.65	0.1740
1A2	129.971	119.65	0.1749
SELECTED	129.97	119.65	0.1745
2A1	129.966	100.05	0.1472
2A2	129.966	100.05	0.1469
SELECTED	129.97	100.05	0.1471
3A1	129.983	80.45	0.1282
3A2	129.983	80.45	0.1285
SELECTED	129.98	80.45	0.1284
4A1	129.975	60.28	0.0947
4A2	129.975	60.28	0.0949
SELECTED	129.98	60.28	0.0948
5A1	129.977	41.93	0.0652
5A2	129.977	41.93	0.0651
SELECTED	129.98	41.93	0.0652
6A1	129.998	22.35	0.0396
6A2	129.998	22.35	0.0407
SELECTED	130.00	22.35	0.0401
1B1	150.025	119.24	0.3887
1B2	150.025	119.24	0.3887
SELECTED	150.03	119.24	0.3887
2B1	150.015	99.91	0.3293
2B2	150.015	99.91	0.3313
SELECTED	150.02	99.91	0.3303
3B1	150.000	99.78	0.3280
3B2	150.000	99.78	0.3264
SELECTED	150.00	99.78	0.3272
4B1	150.030	80.59	0.2666
4B2	150.030	80.59	0.2675
SELECTED	150.03	80.59	0.2671

Table 24. (Continued)

Sample No.	T K	P atm	100 x_2 mole percent
6B1	150.000	42.07	0.1489
6B2	150.000	42.07	0.1496
SELECTED	150.00	42.07	0.1493
7B1	150.010	22.95	0.0818
7B2	150.010	22.95	0.0793
SELECTED	150.01	22.95	0.0805
1C1	162.008	119.10	0.5888
1C2	162.008	119.10	0.5866
SELECTED	162.01	119.10	0.5877
2C1	162.023	99.61	0.5058
2C2	162.023	99.61	0.5068
SELECTED	162.02	99.61	0.5063
3C1	162.003	81.27	0.4134
3C2	162.003	81.27	0.4156
SELECTED	162.00	81.27	0.4145
5C1	161.983	60.38	0.3091
5C2	161.983	60.38	0.3091
SELECTED	161.98	60.38	0.3091
6C1	161.993	42.01	0.2213
6C2	161.993	42.01	0.2197
SELECTED	161.99	42.01	0.2205
7C1	161.999	22.91	0.1182
7C2	161.999	22.91	0.1180
SELECTED	162.00	22.91	0.1181
1D1	173.996	118.77	0.8561
1D2	173.996	118.77	0.8581
SELECTED	174.00	118.77	0.8572
2D1	174.043	99.71	0.7205
2D2	174.043	99.71	0.7273
SELECTED	174.04	99.71	0.7239
3D1	173.992	80.66	0.5907
3D2	173.992	80.66	0.5899
SELECTED	173.99	80.66	0.5903

Table 24. (Continued)

Sample No.	T K	P atm	100 x_2 mole percent
4D1	173.976	60.24	0.4504
4D2	173.976	60.24	0.4508
SELECTED	173.98	60.24	0.4506
5D1	173.971	41.87	0.3071
5D2	173.971	41.87	0.3091
SELECTED	173.97	41.87	0.3081
6D1	173.980	22.92	0.1689
6D2	173.980	22.92	0.1695
SELECTED	173.98	22.92	0.1692
1E1	188.031	119.17	1.232
1E2	188.031	119.17	1.229
SELECTED	188.03	119.17	1.231
2E1	188.026	99.51	1.064
2E2	188.026	99.51	1.065
SELECTED	188.03	99.51	1.065
3E1	188.039	80.72	0.8641
3E2	188.039	80.72	0.8682
SELECTED	188.04	80.72	0.8662
4E1	188.051	60.24	0.6448
4E2	188.051	60.24	0.6414
4E3	188.051	60.24	0.6475
SELECTED	188.05	60.24	0.6446
5E1	187.970	42.35	0.4536
5E2	187.970	42.35	0.4554
SELECTED	187.97	42.35	0.4545
6E1	188.051	42.20	0.4515
6E2	188.051	42.20	0.4517
SELECTED	188.05	42.20	0.4516
7E1	187.999	23.80	0.2458
7E2	187.999	23.80	0.2469
7E3	187.999	23.80	0.2482
SELECTED	188.00	23.80	0.2469
1F1	201.995	119.51	1.721
1F2	201.995	119.51	1.728
SELECTED	202.00	119.51	1.725

Table 24. (Concluded)

Sample No.	T K	P atm	100 x_2 mole percent
3F1	201.982	99.64	1.446
3F2	201.982	99.64	1.448
SELECTED	201.98	99.64	1.447
5F1	202.026	60.17	0.8956
5F2	202.026	60.17	0.8987
5F3	202.026	60.17	0.8963
SELECTED	202.03	60.17	0.8969
6F1	202.016	42.54	0.6127
6F2	202.016	42.54	0.6108
SELECTED	202.02	42.54	0.6118
7F1	202.036	24.61	0.3168
7F2	202.036	24.61	0.3174
SELECTED	202.04	24.61	0.3171
2G1	216.031	99.77	1.947
2G2	216.031	99.77	1.942
SELECTED	216.03	99.77	1.945
4G1	216.048	60.25	1.187
4G2	216.048	60.25	1.167
4G3	216.048	60.25	1.169
SELECTED	216.05	60.25	1.174
5G1	216.060	42.29	0.8153
SELECTED	216.06	42.29	0.8153

Table 25. Experimental Gas Phase Equilibrium Composition in the Helium-Propylene System

Sample No.	T K	P atm	P_{01} atm	100 y_1 mole percent	ϕ
1C6	200.011	118.42	0.26527	0.2295	1.025
1C7	200.012	118.42	0.26528	0.2309	1.031
1C8	200.014	118.42	0.26532	0.2303	1.028
1C9	200.015	118.42	0.26533	0.2291	1.023
SELECTED	200.01	118.42			1.027
2C5	200.009	99.50	0.26524	0.2806	1.053
2C6	200.010	99.50	0.26525	0.2811	1.054
2C7	200.010	99.50	0.26525	0.2811	1.054
2C8	199.997	99.50	0.26505	0.2798	1.050
SELECTED	200.01	99.50			1.053
3C3	199.999	80.79	0.26508	0.3463	1.055
3C4	199.999	80.79	0.26508	0.3471	1.058
3C5	199.999	80.79	0.26508	0.3473	1.059
SELECTED	200.00	80.79			1.057
4C3	200.001	60.24	0.26511	0.4500	1.023
4C4	199.999	60.24	0.26508	0.4489	1.020
4C5	200.003	60.24	0.26514	0.4507	1.024
4C6	200.013	60.24	0.26530	0.4501	1.022
SELECTED	200.00	60.24			1.022
5C4	199.991	41.67	0.26495	0.6451	1.015
5C5	200.003	41.67	0.26514	0.6426	1.010
5C6	199.998	41.67	0.26406	0.6435	1.012
5C7	199.997	41.67	0.26505	0.6420	1.009
SELECTED	200.00	41.67			1.012
6C3	199.996	23.03	0.26503	1.182	1.027
6C4	200.000	23.03	0.26509	1.180	1.025
6C5	199.998	23.03	0.26506	1.180	1.025
6C6	200.001	23.03	0.26511	1.179	1.024
SELECTED	200.00	23.03			1.025
1D3	212.509	118.22	0.53270	0.4686	1.040
1D4	212.513	118.22	0.53282	0.4688	1.040
1D5	212.507	118.22	0.53265	0.4676	1.038
1D6	212.506	118.22	0.53262	0.4674	1.037
SELECTED	212.51	118.22			1.039

Table 25. (Continued)

Sample No.	T K	P atm	P_{01} atm	100 y_1 mole percent	ϕ
2D3	212.496	100.46	0.53234	0.5521	1.042
2D4	212.494	100.46	0.53229	0.5474	1.033
2D5	212.499	100.46	0.53243	0.5485	1.035
SELECTED	212.50	100.46			1.037
3D3	212.487	80.59	0.53209	0.6811	1.032
3D4	212.495	80.59	0.53232	0.6823	1.033
3D5	212.482	80.59	0.53196	0.6863	1.040
3D6	212.484	80.59	0.53201	0.6892	1.044
SELECTED	212.49	80.59			1.037
4D3	212.488	60.24	0.53212	0.9188	1.040
4D4	212.489	60.24	0.53215	0.9185	1.040
4D5	212.492	60.24	0.53223	0.9195	1.041
SELECTED	212.49	60.24			1.040
5D4	212.490	41.05	0.53218	1.344	1.037
5D5	212.487	41.05	0.53209	1.346	1.038
5D6	212.481	41.05	0.53193	1.346	1.039
SELECTED	212.49	41.05			1.038
6D3	212.478	23.45	0.53185	2.389	1.053
6D4	212.487	23.45	0.53209	2.386	1.052
6D5	212.476	23.45	0.53179	2.390	1.054
6D6	212.468	23.45	0.53157	2.398	1.058
SELECTED	212.48	23.45			1.054
1E3	224.997	118.69	0.97955	0.8785	1.064
1E4	224.996	118.69	0.97951	0.8777	1.064
1E5	224.994	118.69	0.97942	0.8781	1.064
1E6	224.997	118.69	0.97955	0.8790	1.065
SELECTED	225.00	118.69			1.064
2E2	224.984	100.86	0.97897	1.029	1.060
2E3	224.984	100.86	0.97897	1.034	1.065
2E4	224.989	100.86	0.97919	1.034	1.065
2E5	224.981	100.86	0.97884	1.038	1.070
SELECTED	224.99	100.86			1.065
3E3	224.984	81.40	0.97897	1.279	1.064
3E4	224.998	81.40	0.97960	1.280	1.064
3E5	224.989	81.40	0.97919	1.279	1.064
SELECTED	224.99	81.40			1.064

Table 25. (Continued)

Sample No.	T K	P atm	P_{01} atm	100 y_1 mole percent	ϕ
4E2	224.979	60.45	0.97875	1.725	1.065
4E3	224.987	60.45	0.97910	1.727	1.066
4E4	224.989	60.45	0.97919	1.727	1.066
4E5	224.984	60.45	0.97897	1.729	1.068
SELECTED	224.99	60.45			1.066
5E2	224.992	40.98	0.97933	2.546	1.065
5E3	224.989	40.98	0.97919	2.545	1.065
5E4	224.996	40.98	0.97951	2.545	1.065
5E5	224.992	40.98	0.97933	2.545	1.065
SELECTED	224.99	40.98			1.065
6E3	224.985	25.47	0.97901	4.093	1.065
6E4	224.984	25.47	0.97897	4.080	1.062
6E5	224.992	25.47	0.97933	4.084	1.062
SELECTED	224.99	25.47			1.063
1F5	239.990	119.92	1.8528	1.702	1.102
1F6	239.986	119.92	1.8525	1.707	1.105
1F7	239.982	119.92	1.8522	1.706	1.105
1F8	239.987	119.92	1.8525	1.706	1.104
SELECTED	239.99	119.92			1.104
2F4	239.986	100.86	1.8525	2.018	1.099
2F5	239.984	100.86	1.8523	2.018	1.099
2F6	239.991	100.86	1.8528	2.026	1.103
2F7	239.985	100.86	1.8524	2.031	1.106
SELECTED	239.99	100.86			1.102
3F5	239.986	80.59	1.8525	2.532	1.101
3F6	239.982	80.59	1.8522	2.548	1.109
3F7	239.982	80.59	1.8522	2.544	1.107
3F8	239.989	80.59	1.8527	2.538	1.104
SELECTED	239.99	80.59			1.105
4F3	239.988	60.25	1.8526	3.376	1.098
4F4	239.997	60.25	1.8533	3.388	1.101
4F5	239.997	60.25	1.8533	3.393	1.105
4F6	239.973	60.25	1.8515	3.388	1.102
SELECTED	239.99	60.25			1.102

Table 25. (Concluded)

Sample No.	T K	P atm	P_{01} atm	100 y_1 mole percent	ϕ
5F5	239.984	41.13	1.8523	4.932	1.095
5F6	239.992	41.13	1.8529	4.929	1.095
5F7	239.993	41.13	1.8530	4.936	1.096
5F8	239.997	41.13	1.8533	4.935	1.095
SELECTED	239.99	41.13			1.095
6F4	240.000	26.09	1.8535	7.605	1.070
6F5	240.002	26.09	1.8536	7.601	1.070
6F6	239.978	26.09	1.8519	7.603	1.071
SELECTED	239.99	26.09			1.070
1G10	254.971	118.43	3.2222	3.103	1.140
1G11	254.968	118.43	3.2219	3.117	1.146
1G12	254.973	118.43	3.2225	3.121	1.147
SELECTED	254.97	118.43			1.144
2G6	254.971	101.20	3.2222	3.647	1.145
2G7	254.975	101.20	3.2227	3.644	1.144
2G8	254.979	101.20	3.2231	3.640	1.143
2G9	254.983	101.20	3.2236	3.645	1.144
SELECTED	254.98	101.20			1.144
3G4	254.968	80.32	3.2219	4.568	1.139
3G5	254.976	80.32	3.2228	4.567	1.138
3G6	254.978	80.32	3.2230	4.572	1.139
SELECTED	254.97	80.32			1.139
4G4	254.984	60.65	3.2237	5.981	1.125
4G5	254.979	60.65	3.2231	5.981	1.125
4G6	254.988	60.65	3.2241	5.980	1.125
SELECTED	254.98	60.65			1.125
5G5	254.976	41.66	3.2228	8.565	1.107
5G6	254.975	41.66	3.2227	8.571	1.108
5G7	254.976	41.66	3.2228	8.574	1.108
5G8	254.971	41.66	3.2222	8.588	1.110
SELECTED	254.98	41.66			1.108
6G5	254.974	25.27	3.2226	13.85	1.086
6G6	254.975	25.27	3.2227	13.84	1.085
6G7	254.971	25.27	3.2222	13.81	1.083
6G8	254.970	25.27	3.2221	13.83	1.085
SELECTED	254.97	25.27			1.085

Table 26. Experimental Values of Equilibrium Liquid Phase Compositions in the Helium-Propylene System

Sample No.	T K	P atm	100 x_2 mole percent
1A1	174.986	118.83	0.4259
1A2	174.986	118.83	0.4309
SELECTED	174.99	118.83	0.4284
2A1	175.000	118.62	0.4241
2A2	175.000	118.62	0.4233
SELECTED	175.00	118.62	0.4238
4A1	174.997	100.39	0.3646
4A2	174.997	100.39	0.3681
SELECTED	175.00	100.39	0.3664
5A1	174.999	80.38	0.2905
5A2	174.999	80.38	0.2930
SELECTED	175.00	80.38	0.2918
6A1	175.007	60.04	0.2323
6A2	175.007	60.04	0.2326
SELECTED	175.01	60.04	0.2325
7A1	175.013	42.21	0.1611
7A2	175.013	42.21	0.1619
SELECTED	175.01	42.21	0.1615
8A1	174.999	22.81	0.0877
8A2	174.999	22.81	0.0874
SELECTED	175.00	22.81	0.0876
1B1	187.503	117.40	0.5979
1B2	187.503	117.40	0.5952
1B3	187.505	117.40	0.5952
SELECTED	187.50	117.40	0.5961
2B1	187.499	99.16	0.5014
2B2	187.499	99.16	0.5018
2B3	187.488	99.16	0.5049
SELECTED	187.50	99.16	0.5027
3B1	187.502	83.51	0.4311
3B2	187.502	83.51	0.4323
SELECTED	187.50	83.51	0.4317

Table 26. (Continued)

Sample No.	T K	P atm	100 x_2 mole percent
4B1	187.494	59.97	0.3121
4B2	187.494	59.97	0.3132
4B3	187.499	59.97	0.3113
SELECTED	187.50	59.97	0.3122
5B1	187.494	41.33	0.2227
5B2	187.494	41.33	0.2222
5B3	187.494	41.33	0.2246
SELECTED	187.49	41.33	0.2232
6B1	187.517	23.10	0.1219
6B2	187.517	23.10	0.1216
6B3	187.521	23.10	0.1231
SELECTED	187.52	23.10	0.1222
1C1	200.014	118.42	0.8157
1C2	200.014	118.42	0.8196
1C3	200.015	118.42	0.8133
SELECTED	200.01	118.42	0.8162
2C1	200.008	99.50	0.6831
2C2	200.008	99.50	0.6863
2C3	199.995	99.50	0.6881
SELECTED	200.00	99.50	0.6858
3C1	199.999	80.79	0.5577
3C2	199.999	80.79	0.5615
3C3	199.999	80.79	0.5556
SELECTED	200.00	80.79	0.5583
4C1	200.008	60.24	0.4296
4C2	200.008	60.24	0.4328
4C3	200.014	60.24	0.4305
SELECTED	200.01	60.24	0.4310
5C1	199.998	41.67	0.2971
5C2	199.998	41.67	0.2958
5C3	199.997	41.67	0.2952
SELECTED	200.00	41.67	0.2960
6C1	200.001	23.03	0.1671
6C2	200.001	23.03	0.1697
6C3	199.987	23.03	0.1708
SELECTED	200.00	23.03	0.1692

Table 26. (Continued)

Sample No.	T K	P atm	100 x_2 mole percent
1D1	212.499	118.22	1.039
1D2	212.499	118.22	1.045
1D3	212.497	118.22	1.051
1D4	212.497	118.22	1.051
SELECTED	212.50	118.22	1.047
2D1	212.499	100.46	0.9213
2D3	212.499	100.46	0.9238
2D4	212.504	100.46	0.9198
SELECTED	212.50	100.46	0.9216
3D1	212.482	80.59	0.7458
3D2	212.482	80.59	0.7465
3D3	212.485	80.59	0.7438
SELECTED	212.48	80.59	0.7454
4D1	212.490	60.24	0.5559
4D2	212.490	60.24	0.5568
4D3	212.493	60.24	0.5552
SELECTED	212.49	60.24	0.5560
5D1	212.485	41.05	0.3844
5D2	212.485	41.05	0.3859
5D3	212.473	41.05	0.3870
SELECTED	212.48	41.05	0.3858
6D1	212.473	23.45	0.2228
6D2	212.473	23.45	0.2263
6D3	212.465	23.45	0.2260
SELECTED	212.47	23.45	0.2250
1E1	224.995	118.69	1.370
1E2	224.995	118.69	1.358
1E3	224.999	118.69	1.368
SELECTED	225.00	118.69	1.365
2E1	224.986	100.86	1.164
2E2	224.986	100.86	1.162
2E3	224.982	100.86	1.170
SELECTED	224.98	100.86	1.165
3E1	224.998	81.40	0.9753
3E2	224.998	81.40	0.9746
3E3	224.988	81.40	0.9789
SELECTED	224.99	81.40	0.9763

Table 26. (Continued)

Sample No.	T K	P atm	100 x_2 mole percent
4E1	224.988	60.45	0.7254
4E2	224.988	60.45	0.7265
4E3	224.982	60.45	0.7291
SELECTED	224.99	60.45	0.7270
5E1	224.995	40.98	0.4799
5E2	224.995	40.98	0.4806
5E3	224.992	40.98	0.4818
SELECTED	224.99	40.98	0.4808
6E1	224.994	25.47	0.2932
6E2	224.994	25.47	0.2975
SELECTED	224.99	25.47	0.2954
1F1	239.984	119.92	1.836
1F2	239.984	119.92	1.840
1F3	239.986	119.92	1.839
SELECTED	239.98	119.92	1.838
2F1	239.988	100.86	1.538
2F2	239.988	100.86	1.541
2F3	239.983	100.86	1.540
SELECTED	239.99	100.86	1.540
3F1	239.983	80.59	1.232
3F2	239.983	80.59	1.233
3F3	239.990	80.59	1.232
SELECTED	239.99	80.59	1.232
4F1	239.989	60.25	0.9507
4F2	239.939	60.25	0.9531
4F3	239.973	60.25	0.9501
SELECTED	239.98	60.25	0.9513
5F1	239.982	41.13	0.6291
5F2	239.982	41.13	0.6315
5F3	239.991	41.13	0.6339
SELECTED	239.99	41.13	0.6315
6F1	239.982	26.09	0.3910
6F2	239.982	26.09	0.3911
6F3	239.991	26.09	0.3876
SELECTED	239.99	26.09	0.3900

Table 26. (Concluded)

Sample No.	T K	P atm	100 x_2 mole percent
1G1	254.972	118.43	2.251
1G2	254.972	118.43	2.256
1G3	254.974	118.43	2.267
1G4	254.974	118.43	2.260
SELECTED	254.97	118.43	2.259
2G1	254.981	101.20	2.004
2G2	254.981	101.20	2.016
SELECTED	254.98	101.20	2.010
3G1	254.962	80.32	1.594
3G2	254.962	80.32	1.600
3G3	254.977	80.32	1.595
SELECTED	254.97	80.32	1.596
4G1	254.979	60.65	1.182
4G2	254.979	60.65	1.179
4G3	254.992	60.65	1.184
SELECTED	254.98	60.65	1.182
5G1	254.975	41.66	0.8148
5G2	254.975	41.66	0.8189
5G3	254.971	41.66	0.8253
SELECTED	254.97	41.66	0.8197
6G1	254.969	25.27	0.4631
6G2	254.969	25.27	0.4671
SELECTED	254.97	25.27	0.4651

APPENDIX F

SELECTION OF PHYSICAL PROPERTY DATA

The calculation of theoretical enhancement factors and the extraction of B_{12}, Henry's law constant, and partial molar volume from binary phase equilibrium data requires a large amount of physical property data for the pure components.

The data required for these calculations are:

(1) The Lennard-Jones (6-12) classical and the Kihara (6-12) core model potential parameters for second virial coefficients.

(2) Third virial coefficient data.

(3) Benedict-Webb-Rubin parameters.

(4) Vapor pressure data.

(5) Saturated molar volume and isothermal compressibility data for the condensed phase. This collection of data for each compound represents the best available values found in the literature.

Two very good summaries of available second and third virial coefficient data are given by David and Hamann[24] and Dymond and Smith.[32] Kihara parameters generally fitted the second virial coefficient data very well, but the Lennard-Jones parameters seemed to be generally somewhat less satisfactory. In several cases where the Lennard-Jones fit was very poor, a least squares program, written by Mullins,[107] was used to determine new parameters. The Lennard-Jones and Kihara parameters selected are presented in Table 27.

Table 27. Intermolecular Potential Parameters and BWR Parameters

Parameter	He	C_2H_4	C_2H_6	C_3H_6	C_3H_8
LJCL (6-12)					
	(107)	(166)	(155)	(This Work)	(109)
e/k, K	6.96	150.76	194.14	167.66	195.0
b_o, cc/gm mole	22.9	227.06	179.42	425.14	379.4
KIHARA					
	(122)	(122)	(164)	(122)	(This Work)
U_o/k, K	9.927	383.00	453.00	475.00	506.00
ρ_o, Å	2.921	2.950	2.840	3.439	3.310
M_o, Å	0.0	8.800	10.17	10.51	12.75
S_o, Å^2	0.0	3.480	5.770	5.260	7.75
V_o, Å^3	0.0	0.0	0.6530	0.0	0.0
M	4.0026	28.0549	30.0708	42.0823	44.0983

BWR liter-atm-K-gm mole	He^{46}	$C_2H_4^4$	$C_2H_6^4$	$C_3H_6^4$	$C_3H_8^4$
A_o	1.308895 (-2)*	3.33958	4.15556	6.11220	6.87225
B_o	1.226171 (-2)	5.56833 (-2)	6.27724 (-2)	8.50647 (-2)	9.73130 (-2)
C_o	4.802198	1.31140 (5)	1.79592 (5)	4.39182 (5)	5.08256 (5)
a	5.759319 (-4)	2.59000 (-1)	3.45160 (-1)	7.74056 (-1)	9.47700 (-1)
b	3.352402 (-4)	8.6000 (-3)	1.11220 (-2)	1.87059 (-2)	2.25000 (-2)
c	2.440703 (-1)	2.1120 (4)	3.27670 (4)	1.02611 (5)	1.29000 (5)
α	2.592255 (-5)	1.78000 (-4)	2.43389 (-4)	4.55696 (-4)	6.07175 (-4)
γ	**	9.23000 (-3)	1.1800 (-2)	1.82900 (-2)	2.20000 (-2)

*Number in parentheses indicates powers of 10.

**Value of γ is a function of temperature = $3.850179 \times 10^{-3} - 2.332414 \times 10^{-5}$ (T) - 7.228731×10^{-8} (T^2) + 6.765171×10^{-10} (T^3).

The problems involved in predicting the third virial coefficient have been discussed in Chapter IV. In the theoretical prediction of the enhancement factor, using Equation (IV-17), the Lennard-Jones (6-12) model and the method of Chueh and Prausnitz were used to predict the third virial coefficients. The Lennard-Jones parameters used were those presented in Table 27, and Table 28 gives the parameters needed by the method of Chueh and Prausnitz.[16] For the fugacity and B_{12} calculations, the method of Chueh and Prausnitz was used. Chueh and Prausnitz state that their method should not be used for calculating C_{111} below $T_{R_1} < 0.80$. This suggestion was followed throughout this work, as Figures 51, 53, 55, and 57 indicate.

The hydrocarbon BWR parameters used in the calculation of the theoretical enhancement factor were taken from the paper of Benedict, et al.[4] The parameters for helium were taken from the thesis of Heck.[46] Heck presents two sets of helium parameters. One set of parameters was determined in his thesis by fitting 423 data points from the data-smoothing calculations of Mann.[89] This set of parameters contained two negative values, and by using the method of Eubanks,[34] one is able to change these signs to positive. The second set of helium parameters presented in his thesis was obtained by Heck[46] from private communications with R. N. Herring (1966). This set contained a value of γ that was temperature dependent. No information was available as to how these parameters were obtained, but they were shown by Heck to calculate the P-V-T data of helium down to 50 K within about one percent. This latter set of helium parameters was shown by Heck to give the best prediction of enhancement

Table 28. Input Parameters for the Calculation of Third Virial Coefficients Using the Method of Chueh and Prausnitz

Component	T_c K	V_c cc/gm mole	d_1	d_{12}	M_{12}
Helium	10.47[16]	37.5[16]	0.0[16]		
Argon	151.2[79]	75.2[79]	0.0[16]	0.0	7.276
Oxygen	154.8[79]	78.0[79]	0.0*	0.0	7.115
Nitrogen	126.2[79]	90.1[79]	0.0[16]	0.0	7.005
Carbon Dioxide	304.2[79]	94.0[79]	3.00[16]	1.50	7.338
Methane	191.1[79]	99.0[79]	0.50*	0.25	6.408
Ethane	305.5[24]	148[24]	1.2*	0.60	7.066
Ethylene	282.4[24]	129[24]	1.40*	0.70	7.006
Propane	370.0[24]	200[24]	1.60*	0.80	7.339
Propylene	365.0[24]	181[24]	1.80*	0.90	7.311

*These values were estimated by plotting third virial coefficient data from David and Hamann[24] on the reduced curve presented by Chueh and Prausnitz.

factors. For this reason, this set of parameters was used in this work. Using Equations (IV-85) and (IV-86), it was possible to calculate the second and third virial coefficients from the BWR equation, Equation (IV-72). These predicted values for B_{11}, B_{12}, B_{22}, C_{111}, and C_{222} are presented in Figures 10, 11, 12, and 13, and in this appendix. All of these BWR parameters are presented in Table 27.

The vapor pressure data used in this work were generally presented in the form of an equation. In these cases, the experimental data used in the fit and any additional experimental data were plotted to check the equation's validity. Vapor pressure data on the hydrocarbons are usually quite old and cover a limited range of temperature. Attempts have been made to put these data on a uniform temperature scale, but usually with very little success.

Saturated molar volume data were available in the literature for all the hydrocarbons studied. These data were collected for each component and the best curve was drawn through these data. P-v-T data for the compressed liquid are extremely scarce for hydrocarbons. Methane is the only hydrocarbon which has been studied over a wide range of temperature and pressure. A curve presented in the thesis of Heck[46] appears to be one of the best methods presently available for estimation of the coefficient of isothermal compressibility, β_T. This curve has been reproduced and is presented in Figure 47. The average compressibility $\bar{\beta}_T$ has been defined in Equation (IV-10). Experimental values for methane were used by Heck[46] in the construction of Figure 47. Limited compressibility data for liquid propane[66] and propylene[36] tend to support the use of this curve

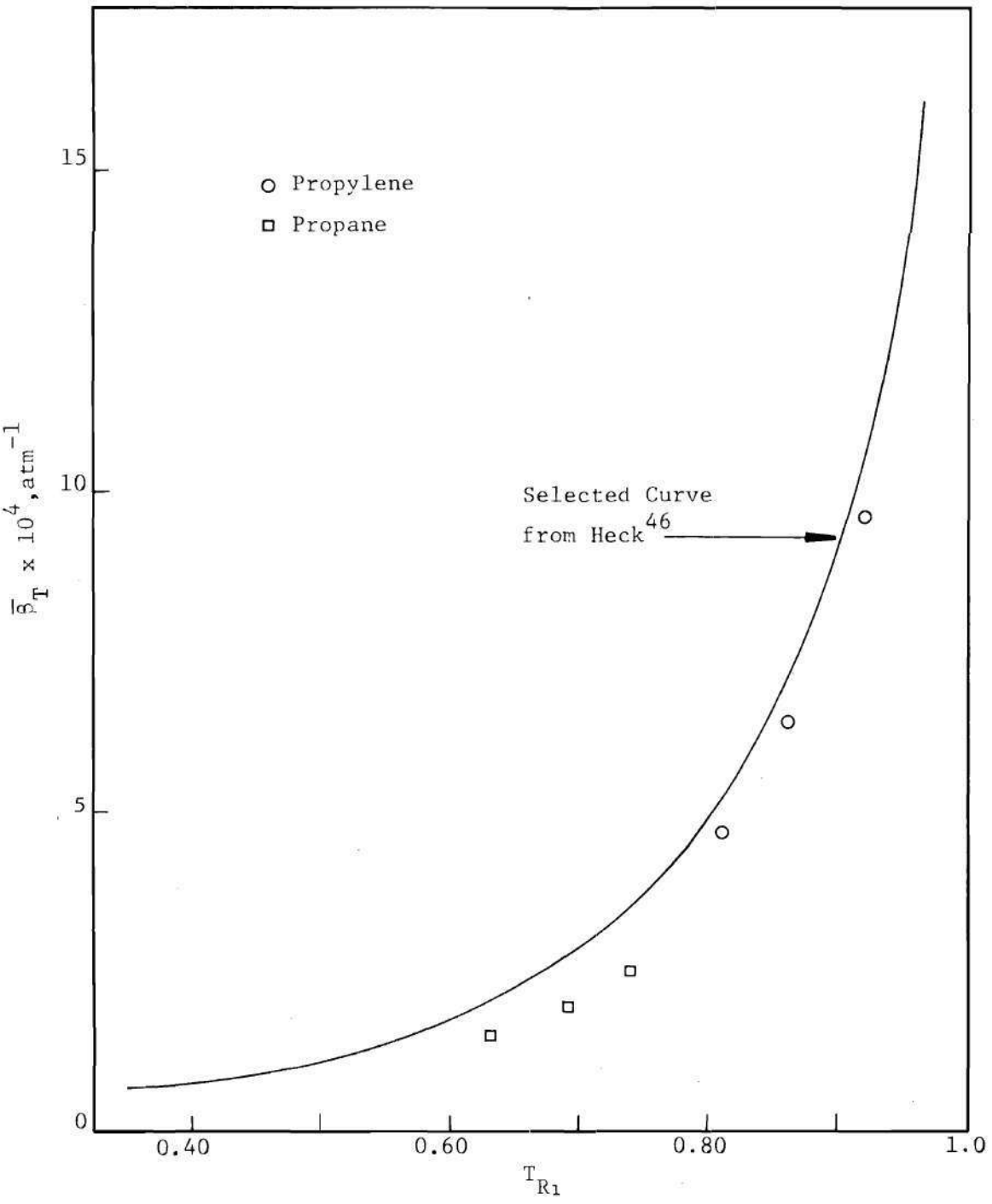

Figure 47. Generalized $\bar{\beta}_T$ versus Reduced Temperature.

for hydrocarbons. A recent paper by Chueh and Prausnitz[19] describes an alternate method of calculating the isothermal compressibility. The method of Heck[46] has been used in this work.

Helium

Since helium is the noncondensible component in this work, the only data required are a description of the P-V-T data for the gas phase. Mullins[107] has presented a good summary of the available second virial coefficient experimental data for helium. The Lennard-Jones parameters were determined by Mullins using a least square procedure on the data of White, et al.[161] Prausnitz and Myers[122] have determined the Kihara core parameters which include the first two translational quantum corrections. Both of these sets of parameters have been shown by Figure 48 to fit the experimental data of Keeson,[68] White, et al.,[161] Canfield, et al.,[12] and Hoover, et al.[58] The third virial coefficient of helium has been measured by Keesom,[68] White, et al.,[161] Canfield, et al.,[12] and Hoover, et al.[58] Figure 49 shows the experimental third virial coefficient curve that was used in most of this work. In the theoretical prediction of the enhancement factors, the third virial coefficients of helium predicted by the various theoretical models are shown in Figure 49.

Ethylene

The second virial coefficient data of ethylene have been measured by Butcher and Dadson,[10] Eucken and Parts,[35] Michels and Geldermans,[99] Roper,[134] Lambert, et al.,[81] and Crommelin and Watts.[22] In Figure 50 a comparison is made between the experimental second virial coefficients

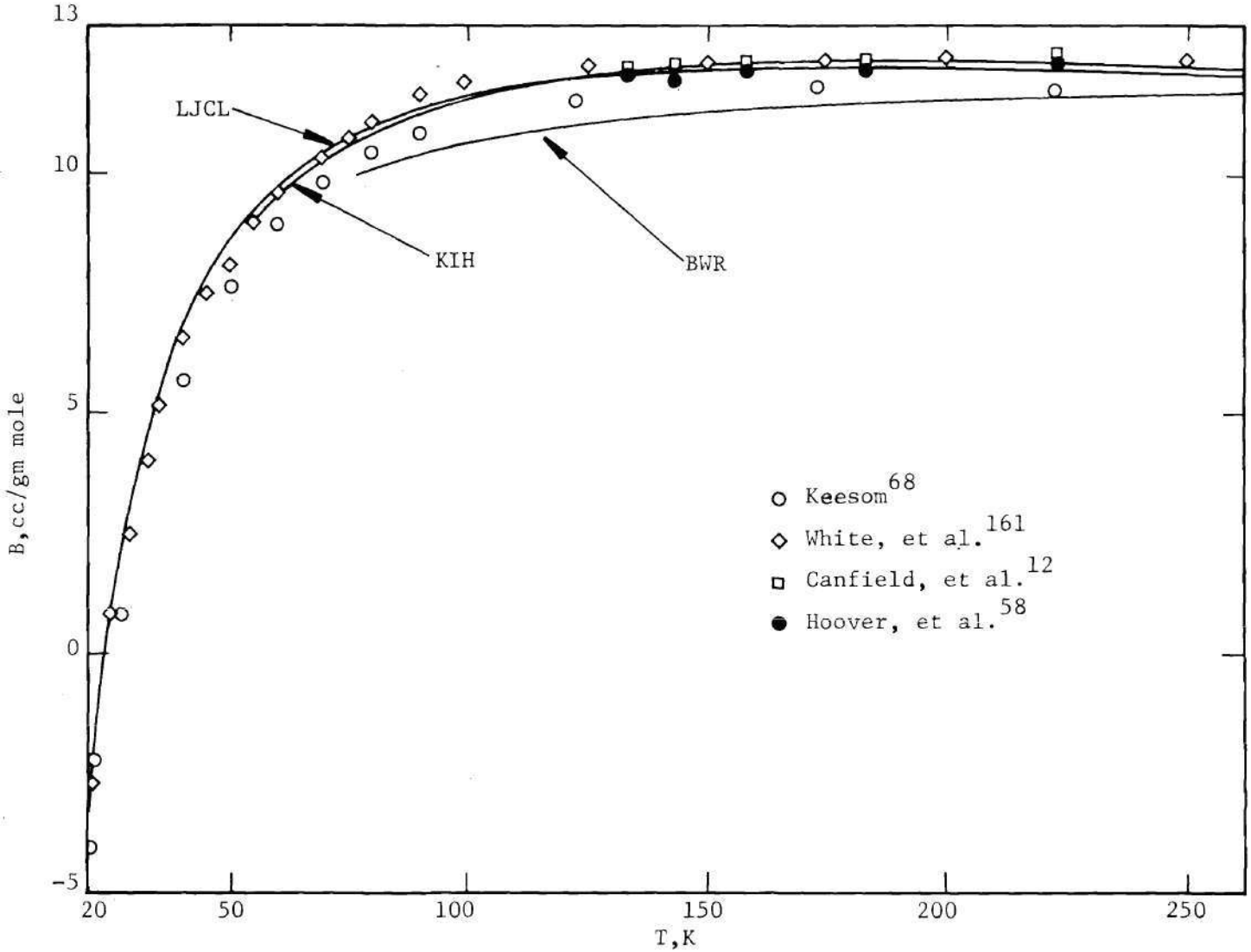

Figure 48. Second Virial Coefficient of Helium.

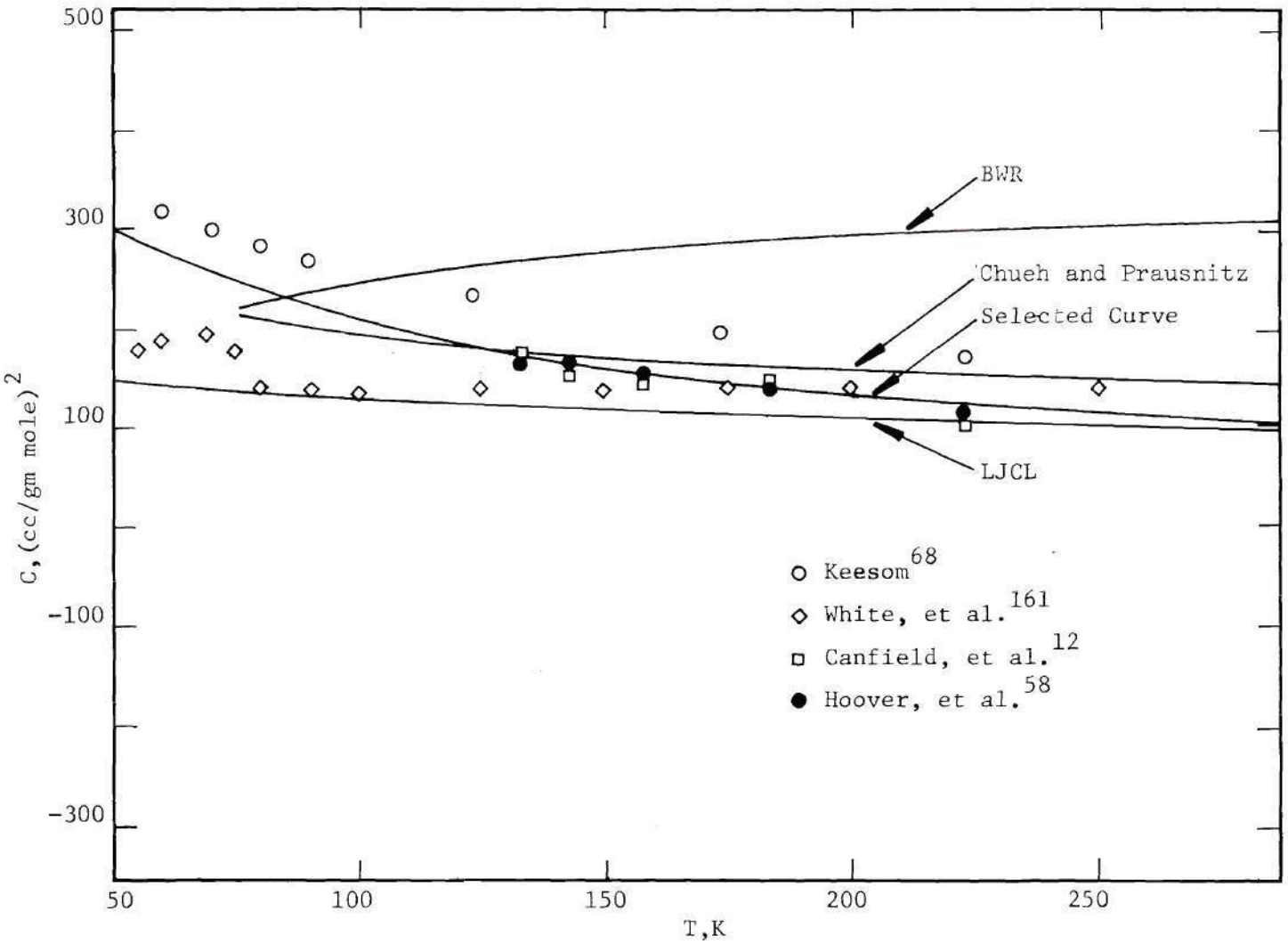

Figure 49. Third Virial Coefficient of Helium.

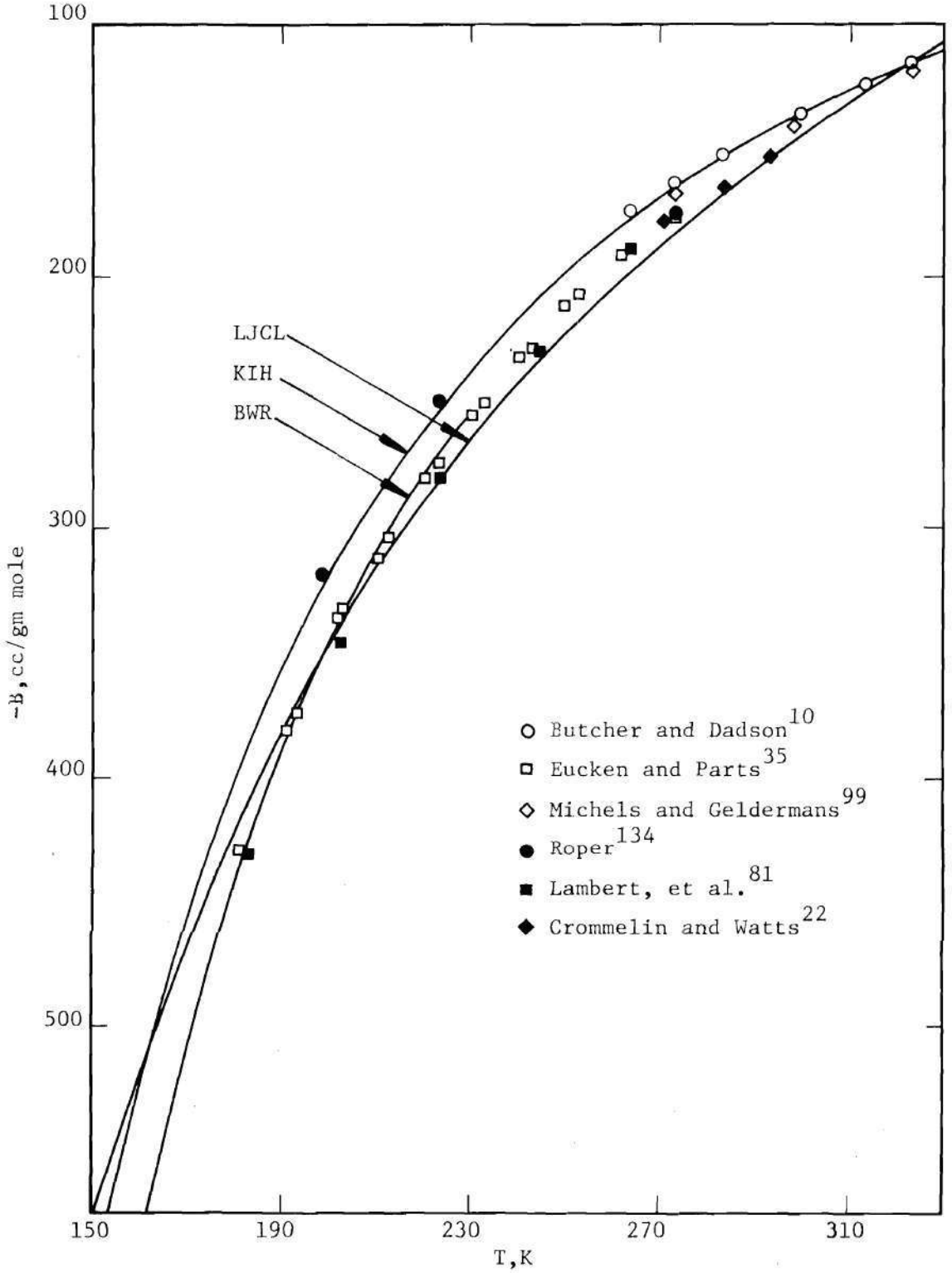

Figure 50. Second Virial Coefficient of Ethylene.

and values calculated from the Lennard-Jones, Kihara, and BWR models. The Lennard-Jones parameters are those obtained by Ziegler, et al.[166] using a least squares program, and the Kihara parameters are from Prausnitz and Myers.[122] The BWR equation predicts second virial coefficients that are in good agreement with experiment.

Experimental and theoretically calculated values of the third virial coefficient of ethylene are presented in Figure 51. Although no experimental data were available in the experimental temperature range of this work, the data of Michels and Geldermans[99] and Butcher and Dadson[10] are presented. The theoretical models LJCL, method of Chueh and Prausnitz, and BWR predict a variety of values for C_{111}. Figure 51 tends to verify that none of the theoretical models satisfactorily represents the experimental values.

A critical survey of existing ethylene vapor pressure data below one atmosphere has been made by Ziegler, et al.[166] Below one atmosphere, the vapor pressure calculated by Ziegler, et al.[166] has been selected, and above one atmosphere the experimental measurements of Michels and Wassenaar[101] have been chosen. In the region of overlap, the two sets of vapor pressure agree within 0.03 K. Values of the vapor pressure below one atmosphere were interpolated directly from the table of values given by Ziegler (one degree intervals). Michels and Wassenaar have presented a fit to their experimental values using the method of least squares. Their equation covers a pressure range of 0.2569 to 47.6481 atmospheres and is given as

$$\log P \text{ (atm)} = - \frac{1243.766}{T} - 11.213927 \times \log T + 0.01102331 \qquad \text{(F-1)}$$

(Continued)

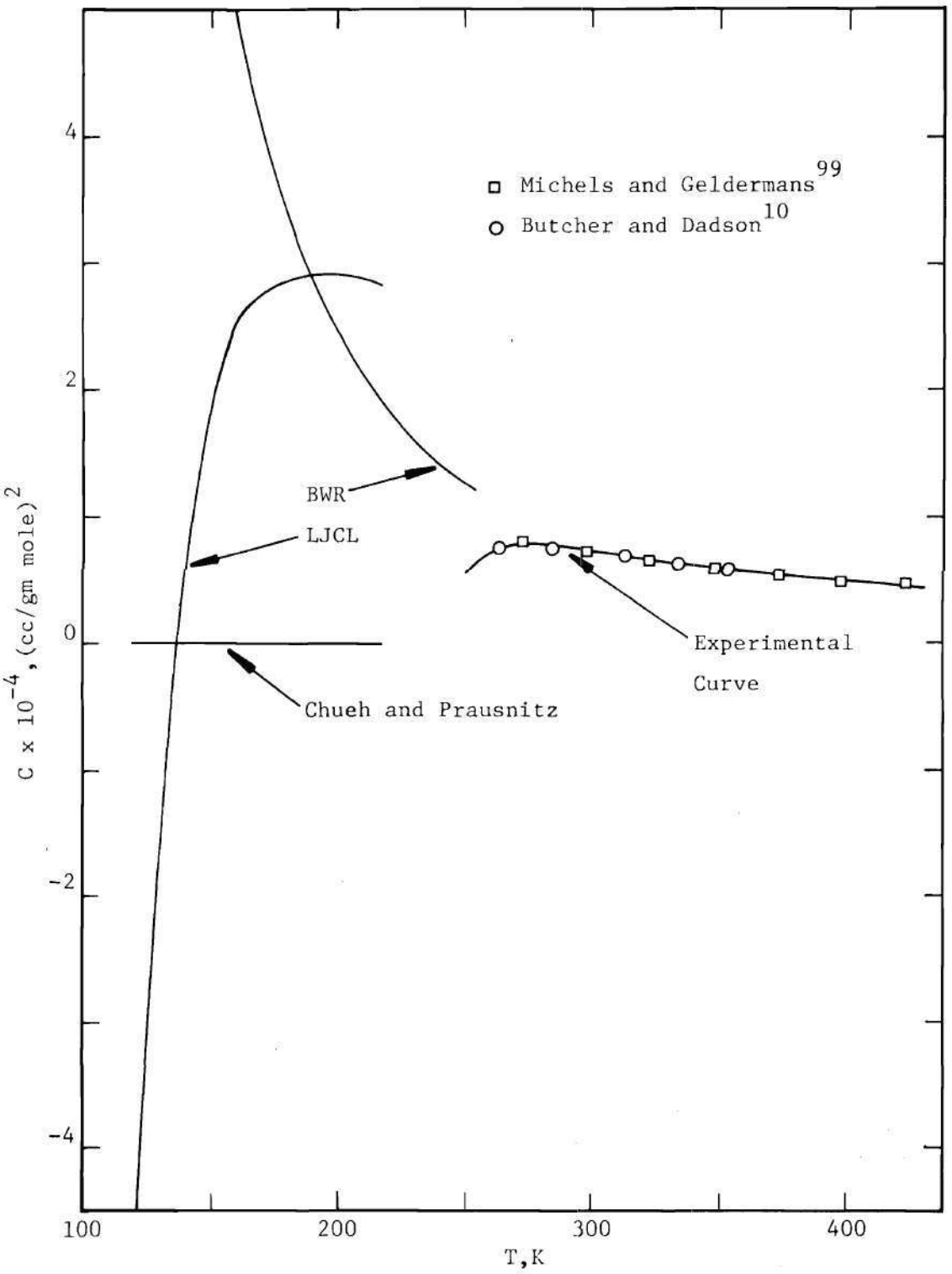

Figure 51. Third Virial Coefficient of Ethylene.

$\times T + 30.470741$

Both Ziegler, et al.[166] and Michels and Wassenaar[101] used the same ice point, 273.15 K, in presenting their data. However, no attempt was made to correct the temperature scales used by these investigators to the 1968 scale, since it was not clear on which scale these measurements had been made. The vapor pressures used in this work are presented in Table 29.

The saturated liquid density of ethylene has been experimentally measured over the temperature range investigated in this work. The data of Mathias, et al.,[92] Maass and Wright,[87] and Maass and McIntosh[86] have been smoothed and selected values are given in Table 29. Below the triple point, 103.97 K, the molar volume values used were those given by Ziegler, et al.[166] Values of the isothermal compressibility, $\bar{\beta}_T$, were read from Figure 47, using the critical temperature of ethylene from Table 28. Values of the isothermal compressibility are presented in Table 29.

Ethane

The second virial coefficient data of ethane have been measured by Eucken and Parts,[35] Michels, et al.,[100] Hamann and McManamey,[44] Lambert, et al.,[81] and Rigby, et al.[132] The comparison between these experimentally measured second virial coefficients and those predicted by various theoretical models is shown in Figure 52. The Lennard-Jones parameters used in this work are those obtained by Tee, et al.[155] The Kihara parameters were essentially those determined by Prausnitz and Myers,[122] but the value of U_o/K has been adjusted by Ziegler, et al.[164] The BWR coefficients predict second virial coefficients that are also shown in Figure 52. These parameters are presented in Table 27.

Table 29. Physical Properties of Solid and Liquid Ethylene

T,K	P_{o1}	v_1^o ℓ/gm mole	$\bar{\beta}_T$ atm^{-1}
	Solid		
91.00	4.77 (-5)*	3.881 (-2)	0.0
95.00	1.43 (-4)	3.897 (-2)	0.0
102.00	7.79 (-4)	3.922 (-2)	0.0
	Liquid		
112.00	4.442 (-3)	4.382 (-2)	7.5 (-5)
122.00	1.7350 (-2)	4.455 (-2)	8.2 (-5)
129.98	4.3482 (-2)	4.515 (-2)	9.0 (-5)
130.00	4.3575 (-2)	4.515 (-2)	9.0 (-5)
150.00	2.6949 (-1)	4.710 (-2)	1.30 (-4)
162.00	6.3200 (-1)	4.845 (-2)	1.47 (-4)
173.99	1.3035	4.992 (-2)	1.80 (-4)
188.02	2.6639	5.177 (-2)	2.30 (-4)
202.01	4.8789	5.400 (-2)	3.05 (-4)
216.04	8.2378	5.665 (-2)	3.95 (-4)

*Number in parentheses indicates powers of 10.

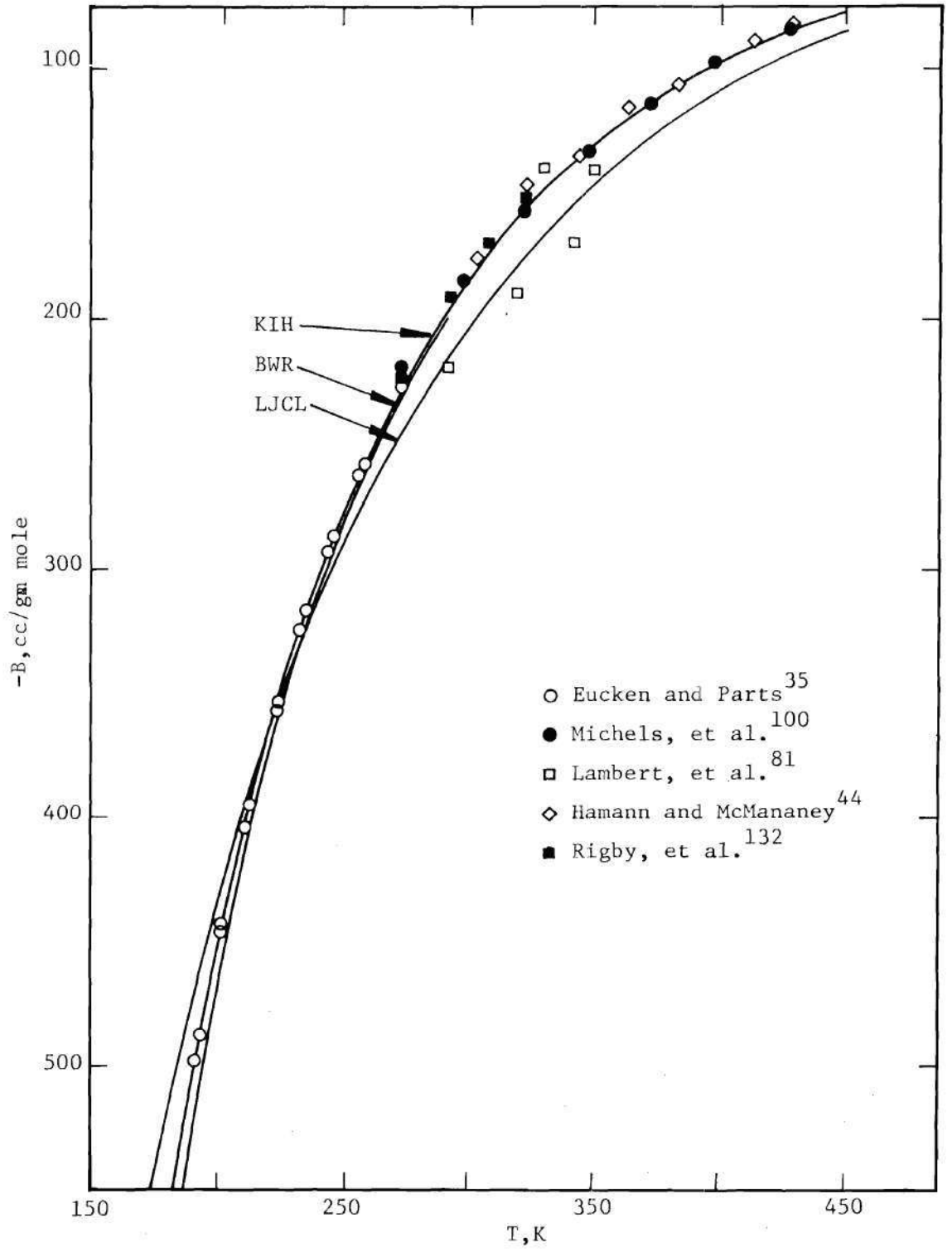

Figure 52. Second Virial Coefficient of Ethane.

Experimental third virial coefficient data for ethane have been presented by Hoover, et al.,[59] Michels, et al.,[100] and David, et al.,[25] who used the data of Reamer, et al.[125] These data include some negative experimental values of C_{111}. The three theoretical models, LJCL, method of Chueh and Prausnitz, and BWR, are shown together with these experimental values in Figure 53. For $T \geq 260$ or $T_{R1} \geq 0.80$, the method of Chueh and Prausnitz gives the best fit of the data. Below this temperature only the LJCL model has the correct qualitative shape.

Ziegler, et al.[164] have calculated the vapor pressure of ethane below one atmosphere, and they have made a critical comparison of the available experimental data. The work of Ziegler, et al.[164] has been selected as the best data below one atmosphere pressure. From the normal boiling point, 184.92 K, to 275.0 K, the equation of Prausnitz, et al.[121] was used. This equation is presented as follows

$$\ln P \text{ (atm)} = 28.495183 - \frac{2437.7237}{T} - 0.012916937 \times T \qquad \text{(F-2)}$$

$$+ 0.000025913 \times T^2 - 2.64150 \times \ln T$$

At the highest temperature, 290 K, used in this work, the vapor pressure value was taken directly from Din,[29] since no equation was found in this range. The above equation and the data of Din agree to within one-fourth percent at all points checked. Values of the vapor pressure used in this work are presented in Table 30.

Values of the saturated molar volume of liquid ethane were taken from the surveys presented by Rossini[135] and Din.[29] The isothermal com-

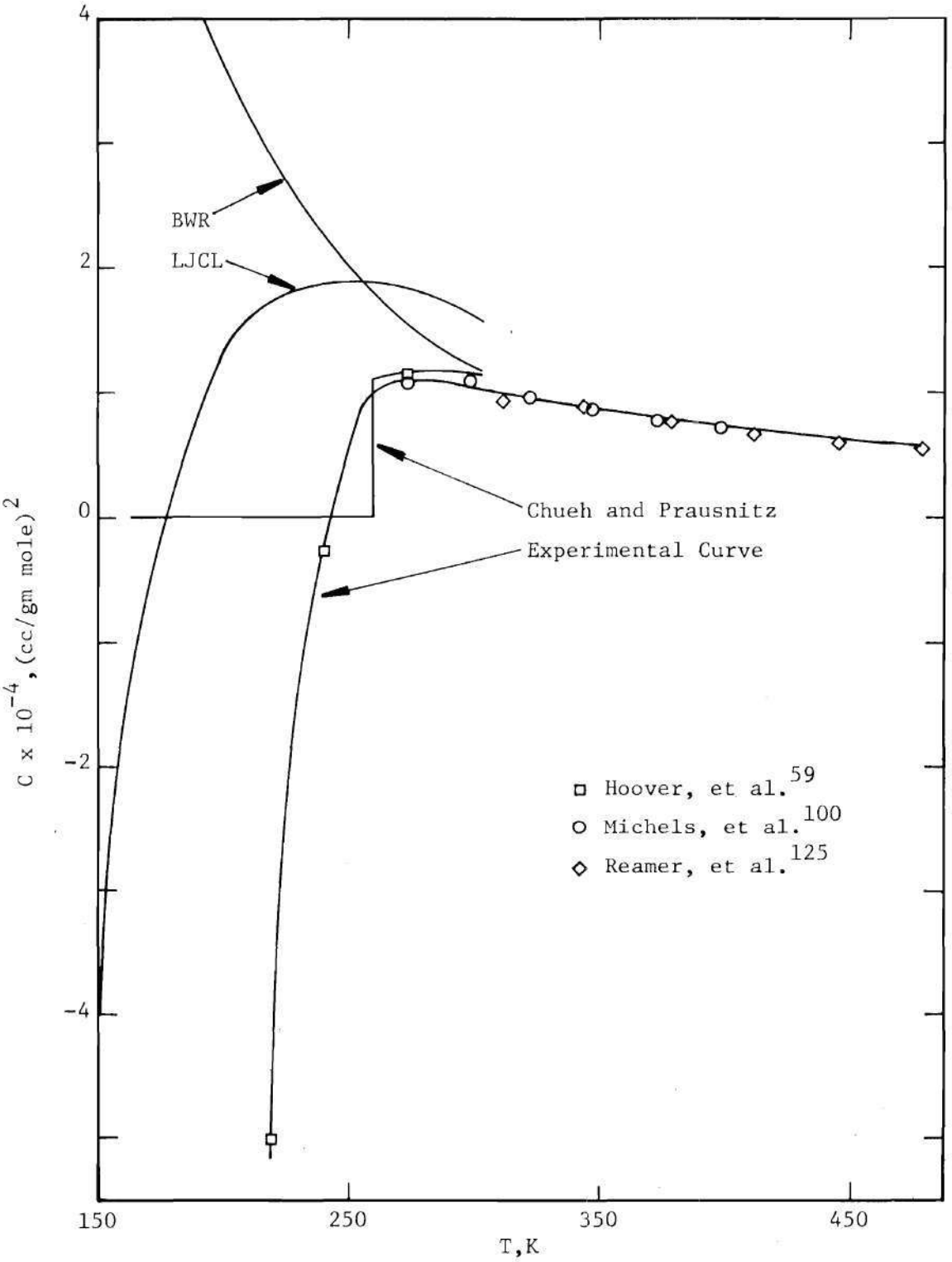

Figure 53. Third Virial Coefficient of Ethane.

Table 30. Physical Properties of Liquid Ethane

T,K	P_{o1} atm	v_1^o ℓ/gm mole	$\bar{\beta}_T$ atm^{-1}
95.00	3.487 (-5)*	4.620 (-2)	6.1 (-5)
102.00	1.618 (-4)	4.677 (-2)	6.5 (-5)
112.00	1.009 (-3)	4.759 (-2)	7.0 (-5)
122.00	4.530 (-3)	4.846 (-2)	7.5 (-5)
130.00	1.254 (-2)	4.915 (-2)	8.0 (-5)
150.00	9.463 (-2)	5.102 (-2)	1.05 (-4)
170.00	4.223 (-1)	5.349 (-2)	1.30 (-4)
200.00	2.153	5.683 (-2)	2.20 (-4)
230.00	6.919	6.140 (-2)	3.70 (-4)
260.00	16.89	6.831 (-2)	6.30 (-4)
290.00	34.65	8.249 (-2)	1.30 (-3)

*Number in parentheses indicates powers of 10.

pressibility values were taken from Figure 47. Both of these results used in this work are presented in Table 30.

Propylene

The second virial coefficient data of propylene have been measured by Roper,[134] Farrington and Sage,[36] Michels, et al.,[102] and McGlashan and Wormald.[97] To obtain estimations of virial coefficients at temperatures below 223 K, the empirical equation developed by McGlashan and Wormald[97] for propylene has been used. The Lennard-Jones (6-12) least squares program written by Mullins was used to obtain suitable molecular parameters. The data of Michels, et al.[102] and McGlashan and Wormald[97] were fitted over the temperature range of 298.15 to 355.38 K. Kihara parameters presented by Prausnitz and Myers[122] represented the available data very well. The BWR coefficients for pure propylene appeared to predict values of the second virial coefficient that were too low. The experimental and theoretical values of B_{111} have been presented in Figure 54. These various parameters are presented in Table 27.

Third virial coefficient data of propylene have been determined by Farrington and Sage[36] and Marcham, et al.[90] The theoretical models are shown together with these experimental data in Figure 55. The LJCL and BWR models predict values of C_{111} that are too high. The method of Chueh and Prausnitz is defined as zero in this temperature range.

A survey of the available vapor pressure data of propylene indicated that there was a sizable amount of data available in the pressure range of interest. The vapor pressure equation given in the API project 44 by

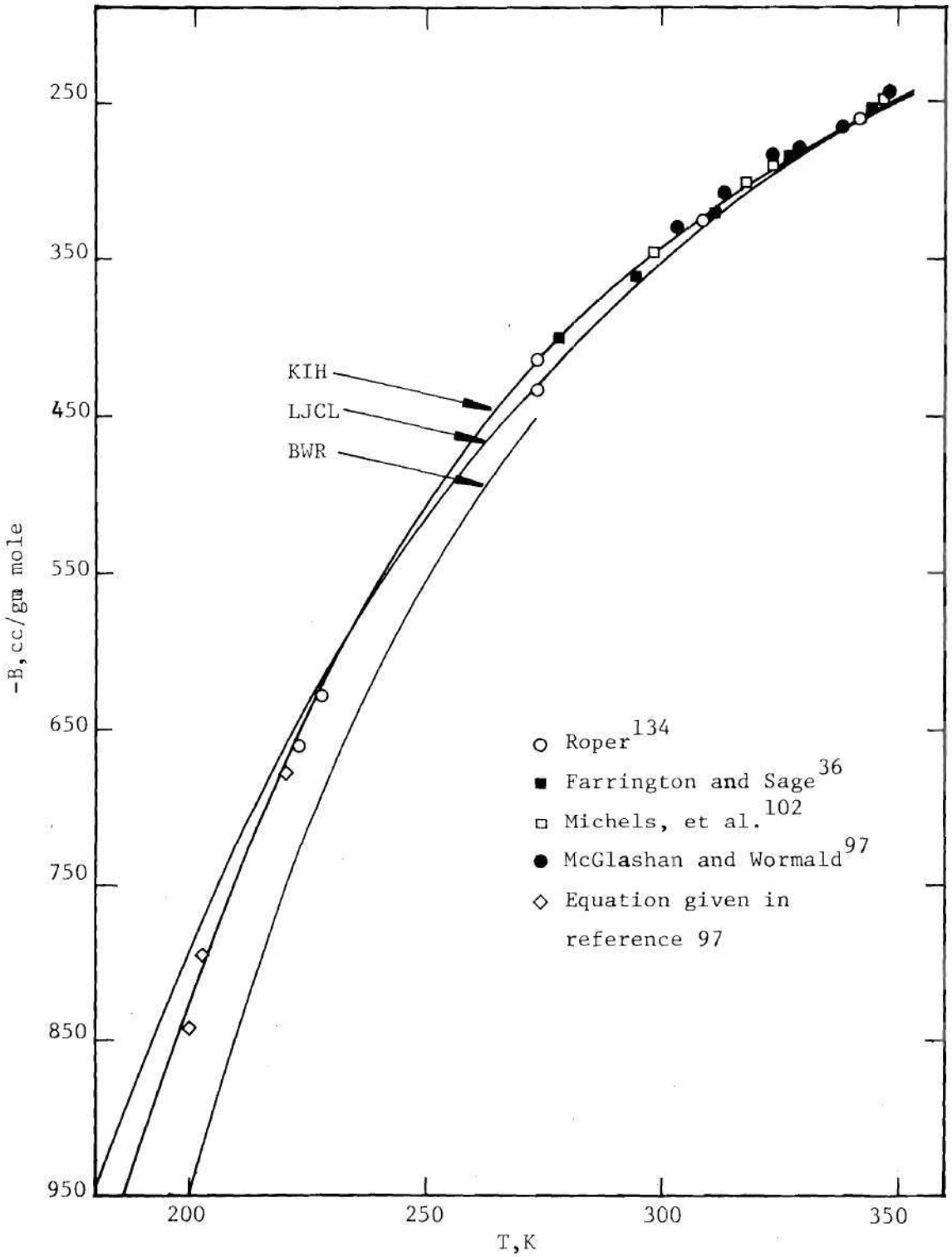

Figure 54. Second Virial Coefficient of Propylene.

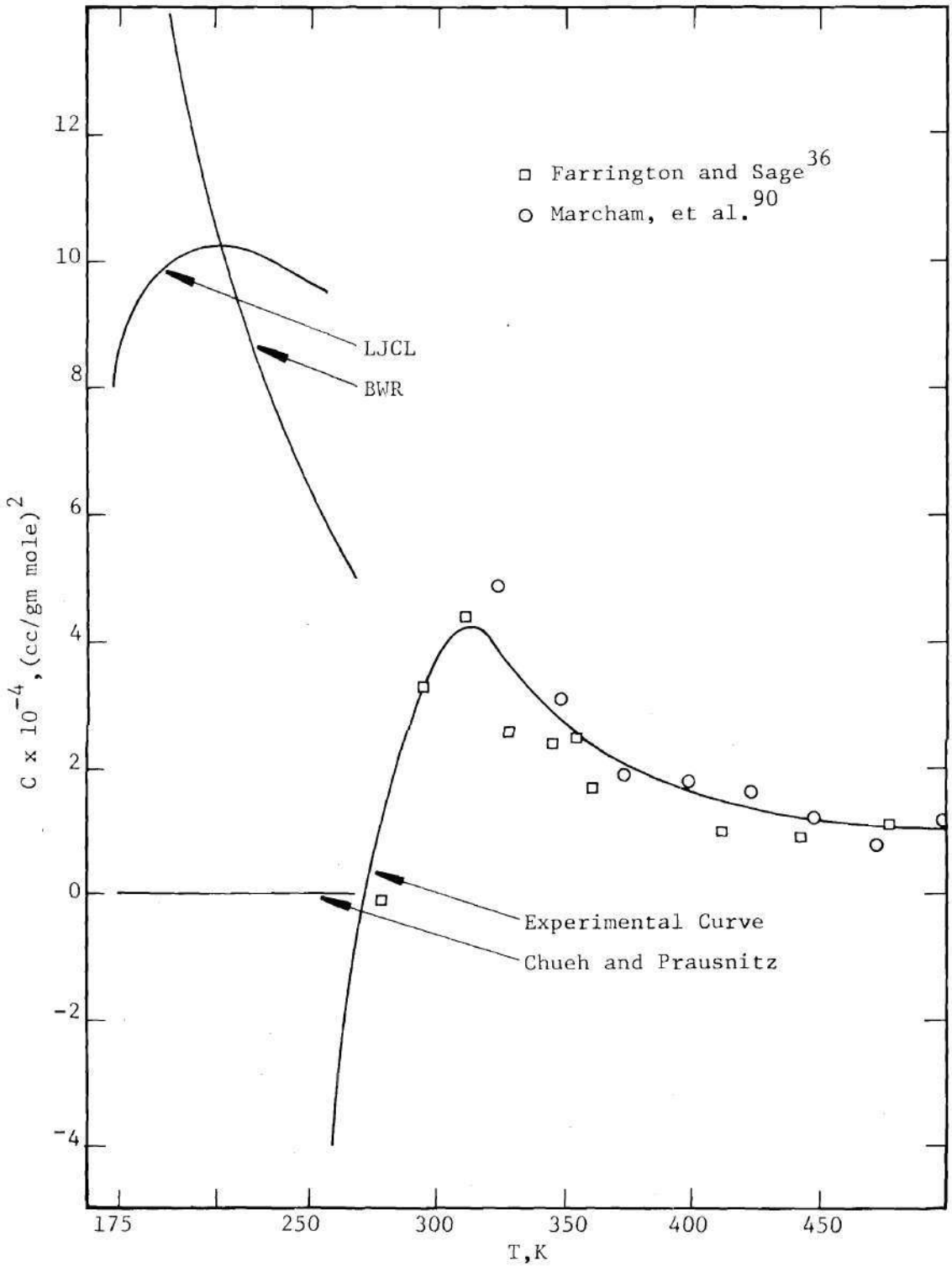

Figure 55. Third Virial Coefficient of Propylene.

Rossini, et al.[135] was used in this work. This equation is given as follows

$$\log P \text{ (mm Hg)} = 6.81960 - \frac{785.00}{t(^{\circ}C) + 247} \qquad \text{(F-3)}$$

This equation was obtained by least squaring the experimental data referenced in their work. Experimental data by Powell and Giauque,[117], Lu, et al.,[84] and Tickner and Lossing,[157] which were not used in the API fit, were shown to agree very well with the above equation.

The density of saturated liquid propylene has been measured by Maass and Wright,[87] Lu, et al.,[84] and the Technical Committee Natural Gasoline Association of America.[154] At low temperatures, several values of density were estimated using the generalized charts of Hougen, et al.[61] These estimated values covered a 25 K temperature range and the overlap region agreed with the experimental data.

Using the definition of average compressibility, $\bar{\beta}_T$, Equation (IV-10), it was possible to estimate several values of $\bar{\beta}_T$ for propylene using the limited data of Farrington and Sage.[36] Three points were calculated, over the temperature range of 4.4 to 87.7°C, using P_m as 120 atmospheres, and these results agreed very well with Figure 47.

The values of vapor pressure, molar volume, and isothermal compressibility used in this work are all presented in Table 31.

Propane

Until about 10 years ago, P-V-T data for propane were quite scarce.

Table 31. Physical Properties of Liquid Propylene

T,K	P_{01} atm	v_1^o ℓ/gm mole	$\bar{\beta}_T$ atm^{-1}
175.00	4.6240 (-2)*	6.307 (-2)	1.10 (-4)
187.49	1.1838 (-1)	6.425 (-2)	1.15 (-4)
200.00	2.6509 (-1)	6.554 (-2)	1.35 (-4)
212.49	5.3218 (-1)	6.704 (-2)	1.65 (-4)
224.99	9.7924 (-1)	6.869 (-2)	1.90 (-4)
239.99	1.8528	7.094 (-2)	2.20 (-4)
254.98	3.2232	7.350 (-2)	2.70 (-4)

*Number in parentheses indicates powers of 10.

The virial coefficients used in this work were taken from Schafer and Kappallo,[139] Dawson and McKetta,[26] McGlashan and Potter,[96] and Hirschfelder, et al.[51] O'Connell and Prausnitz[109] have determined a set of Lennard-Jones parameters which agree fairly well with the experimental data. Due to a shortage of experimental virial coefficient data, the Kihara parameters given by Prausnitz and Myers[122] for propane have been obtained using the Pitzer-Curl empirical equation.[116] In this work their value of U_o/K was changed to 506 and a much better fit to the more recent experimental data was obtained. Figure 56 shows the agreement between the various theoretical models and the experimental data. These various parameters are presented in Table 27.

The only experimental third virial coefficient data come from Reamer, et al.[126] Their values show a maximum and a value of $C_{111} = 0.0$ at higher temperatures than other hydrocarbons. The values predicted theoretically using the LJCL, method of Chueh and Prausnitz, and BWR models are shown together with these experimental data in Figure 57. The LJCL and BWR models again show values of C_{111} that are much higher than experiment.

The available vapor pressure data for propane were smoothed by Canjar and Manning[13] using the Antoine equation. The following form of the equation was obtained

$$\log P \text{ (atm)} = 3.94872 - \frac{813.20}{T(K) - 25.16} + r \qquad \text{(F-4)}$$

for $T \leq 250$ K $\qquad r = 0$

for $T > 250$ K $\qquad r = 0.019 \times 10^{-6} (T - 250)^3$

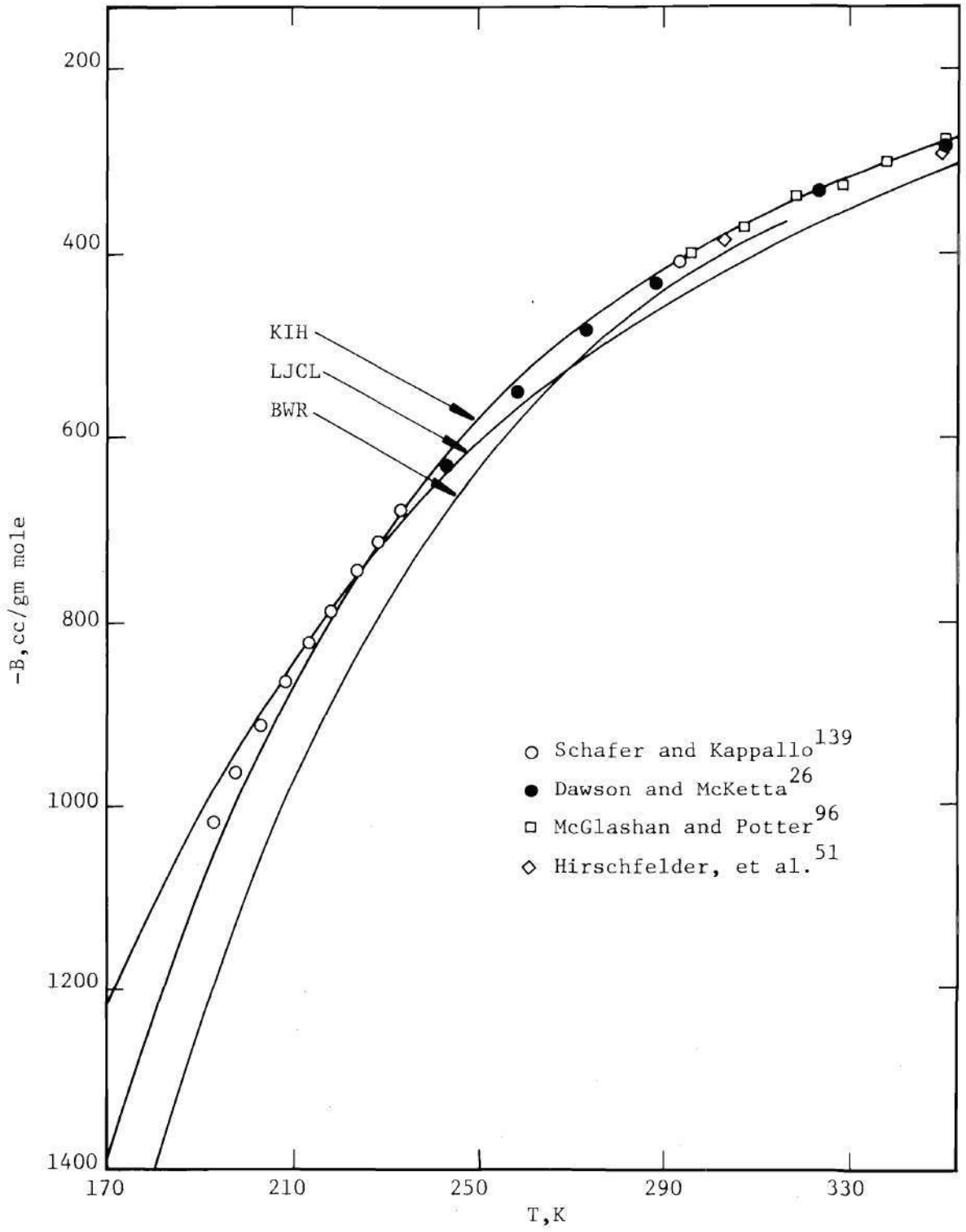

Figure 56. Second Virial Coefficient of Propane.

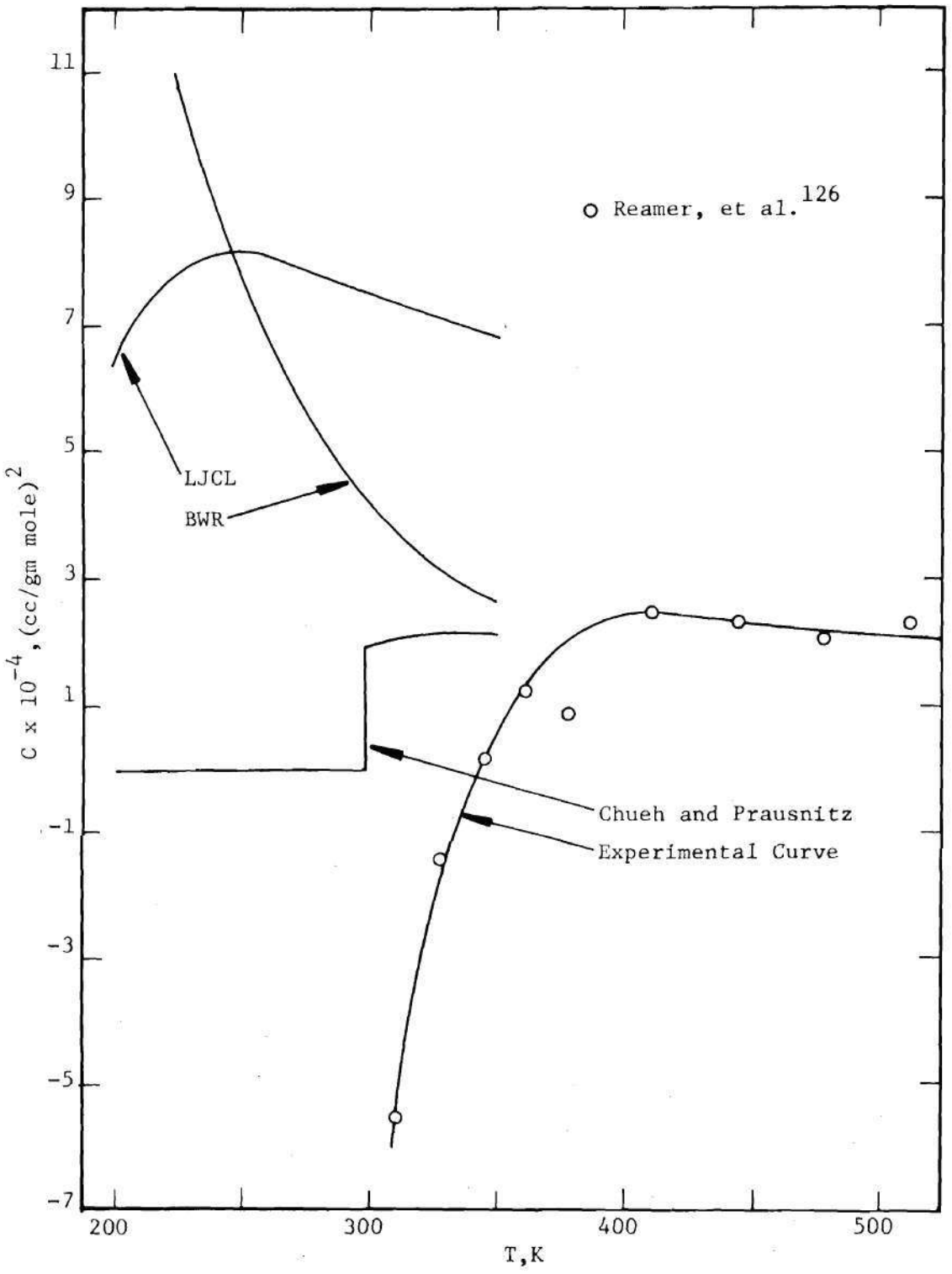

Figure 57. Third Virial Coefficient of Propane.

This equation was used over the range -75 to 75°C, and it compared quite well with the equation given by the API project 44.[135] Values of the vapor pressure used in this work are presented in Table 32.

The saturated liquid density of propane has been measured over the temperature range of interest. The data were taken from Technical Committee Natural Gasoline Association of America,[154] Maass and Wright,[87] and Stearn and George.[149] These experimental data were smoothed, and the values used in this work are presented in Table 32.

Isothermal compressibility data for propane were not found over the entire range of interest. A recent paper by Kahre and Livingston[66] is the only work of any significance. Their work covered the temperature range of -40 to 76.6°C and pressures up to 1,400 psia. These values of $\bar{\beta}_T$ calculated from this paper are shown in Figure 47, and the results compare very favorably with the selected curve of Heck given in Figure 47. The values used in this work are presented in Table 32.

Table 32. Physical Properties of Liquid Propane

T,K	P_{o1} atm	v_1^o ℓ/gm mole	$\bar{\beta}_T$ atm^{-1}
198.15	1.770 (-1)*	7.114 (-2)	1.35 (-4)
223.15	6.941 (-1)	7.452 (-2)	1.75 (-4)
248.15	2.004	7.844 (-2)	2.35 (-4)
273.15	4.675	8.319 (-2)	3.50 (-4)
298.15	9.375	8.934 (-2)	5.00 (-4)
323.15	16.87	9.769 (-2)	7.70 (-4)
348.15	28.14	1.122 (-1)	1.22 (-3)

*Number in parentheses indicates powers of 10.

APPENDIX G

SUMMARY OF SMOOTHED EXPERIMENTAL AND THEORETICAL ENHANCEMENT FACTORS, AND SMOOTHED EXPERIMENTAL SOLUBILITY OF HELIUM

In this appendix the smoothed experimental enhancement factors and liquid phase compositions of the helium-ethane, -ethylene, -propane, and -propylene systems are presented. The data shown here represent all the available experimental data for these systems. These data have been smoothed graphically.

The theoretically predicted enhancement factors are also shown for these four helium systems. The models used to predict the enhancement factor were the Lennard-Jones (6-12) classical, LJCL; the Kihara core model, KIH; the Kihara core model with the K_{12} factor calculated from the correlation of Hiza and Duncan,[53] KIHCK12; the Kihara core model using the experimentally determined K_{12} factor, KIHEK12; and finally the BWR equation using the linear average for the calculation of $(B_o)_{12}$, BWR(LINEAR). These various models are explained in more detail in Chapter IV, and some of these results are shown graphically in Chapter VI. The physical property data required for these calculations are those presented in Tables 27, 28, 29, 30, 31, and 32. The values of K_{12} calculated and experimental are presented in Table 7.

Table 33. Smoothed Experimental and Theoretical Enhancement Factors of Ethane in Helium, and the Smoothed Experimental Solubility of Helium in Liquid Ethane

P atm	ϕ EXP	ϕ LJCL	ϕ KIH	ϕ KIHCK12	ϕ KIHEK12	ϕ BWR	100 x_2
			95.00 K (Hiza and Duncan[53])				
10	1.208	1.132	1.145	1.055	1.039	1.088	0.0[a]
20	1.326	1.275	1.303	1.111	1.078	1.183	0.0
30	1.423	1.427	1.477	1.166	1.116	1.283	0.0
40	1.506	1.589	1.665	1.222	1.153	1.383	0.0
50	1.585	1.761	1.868	1.279	1.190	1.495	0.0
			102.00 K (Hiza and Duncan[53])				
20	1.232	1.222	1.253	1.094	1.066	1.147	0.0[a]
40	1.432	1.467	1.544	1.187	1.130	1.304	0.0
60	1.589	1.734	1.876	1.281	1.192	1.470	0.0
80	1.743	2.022	2.251	1.375	1.253	1.645	0.0
100	1.888	2.392	2.670	1.469	1.312	1.829	0.0
120	2.025	2.657	3.136	1.565	1.372	2.022	0.0
140	2.159	3.002	3.652	1.661	1.431	2.223	0.0
			112.00 K (Hiza and Duncan[53])				
20	1.155	1.168	1.200	1.076	1.054	1.112	0.0[a]
40	1.293	1.346	1.423	1.151	1.105	1.227	0.0
60	1.420	1.533	1.670	1.225	1.155	1.346	0.0
80	1.542	1.728	1.940	1.299	1.204	1.469	0.0
100	1.658	1.930	2.236	1.373	1.252	1.596	0.0
120	1.771	2.139	2.557	1.447	1.300	1.726	0.0
140	1.880	2.353	2.905	1.522	1.347	1.859	0.0
			122.00 K (Hiza and Duncan[53])				
20	1.093	1.131	1.164	1.063	1.045	1.088	0.0[a]
40	1.183	1.265	1.341	1.125	1.088	1.177	0.0
60	1.272	1.402	1.532	1.186	1.130	1.267	0.0
80	1.361	1.541	1.739	1.247	1.171	1.359	0.0
100	1.447	1.683	1.960	1.307	1.211	1.452	0.0
120	1.532	1.825	2.196	1.367	1.251	1.546	0.0
140	1.613	1.969	2.448	1.428	1.290	1.641	0.0

Table 33. (Continued)

P atm	ϕ EXP	ϕ LJCL	ϕ KIH	ϕ KIHCK12	ϕ KIHEK12	ϕ BWR	100 x_2
			130.00 K (Hiza and Duncan[53])				
20	1.075	1.109	1.142	1.056	1.041	1.075	0.025[b]
40	1.145	1.217	1.292	1.109	1.078	1.148	0.055
60	1.215	1.327	1.453	1.163	1.115	1.223	0.080
80	1.284	1.436	1.622	1.215	1.151	1.297	0.100
100	1.351	1.545	1.803	1.267	1.186	1.371	0.125
120	1.418	1.654	1.994	1.319	1.220	1.446	0.150
140	1.483	1.761	2.195	1.371	1.255	1.521	0.175
			150.00 K (Hiza and Duncan[53])				
20	1.027	1.075	1.109	1.048	1.037	1.058	0.060[b]
40	1.055	1.145	1.217	1.089	1.067	1.109	0.120
60	1.082	1.211	1.328	1.129	1.095	1.158	0.190
80	1.108	1.275	1.444	1.168	1.122	1.206	0.290
100	1.136	1.339	1.566	1.207	1.149	1.255	0.310
120	1.162	1.401	1.692	1.245	1.177	1.302	0.430
			170.00 K (Heck[46])				
20	1.029	1.067	1.101	1.056	1.047	1.061	0.129
40	1.058	1.113	1.185	1.089	1.072	1.099	0.257
60	1.086	1.159	1.272	1.123	1.097	1.137	0.381
80	1.114	1.202	1.362	1.155	1.121	1.173	0.509
100	1.142	1.243	1.454	1.188	1.145	1.208	0.637
120	1.168	1.281	1.549	1.221	1.168	1.243	0.757
140	1.193	1.318	1.648	1.253	1.192	1.277	0.870
160	1.213	1.354	1.749	1.285	1.215	1.310	0.980
180	1.231	1.387	1.853	1.318	1.239	1.343	1.074
200	1.245	1.418	1.960	1.351	1.263	1.376	1.151
			200.00 K (Heck[46])				
20	1.067	1.087	1.119	1.090	1.085	1.087	0.240
40	1.099	1.120	1.191	1.123	1.111	1.120	0.500
60	1.122	1.148	1.261	1.153	1.135	1.149	0.763
80	1.140	1.173	1.333	1.183	1.157	1.176	1.025
100	1.156	1.196	1.407	1.210	1.179	1.201	1.275
120	1.168	1.216	1.481	1.239	1.200	1.226	1.512
140	1.177	1.236	1.559	1.266	1.220	1.250	1.740
160	1.186	1.253	1.638	1.294	1.242	1.273	1.950
180	1.193	1.269	1.720	1.322	1.264	1.295	2.125

Table 33. (Concluded)

P atm	ø EXP	ø LJCL	ø KIH	ø KIHCK12	ø KIHEK12	ø BWR	100 x_2
			230.00 K (Heck[46])				
20	1.130	1.125	1.144	1.131	1.128	1.127	0.348
40	1.185	1.177	1.242	1.197	1.188	1.187	0.853
60	1.216	1.205	1.324	1.240	1.225	1.224	1.330
80	1.239	1.225	1.404	1.278	1.257	1.253	1.783
100	1.258	1.241	1.484	1.313	1.286	1.279	2.222
120	1.273	1.253	1.567	1.347	1.313	1.303	2.645
140	1.284	1.262	1.653	1.380	1.340	1.323	3.055
160	1.293	1.271	1.743	1.413	1.365	1.343	3.452
180	1.301	1.275	1.837	1.446	1.391	1.361	3.825
200	1.308	1.279	1.936	1.478	1.415	1.377	4.182
			260.00 K (Heck[46])				
20	1.047	1.052	1.051	1.050	1.050	1.049	0.140
40	1.218	1.227	1.252	1.231	1.228	1.225	1.030
60	1.296	1.303	1.381	1.327	1.318	1.315	1.925
80	1.346	1.344	1.492	1.395	1.379	1.376	2.820
100	1.383	1.367	1.598	1.449	1.427	1.423	3.700
120	1.412	1.382	1.704	1.499	1.469	1.463	4.475
140	1.434	1.390	1.815	1.545	1.507	1.498	5.160
160	1.451	1.395	1.934	1.589	1.544	1.528	5.710
			290.00 K (Heck[46])				
40	1.072	--[c]	--	--	--	1.113	0.480
60	1.272	--	--	--	--	1.514	2.250
80	1.421	--	--	--	--	2.040	4.035
100	1.520	--	--	--	--	2.691	5.730
120	1.583	--	--	--	--	--	7.230
140	1.633	--	--	--	--	--	8.450
160	1.677	--	--	--	--	--	9.430

[a] The composition of the liquid phase has not been experimentally determined and is assumed to be zero in these calculations.

[b] Values of x_2 were estimated.

[c] The blank spaces indicate lack of convergence of theoretical calculations.

Table 34. Smoothed Experimental and Theoretical Enhancement Factors of Ethylene in Helium, and the Smoothed Experimental Solubility of Helium in Liquid Ethylene

P atm	ϕ EXP	ϕ LJCL	ϕ KIH	ϕ KIHCK12	ϕ KIHEK12	ϕ BWR	100 x_2
			91.00 K (Hiza and Duncan[53])				
10	1.100	1.113	1.138	1.037	1.027	1.084	0.0[a]
20	1.173	1.229	1.289	1.074	1.053	1.176	0.0
30	1.238	1.349	1.452	1.110	1.079	1.272	0.0
40	1.296	1.471	1.628	1.146	1.103	1.368	0.0
50	1.348	1.596	1.817	1.180	1.127	1.473	0.0
60	1.395	1.721	2.020	1.215	1.150	1.574	0.0
			95.00 K (Hiza and Duncan[53])				
20	1.147	1.197	1.258	1.066	1.047	1.154	0.0[a]
40	1.267	1.399	1.555	1.130	1.092	1.317	0.0
60	1.370	1.602	1.891	1.191	1.134	1.490	0.0
80	1.460	1.804	2.270	1.251	1.174	1.673	0.0
100	1.542	2.001	2.692	1.309	1.212	1.865	0.0
120	1.617	2.192	3.159	1.366	1.249	2.065	0.0
140	1.684	2.374	3.673	1.423	1.285	2.272	0.0
			102.00 K (Hiza and Duncan[53])				
20	1.118	1.152	1.214	1.055	1.039	1.123	0.0[a]
40	1.217	1.301	1.454	1.108	1.076	1.250	0.0
60	1.302	1.446	1.719	1.158	1.110	1.382	0.0
80	1.378	1.585	2.010	1.207	1.143	1.518	0.0
100	1.447	1.716	2.328	1.255	1.174	1.659	0.0
120	1.510	1.838	2.674	1.301	1.205	1.803	0.0
140	1.567	1.951	3.048	1.347	1.234	1.950	0.0
			112.00 K (Hiza and Duncan[53])				
20	1.080	1.116	1.180	1.053	1.040	1.102	0.0[a]
40	1.157	1.227	1.377	1.105	1.079	1.207	0.0
60	1.231	1.333	1.592	1.155	1.116	1.314	0.0
80	1.302	1.432	1.825	1.204	1.152	1.424	0.0
100	1.368	1.523	2.077	1.253	1.187	1.537	0.0
120	1.432	1.606	2.348	1.301	1.222	1.652	0.0
140	1.488	1.682	2.638	1.349	1.257	1.770	0.0

Table 34. (Continued)

P atm	ϕ EXP	ϕ LJCL	ϕ KIH	ϕ KIHCK12	ϕ KIHEK12	ϕ BWR	100 x_2
			122.00 K (Hiza and Duncan[53])				
20	1.062	1.085	1.148	1.046	1.035	1.083	0.0[a]
40	1.117	1.163	1.306	1.089	1.068	1.164	0.0
60	1.168	1.234	1.475	1.130	1.099	1.247	0.0
80	1.216	1.297	1.655	1.172	1.129	1.330	0.0
100	1.260	1.354	1.846	1.212	1.159	1.414	0.0
120	1.302	1.404	2.048	1.252	1.189	1.499	0.0
140	1.342	1.320	2.263	1.293	1.219	1.584	0.0
			130.00 K (Hiza and Duncan[53])				
20	1.065	1.068	1.130	1.042	1.033	1.073	0.032[b]
40	1.118	1.125	1.264	1.079	1.061	1.140	0.062
60	1.164	1.177	1.407	1.116	1.089	1.209	0.093
80	1.206	1.233	1.556	1.152	1.116	1.276	0.122
100	1.243	1.261	1.714	1.187	1.142	1.345	0.151
120	1.281	1.294	1.880	1.223	1.169	1.413	0.178
140	1.315	1.320	2.054	1.257	1.195	1.482	0.203
			150.00 K (Hiza and Duncan[53])				
20	1.038	1.047	1.106	1.044	1.037	1.064	0.069[b]
40	1.076	1.076	1.205	1.074	1.061	1.112	0.139
60	1.110	1.098	1.307	1.103	1.084	1.160	0.206
80	1.142	1.116	1.413	1.131	1.106	1.207	0.270
100	1.170	1.129	1.523	1.159	1.127	1.253	0.331
120	1.193	1.138	1.637	1.187	1.149	1.298	0.390
140	1.211	1.143	1.754	1.216	1.171	1.343	0.442
			129.98 K (This Work)				
20	1.042	1.068	1.130	1.042	1.033	1.073	0.032
40	1.084	1.125	1.264	1.079	1.061	1.140	0.062
60	1.126	1.177	1.407	1.116	1.089	1.209	0.093
80	1.167	1.223	1.557	1.153	1.116	1.276	0.122
100	1.208	1.261	1.714	1.187	1.142	1.345	0.151
120	1.247	1.293	1.881	1.223	1.169	1.413	0.178

Table 34. (Continued)

P atm	ϕ EXP	ϕ LJCL	ϕ KIH	ϕ KIHCK12	ϕ KIHEK12	ϕ BWR	100 x_2
			150.01 K (This Work)				
20	1.036	1.047	1.106	1.044	1.037	1.064	0.069
40	1.060	1.076	1.205	1.074	1.061	1.112	0.139
60	1.080	1.098	1.307	1.103	1.084	1.160	0.206
80	1.096	1.116	1.413	1.131	1.106	1.207	0.270
100	1.109	1.129	1.523	1.159	1.127	1.253	0.331
120	1.120	1.138	1.637	1.187	1.149	1.298	0.389
			162.00 K (This Work)				
20	1.044	1.048	1.105	1.053	1.048	1.069	0.102
40	1.067	1.064	1.191	1.081	1.070	1.111	0.209
60	1.082	1.078	1.279	1.107	1.091	1.151	0.308
80	1.094	1.086	1.370	1.133	1.111	1.191	0.407
100	1.102	1.091	1.465	1.159	1.132	1.231	0.501
120	1.108	1.092	1.562	1.185	1.152	1.268	0.589
			173.99 K (This Work)				
20	1.054	1.056	1.110	1.067	1.063	1.080	0.147
40	1.080	1.067	1.188	1.095	1.086	1.119	0.297
60	1.096	1.072	1.268	1.120	1.106	1.155	0.445
80	1.107	1.073	1.351	1.145	1.126	1.190	0.591
100	1.115	1.070	1.434	1.170	1.147	1.224	0.731
120	1.120	1.065	1.522	1.195	1.166	1.257	0.862
			188.02 K (This Work)				
20	1.071	1.077	1.122	1.090	1.086	1.102	0.200
40	1.103	1.082	1.199	1.120	1.112	1.142	0.426
60	1.121	1.081	1.274	1.147	1.135	1.176	0.646
80	1.133	1.075	1.350	1.173	1.156	1.209	0.857
100	1.142	1.066	1.430	1.197	1.176	1.240	1.061
120	1.148	1.055	1.510	1.222	1.197	1.270	1.246
			202.01 K (This Work)				
20	1.090	1.100	1.135	1.112	1.110	1.120	0.250
40	1.139	1.110	1.220	1.154	1.148	1.170	0.569
60	1.163	1.104	1.297	1.186	1.177	1.208	0.883
80	1.179	1.093	1.375	1.215	1.200	1.241	1.186
100	1.190	1.079	1.454	1.242	1.224	1.271	1.472
120	1.198	1.062	1.536	1.270	1.247	1.300	1.739

Table 34. (Concluded)

P atm	ϕ EXP	ϕ LJCL	ϕ KIH	ϕ KIHCK12	ϕ KIHEK12	ϕ BWR	100 x_2
			216.04 K (This Work)				
20	1.080	1.113	1.134	1.122	1.121	1.127	0.282
40	1.159	1.143	1.245	1.194	1.189	1.204	0.742
60	1.199	1.139	1.335	1.238	1.229	1.251	1.180
80	1.221	1.135	1.423	1.276	1.264	1.290	1.587
100	1.237	1.122	1.513	1.312	1.294	1.325	1.954
120	1.249	1.086	1.608	1.346	1.324	1.357	2.250

[a] Condensed phase assumed to be pure ethylene.

[b] Liquid composition values taken from this work.

Table 35. Smoothed Experimental and Theoretical Enhancement Factors of Propane in Helium, and the Smoothed Experimental Solubility of Helium in Liquid Propane

P atm	ø EXP	ø LJCL	ø KIH	ø KIHCK12	ø KIHEK12	ø BWR	100 x_2
			198.15 K (Schindler, et al.[140])				
20	1.178	1.021	1.081	1.033	1.024	1.028	0.162
40	1.305	1.025	1.154	1.056	1.037	1.044	0.316
60	1.407	1.024	1.229	1.077	1.049	1.056	0.470
80	1.490	1.018	1.306	1.097	1.060	1.068	0.621
100	1.556	1.007	1.384	1.117	1.073	1.080	0.762
120	1.613	0.9929	1.465	1.138	1.084	1.090	0.904
140	1.665	0.9757	1.548	1.158	1.095	1.099	1.040
160	1.713	0.9554	1.633	1.178	1.107	1.108	1.163
180	1.757	0.9327	1.720	1.198	1.118	1.117	1.282
200	1.800	0.9081	1.808	1.219	1.130	1.125	1.394
			223.15 K (Schindler, et al.[140])				
20	1.115	1.028	1.085	1.049	1.043	1.044	0.278
40	1.207	1.021	1.145	1.068	1.054	1.054	0.540
60	1.282	1.009	1.204	1.087	1.067	1.063	0.783
80	1.342	0.9946	1.266	1.105	1.078	1.070	1.035
100	1.395	0.9759	1.329	1.124	1.088	1.075	1.270
120	1.445	0.9553	1.393	1.141	1.099	1.081	1.490
140	1.490	0.9324	1.458	1.159	1.100	1.086	1.706
160	1.530	0.9078	1.524	1.176	1.121	1.090	1.920
180	1.572	0.8818	1.591	1.194	1.131	1.093	2.130
200	1.612	0.8548	1.660	1.211	1.143	1.097	2.335
			248.15 K (Schindler, et al.[140])				
20	1.078	1.057	1.108	1.081	1.076	1.073	0.380
40	1.145	1.044	1.164	1.103	1.091	1.083	0.785
60	1.200	1.024	1.218	1.122	1.105	1.090	1.180
80	1.245	1.002	1.273	1.140	1.117	1.095	1.563
100	1.285	0.9772	1.329	1.157	1.129	1.098	1.930
120	1.320	0.9509	1.386	1.176	1.140	1.106	2.285
140	1.350	0.9234	1.444	1.192	1.152	1.102	2.620
160	1.382	0.8951	1.504	1.210	1.163	1.104	2.925
180	1.410	0.8661	1.564	1.227	1.175	1.105	3.217
200	1.440	0.8368	1.626	1.244	1.186	1.105	3.480

Table 35. (Continued)

P atm	ϕ EXP	ϕ LJCL	ϕ KIH	ϕ KIHCK12	ϕ KIHEK12	ϕ BWR	100 x_2
			273.15 K (Schindler, et al.[140])				
20	1.042	1.100	1.137	1.120	1.117	1.116	0.480
40	1.088	1.091	1.207	1.158	1.150	1.141	1.070
60	1.128	1.066	1.267	1.184	1.170	1.151	1.650
80	1.162	1.038	1.325	1.208	1.187	1.157	2.200
100	1.192	1.006	1.384	1.229	1.203	1.159	2.750
120	1.215	0.9733	1.444	1.250	1.218	1.161	3.250
140	1.238	0.9395	1.506	1.270	1.233	1.161	3.730
160	1.257	0.9062	1.569	1.290	1.248	1.161	4.160
180	1.275	0.8725	1.633	1.310	1.261	1.159	4.590
200	1.288	0.8395	1.701	1.330	1.276	1.158	4.950
			298.15 K (Schindler, et al.[140])				
20	1.071	1.122	1.137	1.130	1.129	1.132	0.480
40	1.153	1.152	1.247	1.214	1.208	1.207	1.330
60	1.207	1.132	1.324	1.257	1.246	1.236	2.160
80	1.242	1.099	1.392	1.290	1.275	1.252	2.900
100	1.269	1.061	1.457	1.318	1.297	1.262	3.620
120	1.285	1.021	1.522	1.344	1.317	1.266	4.310
140	1.300	0.9808	1.587	1.368	1.335	1.269	4.960
160	1.309	0.9400	1.653	1.389	1.351	1.268	5.580
180	1.317	0.8996	1.719	1.410	1.365	1.265	6.220
200	1.324	0.8603	1.785	1.429	1.379	1.261	6.800
			323.15 K (Schindler, et al.[140])				
20	1.032	1.052	1.054	1.053	1.053	1.054	0.190
40	1.180	1.188	1.265	1.246	1.243	1.243	1.420
60	1.278	1.199	1.399	1.347	1.339	1.329	2.610
80	1.347	1.172	1.512	1.419	1.405	1.379	3.750
100	1.392	1.131	1.619	1.478	1.457	1.411	4.850
120	1.423	1.083	1.728	1.528	1.501	1.433	5.880
140	1.446	1.034	--[a]	1.573	1.538	1.445	6.880
160	1.460	0.9841	--	1.614	1.573	1.452	7.770
180	1.471	0.9352	--	1.652	1.603	1.454	8.580
200	1.478	0.8881	--	1.686	1.628	1.451	9.330

Table 35. (Concluded)

P atm	ϕ EXP	ϕ LJCL	ϕ KIH	ϕ KIHCK12	ϕ KIHEK12	ϕ BWR	100 x_2
			348.15 K (Schindler, et al.[140])				
40	1.155	1.120	--[a]	--	--	1.176	1.280
60	1.323	1.207	--	--	--	1.397	3.220
80	1.434	1.220	--	--	--	1.584	4.970
100	1.516	1.198	--	--	--	1.790	6.590
120	1.576	1.157	--	--	--	--	8.070
140	1.622	1.107	--	--	--	--	9.450
160	1.655	1.051	--	--	--	--	10.73
180	1.679	0.9922	--	--	--	--	11.96
200	1.700	0.9337	--	--	--	--	13.14

[a] The blank spaces indicate lack of convergence of the theoretical calculations.

Table 36. Smoothed Experimental and Theoretical Enhancement Factors of Propylene in Helium, and the Smoothed Experimental Solubility of Helium in Liquid Propylene

P atm	ϕ EXP	ϕ LJCL	ϕ KIH	ϕ KIHCK12	ϕ KIHEK12	ϕ BWR	100 x_2
			175.00 K (This Work)				
20	--[a]	1.004	1.094	1.022	1.019	1.035	0.076
40	--	0.9955	1.188	1.039	1.033	1.064	0.151
60	--	0.9796	1.287	1.057	1.048	1.093	0.224
80	--	0.9573	1.389	1.074	1.061	1.120	0.297
100	--	0.9297	1.494	1.090	1.075	1.145	0.368
120	--	0.8979	1.605	1.107	1.088	1.170	0.437
			187.49 K (This Work)				
20	--	0.9976	1.085	1.024	1.021	1.034	0.107
40	--	0 9808	1.165	1.039	1.034	1.057	0.213
60	--	0.9581	1.249	1.055	1.047	1.080	0.318
80	--	0.9305	1.335	1.070	1.060	1.101	0.420
100	--	0.8989	1.424	1.085	1.071	1.121	0.519
120	--	0.8644	1.515	1.099	1.084	1.141	0.609
			200.00 K (This Work)				
20	1.020	0.9967	1.081	1.029	1.027	1.037	0.142
40	1.029	0.9734	1.152	1.043	1.039	1.057	0.285
60	1.031	0.9455	1.225	1.057	1.050	1.074	0.428
80	1.035	0.9139	1.299	1.071	1.061	1.091	0.567
100	1.036	0.8794	1.374	1.085	1.073	1.108	0.700
120	1.036	0.8428	1.453	1.099	1.085	1.123	0.820
			212.49 K (This Work)				
20	1.025	1.001	1.083	1.038	1.036	1.044	0.190
40	1.036	0.9726	1.147	1.051	1.048	1.061	0.379
60	1.040	0.9406	1.211	1.065	1.059	1.076	0.558
80	1.043	0.9057	1.277	1.078	1.070	1.091	0.738
100	1.044	0.8688	1.345	1.091	1.081	1.104	0.909
120	1.044	0.8306	1.414	1.104	1.092	1.116	1.066

Table 36. (Concluded)

P atm	ϕ EXP	ϕ LJCL	ϕ KIH	ϕ KIHCK12	ϕ KIHEK12	ϕ BWR	100 x_2
			224.99 K (This Work)				
20	1.040	1.011	1.089	1.051	1.049	1.056	0.233
40	1.060	0.9779	1.148	1.064	1.061	1.071	0.475
60	1.068	0.9422	1.207	1.077	1.072	1.084	0.714
80	1.072	0.9043	1.268	1.091	1.084	1.096	0.951
100	1.073	0.8651	1.329	1.103	1.095	1.107	1.175
120	1.074	0.8253	1.393	1.116	1.106	1.117	1.375
			239.99 K (This Work)				
20	1.057	1.028	1.102	1.070	1.069	1.072	0.293
40	1.083	0.9922	1.159	1.086	1.083	1.088	0.613
60	1.096	0.9523	1.216	1.101	1.097	1.101	0.929
80	1.104	0.9109	1.272	1.115	1.108	1.112	1.239
100	1.108	0.8687	1.330	1.127	1.120	1.121	1.540
120	1.109	0.8266	1.388	1.141	1.132	1.130	1.830
			254.98 K (This Work)				
20	1.070	1.051	1.119	1.093	1.092	1.098	0.359
40	1.107	1.014	1.180	1.116	1.114	1.119	0.775
60	1.127	0.9704	1.236	1.133	1.130	1.133	1.179
80	1.138	0.9251	1.292	1.149	1.144	1.144	1.590
100	1.144	0.8796	1.350	1.164	1.157	1.153	1.976
120	1.146	0.8353	1.409	1.179	1.171	1.161	2.284

[a] No results reported for the gas phase.

APPENDIX H

The argon and carbon dioxide gases used in this work were the same as purchased by Liu.[83] The argon was obtained from the Air Products Company with a quoted purity of 99.995 percent, and the carbon dioxide came from Matheson Company with a quoted purity of 99.99 percent. The helium used in this work was obtained from the Air Reduction Company. This helium was the high purity grade, 99.997 percent, as obtained from the Bureau of Mines.

Both hydrocarbons used in this work, ethylene and propylene, were obtained from Phillips Petroleum Company. The quoted purity determination of ethylene was 99.97 percent with the impurities being methane and ethane. The propylene quoted purity was assessed at 99.99 percent with the impurity being mainly propane. Due to the low range of analysis, it was possible to approximately verify these purities and the types of impurities present.

Since all the gases used in this research were of high purity, they were used in the received condition with no further purification.

BIBLIOGRAPHY

1. Barber, C. R., "The International Practical Temperature Scale of 1948," Metrologia 5, No. 2, 35-44 (1969).

2. Barrick, P. L., Heck, C. K., and MacKendrick, R. F., "Liquid Vapor Equilibria of the Helium-Carbon Dioxide System," Journal of Chemical and Engineering Data 13, 352-353 (1968).

3. Benedict, M., Webb, G. B., and Rubin, L. C., "An Empirical Equation for Thermodynamic Properties of Light Hydrocarbons and their Mixtures. II. Mixtures of Methane, Ethane, Propane and n-Butane," Journal of Chemical Physics 10, 747-758 (1942).

4. Benedict, M., Webb, G. B., and Rubin, L. C., "An Empirical Equation for Thermodynamic Properties of Light Hydrocarbons and Their Mixtures," Chemical Engineering Progress 47, No. 8, 419-422 (1951).

5. Bird, R. B., Spotz, E. L., and Hirschfelder, J. O., "Third Virial Coefficient for Non-Polar Gases," Journal of Chemical Physics 18, 1395-1402 (1950).

6. Brandt, L. W., Stroud, L., and Miller, J. E., "Phase Equilibrium in Natural Gas Systems," Journal of Chemical and Engineering Data 6, 6-13 (1961).

7. Brewer, J., "Determination of Mixed Virial Coefficients," Contract No. AF 49(638)-1620, AD 66344F, 98 pages, December 1967.

8. Brewer, J. and Vaughn, G. W., "Measurement and Correlation of Some Interaction Second Virial Coefficients from -125 to 50°C," Journal of Chemical Physics 50, No. 7, 2960-2968 (1969).

9. Burnett, E. S., "Compressibility Determination Without Volume Measurements," Journal of Applied Mechanics 3, A136-140 (1936).

10. Butcher, E. G. and Dadson, R. S., "The Virial Coefficients of the Carbon Dioxide-Ethylene System. I. Pure Gases," Proceedings of the Royal Society (London) A277, 448-467 (1964).

11. Buzyna, G., Macriss, R. A., and Ellington, R. T., "Vapor Liquid Equilibrium in the Helium-Nitrogen System," Chemical Engineering Progress Symposium Series No. 44, 101-111 (1963).

12. Canfield, F. B., Leland, T. W., and Kobayashi, R., "Volumetric Behavior of Gas Mixtures at Low Temperatures by the Burnett Method: Helium-Nitrogen System, 0 to -140°C," Advances in Cryogenic Engineering 8, 146-157 (1963).

13. Canjar, L. N. and Manning, F. S., Thermodynamic Properties and Reduced Correlations for Gases, Gulf Publishing Company, Houston, Texas (1967).

14. Carlson, C. M., Eyring, H., and Ree, T., "Significant Structures in Liquids, III. Partition Function for Fused Salts," Proceedings National Academy of Science 46, 333-336 (1960).

15. Chiu, C. -h. and Canfield, F. B., "Thermodynamic Analysis of Vapor-Liquid and Vapor-Solid Equilibria Data to Obtain Interaction Second Virial Coefficients," Advances in Cryogenic Engineering 12, 741-753 (1967).

16. Chueh, P. L. and Prausnitz, J. M., "Third Virial Coefficients of Nonpolar Gases and Their Mixtures," American Institute of Chemical Engineers Journal 13, No. 5, 896-902 (1967).

17. Chueh, P. L. and Prausnitz, J. M., "Vapor-Liquid Equilibria at High Pressures. Vapor-Phase Fugacity Coefficients in Nonpolar and Quantum Gas Mixtures," Industrial Engineering Chemistry Fundamentals 6, No. 4, 492-498 (1967).

18. Chueh, P. L. and Prausnitz, J. M., "Vapor-Liquid Equilibria at High Pressures. Calculation of Partial Molar Volumes in Nonpolar Liquid Mixtures," American Institute of Chemical Engineers Journal 13, No. 6, 1099-1107 (1967).

19. Chueh, P. L. and Prausnitz, J. M., "A generalized Correlation for the Compressibilities of Normal Liquids," American Institute of Chemical Engineering Journal 15, No. 3, 471-472 (1969).

20. Cook, D., "The Second Virial Coefficient of Carbon Dioxide at Low Temperatures," Canadian Journal of Chemistry 35, 268-275 (1957).

21. Correia, Von. P., Schafer, K., and Schneider, M., "Bestimmung der zwischenmolekularen Krafte aus Ultraschalldispersionsmessungen in Gasgemischen," Berichte der Bunsengesellschaft fur Physikalische Chemie 73, Nr. 6, 507-513 (1969).

22. Crommelin, C. A. and Watts, H. G., "Preliminary Isotherms of Ethylene," Communications Physical Laboratory University of Leiden 189c, 13-16 (1927).

23. Dantzler, E. M., Knobler, C. M., and Windsor, M. L., "Second Virial Coefficients of Some Argon-Hydrocarbon Mixtures and Their Comparison With Chromotographic Values," Journal of Chromatography 32, 433-438 (1968).

24. David, H. G. and Hamann, S. D., "The Gas Imperfections of Hydrocarbons," Proceedings of the Joint Conference in Thermodynamics and Transport Properties of Fluids, London, 74-78 (1957).

25. David, H. G., Hamann, S. D., and Prince, R. G. H., "The Third Virial Coefficient of Ethane," Journal of Chemical Physics 20, 1973-1974 (1952).

26. Dawson, P. P., Jr. and McKetta, J. J., "Z's for Propane and Methylacetylene," Petroleum Refiner 39, No. 4, 151-154 (1960).

27. De Boer, J. and Michels, A., "Contributions to the Quantum-Mechanical Theory of the Equation of State and the Law of Corresponding States. Determination of the Law of Force of Helium," Physica 5, 945-957 (1938).

28. DeVaney, W. E., Dalton, B. J., and Meeks, J. C., Jr., "Vapor Liquid Equilibrium of the Helium-Nitrogen System," Journal of Chemical and Engineering Data 8, No. 4, 473-478 (1963).

29. Din, F., Thermodynamic Functions of Gases, Volume I, II, III, Butterworths, London (1956) and (1961).

30. Dokoupil, Z., "Some Solid-Gas Equilibria at Low Temperatures," Progress in Low Temperature Physics, Vol. III, Edited by C. J. Gorter, North-Holland Publishing Company, Amsterdam, Interscience Publishers, Inc., New York, 454-480 (1961).

31. Dokoupil, Z., Van Soest, G., and Swenker, M. D. P., "On the Equilibrium Between the Solid Phase and the Gas Phase of the Systems Hydrogen-Nitrogen, Hydrogen-Carbon Monoxide, and Hydrogen-Nitrogen-Carbon Dioxide," Applied Scientific Research A5, 182-240 (1955).

32. Dymond, J. H. and Smith, E. B., The Virial Coefficients of Gases, Clarendon Press, Oxford (1969).

33. Eckert, C. H., Renon, H., and Prausnitz, J. M., "Molecular Thermodynamics of Simple Fluid Mixtures," Industrial and Engineering Chemistry. Fundamentals 6, No. 1, 58-67 (1967).

34. Eubanks, L. S., Vapor-Liquid Equilibrium in the System Hydrogen-Nitrogen-Carbon Monoxide, Ph. D. Thesis, Rice Institute, Houston, Texas (1957).

35. Eucken, A. and Parts, A., "Die Molwarmen and Normalschwingungen des Athans und Athylens," Zeitschrift fur Physikalische Chemie B20, 184-194 (1933).

36. Farrington, P. S. and Sage, B. H., "Volumetric Behavior of Propene," Industrial and Engineering Chemistry 41, 1734-1737 (1949).

37. Fedoritenko, A. and Ruhemann, M., "Equilibrium Diagrams of Helium-Nitrogen Mixtures," Technical Physics of U S S R 4, 36-43 (1937).

38. Fowler, R. and Graben, H. W., "Nonadditive Third Virial Coefficient for Intermolecular Potentials with Hard-Sphere Cores," Journal of Chemical Physics 50, No. 10, 4347-4351 (1969).

39. Gibby, C. W., Tanner, C. C., and Masson, I., "The Pressures of Gaseous Mixtures. II-Helium and Hydrogen, and their Intermolecular Forces," Proceedings of the Royal Society (London) A122, 283-304 (1929).

40. Gonikberg, M. and Fastovskii, V., "The Solubility of Gases in Liquids at Low Temperatures and High Pressures, Fourth Article," Foreign Petroleum Technology 9, No. 6, 214-219 (1941).

41. Graben, H. W. and Present, R. D., "Evidence of Three-Body Forces From Third Virial Coefficient," Physical Review Letters 9, 247-248 (1962).

42. Graben, H. W., Present, R. D., McCulloch, R. D., "Intermolecular Three-Body Forces and Third Virial Coefficients," Physical Review 144, No. 1, 140-142 (1966).

43. Haar, L. and Sengers, J. M. H., "Solubility of Condensed Substances in Dense Gases and the Effect on PVT Properties," Journal of Chemical Physics 52, No. 10, 5069-5079 (1970).

44. Hamann, S. D. and McMananey, W. J., "Second Virial Coefficient of Ethane," Transaction of Faraday Society 49, 149-152 (1953).

45. Hanley, H. J. M. and Klein, M., "On the Selection of the Intermolecular Potential Function: Application of Statistical Mechanical Theory to Experiment," National Bureau of Standards Technical Note 360, 82 pages (1967).

46. Heck, C. K., Jr., Experimental and Theoretical Liquid-Vapor Equilibrium in Some Binary Systems, Ph.D. Thesis, University of Colorado, Denver, Colorado (1968).

47. Heck, C. K. and Hiza, M. J., "Liquid-Vapor Equilibrium in the System Helium-Methane," American Institute of Chemical Engineers Journal 13, 593-599 (1967).

48. Herring, R. N. and Barrick, P. L., "Gas-Liquid Equilibrium Solubilities for the Helium-Oxygen System," Advances in Cryogenic Engineering 10, 151-159 (1965).

49. Hill, T. L., Statistical Mechanics, McGraw-Hill, New York (1956).

50. Hirschfelder, J. O., Curtiss, C. J., and Bird, R. B., Molecular Theory of Gases and Liquids, Wiley, New York (1964).

51. Hirschfelder, J. O., McClure, F. T., and Weeks, I. F., "Second Virial Coefficients and the Forces Between Complex Molecules," Journal of Chemical Physics 10, 210-211 (1942).

52. Hiza, M. J., "Solid-Vapor Equilibria Research on Systems of Interest in Cryogenics," Cryogenics 10, No. 2, 106-115 (1970).

53. Hiza, M. J. and Duncan, A. G., "Equilibrium Gas-Phase Compositions of Ethane and Ethylene in Binary Mixtures with Helium and Neon Below 150 K and a Correlation for Deviations from the Geometric Mean Combining Rule," Advances in Cryogenic Engineering 14, 30-40 (1968).

54. Hiza, M. J., Heck, C. K., and Kidnay, A. J., "Liquid-Vapor and Solid-Vapor Equilibrium in the System Hydrogen-Ethylene," Chemical Engineering Progress Symposium Series 64, 57-65 (1968).

55. Hiza, M. J., Heck, C. K., and Kidnay, A. J., "Liquid-Vapor and Solid-Vapor Equilibrium in the System Hydrogen-Ethane," Advances in Cryogenic Engineering 13, 343-356 (1968).

56. Hiza, M. J. and Kidnay, A. J., "Solid-Vapor Equilibrium in the System Helium-Methane," Advances in Cryogenic Engineering 11, 338-348 (1965).

57. Holborn, L. and Otto, J., "Uber die Isothermen einiger Gase bis 400°C und ihre Bedeutung fur das Gasthermometer," Zeitschrift fur Physik 23, 77-94 (1924).

58. Hoover, A. E., Canfield, F. B., Kobayashi, R., and Leland, T. W., Jr., "Determination of Virial Coefficients by the Burnett Method," Journal of Chemical and Engineering Data 9, No. 4, 568-573 (1964).

59. Hoover, A. E., Leland, T. W., and Kobayashi, R., "Negative Virial Coefficients," Journal of Chemical Physics 45, No. 1, 399-400 (1966).

60. Hoover, A. E., Nagata, I., Leland, T. W., Jr., and Kobayashi, R., "Virial Coefficients of Methane, Ethane and Their Mixtures at Low Temperatures," Journal of Chemical Physics 48, No. 6, 2633-2647 (1968).

61. Hougen, O. A., Watson, K. M., and Ragatz, R. A., Chemical Process Principles Part II, John Wiley and Sons, Inc., New York (1965).

62. Hudson, G. H. and McCoubrey, J. C., "Intermolecular Forces Between Unlike Molecules," Transactions of the Faraday Society 56, 761-766 (1960).

63. Huff, J. A. and Reed, T. M., "Second Virial Coefficients of Mixtures of Nonpolar Molecules from Correlations on Pure Components," Journal of Chemical and Engineering Data 8, No. 3, 306-311 (1963).

64. Iomtev, M. B., Morozov, V. S., and Chumak, A. V., "Solid-Gas Phase Equilibrium in the System Helium-Carbon Dioxide," Zhurnal Fizicheskoi Khimii 42, No. 8, 2069-2071 (1968).

65. Jones, A. E. and Kay, W. B., "Part II. Second Virial Coefficients for Helium-n-Butane Mixtures," American Institute of Chemical Engineers Journal 13, No. 4, 720-725 (1967).

66. Kahre, L. C. and Livingston, R. J., "More Accuracy in Liquid Propane Compressibility," Hydrocarbon Processing and Petroleum Refiner 43, No. 4, 119-121 (1964).

67. Kalfoglou, N. K. and Miller, J. G., "Compressibility of Gases. V. Mixtures of Spherically Symmetric Molecules at Higher Temperatures. The Helium-Argon and Helium-Tetrafluoromethane Systems." The Journal of Physical Chemistry 71, No. 5, 1256-1264 (1967).

68. Keesom, W. H., Helium, Elsevier, Amsterdam (1942).

69. Kharakhorin, F. F., "The Phase Relation in Systems of Liquid Gases, First Article, The Binary Mixture Nitrogen-Helium," Foreign Petroleum Technology 9, 397-410 (1941).

70. Kharakhorin, F. F., "Liquid-Vapor Equilibrium in a Helium-Methane System," Inzhenerno-Fizicheskii Zhurnal, Akademiya Nauk Belorusskoi S.S.R. 2, No. 5, 55-59 (1959).

71. Kihara, T., "Determination of Intermolecular Forces from the Equation of State of Gases," Journal Physical Society Japan 3, 265-268 (1948).

72. Kihara, T., "Determination of Intermolecular Forces from the Equation of State of Gases. II.," Journal Physical Society Japan 6, 184-188 (1951).

73. Kihara, T., "Virial Coefficients and Models of Molecules in Gases," Reviews of Modern Physics 25, No. 4, 831-843 (1953).

74. Kihara, T., "Virial Coefficients and Models of Molecules in Gases B." Reviews of Modern Physics 27, No. 4, 412-423 (1955).

75. King, A. D., Jr. and Robertson, W. W., "Solubility of Naphthalene in Compressed Gases," Journal of Chemical Physics 37, No. 7, 1453-1455 (1962).

76. Kirk, B. S., Predicted and Experimental Gas Phase Compositions in Pressurized Binary Systems Containing an Essentially Pure Condensed Phase. Phase Equilibrium Data for the Methane-Hydrogen System from 66.88 to 116.53°K and Up to 125 Atmospheres, Ph. D. Thesis, Georgia Institute of Technology, Atlanta, Georgia (1964).

77. Kirk, B. S. and Ziegler, W. T., "A Phase Equilibrium Apparatus for Gas-Liquid Systems and the Gas Phase of Gas-Solid System. Application to Methane-Hydrogen from 66.88 to 116.53°K and Up to 125 Atmospheres," Advances in Cryogenic Engineering 10, 160-170 (1965).

78. Kirk, B. S., Ziegler, W. T., and Mullins, J. C., "A Comparison of Methods of Predicting Equilibrium Gas Phase Compositions in Pressurized Binary Systems Containing an Essentially Pure Condensed Phase," Advances in Cryogenic Engineering 6, 413-427 (1961).

79. Kobe, K. A. and Lynn, R. E., "The Critical Properties of Elements and Compounds," Chemical Reviews 52, 117-236 (1953).

80. Krichevsky, I. R. and Kasarnovsky, J. S., "Thermodynamical Calculations of Solubilities of Nitrogen and Hydrogen in Water at High Pressures," Journal of the American Chemical Society 57, 2168-2171 (1935).

81. Lambert, J. D., Roberts, G. A. H., Rowlinson, J. S., and Wilkinson, V. J., "Second Virial Coefficients of Organic Vapors," Proceedings of the Royal Society (London) A196, 113-125 (1949).

82. Lin, H. -M. and Robinson, R. L., Jr., "Uncertainties in Intermolecular Pair Potential Parameters Determined from Macroscopic Property Data. I. Virial Coefficients," Journal of Chemical Physics 52, No. 7, 3727-3731 (1970).

83. Liu, K. F., Phase Equilibria in the Helium-Carbon Dioxide, -Argon, -Methane, -Nitrogen, and -Oxygen Systems, Ph. D. Thesis, Georgia Institute of Technology, Atlanta, Georgia (1969).

84. Lu, H., Newett, D. J., and Ruhemann, M., "Two-Phase Equilibrium in Binary and Ternary Systems," Proceedings of the Royal Society (London) A178, 506-525 (1941).

85. Lyckman, E. W., Eckert, C. A., and Prausnitz, J. M., "Generalized Liquid Volumes and Solubility Parameters for Regular Solution Applications," Chemical Engineering Science 20, 703-706 (1965).

86. Maass, O. and McIntosh, D., "Some Physical Properties of Ethane, Ethylene and Acetylene," Journal American Chemical Society 36, 737-742 (1914).

87. Maass, O. and Wright, C. H., "Some Physical Properties of Hydrocarbons Containing Two and Three Carbon Atoms," Journal of the American Chemical Society 43, 1098-1111 (1921).

88. MacKendrick, R. F., Heck, C. K., and Barrick, P. L., "Liquid-Vapor Equilibria of the Helium-Carbon Dioxide System," Journal of Chemical and Engineering Data 13, 352-353 (1968).

89. Mann, D. B., "The Thermodynamic Properties of Helium from 3 to 300 K Between 0.5 and 100 Atmospheres," National Bureau of Standards Technical Note No. 154, National Bureau of Standards, Boulder, Colorado (1962).

90. Marcham, H., Pringle, H. W., and Motard, R. L., "Compressibility and Critical Constants of Propylene Vapor," Industrial and Engineering Chemistry 41, 2658-2660 (1949).

91. Margenau, H. and Kestner, N. R., Theory of Intermolecular Forces, International Series in Monographs in Natural Philosophy, Volume 18, Pergamon Press, Oxford (1969).

92. Mathias, E., Crommelin, C. A., and Watts, A. G., "Le Diametre Rectiligne De L'Ethylene," Annales De Physique 11, 343-353 (1929).

93. Mayer, J. E. and Mayer, M. G., Statistical Mechanics, John Wiley and Sons, New York (1940).

94. McCain, W. D., Jr., Vapor-Liquid Phase Equilibria of the Binary System Argon-Helium, Ph. D. Thesis, Georgia Institute of Technology, Atlanta, Georgia (1964).

95. McCain, W. D., Jr. and Ziegler, W. T., "The Critical Temperature, Critical Pressure and Vapor Pressure of Argon," Journal of Chemical and Engineering Data 12, No. 2, 199-202 (1967).

96. McGlashan, M. L. and Potter, D. J. B., "An Apparatus for Measurement of the Second Virial Coefficients of Vapors," Proceedings of the Royal Society (London) A267, 478-500 (1962).

97. McGlashan, M. L. and Wormald, C. J., "Second Virial Coefficients of Some Alkenes and of a Mixture of Propene and Heptene," Transactions of the Faraday Society 60, 646-652 (1964).

98. Meyers, C. H. and Van Dusen, M. S., "The Vapor Pressure of Liquid and Solid Carbon Dioxide," Journal of Research of the National Bureau of Standards 10, 381-412 (1933).

99. Michels, A. and Geldermans, M., "Isotherms of Ethylene Up to 3000 Atmospheres Between 0° and 150°C," Physica 9, 967-973 (1942).

100. Michels, A., Straaten, Van. W., and Dawson, J., "Isotherms and Thermodynamical Functions of Ethane At Temperatures Between 0°C and 150°C and Pressures Up To 200 Atmospheres," Physica 20, 17-23 (1954).

101. Michels, A. and Wassenaar, T., "The Vapor Pressure of Ethylene," Physica 16, 221-224 (1950).

102. Michels, A., Wassenaar, T., Louwerse, P., Lunbeck, R. J., and Wolkers, G. T., "Isotherms and Thermodynamical Functions of Propene at Temperatures Between 25° and 150°C and at Densities Up To 340 Amagat," Physica 19, 287-297 (1953).

103. Michels, A., Wassenaar, T., and Zweitering, Th., "The Vapor Pressure of Argon," Physica 17, 876-884 (1951).

104. Miller, R. C. and Prausnitz, J. M., "Statistical Thermodynamics of Simple Liquid Mixtures," Industrial and Engineering Chemistry Fundamentals 8, No. 3, 449-452 (1969).

105. Mueller, W. H., Volumetric Properties of Gases at Low Temperatures by the Burnett Method, Ph. D. Thesis, Rice University, Houston, Texas (1959).

106. Mueller, W. H., Leland, T. W., Jr., and Kobayashi, R., "Volumetric Properties of Gas Mixtures at Low Temperatures and High Pressures by the Burnett Method: The Hydrogen-Methane System," American Institute of Chemical Engineers Journal 7, No. 2, 267-272 (1961).

107. Mullins, J. C., Phase Equilibria in the Argon-Helium and Argon-Hydrogen Systems, Ph. D. Thesis, Georgia Institute of Technology, Atlanta, Georgia (1965).

108. Mullins, J. C. and Ziegler, W. T., "Phase Equilibrium in the Argon-Helium and Argon-Hydrogen Systems from 68 to 108°K and Pressures Up To 120 Atmospheres," Advances in Cryogenic Engineering 10, 171-181 (1965).

109. O'Connell, J. P. and Prausnitz, J. M., "Applications of the Kihara Potential to Thermodynamic and Transport Properties of Gases," Symposium Thermophysical Properties, Papers, 3rd, Lafayette, Indiana, 19-31 (1965).

110. Orentlicher, M. and Prausnitz, J. M., "Thermodynamics of Hydrogen Solubility in Cryogenic Solvents at High Pressures," Chemical Engineering Science 19, 775-782 (1964).

111. Orentlicher, M. and Prausnitz, J. M., "Approximate Method for Calculating the Third Virial Coefficient of a Gaseous Mixture," Canadian Journal of Chemistry 45, 373-378 (1967).

112. Percus, J. K. and Yevick, G. J., "Analysis of Classical Statistical Mechanics by Means of Collective Coordinates," Physical Reviews 110, 1-13 (1958).

113. Pierotti, R. A., "The Solubility of Gases in Liquids," Journal of Physical Chemistry 67, 1840-1845 (1963).

114. Pierotti, R. A., "Aqueous Solutions of Nonpolar Gases," Journal of Physical Chemistry 69, No. 1, 281-288 (1965).

115. Pierotti, R. A., "On the Sealed-Particle Theory of Dilute Aqueous Solutions," Journal of Physical Chemistry 71, 2366-2357 (1967).

116. Pitzer, K. S. and Curl, R. F., Jr., "The Volumetric and Thermodynamic Properties of Fluids. III Empirical Equation for the Second Virial Coefficient," Journal of the American Chemical Society 79, 2369-2370 (1957).

117. Powell, T. M. and Giauque, W. F., "Propylene. The Heat Capacity, Vapor Pressure, Heats of Fusion and Vaporization, the Third Law of Thermodynamics and Orientation Equilibrium in the Solid," Journal of the American Chemical Society 61, 2366-2370 (1939).

118. Prausnitz, J. M., "Thermodynamic Representation of High-Pressure Vapour-Liquid Equilibria," Chemical Engineering Science 18, 613-630 (1963).

119. Prausnitz, J. M., Molecular Thermodynamics of Fluid-Phase Equilibria, Prentice-Hall, Inc., Englewood Cliffs, New Jersey (1969).

120. Prausnitz, J. M. and Chueh, P. L., Computer Calculations for High Pressure Vapor-Liquid Equilibrium, Prentice-Hall, Inc., Englewood Cliffs, New Jersey (1968).

121. Prausnitz, J. M., Eckert, C. A., Orye, R. V., and O'Connell, J. P., Computer Calculations for Multi-Component Vapor-Liquid Equilibria, Prentice-Hall, Inc., Englewood Cliffs, New Jersey (1968).

122. Prausnitz, J. M. and Myers, A. L., "Kihara Parameters and Second Virial Coefficients for Cryogenic Fluids and Their Mixtures," American Institute of Chemical Engineers Journal 9, No. 1, 5-11 (1963).

123. Prigogine, I., The Molecular Theory of Solutions, North-Holland Publishing Company, Amsterdam (1957).

124. Prigogine, I. and Mathot, V., "Application of the Cell Method to the Statistical Thermodynamics of Solutions," Journal of Chemical Physics 20, 49-57 (1952).

125. Reamer, H. H., Olds, R. H., Sage, B. H., and Lacey, W. N., "Phase Equilibrium in Hydrocarbon Systems," Industrial and Engineering Chemistry 36, 956-958 (1944).

126. Reamer, H. H., Sage, B. H., and Lacey, W. N., "Phase Equilibrium in Hydrocarbon Systems," Industrial and Engineering Chemistry 41, 482-484 (1949).

127. Reed, R. I., Ion Production by Electron Impact, Academic Press, New York (1962).

128. Reiss, H., "Scaled Particle Methods in the Statistical Thermodynamics of Fluids," Advances in Chemical Physics IX, 1-84 (1965).

129. Reiss, H., Frisch, H. L., Helfand, E., and Lebowitz, J. L., "Aspects of the Statistical Thermodynamics of Real Fluids," Journal of Chemical Physics 32, 119-124 (1960).

130. Reiss, H., Frisch, H. L., and Lebowitz, J. L., "Statistical Mechanics of Rigid Spheres," Journal of Chemical Physics 31, 369-380 (1959).

131. Reuss, J. and Beenakker, J. J. M., "Determination of the Second Virial Coefficient B_{12} of Gas Mixtures," Physica 22, 869-879 (1956).

132. Rigby, M., Dymond, J. H., and Smith, E. B., Unpublished Data (1963).

133. Rodewald, N. D., Davis, J. A., and Kurata, F., "The Homogenous Phase Behavior of the Helium-Nitrogen System," American Institute of Chemical Engineers Journal 10, No. 6, 937-943 (1964).

134. Roper, E. E., "Gas Imperfection," Journal of Physical Chemistry 44, 835-847 (1940).

135. Rossini, F. D., Data on Hydrocarbons and Related Compounds, American Petroleum Institute Research Project No. 44, Selected Values of Properties of Hydrocarbons and Related Compounds Table 24K (Part 1), Sept. 30, 1951.

136. Rowlinson, J. S., Liquids and Liquid Mixtures, Second Edition, Butterworth and Company, London (1969).

137. Rowlinson, J. S., Summer, F. H., and Sutton, J. R., "The Virial Coefficients of a Gas Mixture," Transactions of the Faraday Society 50, 1-8 (1954).

138. Salzburg, Z. W. and Kirkwood, J. G., "The Free Volume Theory of Multicomponent Fluid Mixtures," Journal of Chemical Physics 20, 1538-1543 (1952).

139. Schafer, K. and Kappallo, Von. W., "Thermodynamische Untersuchungen an Binaren Flussigkeitsgemischen von Methylchlorid, Methylbromid, Propan," Zeitschrift fur Electrochemie 66, No. 6, 508-514 (1962).

140. Schindler, D. L., Swift, G. W., and Kurata, F., "Phase-Equilibrium Studies in the Nitrogen-Propane, Helium-Propane, and Helium-Nitrogen-Propane Systems," Proceedings of the Annual Convention, Natural Gas Processors Association, Technical Paper 45, 46-51 (1966).

141. Sherwood, A. E. and Prausnitz, J. M., "Third Virial Coefficient for the Kihara, Exp-6, and Square-Well Potentials," Journal of Chemical Physics 41, No. 2, 413-428 (1964).

142. Sherwood, A. E. and Prausnitz, J. M., "Intermolecular Potential Functions and the Second and Third Virial Coefficients," Journal of Chemical Physics 41, No. 2, 429-437 (1964).

143. Sherwood, A. E., DeRocco, A. G., and Mason, E. A., "Nonadditivity of Intermolecular Forces: Effects on the Third Virial Coefficient," Journal of Chemical Physics 44, No. 8 2984-2994 (1966).

144. Sinor, J. E. and Kurata, F., "Solubility of Helium in Liquid Argon, Oxygen, and Carbon Monoxide," Journal of Chemical and Engineering Data 11, No. 4, 537-539 (1966).

145. Sinor, J. E., Schindler, D. L., and Kurata, F., "Vapor-Liquid Phase Behavior of the Helium-Methane System," American Institute of Chemical Engineers Journal 12, No. 2, 353-357 (1966).

146. Smith, G. E., Sonntag, R. E., and Van Wylen, G. J., "Analysis of the Solid-Vapor Equilibrium System Carbon Dioxide-Nitrogen," Advances in Cryogenic Engineering 8, 162-173 (1963).

147. Solen, K. A., Chueh, P. L., and Prausnitz, J. M., "Thermodynamics of Helium Solubility in Cryogenic Solvents at High Pressures," Industrial and Engineering Chemistry Process Design and Development 9, No. 2, 310-317 (1970).

148. Sood, S. L. and Haselden, G. G., "Prediction Methods for Vapor-Liquid Equilibria in Multi-Component Cryogenic Mixtures," Cryogenics 10, No. 3, 199-207 (1970).

149. Stearns, W. V. and George, E. J., "Thermodynamic Properties of Propane," Industrial and Engineering Chemistry 35, No. 5, 602-607 (1943).

150. Stroud, L., DeVaney, W. E., and Miller, J. E., "Low Temperature Phase Equilibria of Helium-Binary Natural Gases: Hogback Gas," U. S. Bureau of Mines, Report Investigation Number 6278, 16 pages (1963).

151. Stryland, J. C. and Nanassy, A. J., "The Influence of Compressed Gases in the Vapor Density of Mercury and on the Oscillator Strength of the 2537A Line," Physica 24, 935-936 (1958).

152. Stubley, D. and Rowlinson, J. S., "Solubility of Mercury in Compressed Argon," Transactions of the Faraday Society 57, 1275-1280 (1961).

153. Sze, M. M-n. and Hsu, H. W., "Second Virial Coefficients of the Lennard-Jones (6, m) Gases," Journal of Chemical and Engineering Data 11, No. 1, 77-80 (1966).

154. Technical Committee Natural Gasoline Associations of America, "Densities of Liquified Petroleum Gases," Industrial and Engineering Chemistry 34, No. 19, 1240-1243 (1942).

155. Tee, L. S., Gotoh, S., and Stewart, W. E., "Molecular Parameters for Normal Fluids," Industrial and Engineering Chemistry Fundamentals 5, No. 3, 356-363 (1966).

156. Tee, L. S., Gotoh, S., and Stewart, W. E., "Molecular Parameters for Normal Fluids," Industrial and Engineering Chemistry Fundamentals 5, No. 3, 363-367 (1966).

157. Tickner, A. W. and Lossing, F. P., "The Measurement of Low Vapor Pressures by Means of a Mass Spectrometer," Journal of Physical and Colloid Chemistry 55, 733-741 (1951).

158. Van Itterbeck, A., De Boelpep, J., Verbeke, O., Theeuwes, F., and Staes, K., "Vapor Pressure of Liquid Argon," Physica 30, 2119-2122 (1964).

159. Van Itterbeck, A. and Van Doninck, W., "Measurements on the Velocity of Sound in Mixtures of Hydrogen, Helium, Oxygen, Nitrogen and Carbon Dioxide at Low Temperature," Proceedings of the Physical Society (London) 62B, 62-69 (1949).

160. Viswanath, D. S., "Second Virial Coefficients and Force Constants of Gases," Indian Chemical Engineer October, 9-16 (1965).

161. White, D., Rubin, T., Camky, P., and Johnston, H. L., "The Virial Coefficients of Helium from 20 to 300°K," Journal of Physical Chemistry 64, 1607-1612 (1960).

162. Witousky, R. J. and Miller, J. G., "Compressibility of Gases. IV. The Burnett Method Applied to Gas Mixtures at Higher Temperatures. The Second Virial Coefficients of the Helium-Nitrogen System from 175 to 475°K," Journal of the American Chemical Society 85, 282-286 (1963).

163. Yoon, Y. K., Ph. D. Thesis in Progress (Chemical Engineering), Georgia Institute of Technology, Atlanta, Georgia (1970).

164. Ziegler, W. T., Kirk, B. S., Mullins, J. C., and Berguist, A. R., Calculation of the Vapor Pressure and Heats of Vaporization and Sublimation of Liquids and Solids Below One Atmosphere. VII. Ethane. Technical Report No. 2, Project A-764, Engineering Experiment Station, Georgia Institute of Technology, Atlanta, Georgia, December 31, 1964 (Contract No. CST - 1154, National Bureau of Standards, Boulder, Colorado).

165. Ziegler, W. T. and Mullins, J. C., Calculation of the Vapor Pressure and Heats of Vaporization and Sublimation of Liquids and Solids, Especially Below One Atmosphere. IV. Nitrogen and Fluorine. Technical Report No. 1, Project A-663, Engineering Experiment Station, Georgia Institute of Technology, Atlanta, Georgia, April 15, 1963 (Contract No. CST - 7404, National Bureau of Standards, Boulder, Colorado).

166. Ziegler, W. T., Mullins, J. C., and Kirk, B. S., Calculation of the Vapor Pressure and Heats of Vaporization and Sublimation of Liquids and Solids, Especially Below One Atmosphere Pressure. I. Ethylene. Technical Report No. 1, Project A-460, Engineering Experiment Station, Georgia Institute of Technology, Atlanta, Georgia, June 2, 1962 (Contract No. CST - 7238, National Bureau of Standards, Boulder, Colorado).

167. Ziegler, W. T., Mullins, J. C., and Kirk, B. S., Calculation of the Vapor Pressure and Heats of Vaporization and Sublimation of Liquids and Solids, Especially Below One Atmosphere Pressure. II. Argon. Technical Report No. 2, Project No. A-460, Engineering Station, Georgia Institute of Technology, Atlanta, Georgia, June 15, 1962 (Contract No. CST - 7238, National Bureau of Standards, Boulder, Colorado).

168. Ziegler, W. T., Mullins, J. C., and Kirk, B. S., Calculation of the Vapor Pressure and Heats of Vaporization and Sublimation of Liquids and Solids, Especially Below One Atmosphere Pressure. III. Methane. Technical Report No. 3, Project No. A-460, Engineering Experiment Station, Georgia Institute of Technology, Atlanta, Georgia, August 31, 1962 (Contract No. CST - 7238, National Bureau of Standards, Boulder, Colorado).

VITA

James Daniel Garber was born January 10, 1945, in Lafayette, Louisiana, to Nola Marie Grossie and the late Harry Lee Garber. He graduated from Saint Cecilia High School in 1962. From 1962 to 1966 he attended the University of Southwestern Louisiana in Lafayette, Louisiana, where he received the Bachelor of Science degree in Chemical Engineering and graduated With Distinction. In 1966 he enrolled in the graduate division of the Georgia Institute of Technology, where he received an N.D.E.A. fellowship for three years. He received the Master of Science degree in Chemical Engineering in 1968. He is a member of Tau Beta Pi, Phi Kappa Phi, and the Society of the Sigma Xi.

On June 7, 1969, he was married to the former Judith Ann Pickens of Knoxville, Tennessee.